Lehrstuhl für Technische Chemie II
Universität Duisburg-Essen

Surface selective hydrogel grafting of ultrafiltration membranes using macromolecular initiators and the application to increase fouling resistance

Dissertation

Zur Erlangung des akademischen Grades eines

Doktors der Naturwissenschaften

- Dr. rer. nat. –

der Fakultät für Chemie,

der Universität Duisburg-Essen

Vorgelegt von

M.Sc. Mathias Quilitzsch
geboren 1984 in Essen

Essen 2015

Acknowledgements

First of all, I would like to thank Prof. Dr. Mathias Ulbricht for giving me the opportunity to work on this topic. Through all the years in his workgroup I was always grateful for his trust in me and for giving good advice.

I would also like to thank Prof. Dr. -Ing. Stefan Panglisch for his efforts as a co-referent for this work.

I really enjoyed the valuable discussion with all the members of the Technical Chemistry II workgroup in Essen. Especially Anne Vaterrodt, Marc Birkner, Thomas Knoche, Thorsten Pieper and Thorsten van den Berg gave additional impulse to the process of this work. Thanks to the students who worked with me, namely Hanna Thierfeld, Yunfeng Lao and Stephanie van Stiphout and Dominik Drescher. Also the technical and administrative assistance by Inge Danielzik, Tobias Kallweit, Roswitha Nordmann-Silberg and Claudia Schenk is gratefully acknowledged.

I like to thank the German ministry for science and education (BMBF) for funding this project. Also, I appreciate the contribution and valuable input of the project partners in Germany and Israel. Prof. Dr. Viacheslav Freger and Dr. Maria Bass from Technion in Israel for the SIMS-mapping. Prof. Dr. Moshe Herzberg and Eli Asa from Ben Gurion University of the Negev for the QCM measurements and for the warm welcome during my short stay at the Sede Boker campus. Dr. Martin Heijnen, Dr. Michaela Krug and Jinjin Guo from Inge GmbH for providing all sorts of membrane modules and hollow fibres and for the support and opportunity to use the Poseidon filtration unit. Dr. Edoardo Menozzi, BASF for providing the flat sheet membranes.

Furthermore, I like to thank the technical and scientific staff of the different institutes of our university, who contributed with many different measurements – Especially Smail Boukercha for the SEM images, Dr. Ulrich Hagemann for the XPS measurements and Klaus Pärschke for the ellipsometry measurements.

Last but not least, I like to thank my family and especially my wife Polina for believing in me and supporting me all the time. Without you, guys, I would not have been that focused to finish this task.

The work presented here was performed from January 2011 till May 2015 at the Lehrstuhl für Technische Chemie II of the University of Duisburg-Essen and supervised by Prof. Dr. M. Ulbricht.

Disputation: Essen 19.01.2016

Referents: Prof. Dr. M. Ulbricht

Prof. Dr. -Ing. S. Panglisch

Chairman: Prof. Dr. T. Schmidt

I declare that this dissertation represents my own work, except where it is stated by acknowledgements and references. I only used the materials and references named and this work was not submitted to any other university before.

Essen, Sept. 2015

Mathias Quilitzsch

Content

Abstract

Fouling is a major challenge when applying ultrafiltration in water treatment. Membrane grafting is a long known possibility to increase the inherent fouling resistance of polymeric ultrafiltration membranes. On the other hand, many available techniques are not widely established, because they either strongly influence the membrane performance or are not easy to apply and thus not feasible. The aim of the work presented here, was to establish a new grafting technique that is surface selective and easy to apply in ready to use membrane modules. This goal was to be achieved via a new macromolecular initiator that is adsorbed to the membrane selective layer in a first step. Due to its high molecular weight, the initiator is completely rejected by the membrane. In the second step, the initiator activity is used to graft a zwitterionic hydrogel on the membrane surface. A copolymer of butyl methacrylate as adhesive group and N,N-dimethylaminoethyl methacrylate as redox co-initiator was synthesized with varying ratios of both monomers. A thermal macroinitiator was synthesized by modifying a commercial poly styrene-co-maleic anhydride copolymer with a new azo functional group as well as the organic hydroperoxides cumyl- and tert. butyl hydroperoxide. The initiator systems were characterized regarding their behaviour in solvent mixtures by measurements of critical water content and critical micelle concentration. The adsorptive behaviour to polyethersulfone (PES) model surfaces was surveyed via surface plasmon resonance, quartz crystal microbalance and ellipsometry. Suitable conditions leading to a strongly adsorbed monolayer were found for all systems. The initiator activity was surveyed by in situ rheology. A high activity was found for the redox co-initiator system. No activity was found for the azo modified copolymer, while the hydroperoxide based thermal initiators showed a good performance at 65 °C. Zwitterionic [3-(methacryloylamino) propyl] dimethyl (3-sulfopropyl) ammonium hydroxide (SPP) was used as the monomer for membrane modification and N,N´-methylenebis(acrylamide) (MBAA) was used as a cross-linker. It could be proven that both initiator systems are generally suitable for surface selective membrane modification. Since the redox co-initiator caused less unspecific polymerization in the membrane support, this system was used for further studies focusing on membrane performance. The effect of grafting on the membrane surface chemistry was surveyed on PES flat sheet membranes using contact angle, zeta potential, X-ray photospectroscopy and SIMS-mapping. It was found that the modification leads to a more neutral surface charge and higher hydrophilicity. Changes in the elemental composition of the surface indicated that these changes are correlated to successful surface modification.

Fouling tests were performed using Inge Multibore® PES capillary membranes as well as flat sheet samples produced by BASF with similar properties like the Multibore®. The capillaries were potted in filtration modules of different sizes. Fouling tests with bovine serum albumin revealed an increased resistance towards protein fouling in static adsorption tests and during filtration. Tests with extracts from membrane bioreactors (EPS and SMP) showed an increased fouling resistance for the modified membranes. Filtration tests with flower soil extract showed improved anti fouling properties and an increase in TOC rejection due to the modification. Furthermore a good chemical and mechanical stability of the grafting layer could be proven by multiple tests applying or simulating chemical enhanced back wash procedures. Finally the modification was applied in pilot scale modules which are currently surveyed in a long term test.

The developed macromolecular redox co-initiator is well applicable and can be optimized for other membrane types and materials in future work. Also it may be used to graft other polymers on membranes to further improve fouling resistance or other desired properties like MWCO or biocompatibility. Especially the good applicability in membrane modules and the high stability of the grafted layers are expected to make the presented method a versatile and feasible alternative for established techniques. Future work should focus on optimization of the grafting conditions and evaluation of other hydrogel systems to improve the benefits of the grafting.

List of figures

List of abbreviations

AAMPSA	2-Acrylamido-2-methyl-1-propanesulfonic acid
AATAC	(3-Acrylamidopropyl) trimethylammonium chloride
ACN	Acetonitrile
APS	Ammoniumpersulfate
BMA	Butylmethacrylate
CA	contact angle
CEB	chemical enhanced backwash
CF	cross flow
CMC	critical micelle concentration
CP	concentration polarization
CWC	critical water content
DC	degree of cross-linking
DE	dead end
DMAc	N,N-dimethylacetamide
DMAEMA	2-(dimethylamino)ethylmethacrylate
DMF	Dimethylformamide
DMSO	Dimethylsulfoxide
DOM	Dissolved organic matter
EDX	Energy dispersive X-ray
EPS	Extracellular polymeric substances
FR	Fouling resistance
IC	Inorganic carbon
IEP	Isoelectric point
MA	Maleic anhydride
MBAA	N,N′-methylenebis(acrylamide)
MBR	Membrane bioreactor
MF	Microfiltration
MW	Molecular weight
MWCO	Molecular weight cut-off
NF	Nanofiltration
NOM	Natrual organic matter
PBS	Phosphate buffered saline
PDI	Poly dispersity index
PES	Polyethersulfone
PF	Plate and frame
PMMA	Polymethyl methacrylate
PMVE	Poly(vinyl methyl ether)
pSMA	Poly styrene-co-maleic anhydride
PTFE	Polytetrafluoroethylene
PVP	Poly(vinyl pyrrolidone)
Q	Degree of swelling
QCM	Quartz crystal microbalance
RI	Refractive index
SEC	Size exclusion chromatography

SEM	Scanning electron microscopy
SIMS	Secondary ion mass scpectroscopy
SMP	Soluble microbial products
SPP	[3-(Methacryloylamino)propyl]dimethyl(3-sulfopropyl)ammonium hydroxide
TMED	N,N,N,N-tetramethylethylene diamine
TMP	Transmembrane pressure
UF	Ultrafiltration
XPS	X-ray photoelectron spectroscopy
ZP	Zeta potential

List of symbols

$\|R^P\|$	Amplitude difference between incoming and outgoing wave in parallel plane
$\|R^S\|$	Amplitude difference between incoming and outgoing wave in perpendicular plane
A	Surface area, cross section
c_{feed}	Feed concentration
c_{perm}	Permeate concentration
C_{QCM}	Sensor material constant
d	Layer thickness, pipe diameter
Jc_i	Flux through the membrane
K_{ev}	Wave vector of the evanescent field
K_{sp}	Wave vector of the surface plasmon
L	Length
Lp	Permeability
Lp_0	Permeability before fouling
Lp_{after}	Permeability after fouling
m_{dry}	Weight in dry state
m_{perm}	Permeated mass
$m_{swollen}$	Weight in swollen state
n_{QCM}	Overtone number
p_{avg}	Average TMP
Q	Degree of swelling
R	Rejection
Re	Reynolds number
R_f	Fouling resistance
r_g	Radius of gyration of a geometric chain
r_r	Radius of gyration of a real chain
t	Time
TOC_{feed}	Total organic carbon in feed

TOC_{perm}	Total organic carbon in permeate
u	average fluid velocity
w_o	Frequency of incident light
Δ	Phase parameter in ellipsometry
δ_1	Phase difference between components of incoming light
δ_2	Phase difference between components of outgoing light
Δf	Frequency change
ΔI	Changes in streaming current
Δm	Adsorbed mass
Δp	Pressure difference
ΔU	Changes in streaming potential
ε_0	Vacuum permittivity
ε_m	Dielectric constant of the gold film
ε_r	Relative liquid permittivity
ζ	Zeta potential
η	Viscosity
η_g	Refractive index of the glass half cylinder
θ	Angle of incidence
ν	kinematic viscosity
ρ	Complex ratio of total reflection coefficients
Ψ	Amplitude parameter in ellipsometry

1 Introduction

Membranes and membrane processes have developed to an important separation technique. Nowadays, besides the medical applications like blood oxygenators and hemodialysis, membrane processes are widely used in many technical applications[1]. The key advantages of membrane based separation processes over conventional techniques are the lower footprint and energy consumption. Also membrane filtration processes feature an easy scale up by simply increasing the membrane surface area[2]. The major drawback for pressure driven membrane processes is flux decline due to concentration polarization (CP) and membrane fouling. Therefore, in the past decades, many publications have been dealing with strategies to overcome membrane fouling and CP[3]. The industrially established membrane processes for liquid separations can be ordered into different groups according to their rejection characteristics. Microfiltration (MF) is closest to conventional filtration; typical MF membranes reject particles and bacteria in a range from 0.1 to 10 µm. Ultrafiltration (UF) membranes feature pore sizes of 2-100 nm and reject viruses and bacteria but also large macromolecules like many proteins. Reverse osmosis (RO) membranes comprise nominal pore sizes below 0.8 nm. Even though the RO process is still a pressure driven filtration process, the actual separation is more a matter of solubility in the membrane material than of molecular weight. These membranes can remove ions and are used for desalination[1]. Nanofiltration (NF) is a special technique in the border area between UF and RO[4].

UF membranes are widely used for water purification[5], but also in the dairy industry[6] and in the highly profitable biotechnology[7]. UF membranes can be used to remove bacteria and viruses, as well as part of the natural organic matter (NOM) dissolved in surface water[8]. The NOM is the main organic component of surface and ground water. It is composed of substances ranging from macromolecules to low molecular weight molecules. The main fraction of one third to one half of the total organic carbon (TOC) in surface water is formed by humic substances. These are typically polymeric anions containing multiple functional groups in a network of aromatic rings[9]. NF would be capable of directly removing NOM from water, but due to the high energy consumption of NF, a combination of flocculation and MF or UF is usually more energy efficient for NOM removal[8].

A special application for UF membranes in water treatment is the integration in a membrane bioreactor (MBR). A MBR combines the steps of biological treatment and filtration in a single setup. In an aerated tank flocculated biofilms are degrading pollutants in waste water. Fresh water can be extracted from this vessel via UF or MF membranes either directly from the tank (submerged configuration) or in an additional filtration circuit (side-stream configuration)[10]. The

key benefits are the significantly lower footprint of the system combined with the high effluent quality and disinfection capability. Also the sludge production is reduced compared to conventional treatment[11]. Due to the complex nature of the flocculated biomass and feed water composition in MBRs, fouling is not yet fully understood in these systems. However, extracellular polymeric substances (EPS) and soluble microbial products (SMP) are often discussed as main foulants[12].

Typical UF membranes are anisotropic membranes, comprising a thin selective layer over a porous support. Due to its good physico-chemical, mechanical and hydraulic stability, polyethersulfone (PES) is one of the most common materials for fabrication of UF membranes. The main drawback of the material regarding membrane fouling is its hydrophobicity[13]. The hydrophobicity is long known to be an important factor influencing fouling and flux decline during UF[14].

This work was settled in a cooperation project (GelMem, BMBF grant 02WA1261A) between two workgroups in Israel (Moshe Herzberg, Ben Gurion University of the Negev and Viatcheslav Freger, Technion – Israel Institute of Technology), the University Duisburg-Essen and Inge/BASF in Germany. The scope was to modify PES capillary UF membranes manufactured by Inge creating a new UF membrane with improved performance (i.e. fouling resistance and rejection) for application in surface and waste water treatment. Furthermore, the applicability for treatment of MBR effluents was investigated in the project. The main goal of this thesis was to develop a new surface grafting technique which is applicable in ready to use membrane modules. By decoupling the grafting step from the membrane fabrication, the feasibility of the process was meant to be increased. The developed method also had to be surface selective to avoid undesired grafting in the membrane support and thus minimize performance loss. The approach to achieve surface selectivity was to use a surface active macromolecule that is adsorbed to the membrane surface in a first step and then acted as an initiator in the subsequent membrane grafting process.

2 Theoretical Background

2.1 Ultrafiltration

Ultrafiltration uses membranes with typical pore sizes of 2-100 nm. It thus covers the separation range between RO and MF and can typically reject materials like viruses and bacteria[1]. Figure 2-1 shows the typical characteristics of these filtration processes in comparison to conventional filtration.

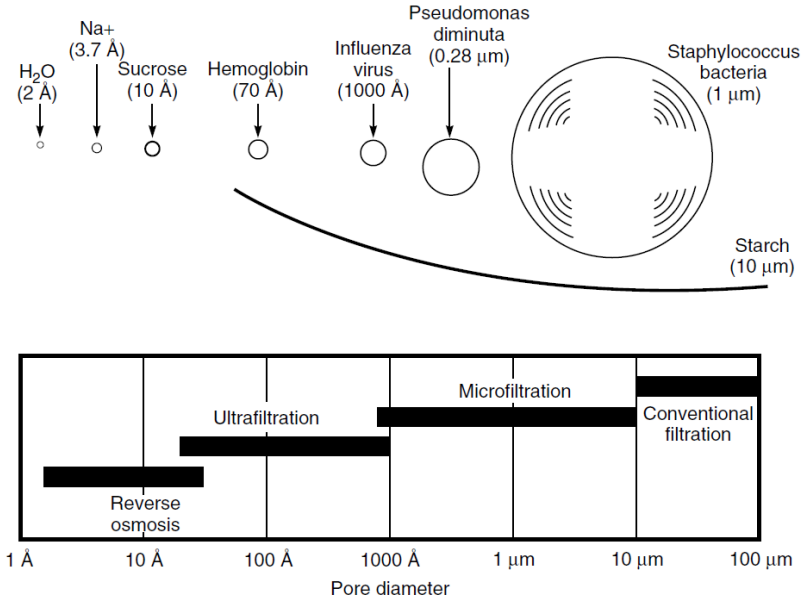

Figure 2-1 Characterization of separation processes regarding their pore diameter and typically rejected materials[1].

Nitro cellulose based UF membranes have already been available in the 1920, but the first membranes capable of large scale application were the Loeb-Sourirajan type anisotropic membranes. Due to their anisotropic structure of a filtration layer with fine pores on a more porous sublayer, these membranes can achieve higher fluxes at similar rejection compared to isotropic membrane filters. Therefore UF membranes are usually screen filters where the rejection takes part on the membrane surface, while MF membranes are either screen or depth filters[1]. The main challenges for UF membranes are flux decline due to membrane fouling and the resulting need for intensified cleaning and hence reduced membrane lifetime and higher cost. The different effects and strategies to cope with membrane fouling are discussed in the following sections.

2.2 Flux decline in membrane processes

Generally membrane filtrations can either be performed in dead-end (DE) or cross-flow (CF) mode (Figure 2-2):

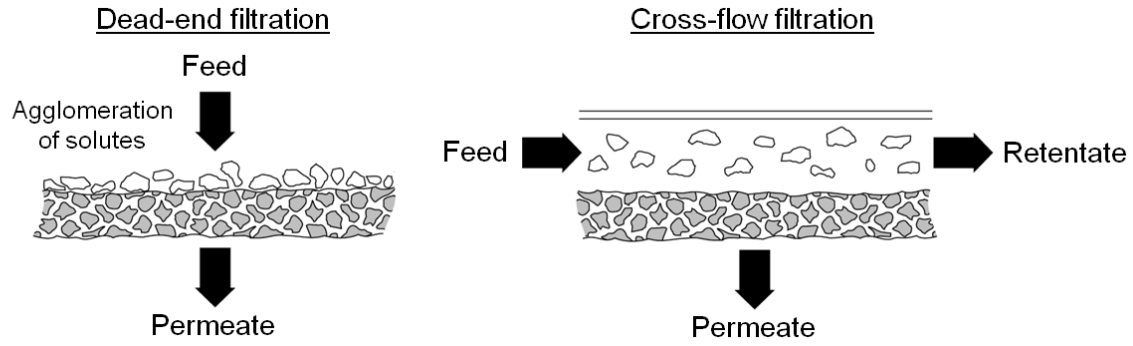

Figure 2-2 Principle of dead-end (left) and cross-flow (right) operation modes[1].

In DE filtration, the concentration of solutes on the feed side of the membrane constantly increases. In CF mode, the feed solution is passed across the membrane surface and concentrate is constantly transported from the feed side. Thus a steady state concentration can be achieved. Usually UF membranes feature a quite high pure water flux, but decline in flux when solutes are rejected by the membrane[1]. In most cases, three different stages of flux development can be observed during UF:

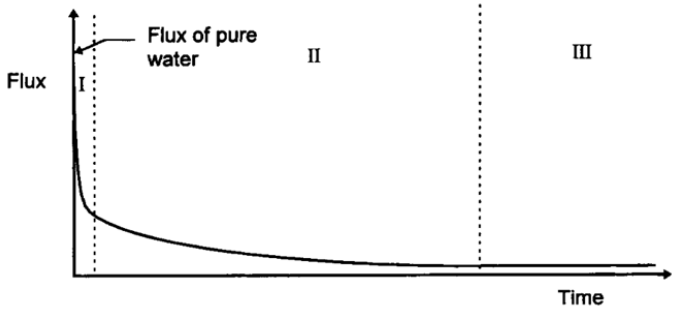

Figure 2-3 Three stages of flux development during UF and MF; I: rapid flux decline at the beginning, II: long term gradual decrease, III: steady state flux[15].

In stage I the flux drops rapidly from the initial water flux. Stage II can be observed in all UF processes. Here the flux decreases slowly, often over weeks. Stage III characterizes steady state flux where no flux decline is observed[15]. The flux decline can be attributed to CP or membrane fouling increasing the membrane resistance or decreasing the driving force through the membrane. CP is reversible[16]. Fouling effects, leading to an increased membrane resistance can be divided into three different kinds of fouling: pore narrowing, blocking of pores and cake layer formation which leads to an additional resistant layer on top of the membrane[15]. Physical cleaning is usually not sufficient to neutralize fouling effects caused by the blocking of

pores. Therefore chemical cleaning steps are often necessary. Since the chemical cleaning reduces the membrane lifetime, its application should be reduced to a minimum[17, 18]. For the named reasons, membrane fouling is considered one of the major challenges in UF[19, 20].

2.2.1 Concentration polarization

Concentration polarization is one of the main limiting factors for high flux UF membranes[21]. Generally, when a solution containing different components is separated by filtration, one of the components will be concentrated on the feed side. This will form a boundary layer with increasing concentration of one component towards the membrane separation layer (Figure 2-4):

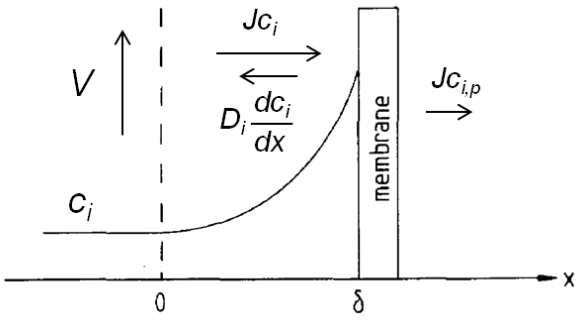

Figure 2-4 Schematic representation of the phenomenon of CP in a cross-flow system, with the boundary layer thickness *δ*, cross-flow velocity *V*, and concentration of component *i* in dependence of longitudinal position *x*[1, 22].

The mass transport in this boundary layer can be described in Eq. 1 as a simple mass balance between the solute flux towards the membrane (Jc_i) and back transport via diffusion described by Fick´s law ($D_i \frac{dc_i}{dx}$):

$$Jc_{i,p} = Jc_i - D_i \frac{dc_i}{dx} \quad (1)$$

The concentration gradient as a driving force is only present in the boundary layer. Therefore the effect of CP is strongly dependant on the boundary layer thickness. As a result, the easiest way to reduce the amount of CP is to increase turbulent mixing on the feed side and thus reduce the size of the boundary layer[1]. CP is reversible but it can facilitate adsorption processes and thus irreversible fouling[23]. Besides increasing the membranes resistance and hence the energy demand, the effect of CP also reduces the rejection for certain solutes. This is due to the increased concentration of solute on the feed side of the membrane which causes a larger driving force for the solute to permeate through the separation layer[24].

2.2.2 Membrane fouling

CP usually leads to precipitation and/or adsorption of rejected macromolecules on the membrane surface or inside the membrane pores. In this case membrane fouling occurs. Generally two different modes of fouling can be distinguished, depending on the size of solutes compared to the membranes pore size (Figure 2-5).

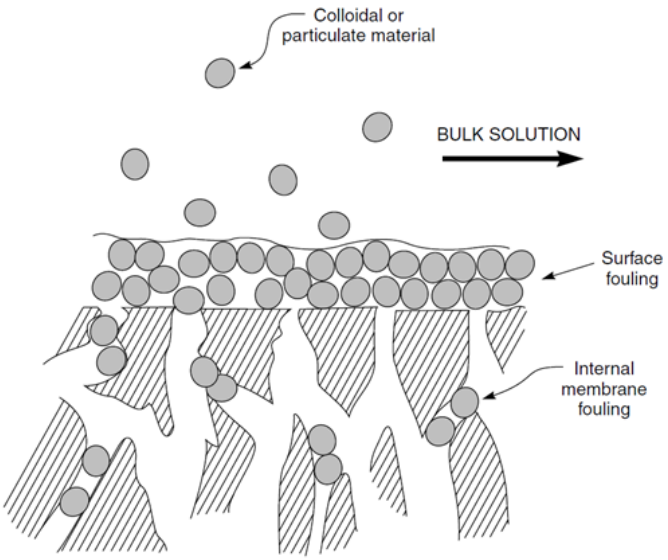

Figure 2-5 Schematic representation of different fouling modes in UF[1].

When the solutes are large enough to be rejected by the membrane, surface fouling occurs. A cake layer is formed on the membrane surface and causes an increase of its hydraulic resistance. The second mode occurs when the solute size is comparable to the membranes pore size. In this case internal fouling occurs inside the pores. This pore plugging is usually irreversible by physical methods and can only be removed by chemical cleaning[1].

In practice it is often difficult to investigate membrane fouling under similar conditions in laboratory experiments and in practical application. The main reason is that most laboratory studies operate at constant pressure, while technical applications usually use a constant flux operation mode[25].

In the following section the different types of membrane fouling are discussed.

Organic fouling

Due to the complex nature of natural feed solutions and especially the composition of dissolved organic matter (DOM) in these solutions, organic fouling is not yet fully understood. The main components believed to be responsible for organic fouling during UF water treatment are proteins, humic substances and polysaccharides[26]. The hydrophobic humic substances

generally represent the largest part of DOM in surface water[27]. They are known to cause severe membrane fouling during UF, especially in the presence of bivalent metal ions. Also the membrane hydrophilicity can be significantly reduced, making it prone to subsequent fouling[28, 29].

Soluble microbial products (SMP) and extracellular polymeric substances (EPS) are believed to be the main fouling components in MBRs[30]. Both EPS and SMP are comprised of microbially produced organic substances but are not living cells. EPS generally consist of polysaccharides, proteins and nucleic acids, but due to the complex composition a detailed analysis is often difficult. The EPS are forming the matrix of biofilms and adhere them to surfaces[31]. For this reason, an EPS resistant surface may also be more resistant towards biofouling. SMP consist of soluble cellular components either released during cell lysis or being excreted by living cells[32].

Particle fouling

Especially in MBRs the loading with suspended solids is often very high. Fouling by particles can therefore have an important influence on the filtration process. The interplay of particle size, membrane structure and filtration conditions is very important for this type of fouling[33]. Also electrostatic interactions are very important for colloidal fouling. The formation of electrostatic double layers prevents particles from coagulation by increasing the repulsion between particles[34]. A charged membrane surface can similarly reduce the extend of membrane fouling by creating an electrostatic repulsion towards particles bearing a negative charge[1]. The discussed electrostatic interactions are strongly influenced by the electrolyte concentration in the feed solution, since higher electrolyte concentrations reduce the electrostatic repulsion[34].

Biofouling

In all water treating membrane processes, biofouling is a concern[35]. Biofouling in general describes the growth of microorganisms on surfaces. In contrast to other fouling mechanisms, the foulant is a living organism so that reducing the amount of foulant (i.e. bacteria) in the feed solution will not necessarily reduce the amount of biofouling[36]. Biofouling generally occurs after a first layer of the substances responsible for organic fouling is adsorbed on the membrane surface[37]. In all laboratory scale experiments presented in this work, NaN_3 was used as an inhibitor to prevent biological growth and avoid biofouling. However biofouling can be a concern in the long term testing of pilot modules.

Scaling

Briefly, this type of fouling occurs when the feed water contains a high load of inorganic salts which are rejected by the membrane. Due to the CP, their solubility is exceeded and the salts

precipitate on the membrane surface[38]. Since the used UF membranes in this work have no selectivity towards inorganic salts, problems due to scaling are not of concern.

2.3 Strategies to overcome membrane fouling

Different strategies can be employed to overcome membrane fouling and concentration polarization. The influencing factors are illustrated in Figure 2-6.

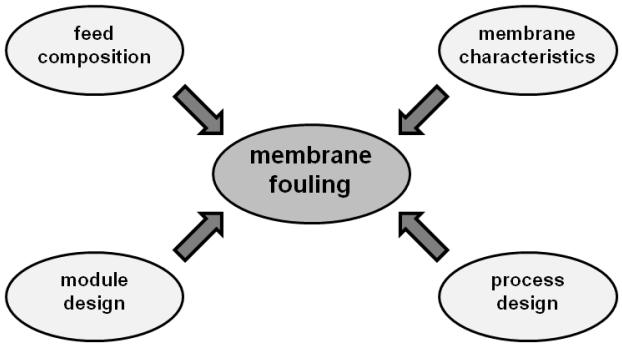

Figure 2-6 Strategies to overcome membrane fouling.

Generally, the factors affecting flux decline in membranes can be allocated to either the operation conditions (i.e. dead-end vs. cross-flow, back flushing etc.), the module design (i.e. hydrodynamic conditions due to spacer design, module type), feed composition (i.e. foulants, pH) or the membrane characteristics (i.e. molecular weight cut-off, hydrophilicity)[3]. In the following section, the different factors are discussed in detail.

2.3.1 Influence of process design

Changing the filtration process from dead-end to cross-flow mode will strongly influence the membrane performance. In cross-flow filtration of protein solutions, the cross-flow velocity has been shown to have significant influence on the CP and hence on fouling and filtration performance[39]. Due to the need of higher pump rates in cross-flow operation, it is usually more costly than dead-end filtration.

The concept of a critical flux is of great importance for the process design in membrane filtration processes. The critical flux marks the permeate flux rate at which the repulsion between solutes or particles is overcome. This leads to aggregation at the surface. Below the critical flux no fouling occurs[40]. Field et al. described two different types of critical flux in microfiltration[41].

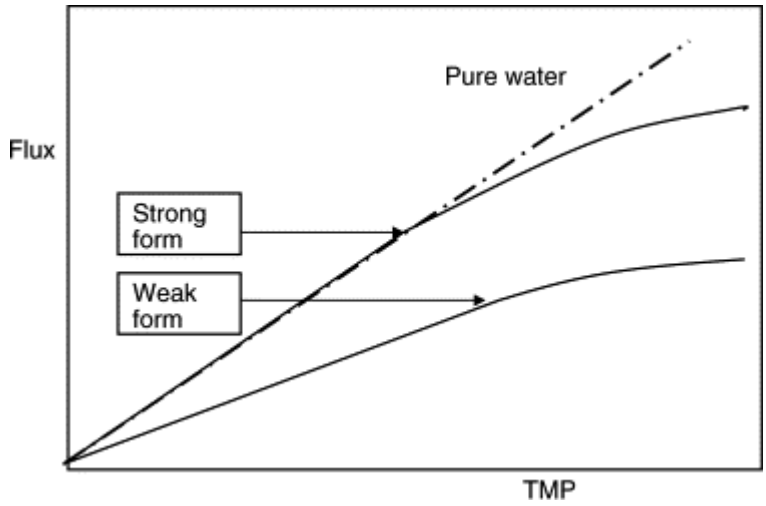

Figure 2-7 Strong and weak form of critical flux concept[40, 41].

The pure water flux vs. transmembrane pressure (TMP) is used as a reference. The strong form of critical flux is characterized by the point where the flux curve of a solution deviates from the pure water line. In case of rapid fouling the curve can also be lower from the start. In these cases a weak form of critical flux is observed. This critical flux is determined as the point where the flux curve deviates from linear behaviour[40]. The form and extend of the critical flux are depending on the feed composition as well as on membrane pore size and porosity[42]. It is therefore important to adjust the filtration conditions of each separation problem carefully to the given conditions.

Especially in DE mode, the permeate flux is important for the hydraulic resistance of the fouling layer[25]. A very interesting approach for point of use drinking water production uses the fact that a forming biofilm maintains open flow channels and thus prevents membrane fouling at ultra low fluxes. According to this approach steady state DE filtration of surface water can be carried out for 50 days without need of any membrane cleaning steps[43].

2.3.2 Membrane characteristics

Membrane characteristics like porosity and pore size but also the chemical properties of the material can have a vast influence on the fouling behaviour:

An obvious characteristic of a membrane is its pore size and resulting permeability and rejection. Varying the pore size of the used membranes is known to influence the filtration performance especially in complex feed solutions with many different solute and particle sizes like in an MBR[33].

The hydrophilicity of the membrane can be modified by blending the membrane polymer. In recent studies, improved antifouling properties combined with high permeability and low MWCO

could be achieved by blending the base polymer with surface tailored nanoparticles[44] or novel block copolymers[45]. A broadly applied measure to increase membrane hydrophilicity is the blending of the hydrophobic base polymer with water soluble polymeric additives like poly(vinyl pyrrolidone) (PVP)[46]. Most of the polymer is leached out from the membrane, but usually a sufficient amount remains and increases the hydrophilicity.

Besides hydrophilicity, surface charge can also govern anti fouling properties. Since colloids often bear a negative charge, a slight negative charge of the membrane surface can help to avoid membrane fouling by particles[1] (cf. Particle fouling, page 7).

2.3.3 Feed composition

The feed composition is of great importance for the fouling behaviour. Obviously the nature (molecular weight, hydrophilicity, particle size) of substances which are present in the feed will have a large influence on the fouling. These can be changed to some extend by feed pretreatment. The most common feed pretreatment in UF is flocculation. A flocculation pretreatment can effectively increase the rejection of NOM and in addition significantly reduce membrane fouling[47, 48]. Another pretreatment is preoxidation with gaseous or liquid oxidizing agents. Besides the reduction of organic fouling, this technique is also capable of reducing biofouling by suppressing bacterial growth. The main drawback is the aggressiveness usually also damaging polymeric membranes[49].

The addition of granular polyethylene glycol (PEG) particles in an MBR has been shown to suppress reversible fouling of the used MF membranes[50]. On the other hand, the absence of a reversible fouling layer was found to promote irreversible fouling[50].

2.3.4 Module design

Another important factor, influencing the membrane fouling is the type and geometry of membrane modules. Tubular and plate and frame (PF) modules can be used for feed solutions with a very high fouling propensity. Tubular modules offer a high fouling resistance at the cost of higher energy consumption. PF modules are less fouling resistant than tubular modules, but also cheaper to manufacture. Capillary modules feature the advantage of a high packing density and thus high membrane surface area per module. Other than PF and tubular modules, capillary modules can be cleaned by back flushing. On the other hand, high loads of particles should be avoided to prevent blinding of the membrane by plugging the entrance of single capillaries. Spiral wound modules contain a large sheet of membranes rolled and separated by spacers. In these modules, the spacer design is known to strongly influence fouling[1]. It has

been shown that new geometries like zig zag shaped[51] or helically microstructured feed spacers[52] can significantly change the filtration performance.

2.4 Membrane modification

As discussed in Chapter 2.3.2, the membrane characteristics can strongly influence the fouling behaviour. Blending of the membrane base polymer however also changes the membranes overall properties. Besides the filtration behaviour, also properties like mechanical strength and chemical resistance will be influenced[53, 54]. Therefore a more elegant way is the modification of an established membrane in a way that does not reduce mechanical strength and chemical resistance.

Thin film composite UF membranes with new properties can be prepared by coating thin (< 1 µm) polymer films on a porous support[55]. Internal fouling is completely avoided in such membranes due to the nonporous nature of the selective layer. The main draw-back however is the low permeability[56].

A very promising and often applied way is the modification with hydrogels or brushes of hydrophilic polymers. Due to their hydrophilic nature, the tendency for unspecific adsorption of feed components and hence fouling is significantly decreased[57]. Known chemical factors increasing resistance towards protein adsorption and hence organic fouling are[58]:

- High hydrophilicity
- H-bond acceptor but not donor groups
- No net charge

Polyethylene glycol (PEG) derivatives meet these requirements and are long known for their good resistance to protein fouling[59]. The main drawback of PEG based modifications is its relatively low chemical stability[60]. Grafting with more stable zwitterionic sulfobetaine derivatives is reported to also feature good anti fouling properties at a much higher chemical stability[61]. They have been shown to strongly decrease protein adsorption and cell adhesion[62].

Besides the chemical properties, it has been found that a high swelling degree of hydrogel coatings can lead to a kind of physical “dilution” of the surface[63]. In that study it has been shown that highly swollen hydrogels can significantly reduce the amount of bacterial attachment to polymeric membranes.

Besides a mere increase in fouling resistance, hydrogel grafting can also be employed to create stimuli responsive membranes[64, 65].

Grafting techniques can be classified either as grafting-from or grafting-to. In case of grafting-to techniques, a functional polymer is immobilized on the polymer surface. In grafting-from techniques, chain growth starts at the membrane surface and a functional polymer is synthesized from the surface. Grafting-from techniques generally feature higher grafting densities, since only the monomers need to diffuse to the surface[57].

Different techniques for radical initiated grafting of monomers on membrane surfaces can be employed. Radicals at the surface can be generated by plasma treatment, UV or electron beam irradiation, or by chemical reactions.

One often applied method uses the inherent capability of PES to absorb UV light and form radicals upon UV irradiation[66, 67]. The main advantage is the simplicity of the process, since no additional radical starter is needed. Furthermore, the method is surface selective due to the low penetration depth of UV light. However, the conditions have to be carefully chosen, since too high UV doses can damage the base membrane and thus decrease rejection[66].

Plasma induced grafting is a possible technique for surface modification of PES membranes. Plasma treatment can directly be applied to increase the surface hydrophilicity of the membrane by partial oxidation. Since this effect is only temporary due to reorientation effects[68], more permanent approaches use plasma treatment for radical creation and subsequent grafting of hydrogels[69]. The approach has even been used to graft outside-in hollow fibre membranes[70]. A wide variety of monomers can be grafted onto PES membranes by plasma treatment. Also zwitterionic monomers like the system used in this study can be grafted by plasma treatment. The so created membranes have been shown to feature significantly increased anti fouling properties[71]. The cited studies were all performed under vacuum conditions. Even though possibilities for polymer treatment under atmospheric plasma conditions exist[72], the main drawback for large scale application is the need of complex equipment.

Another irradiation based technique uses electron beams to generate surface radicals for subsequent grafting. The method can be used to graft different polymers on the membrane surface and is very surface selective. The main drawback is an electron beam induced cross-linking of the polymer accompanying the grafting procedure and leading to different mechanical properties[73].

Besides the irradiation based techniques, surface initiated atom transfer radical polymerization (SI-ATRP) is an interesting technique for membrane grafting. The technique is independent of external energy sources and allows a good control over the length of grafted polymer brushes. The latter is interesting especially when preparing stimuli responsive membranes[74]. Also precise tuning of the membranes MWCO is possible by ATRP[75]. The main drawback is the lack

of surface selectivity, since generally an ATRP initiator needs to be adsorbed or incorporated into the membrane first and these are usually small molecules. ATRP has also been used to graft a zwitterionic methacrylate, very similar to the SPP used in this study onto a polysulfone membrane[76]. Also the use of polycationic ATRP macro initiators has been reported as a versatile way to apply ATRP on PES substrates[77]. Another study reported the use of macromolecular photoinitiators for UV initiated coating of membrane surfaces with hydrogels[78]. The key factor in the latter two cases is the surface activity of the macromolecular initiators. This will be discussed in detail in the following chapter.

2.5 Surfactants at interfaces

Surfactants are surface active substances consisting of hydrophilic and hydrophobic parts. When immersed in water they have a strong driving force towards the air-water interface, arising from the strong hydrogen bonding of surrounding water molecules. The orientation in a monolayer at the surface is therefore a spontaneous effect. At concentrations above the critical micelle concentration (CMC), the surfactant molecules are aggregating with other surfactant molecules to form micelles. At concentrations above the CMC, the system is in equilibrium between a saturated surfactant monolayer at the surface, a few free surfactant molecules and the micelles. Due to the dynamic nature of micelles and the rapid interchange of molecules between micelles and solution, the concentration of unassociated molecules remains almost constant when increasing the concentration above the CMC. The CMC is largely affected by the length of the hydrocarbon chain in case of straight single chain surfactants. Branching usually leads to higher CMC at similar number of carbon atoms. Benzene rings in the chain reduce the CMC less than six CH_2 groups would[79].

The adsorption efficiency of the surfactant to the surface is correlated to the free energy changes of the individual groups in the surfactant. For example in straight-chain surfactants in water of the type $CH_3(CH_2)_n$-M (M as the hydrophilic head group), the adsorption efficiency is directly correlated with the chain length of the hydrophobic group. Other factors favouring efficient adsorption are[80]:

- Straight hydrophobic groups rather than branched (containing the same number of C atoms)
- Single hydrophilic group at the end of a hydrophobic group rather than one or more at a central position (head-tail structure)
- No net charge in the hydrophilic group

For ionic head groups the efficiency can be increased by either increasing the ionic strength in the solvent or exchanging the counter ion for a less hydrated one[80].

Besides the typical low molecular weight surfactants, macromolecular surfactants are a field of growing interest. This class of polymers contains all sorts of amphiphilic polymers. Due to the larger size of polymeric surfactants, their structure can have a much broader influence on their behaviour. According to their structure, macromolecular surfactants are separated in two sub classes. Macrosurfactants are a class of polymers in which the hydrophilic and hydrophobic part are well separated. Typical representatives of this class are block copolymers, comprising hydrophilic and hydrophobic blocks. The second class, to which also the macromolecular initiators in this work belong, are the polysoaps. Here the hydrophobic and hydrophilic parts are distributed along the polymer backbone[81]. Possible structures of representatives of the two classes are shown in Figure 2-8.

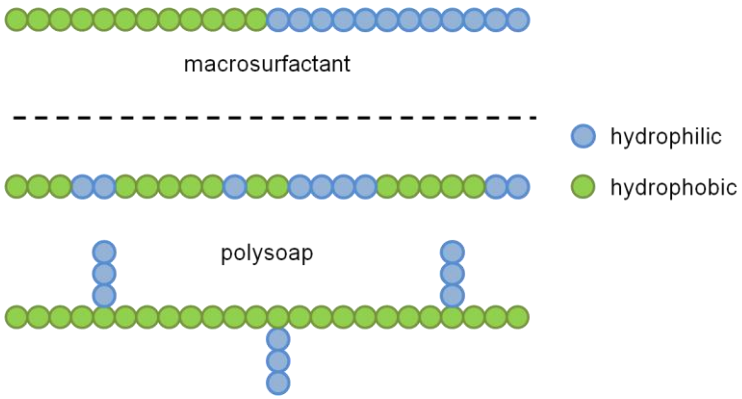

Figure 2-8 Possible structures for macrosurfactants and polysoaps.

Besides these two classes, more complex structures like branched copolymers can also be synthesized[81].

While macromolecular surfactants have most properties in common with their low molecular weight counterparts, several additional properties can be added by changing their structure and molecular weight. Especially in the class of well ordered macrosurfactants fine tuning can be used to create self-assembling structures[81]. Such self-assembly in micelles can be much stronger than the adsorption to hydrophobic surfaces. In cases, where the hydrophobic block is highly hydrophobic, the micelles are kinetically “frozen” and no exchange between unimers and micelles occurs. This is typically the case for CMCs $< 10^{-4}$ wt %[82]. In case of weakly hydrophobic diblocks the adsorption is much faster due to the lower stability of the micelles. This is typically the case for CMCs in a range of ~1 – 5 wt %[82]. Micelles do not adsorb directly, but the adsorbing species is the unimer, which is in equilibrium with the micelles on the other hand[83]. The properties of block copolymers can be tuned in ways that allow their arrangement into surface micelles rather than homogenous monolayers. Thus nanostructured surfaces can be created by self-assembly on the substrate. Random copolymers on the other hand always

feature a homogenous distribution on the macroscopic level, since their functional groups are randomly distributed along the polymer backbone[84].

In 1989 a study has surveyed the use of different polyethylene oxide (PEO), polypropylene oxide (PPO) and polybutylene oxide (PBO) block copolymer surfactants to cover hydrophobic polymer surfaces and reduce protein adsorption[85]. However, the stability of such systems has been doubted by the authors, since proteins could displace the surfactant from the surface. More recent works in the field of low fouling UF membrane preparation are focussed on the self-assembling properties of PEO-b-PPO and PEO-b-PBO block copolymers[86, 87]. In the named studies, the block copolymers are added directly to the membrane dope solution. During the phase separation process the block copolymer assembles at the polymer water interface and thus makes the produced membrane more hydrophilic[86].

2.5.1 Macromolecular initiators

Different approaches exist, where a polyionic macromolecular initiator is used for surface modification of nonporous materials[77, 88]. Also for the modification of NF membranes, the use of a macromolecular photo initiator has been reported[89].The concept uses the macromolecules stronger interaction and thus higher driving force for adsorption compared to low molecular weight compounds.

Macromolecules containing thermally cleavable azo side groups as radical starters are long known as precursors for graft copolymers[90]. Such polymers can be achieved via free radical co-polymerization of azo group containing monomers with other monomers[91]. Polymers, containing peroxide groups, are another long known possibility for synthesis of graft or block co-polymers depending on whether the peroxide bond is located in the main chain or in the backbone[92].

In 1999 Anders et al.[93] have presented a thermal grafting method for surface modification with hydrogels, based on different types of thermal macro initiators. Even though these polymers were insoluble in water and hence no actual surfactants, they can be used as a starting point for the modifications in this study.

3 Concept

3.1 Aim

The aim of this work is to establish a new hydrogel grafting process for UF membranes that is applicable in ready to use membrane modules. The concept is based on a macromolecular initiator which is used to graft a zwitterionic hydrogel on the PES membranes. In the following Chapter, the general concept and the different strategies to achieve a macromolecular initiator as well as the used hydrogel system are described. As discussed in Chapter 2.3, different strategies are employed to reduce membrane fouling. Many established grafting techniques (as discussed in Chapter 2.4), either lack surface selectivity or are only applicable on flat sheet membranes but not inside capillaries or modules. The goal of the work presented here is therefore to establish a new grafting technique that is surface selective and can be applied without direct access to the membranes selective layer.

3.2 Macromolecular initiator mediated grafting

As discussed in Chapter 2.5, macromolecular surfactants carrying initiator active groups can be used to immobilize initiator groups on membrane surfaces. The scope of this work is modification of UF membranes. These are capable of rejecting macromolecules of sufficient size, but smaller molecules will penetrate into the membrane support. High surface selectivity of the grafting procedure can therefore only be achieved, when the macromolecular initiator is completely rejected by the used membrane.

The two-step modification procedure with separate initiator immobilization and grafting steps is shown in Figure 3-1.

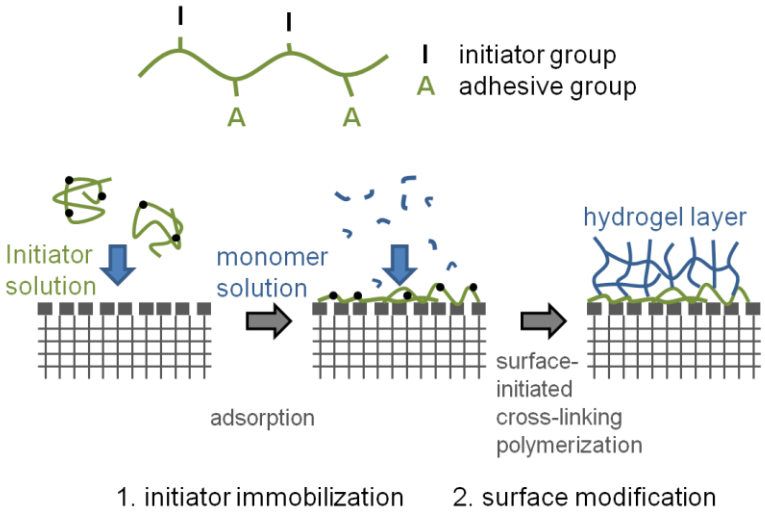

Figure 3-1 Two-step process for surface selective modification of filtration membranes, using a macromolecular initiator.

The macromolecule contains initiator- and adhesive functionalities. The macromolecular initiator is filtered through the membrane in a premodification step. When the hydrodynamic radius of the molecules is large enough to be rejected by the used membrane, adsorption will only take place on the selective layer. Also when the colloidal properties and filtration conditions are well adjusted (cf. Chapter 2.5 and Chapter 2.3.1), the macromolecule should form a saturated monolayer on the surface. Therefore the effect of the initiator on membrane performance is expected to be low. The second step is a surface initiated cross-linking polymerization forming a thin hydrogel layer on top of the membrane.

Since the modification procedure shall be applied to capillary UF membranes which are potted in modules, photo initiation is not an option here. Two possible alternatives for the initiation step are developed. The different initiation mechanisms of a redox co-initiator and a thermal initiator are discussed in the following:

Redox co-initiator

The prototype for the initiation step used here is the often used N,N,N,N-tetramethylethylene diamine (TMED), shown in Figure 3-2.

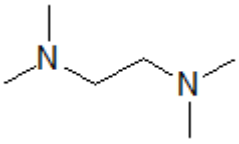

Figure 3-2 Structural formula of TMED.

TMED is a well known redox co-initiator which is often used in combination with ammonium persulfate (APS) for polymer hydrogel synthesis. Many different substituted mono- and diamines have been reported to facilitate radical formation from APS. Reaction rates are generally higher for higher substitution of the amine and higher for ethyl diamines than monoamines[94]. A proposed reaction mechanism for radical formation from the TMED/APS redox couple involves a cyclic intermediate state (Figure 3-3).

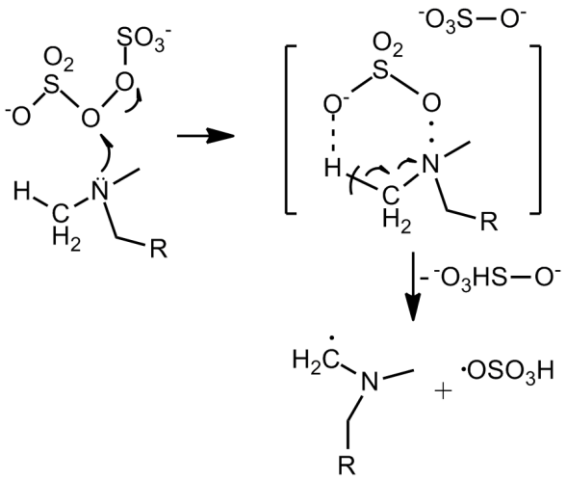

Figure 3-3 Proposed reaction mechanism for radical formation by APS/amine redox couple[89].

Observed higher reaction rates for TMED than for other tertiary amines have been explained by a co-promoting effect of the second amine group[94].

Due to the vast variety of available methacrylate monomers, these were chosen for initiator synthesis via free radical polymerization. The molecular formulas of the used monomers 2-(dimethylamino)ethylmethacrylate (DMAEMA) and butylmethacrylate (BMA) are given in Figure 3-4.

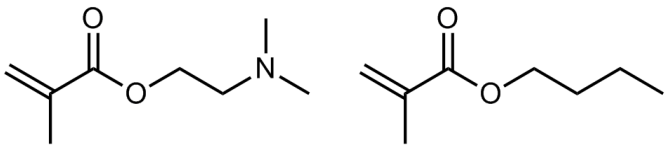

Figure 3-4 Structural formula of DMAEMA (left) and BMA (right).

DMAEMA contains a tertiary amine group that should serve as redox partner for APS in the initiation step. BMA contains a hydrophobic chain which is used to adjust the polymer hydrophobicity and hence the adsorption to PES. The structure of the macromolecular initiator is shown in Figure 3-5.

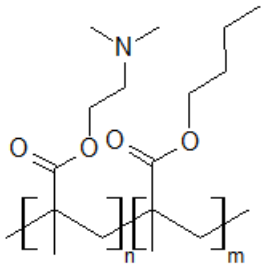

Figure 3-5 Structure of synthesized macromolecular redox co-initiators.

A main advantage in the use of the toolbox like methacrylate monomers is the adjustability of interactions with materials, once the principle is established. Besides BMA, other methacrylate monomers are available, which could serve as a side group. For example, partially fluorinated methacrylate compounds like hexafluorobutyl methacrylate with comparable reactivity[95] could replace BMA. The initiator system could thus be optimized for other membrane materials like the fluorinated polyvinylidene fluoride.

Thermal initiator

An alternative initiation mechanism relies on thermal activation of the macromolecular initiator instead of a co-initiation.

The macromolecular thermal initiators presented by Anders et al.[93] were insoluble in aqueous solution (cf. Chapter 2.5.1). Therefore they had to be dip coated on the base material from a solution in organic solvents. In order to apply the initiator system to membranes, the initiator should act like a surfactant forming a saturated monolayer on the membrane surface. A thick dip coating of an insoluble polymer would likely lead to a severe flux decline of the membrane. Therefore, poly styrene-co-maleic anhydride (pSMA) was used as the base polymer for modification in this work (Figure 3-6).

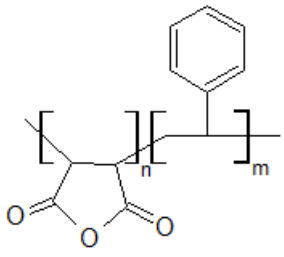

Figure 3-6 Poly(styrene-co-maleic anhydride) n = 0.26 m = 0.74 for Xiran SZ26120.

The polymer is available with different MW and several grades of the polymer can be solubilised in water[96]. Part of the maleic anhydride (MA) groups will be modified with organic hydroperoxides to form perester side groups or 4-[(1,1-dicyanoethyl)azo]benzyl alcohol (azo-benzylalcohol) to form azo side groups. Subsequently the rest of the MA groups will be

hydrolysed to achieve water solubility. It is crucial to adjust the ratio of modification and hydrolysis of the MA in a way that the polymer acts as a surfactant, while granting high activity.

3.3 Monomers for grafting

In the second step of the modification procedure (Figure 3-1) the adsorbed initiator is activated to initiate a radical graft polymerization on the membrane surface. Different monomers and cross-linkers may be used in this step. The main requirements are good water solubility and polymerization ability by free radical polymerization. For the proof of concept a monomer system with known antifouling properties shall be used. As discussed in Chapter 2.4, sulfobetaines are a promising material for surface modification.

The sulfobetaine [3-(methacryloylamino)propyl]dimethyl(3-sulfopropyl)ammonium hydroxide (SPP) is used as the zwitterionic monomer for hydrogel preparation in this work. The formula is shown in Figure 3-7.

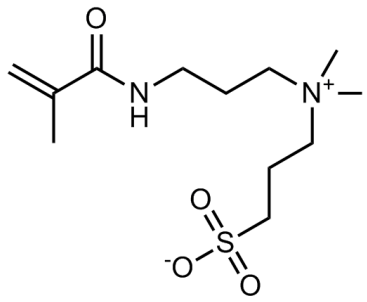

Figure 3-7 [3-(Methacryloylamino) propyl] dimethyl (3-sulfopropyl) ammonium hydroxide (SPP).

Similarly good antifouling properties have been reported for copolymers of anionic and cationic monomers[97]. Therefore mixtures of anionic 2-acrylamido-2-methyl-1-propanesulfonic acid (AAMPSA) and cationic (3-acrylamidopropyl) trimethylammonium chloride (AATAC) are also tested (Figure 3-8).

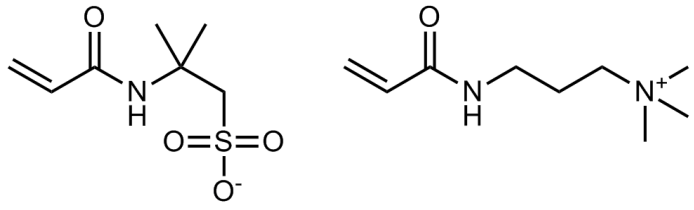

Figure 3-8 2-Acrylamido-2-methyl-1-propanesulfonic acid (AAMPSA) (left) monomers and (3-acrylamidopropyl) trimethylammonium chloride (AATAC) (right).

The methacrylamide SPP and the acrylamides AATAC and AAMPSA are chosen instead of the more commonly available methacrylate or acrylate derivatives due to their higher hydrolytic stability[98] under typical conditions for membrane cleaning.

3.4 Work plan

Both hydrogel systems are first tested in bulk experiments for their suitability (cf. Figure 4-3). The more promising system is then used for further experiments. The initiators are tested for their suitability regarding adsorptive behaviour and initiator activity. The best suited initiator is then used to modify membranes. The membrane modification is first optimized on flat sheet membranes using different fouling substances. Subsequently the modification is transferred to lab scale modules and ultimately employed to a full scale pilot plant module for long term operation tests. The main goal of this work is to prove the applicability of the concept of a macromolecular initiator for membrane modification. The creation of a modified membrane with improved antifouling properties with the aim to indicate directions for future work are also in the scope of this work.

4 Experimental

4.1 General materials

Unless otherwise stated, the term water will refer to ultrapure water (18.1 MΩ cm^{-1}) produced using a Milli-Q RO System (Millipore, USA).

The Membranes used in this work are either flat sheet or capillary membranes. The ultimate goal was the modification of Inge Multibore® PES capillary membranes (Figure 4-1).

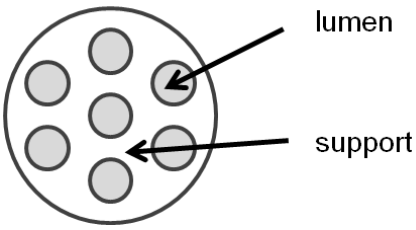

fibre diameter: 4 mm

lumen diameter: 0.9 mm

pore size: app. 20 nm

Figure 4-1 Cross section of a multibore fibre containing 7 capillary membranes.

The Multibore® membrane contains seven capillary membranes in a single fibre surrounded by a porous support. For filtration and modification of the fibres, the support on the feed side has to be sealed without closing the lumen. Therefore Inge/BASF (Germany) has provided ready to use membrane modules in different sizes containing different numbers of fibres.

Module type	Number of fibres	Fibre length [cm]	Surface area [cm²]
Flat sheet	-	-	3.1
Lab scale	1	20	40
Poseidon plant	5	20	200
Pilot plant	5	140	1400

The so prepared fibres are not accessible in the module and thus several important surface characterizing techniques are not applicable. Therefore BASF developed flat sheet membranes from the same base material and with similar properties like the Multibore® membrane. These have been provided and used for all experiments on flat sheets. Since grafting had often a huge influence on the overall membrane performance (i.e. reduced permeability), the commercial PES membrane Nadir UP020 (Microdyn Nadir, Germany) was used for comparison in some fouling tests. The permeabilities of the used membrane types are summarized in Table 4-1.

Table 4-1 Initial water permeabilities of used membrane types.

Membrane	Permeability (water) [L/hm²bar]	Deviation [L/hm²bar]
Multibore	1000	100
Flat sheet	670	120
Nadir UP020	400	40

4.2 Sulfobetaine-methacrylamide

For first experiments (mainly bulk hydrogel preparation and modification of dense films) SPP with a purity of 96 % was supplied by Sigma Aldrich (USA). Since Sigma Aldrich discontinued sales of the monomer, the supplier was changed to Chemical Point (Germany). This batch of SPP was used for the first membrane modification experiments. Due to the poor quality of the monomer (mainly a large fraction of insoluble polymer chunks), another batch was self synthesized. The synthesis is derived from a literature source.[99] Briefly 20 mL [3-(dimethylamino)propyl]methacrylamide (0.11 mol) was dissolved in 20 mL dry acetonitrile (ACN) and 9.7 mL (0.11 mol) 1,3-propanesultone were added. The mixture was heated up to 35 °C for 3 h. After cooling to room temperature, the formed white precipitate was filtered, washed three times with 30 mL ACN and hence 3 times with 30 mL diethylether. The self synthesized SPP was used for all membrane modifications unless stated otherwise.

4.3 Bulk hydrogel preparation

Besides the zwitterionic SPP monomer, a mixture of anionic and cationic monomers was also tested for bulk hydrogel preparation.

Figure 3-8 shows the structures of the used monomers (3-acrylamidopropyl) trimethylammonium chloride (AATAC) (75 %) solution in H_2O and 2-acrylamido-2-methyl-1-propanesulfonic acid (AAMPSA) (99 %) both Sigma Aldrich. Both monomers were used as provided without further purification. N,N´-methylenebis(acrylamide) (MBAA) (97 %) (Sigma-Aldrich, USA) was used as cross-linking agent.

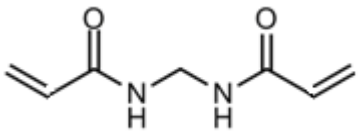

Figure 4-2 N,N´-methylenebis(acrylamide) (MBAA).

The degree of cross-linking (DC) was determined by calculating the weight ratio of crosslinker (m_{MBAA}) to monomer ($m_{Monomer}$) using Eq. 2.

$$DC = \frac{100 \cdot m_{MBAA}}{m_{monomer}} \quad [-] \qquad (2)$$

Compositions were varied, while the starting point for determining optimum conditions was derived from an older work in the group[79]. Typically a mixture of AATAC and AAMPSA with a molar ratio of 1:1 containing 0.8 mol/L total monomer and a DC of 6.7 was prepared by dissolving 2.07 g AAMPSA (10 mmol) and 2.48 mL AATAC (10 mmol containing 0.62 mL water) and 222 µL TEMED (1.4 mmol) in 25 mL water. 43.3 mg APS (0.18 mmol) were added to start the gelation. In some cases NaCl was added to minimize possible electrostatic interactions. The tested compositions can be found in Table 4-2.

Table 4-2 Composition of monomer solutions for bulk hydrogel synthesis from AATAC/AAMPSA 1:1 with 0.8 M total monomer and DC 6.7

NaCl [mmol/L]	**persulfate [mmol/L]**	**TMED [mmol/L]**
0	7.5	30
100	7.5	30
200	7.5	30
0	30	30
100	30	30
200	30	30
0	30	120
100	30	120
200	30	120
0	7.5	120

For comparison, a hydrogel containing 0.8 mol/L SPP with a DC of 6.7 was prepared similarly.

The gelated samples were washed in 50 mL water for 24 h changing the water once after 3 h. TOC was determined in both washing waters to estimate total conversion of monomers.

The samples where cut into cubic pieces of ~1 cm³. Swelling degree of these samples was determined by immersing in water or a solution containing different NaCl concentrations for at least 24 h. The samples where then padded dry with lab paper and weighed to determine weight in swollen state ($m_{swollen}$). Then the samples where dried in vacuum at 60 °C for at least 24 h and their weight was determined again (m_{dry}). The Degree of Swelling (Q) was determined using formula 3.

$$Q = \frac{m_{swollen}}{m_{dry}} \quad [-] \qquad (3)$$

Elemental analysis (C, H, N, S, O) was performed for AATAC/AAMPSA samples using an Euro EA elemental analyzer (Eurovector, Italy). The N/S ratio was determined to estimate the

incorporation of both monomers, by comparing measured values to theoretical values for ratios of 2:1, 1:1 and 1:2.

4.4 Macromolecular initiator systems for membrane modification

4.4.1 Synthesis

4.4.1.1 Macromolecular redox co-initiators

2-(Dimethylamino)ethylmethacrylate (DMAEMA) 98 % (Sigma-Aldrich, USA) containing 700-1000 ppm monomethyletherhydroquinone as inhibitor and butylmethacrylate (BMA) 99 % (Sigma-Aldrich, USA) containing 10 ppm monomethyletherhydroquinone as inhibitor were used as delivered.

2,2´-Azobis(2-methylpropionitrile (AIBN) (98 %, Sigma-Aldrich, USA) was used as thermal initiator for polymerization. Different monomer ratios and AIBN concentrations were used (given in Table 4-2).

Table 4-3 Varied compositions of reaction solutions (total monomer concentration = 2 mol/L)

Initiator	BMA:DMAEMA	c(AIBN) [mmol/L]
MB11	1:1	25
MB12	1:2	25
MB13	1:3	25
MB14	1:4	25
MB12(155)	1:2	6.25
MB10	pure DMAEMA	25

The standard synthesis procedure was similar for all prepared initiators. Exemplary, it shall be described for MB12(155), which was the initiator used for membrane modification. 4.56 mL DMAEMA (27 mmol) and 8.41 mL BMA (53 mmol) were dissolved in 40 mL DMF. Oxygen was removed by bubbling with Ar, while the solution was heated to 80 °C (~15 min). 32.8 mg AIBN dissolved in 50 µL DMF were added. After 3 h reaction time the reaction mixture was precipitated in water. After stirring over night, the viscous polymer precipitate was immersed in fresh water. After another 6 h of stirring, the polymer was dried in vacuum at 60 °C over night.

The conversion was estimated by weighing the dried precipitate.

4.4.1.2 Synthesis of macromolecular thermal initiator

The commercial polystyrene-co-maleic anhydride (pSMA) Xiran® SZ26120 (Polyscope, Netherlands) was used as educt for all modification based thermal initiators.

The polymer has an M_w of 120 KDa with a PDI of 2 and contains 26 % maleic anhydride (MA) groups. The polymer can be solubilised in water by hydrolysis of the MA groups. The modification procedure for both thermal initiators followed closely the experiments by Anders et.al.[93] After partial modification of MA groups with either and azo functional or peroxide side group, the remaining MA groups were hydrolysed leading to the product given in Figure 4-3.

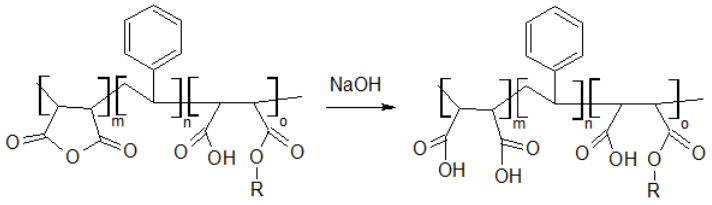

Figure 4-3 Hydrolysis step after partial modification of MA groups with peroxide or azo functional side group R.

Modification with a new azo group

The azo functional group was synthesized using a synthesis method described by Kerber et al.[100]. 4-nitrobenzylalcohol (99 % Aldrich, USA) was reduced using zink (≤ 10 µm, ≥ 98 %, Aldrich, USA). The aminobenzylalcohol was then diazotized at temperatures below 0 °C. The diazonium salt solution was filtered and added to a solution of methylmalodinitrile. The formed precipitate was then filtered and dried. The methylmalonodinitrile was synthesized using a procedure described by Ghorai et al.[101]. The complete synthesis route is given in Figure 4-4.

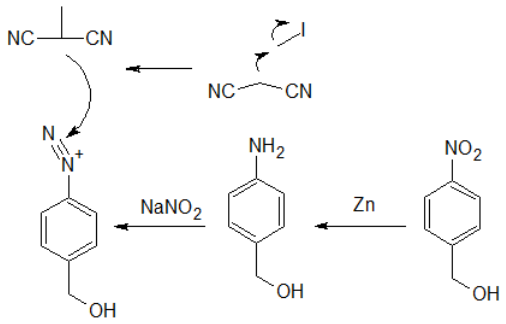

Figure 4-4 Synthesis of azo-benzyl alcohol.

Modification of pSMA was carried out following the modification procedure for poly(1-octadecene-co-maleic anhydride) described by Anders et al.[93]. 1 g pSMA (2.54 mmol maleic anhydride) was dissolved in 15 mL dry THF under Ar atmosphere. The solution was added to a solution of 56.7 mg (2.6 mmol) azo-benzylalcohol in dry THF. The mixture was stirred 3 days at room temperature under Ar atmosphere. The reaction scheme is shown in Figure 4-5.

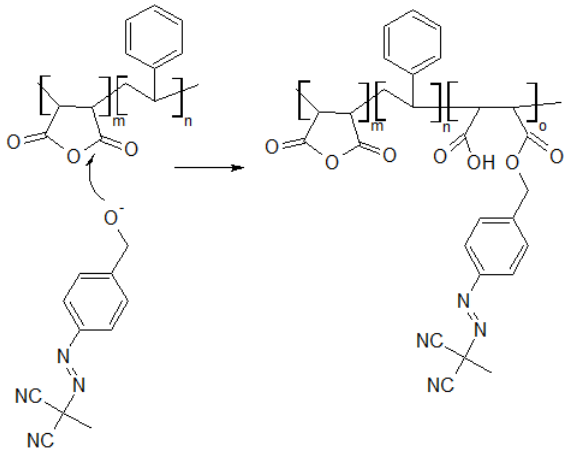

Figure 4-5 Introduction of azo group into pSMA.

Differing from literature, the remaining MA groups were hydrolysed by adding 15 mL 1 M NaOH and stirring for another day to achieve the modified polymer in the hydrolysed form like shown in Figure 4-3 (with R as the azo side group). The solvent was removed by oil pump vacuum. The obtained yellow powder was dissolved in 15 mL water and neutralized with 1 M HCl. Purification was achieved by dialysis (MWCO 6000-8000 Da) against water for 2, 3 and 12 hours. Finally water was removed (25 mbar, 28 °C) and the polymer was dried in vacuum at room temperature.

Modification with hydroperoxides

The modification of maleic anhydride copolymers first described in a patent by Steinert et al.[102] was also described by Anders et al.[93]. In this work, the described process was applied to modify pSMA using *tert*-butyl hydroperoxide (Peroxan BHP 70, 70 % solution in water, Pergan, Germany) and cumyl hydroperoxide (Peroxan CU-90 L, containing 10 % Cumol, Pergan, Germany). The hydroperoxides where kindly supplied by Pergan GmbH as free samples. The chemical structures are shown in Figure 4-6.

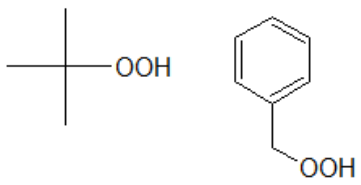

Figure 4-6 Chemical structures of *tert*-butyl hydroperoxide (left) and cumyl hydroperoxide (right).

5 g pSMA (containing 12.7 mmol MA) were dissolved in 15 mL acetone under Ar atmosphere. 1.77 mL Et_3N (12.7 mmol) were added. After 10 min. 1.75 mL *tert*-butyl hydroperoxide (12.7 mmol) were added. The reaction scheme is given in Figure 4-7.

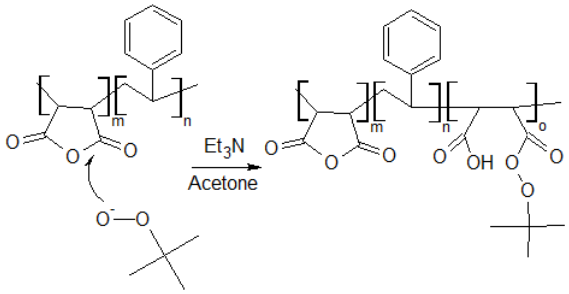

Figure 4-7 Modification with *tert*-butyl hydroperoxide.

After 4 h reaction time 50 mL 1 M NaOH were added to hydrolyse unreacted MA groups. This should yield the modified polymer in the fully hydrolysed form as given in Figure 4-3 (with R as the respective peroxide side group). After stirring over night HCl was added until a white precipitate formed. The precipitated polymer was filtered and washed with 0.1 M HCl and subsequently with water. The product was then freeze dried.

4.4.2 Characterization

4.4.2.1 General characterization

Nuclear magnetic resonance (NMR)

Most NMR experiments in this work were performed using a DMX300 (Bruker, USA) 300 MHz NMR. 500 MHz NMR spectra were recorded using a DRX500 NMR (Bruker, USA).

To determine the BMA/DMAEMA ratio in the redox co-initiators, 300 MHz ^{1}H-NMR spectra were recorded in $CDCl_3$ and the ratio of peak areas of δ=1.4 ppm (CH_2 in BMA) and δ=2.56 ppm (CH_2 in DMAEMA) was calculated directly giving the ratio of monomer units (cf. Appendix Figure 11-1).

To estimate the modification ratio for hydroperoxide modified pSMA, 500 MHz ^{1}H-NMR spectra were recorded using dimethylsulfoxide (DMSO) as solvent. For *tert*-butyl hydroperoxide the Me proton peak (δ=1.14 ppm) was correlated to the broad aromatic band of styrene groups in the base polymer (δ=5.7-7.7 ppm) (cf. Appendix Figure 11-4).

The degree of modification with cumyl hydroperoxide was roughly estimated by integrating the band area for CH groups in MA (δ=2.8 - 3.26 ppm) and calculating the expected band area for aromatic protons from the styrene groups (δ=5.7 - 7.7 ppm). This was then subtracted from the combined band and peak area of all aromatic protons to achieve the peak area of aromatic protons in the cumyl side group. Subsequently the latter was correlated with the CH band δ=2.8-3.26 ppm (cf. Appendix Figure 11-5).

Size exclusion chromatography

Size exclusion chromatography (SEC) was used to determine the molecular weight (MW) of the synthesized macromolecular initiators and co-initiators as well as to determine the molecular weight cut-off (MWCO) from sieving curves.

For MW determination of synthesized polymers, a dual detector for refractive index and viscosity (ETA-2020, WGE Dr. Bures, Germany) was used. For the MW determination a solution of 4 g/L in DMF was prepared. A Gram Column (PSS, Germany) with 10 µm particles was used at a flow rate of 1 mL/min, 200 µL injection volume and room temperature.

For MWCO determination, a RI-101 refractive index detector (Showa Denko, Japan) was used. The filtration procedures and feed compositions for MWCO determination are described in the respective Chapters in the membrane section (Chapters 4.5.3.2 and 4.6.3.3).

Elemental analysis

Elemental analysis (C, H, N, O) was performed using the same analyser as for bulk hydrogel analysis (cf. Chapter 4.3). Theoretical compositions were calculated for the different macromolecular initiators and co-initiators and compared to the measured compositions.

For the redox co-initiators the elemental composition in case of similar reactivity or 100 % conversion was calculated based on the educt mixture.

The theoretical composition of azo based macro initiators was calculated for a modification of 10 % of MA groups in the polymer (assuming 24 % mol MA as specified by manufacturer). The composition of peroxide based macro initiators was calculated assuming a conversion of 50 % mol of the MA groups. In both cases full hydrolysis of all remaining MA groups was assumed.

UV-VIS spectroscopy

A Cary 50 Probe UV-VIS spectrophotometer (Varian, USA) was used to characterize the new synthesized azo-benzyl alcohol, as well as the azo modified pSMA according to Anders et al.[93]. Solutions with a concentration of 1 g/L were measured at a wavelength range of 200 – 600 nm.

4.4.2.2 Colloidal properties

The macromolecular initiators synthesized in this work all contain hydrophilic and hydrophobic groups. In case of the redox co-initiators the DMAEMA group is expected to be hydrophilic in its protonated state. In the pSMA based thermal initiators, maleic acid groups will serve as hydrophilic parts after hydrolysis. The BMA group in the redox- and the styrene group in the

thermal macro initiators will form a hydrophobic part making the macromolecules to some extend amphiphilic. The schematic structures of the synthesized polymers with hydrophilic groups randomly located in a hydrophobic polymer are illustrated in Figure 4-8.

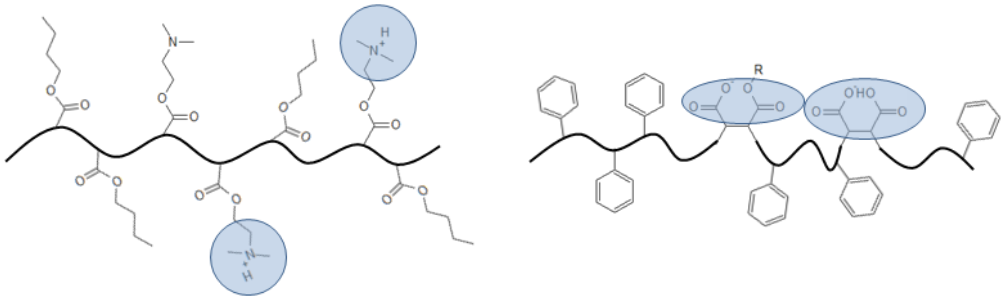

Figure 4-8 Structural illustration of the amphiphilic nature of synthesized macromolecular redox co-initiator (left) and thermal initiator (right), with blue parts illustrating hydrophilic units.

To understand the processes during adsorption to surfaces, the tendency to form aggregates in aqueous solution was investigated, determining critical water content (CWC) and the critical micelle concentration (CMC).

Critical water content

The CWC was determined by an established method found in literature[103]. Here part of the ternary phase diagram water/solvent/polymer was investigated by dissolving the polymer in a solvent and adding water stepwise. Solutions containing 1 g/L of the redox co-initiators were prepared in ethanol and *iso*-propanol. A series of samples was prepared containing water in increments of 5 % Vol. ranging from 0 to 40 %. In the area, where visible precipitate formed, 15 more samples were prepared with 1 % increments in water content. After at least 20 min waiting time, the light absorbance at 650 nm was measured using a Cary 50 Probe UV-VIS spectrophotometer (Varian, USA). The absorbance was plotted and the CWC was calculated from the interception of the curves before and during formation of aggregates. A typical plot for CWC determination is shown in Figure 4-9.

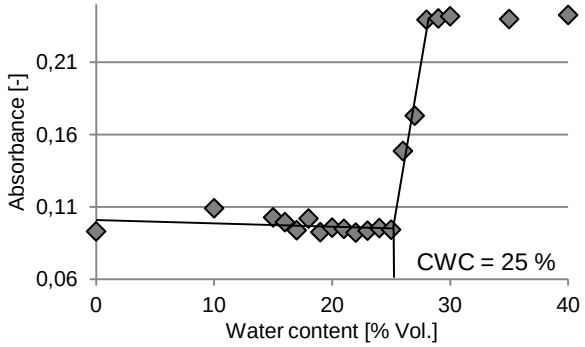

Figure 4-9 Determination of CWC from turbidity measurements.

DMAc was used to dissolve the pSMA based thermal macro initiators (1 g/L) for CWC determination in a similar way.

Critical micelle concentration

To determine the CMC, at which the first formation of micelles occurs, the pyrene fluorescence spectroscopy method[104] was used. When adding an amphiphilic block copolymer to water in increasing concentrations, it will start forming aggregates above this concentration. The method to determine the point of micelle formation uses pyrene as a probe molecule. The fluorescence spectrum of pyrene in very low concentrations ($2 \cdot 10^{-6}$ mol/L) is dependent on the polarity of its environment[105]. Due to its poor water solubility, pyrene will be incorporated into forming micelles as soon as they are formed. This results in an intensity shift in the fluorescence spectrum. More precisely, the intensity ratio of the first and third vibrational band will shift and increase[106].

The experiments in this work were performed according to former work in the workgroup[107]. Stock solutions of all polymers were prepared at a concentration of 1 g/L in their respective solvent mixture or pure water. Pyrene was added to a concentration of 1 µmol/L from a pyrene stock solution of 2 mmol/L in ethanol. Dilutions generally ranging from 0.1 mg/L to 1 g/L were prepared keeping the pyrene concentration constant. All samples were equilibrated in darkness for two hours and fluorescence was measured using a Cary Eclipse (Varian, USA) spectrophotometer. The emission wavelength was 343 nm and the recording range was 360-420 nm with emission and excitation slit widths of 5 nm. The band ratio of emission bands 384 nm to 374 nm was plotted half logarithmical and the CMC was determined as point of interception between the two straight lines representing unimer presence at low concentrations and micelle formation at increasing concentration (Figure 4-10).

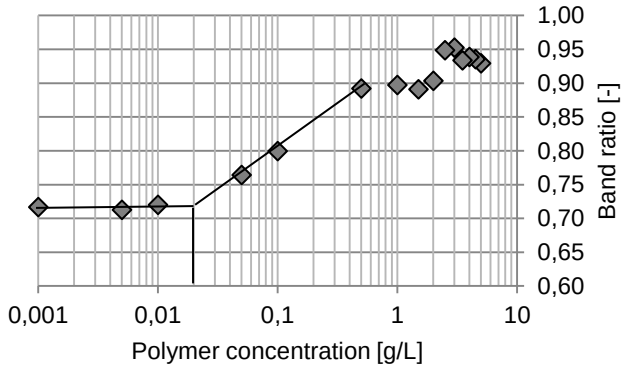

Figure 4-10 Band intensity ratio 384 nm : 374 nm in pyrene emission spectrum in dependence of the concentration of redox co-initiator.

4.4.2.3 Adsorption behaviour to PES model surfaces

For the experiments in this part individual coating procedures had to be developed for each sensor type. Spin coating was used to achieve thin (< 100 nm) polymer layers on top of different sensor materials. Even though theoretical models trying to predict the layer thicknesses of spin coated layers in dependence of coating conditions exist[108], a simple trial and error method was applied here to find suitable conditions. Starting with a preparation method for thin PES films on silica wafers described in literature[109], the coating process was optimized for each sensor type. The detailed procedures will be given in the subsequent subChapters. In all cases dichloromethane (p.a. quality, Aldrich, USA) was used as solvent. After dissolving the desired amount of PES (Ultrason, BASF, Germany) over night, the solutions where filtered through a 0.2 µm polytetrafluoroethylene (PTFE) syringe filter in order to remove dust.

Solutions of the macromolecular redox co-initiator were always prepared by dissolving the desired amount in *iso*-propanol (99.7 %, Bernd Kraft, Germany), then adding 1 M HCl and finally filling up with water to a total solvent composition of 20 % vol *iso*-propanol and 80 % vol water containing 10 mmol/L HCl. The same solvent composition without co-initiator was used as background solution.

Ellipsometry

Ellipsometry is a commonly used technique to derive thicknesses or optical properties of layers on reflecting substrates. However instead of actually measuring thickness or refractive index of a material, the ellipsometry setup determines differences in polarization of the reflected light. Two parameters are actually measured: The parameter delta (Δ) combines the phase difference between the parallel and perpendicular components of the incoming light wave (δ_1) with the components of the outgoing wave (δ_2) via Eq. 4.1.

$$\Delta = \delta_1 - \delta_2 \qquad [°] \tag{4.1}$$

The parameter Psi (Ψ) combines the changes in amplitude between incoming and outgoing light for perpendicular and parallel components (Eq. 4.2).

$$\tan \Psi = \frac{|R^P|}{|R^S|} \qquad [-] \tag{4.2}$$

Where $|R^P|$ and $|R^S|$ are the amplitude ratios of the outgoing to incoming waves for parallel and perpendicular components respectively. Both values are connected via the fundamental equation of ellipsometry (Eq. 4.3).

$$\rho = \tan \Psi e^{j\Delta} \qquad [-] \tag{4.3}$$

With the complex ratio ρ of the complex total reflection coefficients (Eq. 4.4).

$$\rho = \frac{R^P}{R^S} \qquad [-] \tag{4.4}$$

Since the reflection coefficients and phase shifts upon reflection are depending on the refractive index and the layer thickness of the surveyed film, these parameters can be derived from the measured Ψ and Δ values via mathematical fitting methods. However it is important to keep in mind that assumptions regarding the structure and properties of the surveyed system have to be made[110].

In this work a MM-16 ellipsometer (HORIBA Jobin Yvon, Germany) was used. The obtained Δ and Ψ values were evaluated using the software DeltaPsi 2 (HORIBA Jobin Yvon, Germany). Ellipsometry was used for the sole determination of PES layer thicknesses on sensors but also to determine thicknesses of adsorbed initiator layers on model surfaces. For the latter, 9x9 mm silicon wafer pieces were spin coated. These chips were cleaned in peroxomonosulfuric acid for 2 h at app 60 °C. Before spin coating they were rinsed and stored in water. The chips were then dried in Ar gas and spin coated for 40 s at 40 rps with 50 µL of a 1 % PES solution. The samples were dried at room temperature over night.

In order to determine layer thicknesses of adsorbed macromolecular redox co-initiators, spin coated chips were immersed in a solution of 5 g/L for two hours. Then the samples were rinsed with the standard solvent mixture and finally in water. After drying over night, layer thickness was determined by ellipsometry. A model containing the determined refractive index *n* and layer thickness *d* of the PES sub layer was constructed (Figure 4-11).

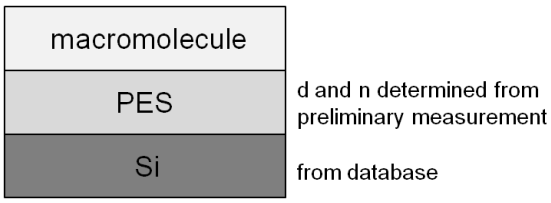

Figure 4-11 Multilayer model used for determination of the thickness of adsorbed macro initiator.

Characteristic values for a Si layer covered with a SiO_2 skin layer were taken from the software´s database. The *n* and *d* values from one single measurement of the PES coated sensor were used for the *n* and *d* determination of all adsorbed macromolecular layers, neglecting any inhomogeneities in the spin coated PES layers.

Azo modified and unmodified pSMA was dissolved in different concentrations (0.1 g/L and 1 g/L) in pure water and in water containing 20 % vol. DMAc. The spin coated chips were immersed in these solutions for 30 minutes and then rinsed with water and dried with Ar before performing ellipsometry measurements.

Surface Plasmon resonance

Surface plasmon resonance (SPR) is a versatile and widely applied method to monitor interactions of solutes and surfaces. In this work a Kretschmann[111] type attenuated total reflection spectrometer was used. The configuration is shown in Figure 4-12.

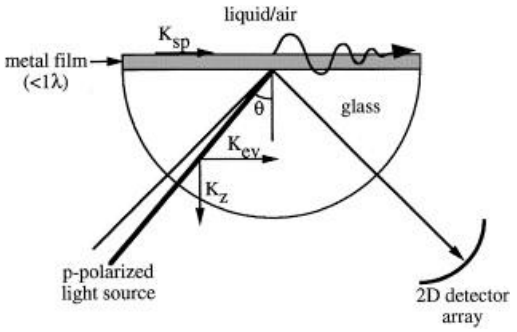

Figure 4-12 Kretschmann configuration SPR detector[112].

A parallel polarized monochromatic light beam is totally reflected on the interface between a glass half cylinder and a medium of less optical density. This will create an evanescent field with a penetration depth of its wavelength. The other side of this interface is covered with a thin metal film exhibiting free electron behaviour (here gold). At a certain angle of incidence, the plasmon resonance angle, surface plasmons in the metal film will be excited. This results in an energy loss of the reflected light beam, which can be detected. The condition for plasmon resonance is that the wave vector of the evanescent field K_{ev} and the wave vector of the surface plasmon K_{sp} are coherent ($K_{ev} = K_{sp}$). The angle of incidence θ is connected to K_{ev} by Eq. 5.1.

$$K_{ev} = \frac{w_o}{c}\eta_g \sin\theta \tag{5.1}$$

With w_o as the frequency of incident light, η_g the refractive index of the glass half cylinder and c the vacuum speed of light. On the other hand, the plasmon wave vector K_{sp} is depending on the refractive index on the solvent side η_s via Eq. 5.2.

$$K_{sp} = \frac{w_o}{c}\sqrt{\frac{\varepsilon_m+\eta_s^2}{\varepsilon_m+\eta_s^2}} \tag{5.2}$$

Where ε_m is the dielectric constant of the gold film. From this it is clear that the angle, at which plasmon resonance and thus intensity loss in the reflected light occurs, is depending on the refractive index on the solvent side. By this technique changes in refractive index to up to 300 nm can be sensed. The actual measuring procedure is depicted schematically in Figure 4-13.

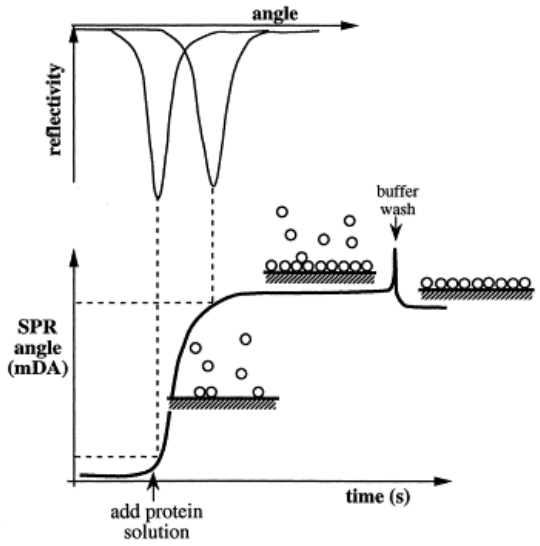

Figure 4-13 Dip in reflectivity due to SPR in dependency of incidence angle[112].

By constantly changing the angle of incidence and monitoring the reflected intensity, a dip at the SPR angle will be recorded. By following the position of the minimum of this dip, the adsorption or desorption of material at the surface expressed as changes in the dip position can be monitored[112].

For this work an IBIS I SPR system (Xantec, Germany) with a constant emission wavelength of 670 nm was used. The sensors (Xantec, Germany) consisted of 50 nm gold layers on glass slides. Recycled sensors were first cleaned in DMF for 12 h and then rinsed in water. All sensors were then cleaned in a concentrated solution of potassium dichromate in concentrated sulfuric acid for 5 min and immediately rinsed with water and dried with Ar gas[113]. The sensor

discs were then immediately spin coated with 200 µL of a 0.25 % PES solution at 42 rps, resulting in a layer thickness of 60 nm PES.

For a typical experiment a 5 g/L solution of macro initiator was prepared. The sensor was equilibrated with 50 µL background solution (either water or the used solvent mixture) in the cuvette until the baseline was stable for at least 10 minutes. Then 40 µL background solution were removed and replaced with 40 µL initiator solution. 10 µL were always left in the cell to avoid a baseline shift due to sensor dewetting. The sample solution was mixed by constantly pumping 25 µL out and in. After the angle shift was stable, the sensor was "rinsed" by removing 40 µL of the sample solution and replacing with background solution. This has been repeated three times. To test, whether this is sufficient to remove all effects of analyte in the cuvette, the cuvette was rinsed constantly for one minute using constant dosing and a drainage pump. However, since the sensor surface will be frequently left uncovered by solvent, the method was only used on some samples.

Quartz crystal microbalance

The quartz crystal microbalance (QCM) uses an oscillating quartz crystal to determine adsorbed mass. The measurement uses the fact that adsorbed mass on the crystal will result in a decrease of its oscillation frequency. The correlation between adsorbed mass Δm per surface area A is expressed in the Sauerbrey equation (Eq. 6).

$$\frac{\Delta m}{A} = -\frac{C_{QCM} * \Delta f}{n_{QCM}} \qquad [\text{g cm}^{-2}] \qquad (6)$$

With the frequency change Δf, the overtone number n_{QCM} and a constant C_{QCM}, summarizing material constants of the sensor[114].

The QCM-D, E4 type sensors (Q-Sense, Sweden) were thoroughly cleaned in a solution of saturated ammonia solution, 30 % H_2O_2 in water (1:1:5) for one hour. Spin coating was performed at 40 rps with 45 µL of a 0.33 % PES solution for 1 min.

The adsorption of macromolecular redox co-initiators was surveyed under flow through conditions (150 µL min^{-1}) at 25 °C. A solution of 5 g/L of each polymer was prepared. The sensors were first equilibrated in water flow for 20 min. In the second step background solution (*iso*-propanol/water/HCl) was flowing for 20 min. Switching to the initiator solution, the response was monitored until a stable frequency was observed (~30 min). Then the sensor was rinsed with background solution for 20 min and finally with water. The frequency change in the ninth overtone between the measurements in water was determined and used to calculate the adsorbed mass of initiator according Eq. 6.

4.4.2.4 Initiator activity from in-situ rheology

Rheology was used to determine the gelation time for monomer solutions with and without initiators and co-initiators under different conditions. Using rheology in oscillation mode to survey cross-linking kinetics is a commonly known technique[115, 116]. The gelating sample is contained between a fixed plate and the measuring head. The head is oscillating at low amplitude, while the required force in dependency of the phase is monitored. From this data, the storage and loss modulus can be derived. The point of interception determines the gelation point[117].

In this work a Physica MCR301 rheometer (Anton Paar, Austria) with a plate/plate geometry (Ø = 50 mm, gap height 0.1 mm) was used. The frequency was 10 rad/s and the amplitude was 0.1 mrad. The redox co-initiators had to be dissolved in water for these tests, since the co-solvents ethanol and *iso*-propanol are expected to catalyze persulfate decomposition and radical formation[118]. The water solubility of the polymers decreases with increasing pH as well as with increasing amount of adhesive groups (BMA). In order to perform tests at a broader pH range, a pure pDMAEMA polymer was synthesized for these tests (cf. Chapter 4.4.1.1). The only other water soluble polymer was MB11 containing DMAEMA and BMA in a ratio of 1:1. For reference, the monomelucular diamine TMED was also used as co-initiator for these tests. Monomer solutions containing 0.56 mol/L SPP (DC 6.7) and 30 mmol/L amine groups were prepared for each co-initiator. The pH was adjusted to 4, 6 and 8 by adding 1 M NaOH. APS was added to these solutions to give a concentration of 7.5 mmol/L 90 s before starting the measurement. Generally the measurements were carried out at 20 °C. In an additional series with MB11, the influence of higher temperature (40 °C) and higher APS concentration (22.5 mM) was surveyed.

The activity of the azo-pSMA initiator was tested at concentrations of 1 g/L and 27 g/L polymer 0.56 M SPP (DC 6.7) at 80 °C.

From the peroxide modified polymers a solution containing 12 mmol/L peroxide (assuming full modification) was prepared by dissolving 12 mg in 50 µL DMAc and filling up with 2 mL monomer solution (0.56 M SPP, DC 6.7). The measurements were performed at temperatures ranging from 65 °C to 80 °C with both initiators and for comparison with the pure monomer mixtures.

4.5 Flat sheet membranes

4.5.1 Modification procedure

Sample preparation

The received flat sheet samples were removed from their sealing and immersed in a mixture of 50 % glycerol in water containing 10 mmol/L NaN_3 in order to avoid drying during long term storage. For modification and analysis, circular samples with a diameter of 25 mm were cut out. The samples were first immersed in *iso*-propanol over night and then washed three times with ultrapure water for 20 min. The samples were then stored in 10 mM NaN_3 solution.

4.5.1.1 Using macromolecular redox co-initiator

For a typical modification procedure, a 1 g/L solution of the macro-initiator was prepared like described in Chapter 4.4.2.3. Membrane samples were premodified with this solution by filtering 5 mL out of 15 mL in dead-end mode at 0.4 bar under stirring (300 rpm) in an Amicon type stirred dead-end filtration cell (Merck Millipore, USA). The samples were rinsed thoroughly and pure water permeability was determined. Thereafter they were either directly modified or stored in 10 mM NaN_3 solution for later use. In the latter case, the samples had to be rinsed two times with water for 20 min on a shaker prior to hydrogel modification.

A typical monomer solution (25 mL 0.25 M SPP, DC 6) was prepared by dissolving 1.828 g SPP and 0.122 g MBAA in ultrapure water and filling up to 25 mL. The solution was degassed by bubbling with Ar for 20 min. 5 min before the end of degassing, 250 µL of a 0.5 M APS solution were added. The premodified membrane samples were transferred to snap cap vials during the next 5 min with the selective side up. After degassing, 4 mL of the solution were added to each vial to completely cover the samples. The vials were sealed and after 2 h the samples were removed and rinsed for 1 h in water. Thereafter the samples were kept in 10 mM NaN_3 solution for at least 10 h before measuring water permeability again. The procedure was generally carried out with three premodified and three pristine samples simultaneously for comparison. The pure water permeability was measured after premodification with the macromolecular redox co-initiator and after hydrogel modification in order to rate the permeability decrease.

4.5.1.2 Using macromolecular thermal initiator

Since the azo modified pSMA did not show thermal initiator activity at temperatures up to 80 °C, the thermally initiated modification was only carried out using ^{t}Bu-OO-pSMA.

To prepare 100 mL solution of the thermal macro initiator, 10 mg ^{t}Bu-OO-pSMA was immersed in 2 mL DMAc for 20 min. The partly dissolved polymer was then filled up to approx. 50 mL with 100 mM NaOH solution and kept on the shaker until all solids were dissolved (about 30 min). The solution was then filled up to 100 mL with 100 mM NaOH and directly used for premodification. For first experiments 10 mL of 15 mL were filtered in dead-end mode at 0.4 bar and 300 rpm. Since this led to severe flux decline, more samples were prepared filtering only 2/15 mL and also by just adsorbing the macromolecular initiator for 10 min in the filtration cell without flux. The so prepared samples were stored at 4 °C in water for a maximum of 1 hour before the second modification step.

The monomer solution was prepared similarly like for the redox initiated modification (Chapter 4.5.1.1). During the degassing step the solutions were heated up to 65 °C in a three neck flask with chiller. After 10 min heating and bubbling with Ar 4 mL aliquots of the solution were transferred into snap cap vials, containing the membranes. The vials were sealed and stored in an oven at 65 °C. After one hour the samples were removed and rinsed in water for one hour on a shaker and then stored in 10 mM NaN_3 solution over night.

4.5.2 Characterization of surface properties

4.5.2.1 Scanning electron microscopy

An ESEM Quanta 400 FEG scanning electron microscope (FEI, USA) was used to generate high resolution pictures of surface and cross section of modified and unmodified membrane samples. Prior to scanning electron microscopy (SEM), all samples were rinsed thoroughly and dried in a vacuum oven (50 °C, 10 mbar abs) over night. The samples were cooled with liquid nitrogen and broken for pictures of the cross-sections. Surface and cross-section were then sputtered with an 8 nm Au/Pd layer using an EMITECH automatic coater K550 (Quorum Technologies, UK). SEM pictures were recorded under vacuum conditions.

Energy dispersive X-ray (EDX) was used on the cross section of the membrane, scanning an area of 100 x 100 nm in the upper and lower part of each membrane. The C, O, N and S contents of pristine and premodified membranes and membranes after grafting with 0.1 M SPP (DC 3.35) and 0.5 M SPP (DC 3.35) were determined.

4.5.2.2 Secondary Ion Mass Spectroscopy

Secondary Ion Mass Spectroscopy (SIMS) in a surface scanning mode (SIMS-mapping) was used to evaluate the homogeneity of the created grafting layers.

Generally in SIMS, a sample is exposed to a focused primary ion beam in vacuum. The impact transfers all or part of its kinetic energy into the sample. This can occur by elastic or inelastic collisions. If the transferred energy is higher than the binding energy of certain molecules, these can be fragmented and released from the surface. The composition and concentration of these fragments is strongly depending on the kinetic energy and hence on the type of primary Ion source. The secondary ions released from the samples surface can then be separated and analyzed in a time of flight mass spectrometer to create the SIMS spectrum[119].

Since the primary ion beam can be controlled by electrostatic lenses and deflectors, it can be focused on a specific area of interest on the sample. By scanning the sample with the Ion beam and collecting SIMS spectra from different spots, a two dimensional map of mass spectra can be generated. The lateral resolution of this technique is limited by the volume of the collision cascade, which is induced by the impact of the primary Ion. Typically, the diameter of this volume is ~10 nm. Most instruments operate with a lateral resolution of 50-100 nm. Since each scan removes material from the surface, it is even possible to generate three dimensional depth scans of the sample. However, the main drawback is the enormous amount of collected data, since a full mass spectrum is created for each measuring spot. It is thus important to identify secondary ions, which are specific for a substance of interest on the sample. Colour scale images can then be generated by monitoring the amount of the specific ion for each spot[119].

A direct correlation of the recorded ion signals to a concentration at the sample surface is difficult. The main reason is a possible influence of the matrix on secondary ion yield. Due to matrix effects, it can vary over several orders of magnitude. During the two dimensional scanning the matrix can be expected to be similar at all spots of the same sample. The intensity distribution can therefore still be correlated to a concentration distribution at the surface. However the direct comparison of different samples can be difficult[119].

The SIMS-mapping images in this work were created using a TOF SIMS5 (ION-TOF GmbH, Germany) with a 25 keV Bi_1^+ or Bi_3^+ ion beam. To achieve depth information, the surface was sputter cleaned with a 200 eV Cs^+ ion beam.

4.5.2.3 ATR-IR Spectroscopy

The attenuated total reflection technique enables IR measurements on optically dense samples. Briefly, the IR beam is sent through a crystal in an angle to create total reflection at the crystal to sample interface. This will create an evanescent wave interacting with the sample and thus creating the spectrum. This is schematically presented in Figure 4-14.

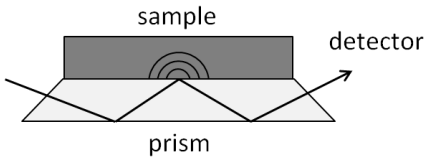

Figure 4-14 ATR-IR principle according to Lit[120].

The main advantage for this work is the relative surface sensitivity, since the method is measuring IR spectra of the upper few microns (~2 µm) of the sample[120, 121].

In this work a Varian 3100 FT-IR Excalibur spectrometer (Agilent Technologies, USA) equipped with the ATR extension MIRacle (Pike Technologies, USA) containing a diamond/ZnSe crystal (refractive index 2.4, angle of incidence 45°) was used. All samples were dried in a vacuum oven at 45 °C over night before the measurement. Only the thermal initiator samples were freeze dried instead to avoid thermally induced decomposition.

4.5.2.4 X-Ray Photoelectron Spectroscopy

X-Ray photoelectron spectroscopy (XPS) is a surface sensitive technique, which provides chemical information about the upper 2 – 20 atomic layers of a substrate. Information about the elemental composition as well as the binding properties of the upper few nm can thus be obtained. Briefly, the surface is irradiated with X-rays, causing surface atoms to emit electrons. The energy of theses electrons is depending on the characteristic energy of the electron in the atom, from which it is emitted. Therefore the emitting atom can be determined by detecting the electron energy. If the precision of the instrument is high enough, further information about the binding state of each element can be gathered from chemical shifts in the binding energies[122].

The XPS measurements in this work were performed using the hemispherical electron energy analyzer Phoibos 100 (SPECS, Germany) and a Mg anode as X-ray source. The pristine membrane samples were washed in *iso*-propanol for 12 h. Modified and premodified samples were rinsed in water for 12 h. All samples were then dried in a vacuum oven (45 °C, 10 mbar abs) over night. Samples of the flat sheets could directly be fixed to a sample holder with double sided adhesive tape. Samples of the multibore had to be cut out of the fibre and pressed flat onto the tape to achieve a flat surface. In case of the premodified and modified multibore, the module was destroyed and a membrane sample was cut from the middle of the fibre to avoid contamination with sawdust from the module housing. The determined elemental compositions were compared to calculated theoretical values.

4.5.2.5 Contact angle

All contact angles were measured using an OCA 15 plus system (Dataphysics, Germany). Captive air bubble in water was used as measuring mode to avoid rearrangements or defects, that could occur during drying[123]. Also, this mode is beneficial for modified membranes, since the hydrogel layer can be measured in swollen state and quick absorption of a droplet in sessile drop mode is avoided. Every angle was determined as the average of 15 single measurements.

In order to determine CA of hollow fibres, an Inge single bore membrane was used. The Membrane was prepared by Inge with similar characteristics like the multibore membrane. Samples of this fibre were cut in longitudinal direction and unfolded. By fixing the membrane to a glass slide, a flat surface could be generated and was surveyed using captive bubble and sessile drop method. A photograph and a microscopic side view of the samples is shown in Figure 4-15.

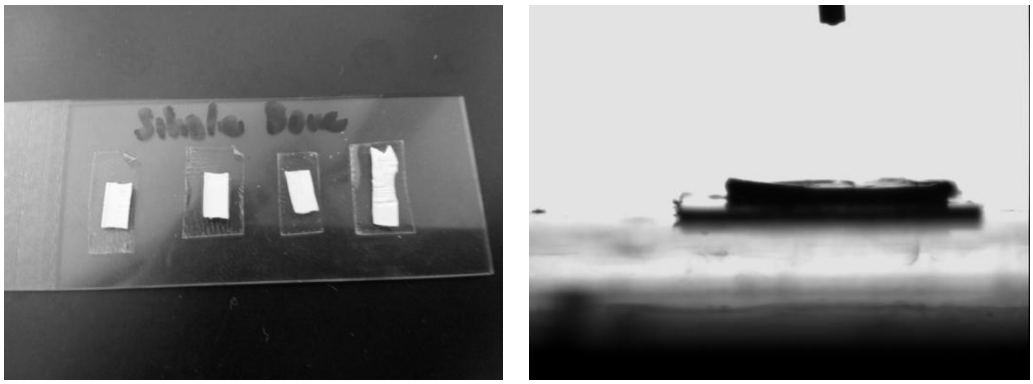

Figure 4-15 Preparation for contact angle measurement on single bore membrane. Left: top view. right: side view (microscope).

4.5.2.6 Zeta potential

The electrokinetic characterization of polymer surfaces is of great importance to understand adsorption processes or interactions with cells. Generally, at the solid liquid interface an electrical double layer will be formed by selective adsorption of Ions. By applying a liquid flow, the mobile ions will be transported in the flow direction. This current can be measured as a streaming current. However, this transport will cause a charge separation, building up a streaming potential. In steady state this potential is countered by a back current depending on the conductivity in the flow channel. Streaming current and streaming potential will vary with changes in the applied pressure[124]. Measuring changes in streaming current ΔI or streaming potential ΔU in dependence of the applied pressure difference Δp, the zeta potential ζ can be derived. The zeta potential (ZP) characterizes the charge at the shear plane between mobile and adsorbed ions. In this work, the Helmholtz-Smoluchowski equation was used to calculate the ZP from streaming current (Eq 7).

$$\zeta = \frac{dI}{dp} \cdot \frac{\eta}{\varepsilon_r \cdot \varepsilon_0} \cdot \frac{L}{A} \quad [V] \quad (7)$$

Where η is the electrolyte viscosity, ε_r the relative liquid permittivity, ε_0 the vacuum permittivity, L the length of the streaming channel and A the cross section of the streaming channel[125].

A SurPASS electrokinetic analyzer (Anton Paar, Austria) was used for all ZP determinations. For flat sheet samples, the adjustable gap cell was used and all experiments were performed with a gap height of 100 (± 10) µm. 1 mM KCl solution was used as electrolyte and all samples were equilibrated at least 20 min in this solution before measuring. The measurements were typically performed in the pH range from 3 – 10, always starting at low pH and titrating with 10 mM KOH solution in pH steps of 0.5. At each step the cell was rinsed for 180 s and two measurements were performed in each direction, varying Δp from 0 to 400 mbar.

4.5.3 Filtration performance

4.5.3.1 Permeability

The combination of permeability and rejection (or MWCO) is the main characteristic of every UF membrane. In this work permeability was also investigated to evaluate the different grafting techniques. A decrease in permeability can be expected upon grafting of a dense hydrogel network on the selective layer or in the porous support, since this will increase the hydrodynamic resistance by narrowing the flow channel in the support or reducing effective pore size.

A standard Amicon type stirred cell (Millipore, USA) (⌀ = 25 mm, active area = 3.14 cm²) was used for permeability tests. Due to the large number of samples, a setup with three parallel cells was used (Figure 4-16).

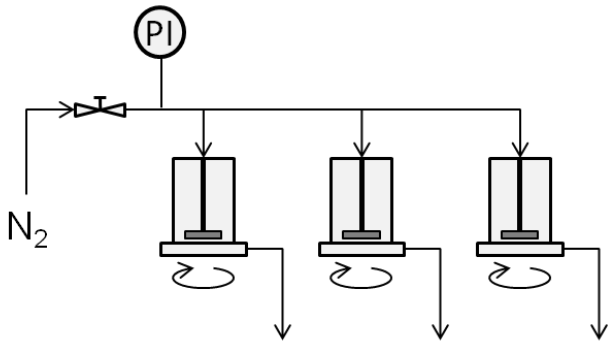

Figure 4-16 Filtration setup containing three Amicon stirred filtration cells.

The setup consisted of three Amicon cells pressurized by N_2 gas. For water permeability measurements membranes were first equilibrated in water for 1 h and subsequently rinsed 5 min at 0.8 bar. For each permeability measurement, permeate was collected for 10 min at 0.4 (± 0.02) bar, recording the pressure at the beginning and end. The permeability *Lp* was then calculated according to Eq. 8.

$$Lp = \frac{m_{perm} \cdot \rho}{t p_{avg} A} \quad \text{[L/h m² bar]} \qquad (8)$$

With m_{perm} as the permeated mass, the density ρ, the filtration time *t*, the average TMP p_{avg} and the filtration area *A*. The effect of temperature or solutes on permeate density was ignored and a density of 1 g/cm³ was used. Since the membranes used often had different initial water permeabilities, the changes due to grafting or during the stability tests were expressed as relative changes according to Eq. 9.

$$relative\ change = 100\% \cdot (1 - \frac{Lp_{after}}{Lp_{initial}}) \qquad [\%] \qquad (9)$$

4.5.3.2 Rejection and molecular weight cut-off

According to IUPAC definitions[126], the MWCO is determined by the molecular weight of a molecule for which the rejection of the membrane is 90 %. According to the same recommendations, the rejection (*R*) is calculated according to Eq. 10.

$$R = 100\ \% \cdot (1 - \frac{c_{perm}}{c_{feed}}) \qquad [\%] \qquad (10)$$

Where c_{perm} and c_{feed} are the concentrations in permeate and feed respectively. For the actual filtration, mixtures of dextran standards with different molecular weight distribution were used. The method is a standard characterization often used in the workgroup[127]. A composition of dextran with a broad molecular weight distribution around the expected MWCO of the surveyed membrane was prepared. The dextran composition for 1 L feed solution is given in Table 4-4.

Table 4-4 Dextran composition in the feed solution for MWCO determination.

Mw [kDa]	amount [g/L]
70	0.25
100	50
168	0.25

The total dextran concentration was 1 g/L. The solution contained 10 mmol/L NaN_3 for anti-microbial stabilization. The molecular weight distribution of the feed solution is shown in Figure 4-17.

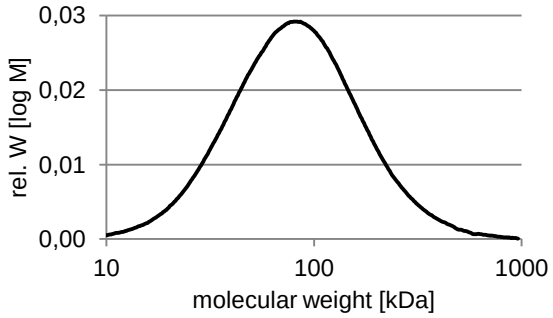

Figure 4-17 Molecular weight distribution in the feed solution for MWCO determination.

Samples with 44 mm diameter were used for the dextran filtration. To minimize the effect of CP on the rejection[128], the flux through the membrane was kept minimal by using the lowest possible (limited by the experimental setup) pressure of 0.03 bar. The MW distribution of permeate and feed was determined via SEC. The sieving curve was then calculated, via Eq. 10 for each molecular weight and the MWCO was determined as the MW where rejection reached 90 %.

According to Sarbolouki[129], the hydrodynamic radius of dextran (r) can be estimated as the average of the radius of gyration of a real chain (r_r = 0.096M$^{0.59}$) and the radius of a geometric chain (r_g = 0.128M$^{0.5}$) (Eq. 11).

$$r = \frac{0.096M^{0.59} + 0.128M^{0.5}}{2} \quad \text{[nm]} \qquad (11)$$

4.5.3.3 Fouling experiments

Bovine serum albumin

Bovine serum albumin (BSA) (MW~66 kDa, >98 % pure, Gerbu Biotech, Germany) was used as a model foulant to investigate protein fouling. The molecule is used as a common model protein for protein filtration and protein fouling[130-132]. BSA has a molecular weight of 66 kDa and an isoelectric point (IEP) of 4.7[132]. In phosphate buffered saline (PBS) solution at a pH of 7.4 the protein will therefore be negatively charged. The main advantages compared to the other foulants used in this study are constant quality compared to extracts from flower soil and MBR and the better availability (i.e. lower effort and price) compared to MBR extracts. BSA fouling was therefore used as a screening test to evaluate the effect of hydrogel grafting on membranes.

1 L PBS solution was prepared dissolving 8 g NaCl, 0.2 g KCl, 0.27 g KH_2PO_4 and 3.58 g $Na_2HPO_4 \cdot 12\ H_2O$ in water.

To avoid concealing effects due to different flux conditions in grafted and pristine membranes (arising from significantly lower permeabilities), first fouling tests were performed as static adsorption tests. The membrane was mounted to the filtration cell and permeability was determined as described in Chapter 4.5.3.1. The water was removed and a 1 g/L solution of BSA was inserted and left in the sealed cell without stirring or flux for 1 h. Thereafter cell and membrane were rinsed thoroughly with water and permeability was measured again. Fouling resistance R_f was calculated according to Eq. 12.

$$R_f = 100\,\% \frac{Lp_{after}}{Lp_0} \qquad [\%] \tag{12}$$

Where Lp_0 is the permeability before and Lp_{after} is the permeability after fouling.

To evaluate protein fouling under filtration conditions, BSA UF experiments were carried out. After measuring water permeability, each cell was filled with 15 mL of a 1 g/L solution in PBS. 10 mL of the solution were filtered at 0.4 (± 0.02) bar at a stirring rate of 300 rpm. The cell was then rinsed and water permeability was measured again. Fouling resistance was calculated using Eq. 12. TOC of permeate (TOC_{perm}) and feed (TOC_{feed}) were determined to calculate the rejection R according to Eq. 13.

$$R = 100\% \cdot (1 - \frac{TOC_{perm}}{TOC_{feed}}) \qquad [\%] \tag{13}$$

Membrane bioreactor extracts

Since BSA is not a foulant, typically encountered in surface or waste water, a foulant closer to reality was used for the most promising membranes – EPS and SMP were used for this purpose. The substances have been extracted by a project partner (Ben Gurion University of the Negev) from a 200 L MBR treating municipal wastewater at the Sede Boqer desert campus of the Ben Gurion University in Israel. The known information about the compositions is shown in Table 4-5.

Table 4-5 Known components of used EPS[133].

Organic matter	Content in EPS [%]	Content in SMP [%]
Polysaccharides	40.7	102.5 (± 10)
Proteins	21.8	5.3
TOC	36.6	36.4
TN	9.1	3.1

Most fouling tests were performed with solutions of 40 mg/L SMP or 10 mg/L EPS. The foulant was dissolved in phosphate buffered saline (pH 7.4). First the permeate flux for each membrane was adjusted to 0.15 (±0.01) mL/min with pure buffer as solvent. Then the measuring cell was

filled with 15 mL of the solution and dead-end filtration was performed at constant pressure until 10 mL had passed the membrane. Another set of membranes was used to filter 10 mL of 15 mL of a 25 mg/L EPS solution at 0.4 bar. The permeability of pure buffer solution was determined before (Lp_0) and after (Lp_{after}) the tests in order to determine the fouling effect. Fouling resistance (R_f) was calculated using Eq. 12.

The samples used to filter the higher EPS concentration were immersed in PBS solution on a shaker for 24 hours and Lp_{after} was measured again. Irreversible fouling was calculated from this according to Eq. 12.

5 mL of permeate and 2 mL of retentate were collected to determine the TOC rejection. The samples were diluted 4 and 10 times respectively before the measurement. The TOC rejection was then calculated according to Eq. 13. Since the used concentrations were low, UV absorption at 284 nm was also tested as a method for concentration determination. 2 mL samples of feed and permeate were measured and the concentration was determined with a 5 point calibration curve. The rejection was calculated according to Eq. 10.

Flower soil extract

Searching for a fouling substance, which leads to significant fouling within relatively short time (i.e. one day) of operation, the project partner Inge has developed a flower soil extract. For tests with hollow fibre modules, the extract was prepared as follows: 750 g of flower soil (OBI, Living garden Blumenerde, composed mainly of bog peat, compost and clay) were soaked in 3 L of a 0.25 M NaOH solution in warm tap water. The mixture was left over night and then filtered through a 900 µm and a 90 µm filter (Inge used a 100 µm Filter instead of 90 µm for the second filtration step). The solution was then neutralized by adding 1 M HCl solution until a pH of 7 was reached. To increase biological stability, 30 mL of a 10 mM NaN_3 Solution were added.

The composition of the similarly prepared flower soil extract was analysed by Inge and is given in Figure 4-18.

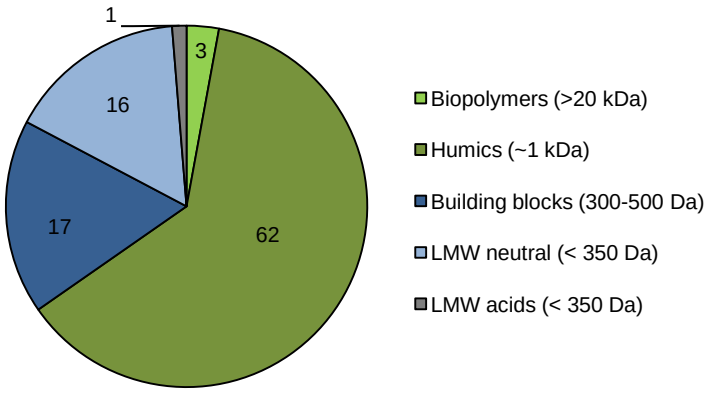

Figure 4-18 Composition of DOC in flower soil extract created from OBI living garden flower soil[134].

The main component of the DOC was formed by humic substances. Only 3 % of the extracts DOC were composed of biopolymers larger than 20 kDa. In real surface water the content of larger polymers (>100 kDa) is usually higher (~15 – 22 %[135]) while the content of low molecular weight compounds (LMW) is usually lower. Since the main part of DOC in surface water is formed by humic substances (70 – 80 %[135]), the flower soil extract seems an appropriate model system for surface water.

For preliminary tests with flat sheet samples, a different flower soil (Netto, Compo-Sana, mainly composed of bog peat (95 %) and clay) was treated similarly.

A dead-end filtration without stirring was performed as follows: a water flux of 1.1 (± 0.1) mL/min was adjusted. Then the flower soil extract was filled in the cell and filtered 20 min without stirring or adjusting the pressure. After this the sample was simply rinsed with clear water and the filtration was repeated. This sequence was carried out three times. The same samples were then used for filtration under stirring at 300 rpm until 40 mL permeate had passed the membrane. Permeate samples were collected during filtration with and without stirring and rejection was determined as TOC decrease according to Eq. 13. The permeate flux was monitored gravimetrically in 30 s intervals.

In order to monitor changes in hydrophilicity, CA was measured before and after the fouling tests. To evaluate possible changes due to the chemical cleaning usually applied to membrane modules (cf. Chapter 4.6.4), the fouled flat sheets were soaked first in 0.03 M NaOH solution and hence in 0.03 M H_2SO_4 solution. After each step, the membrane was equilibrated in water for 20 min and CA was measured again.

4.5.3.4 Stability tests

In order to determine the stability of applied modifications, two tests were performed. To rate the stability under hydrolytic conditions, the water permeability was measured collecting permeate for 10 min. Then the membrane was turned upside down and back flushed 30 min with 0.1 M NaOH at 0.4 bar. The sample was then thoroughly rinsed with water, equilibrated in water for 10 min and water permeability was measured again. This procedure was repeated three times.

To rate the stability under oxidative conditions, the membrane was immersed in 1 % H_2O_2 solution on a shaker for 30 min instead of the backwash step with NaOH. Permeability was determined similarly after each immersion and subsequent rinsing with water.

For better comparability the measured permeabilities (*Lp*) were expressed as relative permeabilities according to Eq. 14.

$$relative\ permeability = 100\% \frac{Lp}{Lp_0} \quad [\%] \qquad (14)$$

Were in this case Lp_0 means the initial permeability of pristine samples and the permeability after grafting for grafted samples respectively.

4.6 Membrane modules

4.6.1 Filtration setup and module design of lab scale modules

To be able to modify and characterize the Inge Multibore® capillary membrane, small lab scale modules were designed. The modules were produced by Inge.

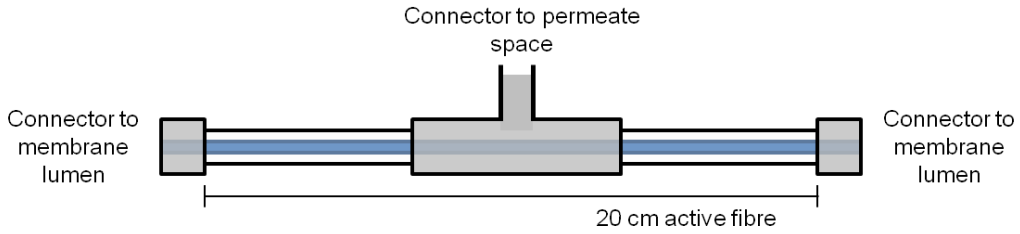

Figure 4-19 Design of lab scale modules containing a single multibore fibre (blue).

The lab scale module shown in Figure 4-19 contains a 20 cm multibore fibre (filtration area = 0.004 m²) potted in a transparent tube. The lumen is fitted with two connectors. The permeate side has one connector enabling backwash at high pressures.

To perform filtration experiments and initiator pre modification with modules, a filtration setup suitable for cross-flow and dead-end filtration was designed (Figure 4-20).

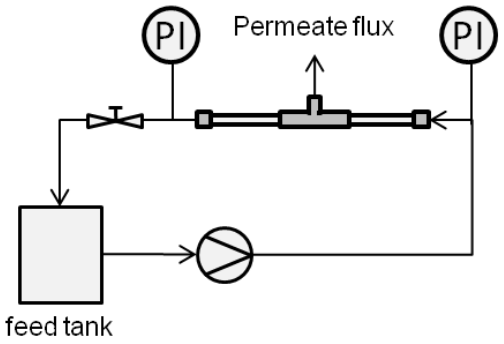

Figure 4-20 Filtration setup for cross-flow and dead-end operation of lab scale modules.

The setup as shown in Figure 4-20 consisted of a stirred tank as feed reservoir. A peristaltic pump (323, Watson-Marlow, Germany) was used to generate the desired feed streams. Two pressure indicators before and after the module, were used to determine the average transmembrane pressure (TMP) as average of the pressure before and after the module. An adjustable hose clamp was used to set the desired TMP in case of cross-flow operation. For dead-end operation, the clamp was tightly closed after filling the module with feed solution. All equilibration steps were performed in a recirculation mode with the permeate flowing back to the feed tank.

In case of experiments under cross-flow conditions, the Reynolds number in pipes (*Re*) can be calculated according to Eq. 15.

$$Re = \frac{u \cdot d}{\nu} \qquad [-] \qquad (15)$$

With the average fluid velocity *u*, the pipe diameter *d* and the kinematic viscosity *v*. When *Re* < 2300, the flow is laminar. An intermediate flow condition between laminar and turbulent flow occurs for 2300 < *Re* < 4000. Above *Re* = 4000 the flow is strictly turbulent[136].

4.6.2 Modification in modules

The module was first equilibrated for 30 min in a solution of 20 % *iso*-propanol and 10 mmol/L HCl in ultrapure water. Hereafter the solution recirculated for 1 h with an average TMP of 0.4 bar (± 0.05 bar). The solvent mixture was then replaced by 250 mL solution of the macromolecular redox co-initiator, prepared similar like for flat sheet modification (cf. Chapter 4.5.1.1). The solution was recirculated at 0.4 bar and 50 rpm for 10 min. Samples of permeate and feed were collected to determine rejection gravimetrically. For comparison the standard solvent mixture was also filtered through a module and a permeate sample was collected and dried.

After this the module was removed from the filtration setup and both setup and module were rinsed with water. The module was then equilibrated in water for 1 h without flux. Subsequently Ar saturated water was filtered through the membrane at an average TMP of 0.4 bar for 30 min. The permeate side was sealed to avoid permeation through the membrane during subsequent modification. For modification the so prepared module was connected to a valve and fixed in a vertical position (Figure 4-21).

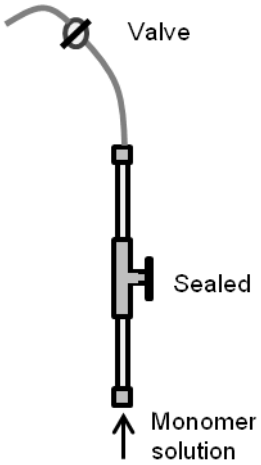

Figure 4-21 Module installation for in module grafting procedure.

A syringe was used to fill the module with a monomer solution, prepared similar to the solutions for flat sheet modification (cf. Chapter 4.5.1). After 5 mL of the solution passed the valve, the valve was closed. The module was left for 2 h and then rinsed with water. For washing, the module was mounted into the filtration setup and water was recirculated at a pump rate of 10 rpm with the pressure clamp (cf. Chapter 4.6.1) open (i.e. minimal possible TMP) for 1 h. After this the module was left at least 12 h filled with fresh water.

4.6.3 Characterization

4.6.3.1 Determination of zeta potential in modules

Under certain prerequisites, ZP can also be determined in capillary membranes. If the measurement is performed as a streaming potential measurement, different problems will occur. Due to the generally high porosity of the electrolyte filled membrane support, back current can be much stronger than for non porous samples. Also, often the membrane will be surrounded by electrolyte, that can contribute to conductivity. To avoid these often hard to quantify contributions, it was suggested to use streaming current measurements[137]. To measure ZP in the single fibre modules an adapter was constructed, fitting the electrodes of the SurPASS analyzer to the modules. Flow checks revealed that the flow is strictly laminar up to a Δp =

300 mbar in the modules used here. Prior to the measurement, the module was filled with electrolyte and the permeate compartment was sealed. The module was equilibrated for at least 1 h. Streaming current measurements were performed with ramps up to 200 mbar (Re = 1160) over a pH range from three to 10 in steps of 0.5. 1 mM KCl was used as electrolyte in all cases.

To estimate the sensitivity of the method, a module was first measured in pristine state. Then it was premodified with a polycation (poly trimethylaminoethyl methacrylate M = 16867 g/mol) used for layer by layer modification in a different study in the workgroup[138] and ZP was measured again. Unlike all other ZP measurements, this run was performed with a titration sequence going from high pH (10) to low pH (3) using 10 mM HCl.

4.6.3.2 Permeability

Permeability checks were done in cross-flow mode at a pump rate of 50 rpm and TMP of 0.4 (± 0.1) bar. Before permeate collection, each module was run for at least 1 h under these conditions until all indicated pressures where stable. Permeate was collected for 10 min and TMP was measured at the beginning and end of sample collection. The average TMP was calculated as average of these values. A second measurement was performed after another 20 min of recirculation.

4.6.3.3 Rejection

The same Feed composition and calculation methods like for flat sheet membranes (cf. Chapter 4.5.3.2) were used to determine the MWCO of membrane modules. Instead of dead-end operation, the filtration was performed in cross-flow mode. The pump rate was set to 50 rpm and the pressure clamp was adjusted to set a TMP of 30 mbar. The retentate flux was then ~80 mL/min. The initial permeate fluxes were 0.15 mL/min (400 mL/min m²) for modified and 0.2 mL/min (500 mL/min m²) for unmodified modules.

4.6.3.4 Fouling experiments

BSA

To determine, if the grafting in modules was similarly beneficial like on flat sheet samples, BSA fouling experiments were performed prior to experiments with flower soil and MBR extracts. The modules were equilibrated in PBS (cf. Chapter 4.5.3.3) solution for at least 1 h and PBS permeability was determined. Then the buffer was replaced by a 1 g/L BSA solution. This solution was recirculated for 20 min at 0.4 bar. Setup and module were rinsed with buffer and

buffer permeability was determined again. The fouling resistance was calculated according to Eq. 12.

Membrane bioreactor extracts

Due to the low amounts of EPS and SMP available and high material demand of the test, only one pristine and one modified module were used. The setup was filled with PBS buffer and cross-flow velocity was adjusted to 103 mL/min (Re = 3700). Permeate flux was set to 4.25 mL/min by adjusting the pressure clamp and pump speed, keeping the cross-flow velocity constant. Solutions with concentrations of 10 mg/L EPS or 40 mg/L SMP in PBS (pH 7.4) were used as feed. The filtration was carried out for 80 min. PBS flux was measured for 10 min before and after the fouling test. During the fouling test, permeate flux was measured every 10 min for 5 min in the first 30 min and subsequently every 15 min.

After this the cross-flow velocity was doubled (Re = 7400) and the module was rinsed with PBS for 5 min with the pressure clamp open (i.e. lowest TMP). After this simple cleaning step the permeability was determined again.

A chemical cleaning step was performed by back flushing the module with 150 mL 50 mM NaOH solution at a pump rate of 6 rpm and a pressure of 0.5 (± 0.05) bar. After this the feed side was rinsed with 750 mL of the same NaOH in the opposite direction of the cross-flow at 200 rpm with an open pressure clamp. Finally, the module was rinsed with water and permeability was measured again.

Flower soil extract

Flower soil fouling was investigated in cross-flow and dead-end mode in the small lab scale modules.

The pump rates were set to the lower limit for both modules to generate a water permeate flux of 5 mL/min in dead-end mode. The pump rates were 5 rpm and 0.4 rpm for the modified and pristine module respectively. A feed solution containing 20 mg/L TOC was then filtered in dead-end mode. The TMP was monitored for a filtration time of 2 h. After 1 h samples were collected to determine TOC rejection according to Eq. 13. Pure water permeability was measured before and after the test to determine the fouling resistance according to Eq. 12.

In cross-flow operation, a permeate flux of 20 mL/min (300 L/hm²) pure water was set. The needed TMP was maintained during the filtration experiment. A feed solution with 250 (± 10) mg/L TOC was recirculated for 20 h at this pressure. In the end samples of permeate and retentate were collected for TOC determination. TOC rejection was calculated according to

Eq. 13. Pure water permeability was measured two times before and after the fouling test and the fouling resistance was calculated from the average values according to Eq. 12.

4.6.4 Experiments with automated filtration unit for five fibre modules

The medium lab scale modules used in this section contained five multibore fibres with a length of 20 cm featuring a membrane surface area of 0.02 m². All modules used here contained membranes from the same batch.

A Poseidon inspector filtration unit (Convergence, Netherlands) was used to evaluate long term stability and fouling resistance during multiple application cycles. A simplified flow sheet of the main components is shown in Figure 4-22.

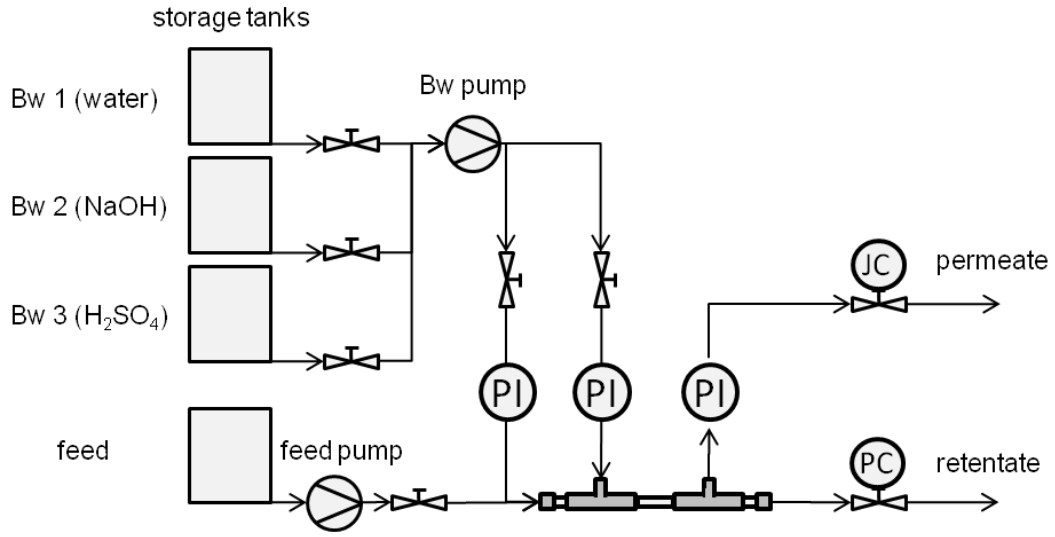

Figure 4-22 Simplified flow sheet of the automated filtration unit.

Briefly, the setup consisted of two separate pumps (Bw and feed pump), a pressure control (PC) at the retentate side and a flux control (JC) at the permeate side. The setup could be operated in dead-end, as well as cross-flow mode. Furthermore, the back wash pump could be used to back wash with chemicals from three different tanks. Every back wash step in this section was carried out with a flux of 100 mL/min unless stated otherwise.

A standard chemical enhanced backwash (CEB) cycle consisted of cleaning steps with NaOH and H_2SO_4 (both 30 mM). The sequence was 3 min backwash with NaOH, 15 min soaking with NaOH, 3 min backwash with tap water, 3 min backwash with H_2SO_4, 15 min soaking with H_2SO_4 and 3 min backwash with tap water.

4.6.4.1 Flower soil fouling in cross-flow mode

Fouling tests in cross-flow mode were performed to evaluate the influence of turbulence on the fouling behaviour.

First the flux through the membrane was increased stepwise in order to determine the “critical-flux”, where enough fouling occurs to be detected within short time (i.e. 8 h). Feed stream velocity was kept constant at 542 mL/min by the two pumps of the filtration unit (feed pump 249 mL/min and back-wash pump 293 mL/min). On the concentrate side a valve decreased the concentrate flux stepwise to adjust permeate flux from 22 mL/min to 33 mL/min in 1.7 mL steps every 15 min. For a flux of 19.8 ml/min (59.4 L/hm²) a detectable fouling expressed as increase in TMP occurred. This flux was then used for all subsequent tests with a newly modified and a pristine module. TMP was constantly recorded and samples of permeate and retentate were collected for TOC analysis.

4.6.4.2 Flower soil fouling in dead-end mode

The experiments with lab scale modules were performed in cross-flow mode (cf. Chapter 4.6.3.4) to provide a better comparability to the turbulent conditions in the stirred cells (cf. Chapter 4.5.3.3). In real treatment of surface water, cross-flow operation is usually too costly a measure of fouling control. A more efficient and the typical operation mode is dead-end filtration and the use of a coagulant to remove foulants from the feed[27]. The modification, which performed best in all preliminary tests on flat sheets was tested in a standard test, usually applied by Inge to all newly developed membranes:

A feed solution containing 0.003 g/L organics was prepared by diluting the stock solution of flower soil extract (cf. Chapter 4.5.3.3). The absorbance at 287 nm was then measured and concentrate or water were added until absorbance was 0.275. A feed stream of 25 mL/min was maintained using the feed pump. The retentate valve was closed so that the permeate stream was equal to the feed stream. The resulting TMP was constantly measured. A backwash step with tap water was carried out every 20 min. Once the TMP reached 0.8 bar, a CEB was carried out. The procedure was repeated four times and cycle duration was monitored as a measure for fouling resistance. A standard module was always running the same sequence on a second setup with the same feed for comparison.

4.6.4.3 Long term chemical stability

To evaluate long term stability, 22 CEB cycles were carried out. Each cycle was followed by a 10 min measurement of water permeability as measure for grafting integrity. Due to the limited

number of available modules, the test was conducted with modules that were used for flower soil fouling experiments before. A module modified with 0.25 M SPP DC 6.7 and a pristine module were used.

4.6.5 Scale up to pilot modules

The modification was also applied to 1.4 m five fibre pilot scale modules with a surface area of 1400 cm². Since the pumps were not capable to deliver high enough fluxes to achieve identical filtration conditions during initiator immobilization, some adaptations had to be made. To make the conditions as comparable as possible, the highest possible pump rate of 300 rpm was set. The TMP was then adjusted to achieve the same flux to linear velocity ratio like in the lab scale modules. The modules were equilibrated in the solvent mixture (20 % *iso*-propanol, 10 mM HCl) for 3 hours. 1 L of a 1 g/L initiator solution was then filtered at 0.3 bar and a linear velocity of 22 cm/s (with recirculation of retentate and permeate). The subsequent modification procedure was identical to the modification of lab scale modules (cf. Chapter 4.6.2), using a 0.25 M SPP solution with a DC of 6.7. All other factors were identical to the conditions used for lab scale modification. 100 mL of modification solution were needed to fill the lumen side of the pilot scale modules completely.

Pure water permeability was determined before and after the modification procedure as an indicator for successful grafting. Two modules were then run by Inge/BASF in a pilot plant treating a mixtures of municipal waste water and river water, in order to be compared with standard modules. The content of waste water was slowly increased from 20 % (2 weeks operation). The first steps were to 25 % waste water and 30 % (each after 1 week operation) and then in 10 % steps every week. The final feed contained 60 % waste water. The long term experiment will be finished in 10/2016 and will be concluded by a membrane autopsy.

5 Results

5.1 Synthesis of bulk hydrogels

To find optimum conditions for bulk hydrogel preparation, different compositions were tested. NaCl was added to evaluate possible influence on the reactivity of the ionic monomers. Table 5-1 shows the tested compositions.

Table 5-1 Preparation of bulk gels from 1:1 mixture of AATAC and AAMPSA (0.8 M total monomer, DC 6.7)

NaCl [mmol/L]	APS [mmol/L]	TMED [mmol/L]	Gelation time
0	7.5	30	> 7 d
100	7.5	30	> 7 d
200	7.5	30	> 7 d
0	30	30	> 7 d
100	30	30	> 7 d
200	30	30	> 7 d
0	30	120	< 1 min
100	30	120	< 1 min
200	30	120	< 1 min
0	7.5	120	< 1 min

Solutions with 7.5 mmol/L persulfate and 30 mmol/L TMED were not gelating within one week. Increasing the persulfate concentration brought no increase in gelation speed, while increasing the TMED concentration led to gelation within one minute. An effect of salt concentration on gelation time was not detected. Similar starting conditions were used for SPP (Table 5-2).

Table 5-2 Preparation of bulk gels from SPP with 0.8 M monomer content and DC 6.7 (no NaCl added)

APS [mmol/L]	TMED [mmol/L]	Gelation time
7.5	30	< 1 min

The zwitterionic SPP solution did gelate much faster than the mixtures of anionic and cationic monomers. Also a much lower TMED concentration was needed here.

The conversion was determined by TOC to be 80 (± 1) % for AATAC/AAMPSA samples and 87 (± 1) % for the SPP DC 6.7 sample. The compositions of the bulk hydrogels prepared from a 1:1 (mol:mol) mixture of AATAC and AAMPSA are given in Table 5-3.

Table 5-3 N/S ratio determined by elemental analysis compared to theoretical values of different AATAC/AAMPSA ratios (assuming complete incorporation of MBAA

AATAC/AAMPSA monomer [mol/mol]	N/S [-]
1 (0 mM NaCl)	1.4
1 (200 mM NaCl)	1.5
2 (theor.)	2.4
1 (theor.)	1.4
0.5 (theor.)	0.7

The N/S ratio of the samples containing 200 mM NaCL was slightly higher than without NaCl. However both samples have N/S ratios very close to the expected ratio for similar reactivity (1.4).

Swelling experiments were performed to rate the homogeneity of charge distribution especially in the anionic/cationic copolymers. The results are given in Figure 5-1.

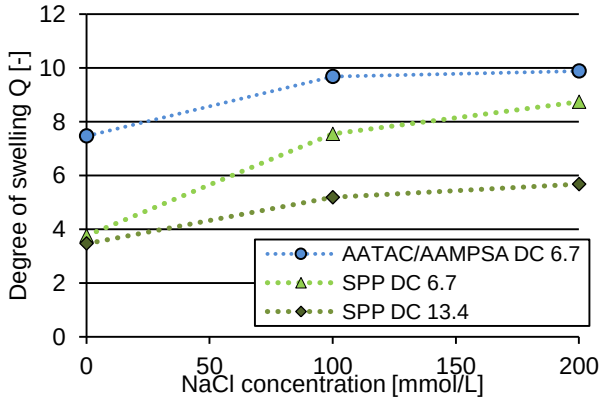

Figure 5-1 Degree of swelling in dependency of NaCl concentration for bulk hydrogels with different composition.

The swelling in the absence of salt was about two times higher for the AATAC/AAMPSA hydrogel than for both SPP based hydrogels. Both bulk hydrogels showed higher swelling at increased salt concentrations. The increase in swelling was stronger for the SPP hydrogel. At the highest salt concentration the swelling degree was almost similar to the swelling degree of AATAC/AMMPSA (8.7 and 9.9). With increased cross-linker content the degree of swelling was lower but still increased upon addition of salt. Interestingly at the absence of salt, both SPP hydrogels showed a similar swelling degree, independent of the DC.

5.2 Macromolecular initiator systems

5.2.1 General characterization

5.2.1.1 Redox co-initiator

In the following section, results for the different redox co-initiators are discussed. Four different co-initiators with BMA:DMAEMA ratios of 1:1 to 4:1 were prepared. In cases where quantitative relations are shown, the ratio is usually given directly as a number. In more complex figures, identifiers were used. The identifiers start with MB followed by two digits giving the ratio of DMAEMA to BMA. For example MB12 means a polymer with a ratio of DMAEMA to BMA of 1:2 and so on.

Nuclear magnetic resonance

The reaction yield was determined gravimetrically to be 60 (± 10) % for all BMA/DMAEMA ratios. ^{1}H-NMR was used to analyze the composition of the macromolecular redox co-initiators. The so determined ratios of monomer units in the polymers versus their ratio in the prepared educt mixture are given in Table 5-4.

Table 5-4 Ratio of monomer units derived from ^{1}H-NMR

Relation BMA:DMAEMA	^{1}H-NMR ratio BMA:DMAEMA [-]	Error [-]
1:1	1.1	0.02
2:1	2.05	
3:1	2.96	0.04
4:1	3.95	0.05

At low relative BMA contents (1:1 and 2:1), slightly more BMA was incorporated in the polymer. When increasing the BMA content in the educt mixture, the BMA content in the polymer was slightly lower in relation to the expected values (2,96 and 3,95 for 3:1 and 4:1). However this effect was low in relation to the given error.

Size exclusion chromatography

SEC was used to determine the MW of the initiators; the results are given in Table 5-5.

Table 5-5 Weight average MW determined by SEC using RI/viscosity dual detector with universal calibration

BMA:DMAEMA	[AIBN](mmol/L)	M_w [kDa]	PDI
1:1	25	42	2
2:1	25	157	3.1
3:1	25	62	2.1
2:1	6.25	344	2.2

The weight average molecular masses showed a broad variety. The first three rows in Table 5-5 show the results for polymers synthesized with higher initiator content. Except for the polymer with a BMA:DMAEMA ratio of 2:1, the polymers comprised narrow PDIs slightly above 2 and weight average molecular masses of 40 to 60 kDa. Both PDI and molecular weight were significantly higher for the polymer synthesized with a monomer ratio of 2:1 and high initiator content. By reducing the initiator content by a factor of 4, the molecular weight could be increased, maintaining a low PDI. The so synthesized copolymer with an M_w of 344 kDa was used for all membrane modifications.

Elemental analysis

Te elemental compositions determined by elemental analysis are summarized in Table 5-6.

Table 5-6 Elemental composition determined by elemental analysis of synthesized macromolecules

Relation BMA:DMAEMA	C [%]	H [%]	N [%]	O [%]
1:1	64.4	9.8	4.8	21.4
2:1	65.5	9.7	3	21.8
3:1	67.9	10.4	3	18.7
4:1	65.6	9.8	2.7	21.9

For comparison the theoretical values for similar reactivity or 100 % conversion were calculated and are given in Table 5-7.

Table 5-7 Elemental composition of p-BMA-co-DMAEMA calculated for different monomer ratios

Relation BMA:DMAEMA	C [%]	H [%]	N [%]	O [%]
1:1	64	10.1	4.7	21.3
2:1	65.1	10	3.2	21.7
3:1	65.7	10	2.4	21.9
4:1	66.1	9.8	1.9	22

Since only the DMAEMA monomer unit contains N, the theoretical N content was decreasing with increasing amount of BMA. The determined N contents (Table 5-6) were decreasing as well. However this decrease was not as pronounced as expected. Overall an increase in C content would be expected with decreasing the DMAEMA content. The H and O content should

stay similar. Roughly the measured compositions followed the same trend as the calculated values. The only exception was the polymer with a ratio of 3:1. Here the O content was lower (18.7 % instead of 21.9 %), while all other values were higher than expected.

IR spectrum

The IR spectrum of the redox co-initiator used for membrane modification (MB12) is given in Figure 5-2.

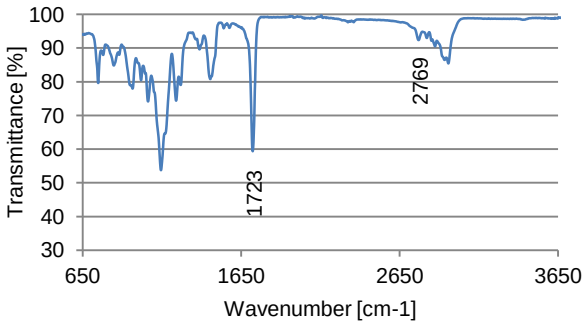

Figure 5-2 ATR-IR spectrum of MB12.

Two important bands were found in the spectrum. The absorption at 1723 cm^{-1} can be attributed to C=O in the ester groups along the polymer backbone (cf. Figure 3-5). The band at 2769 cm^{-1} can be attributed to C-H in R_2NCH_3 of the DMAEMA group[139].

5.2.1.2 Azo based thermal initiator

Due to the poor solubility of azo modified pSMA in polar und unpolar NMR solvents, only low peak intensities could be achieved in the spectrum (Appendix Figure 11-3). A quantification of the modification based on NMR was thus not possible.

Size exclusion chromatography

The changes in molecular weight due to hydrolysis and modification were monitored by SEC, the results are given in Table 5-8.

Table 5-8 Weight average MW of pSMA before and after azo modification and hydrolysis determined by SEC using PMMA calibrated RI detector and universal calibration with RI/viscosity dual detector.

Evaluation	Polymer	M_W [kDa]	PDI
Universal calibration	pSMA	108 (± 12)	2.2 (± 0.2)
	pSMA hydrolysed	149	1.8
	azo modified pSMA	110	2.0
RI with PMMA calibration	pSMA	118 (± 17)	2.0 (± 0.03)
	pSMA hydrolysed	149	1.8
	azo modified pSMA	110	2.0

M_w given by the manufacturer for pSMA was 120 kDa with a PDI of 2. The average of two performed measurements was quite close to these values for both calibrations. Evaluation with the universal calibration gave a slightly lower M_w and higher PDI. For the hydrolyzed and azo modified polymers both evaluation methods delivered similar results. By just hydrolysing the polymer, the M_w increased while the PDI was decreased. The azo modification (also including a hydrolysis step) did not change the M_w or PDI significantly compared to the given deviations from the two pSMA measurements.

Elemental analysis

Due to the mentioned problems to determine modification degree from NMR, EA was the most important analysis for the azo based thermal initiator. The data is given in Table 5-9 in direct c

Table 5-9

Table 5-9 EA data of unmodified, hydrolysed and azo-modified pSMA compared to theoretical values

	C [%]	H [%]	N [%]	O [%]	Σ
pSMA	79.1	6.1	0	12.7	97.9
theoretical	81.4	6.28	0	12.32	100
pSMA-hydrolysed	68.3	6.3	0	19.4	94
exp. 100 % hydrolysis	77.95	6.54	0	15.52	100
azo modified pSMA	64.3	6.4	0.9	20.3	91.9
exp. 10 % modif.	77.47	6.43	1.3	14.81	100

The values determined for the pSMA as purchased were very similar to the theoretical values. After hydrolysis and after azo modification, the determined oxygen content was significantly higher than the expected values. The determined carbon content was lower than the calculated values in both cases and the N content was lower for the azo modified polymer than expected for a modification of 10 % of the MA groups. Also the total composition must have contained other elements than C, H, N and O since the sum is only 94 % for the hydrolysed and 92 % for the modified polymer.

UV-Vis spectroscopy

The UV-Vis spectra of azo modified and hydrolysed pSMA are given in Figure 5-3 (right). For comparison the UV-Vis spectrum of azo-benzyl alcohol is given on the left side.

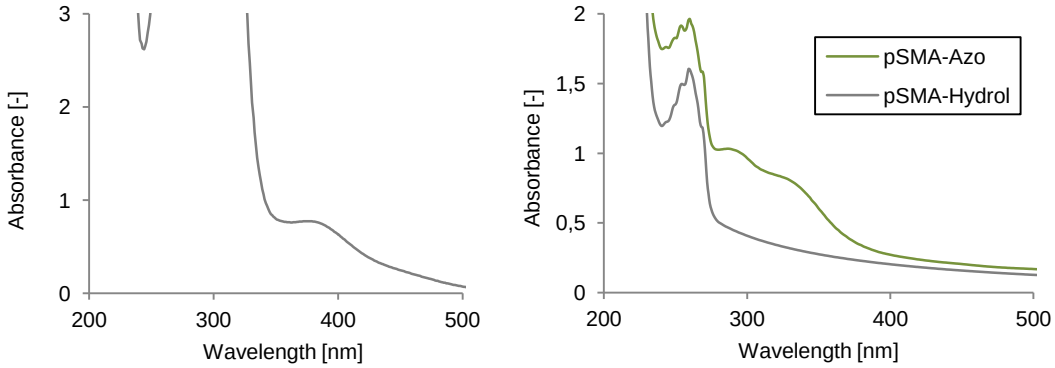

Figure 5-3 UV-VIS spectra of 0.5 g/L azo-benzyl alcohol (left) in water and 1 g/L modified and hydrolysed pSMA (right).

The spectrum of azo-benzyl alcohol showed a strong absorption (ε>4000 L mol^{-1} cm^{-1}) in the range of 270 nm to 300 nm. For an isolated azo group in cis configuration, an n → π* would be expected at λ_{max} = 353 nm with ε = 240[139]. In the conjugated azo-benzyl alcohol however a much stronger absorption can be found at λ_{max} = 289 nm with ε = 14000[93]. Comparing the spectra of modified and hydrolysed pSMA (Figure 5-3 right), additional bands at 290 nm and 330 nm occurred in azo-pSMA.

Infrared spectra

The IR spectra of pSMA before and after hydrolysis and after modification are shown in Figure 5-4.

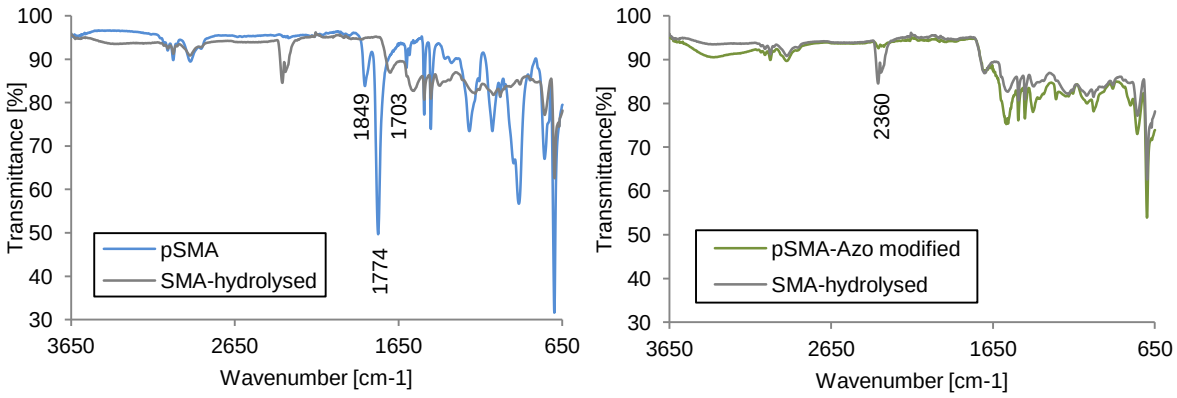

Figure 5-4 ATR-IR spectra of original pSMA (left) and azo modified pSMA (right) compared to spectra of hydrolysed pSMA.

Comparing the IR spectra of pSMA before and after hydrolysis (Figure 5-4 left) the characteristic dual band for anhydrides (1774 and 1849 cm-1) disappeared upon hydrolysis and a new band for carboxylic acids (1703 cm^{-1}) occurred. Comparing the spectra for azo modified and hydrolysed pSMA (Figure 5-4 right) no significant changes were detected. The disappearing band at 2360 cm^{-1} can be attributed to interfering CO_2[139].

5.2.1.3 Peroxide based thermal initiator

Nuclear magnetic resonance

The degree of modification of the MA groups in pSMA was determined from NMR spectra (spectra can be found in the appendix Figure 11-4 and Figure 11-5). The results for peroxide modified pSMA are given in Table 5-10.

Table 5-10 Degree of peroxide modification determined from ^{1}H-NMR.

Modification	Modified MA groups [% mol]	Deviation [%]
^{t}Bu-OO-pSMA	36	1
Cumyl-OO-pSMA	72	20

The presented values are average values of three manual integrations with the resulting deviation. In ^{t}Bu-OO-pSMA, 36 % of the maleic anhydride groups were modified. The deviation of the evaluation was 1 %. The determined degree of modification was higher (72 %) for the cumyl modification but also with a high deviation of 20 %.

Size exclusion chromatography

SEC was performed with the peroxide modified pSMA. Also the unmodified pSMA was measured once more for comparison (cf. Table 5-9). The determined MW are given in Table 5-11.

Table 5-11 MW of SEC for pristine and peroxide modified pSMA.

Evaluation	Polymer	Mw [kDa]	PDI
Universal calibration	pSMA	123	2.5
	tBu-OO-pSMA	223	2.3
	Cumyl-OO-pSMA	313	2.4
RI with PMMA calibration	pSMA	124	2.1
	tBu-OO-pSMA	114	1.9
	Cumyl-OO-pSMA	140	2

The M_w determined for the base polymer was still very close to the 120 kDa provided by the manufacturer. However the PDI was higher in case of the universal calibration (2.5 instead of

2.03 cf. Table 5-9). The evaluation by mere retention time (RI with PMMA) still delivered a similarly low PDI.

Both modifications increased the determined MW by universal calibration. The MW after cumyl peroxide based modification was 2.5 times higher, while the determined value after ^{t}Bu peroxide based modification was 1.8 times higher than those for the base polymer.

The MW determined using the PMMA calibration was slightly decreased after modification with ^{t}Bu hydroperoxide, while modification with the cumyl hydroperoxide slightly increased the apparent M_w. In both cases the PDI was relatively unchanged compared to the base polymer.

Elemental analysis

The data from EA of the peroxide modified and unmodified pSMA compared to theoretical values are summarized in Table 5-12.

Table 5-12 Elemental analysis of peroxide modified and unmodified pSMA compared to theoretical values

	C	H	N	O	Σ
pSMA	81.1	6.22	0	12.55	99.87
Theoretical	81.4	6.28	0	12.32	100
^{t}Bu-OO-pSMA	80.55	6.20	0	13.15	99.9
exp. 100 %	77.95	6.54	0	15.52	100
exp. 50 %	77.04	6.91	0	16.05	100
exp. 0 %	76.26	7.23	0	16.51	100
Cumyl-OO-pSMA	69.90	7.50	1.41	16.35	95.16
exp. 100 %	77.95	6.54	0	15.52	100
exp. 50 %	77.89	6.42	0	15.69	100
exp. 0 %	77.85	6.33	0	15.82	100

The composition of pSMA was measured again for reference. Compared to the previously shown data (cf. Table 5-9) the contents in H and O only varied around 0.1 %. The determined C content was slightly (1 %) higher. For both modifications, the determined compositions were well out of the region of the expected values for either 100 % modification or no modification at all. Also for the cumyl modified polymer, traces of N were detected.

IR spectra

The ATR-IR spectra of ^{t}Bu-OO-pSMA and cumyl-OO-pSMA are shown in comparison to the spectra of the base polymer in Fig. 5-5.

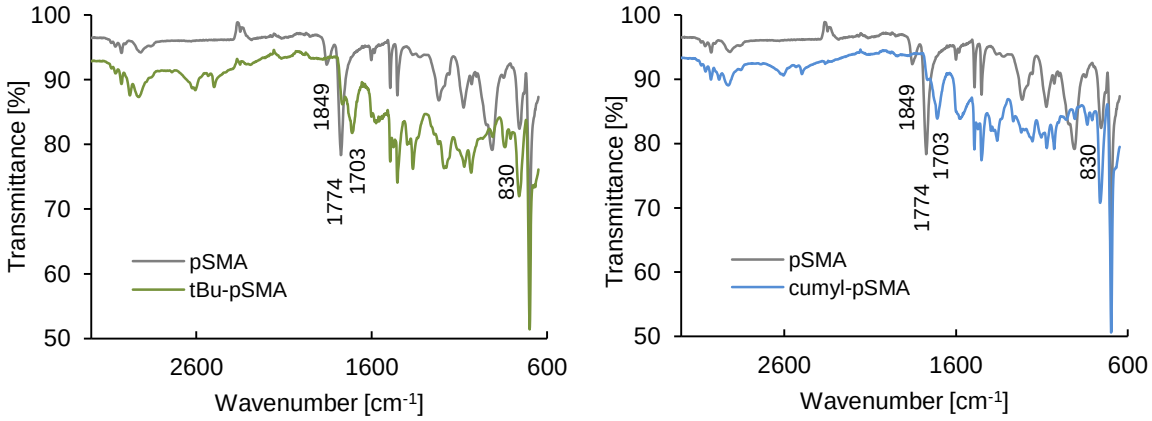

Figure 5-5 ATR-IR spectra of original, ^{t}Bu-OO-H modified (left) and cumyl-OO-H modified (right) pSMA.

A similar change like in Figure 5-4 (left) was observed in both spectra due to the hydrolysis of MA groups. Another change was a new occurring band at 830 nm in both spectra. In the same area often asymmetrical stretching of peroxide bonds occurs in organic peroxides[140].

5.2.2 Colloidal properties

5.2.2.1 Redox co-initiator

Critical water content

The CWC for 1 g/L solutions of redox co-initiators with different BMA:DMAEMA ratios in ethanol and *iso*-propanol is given in Figure 5-6.

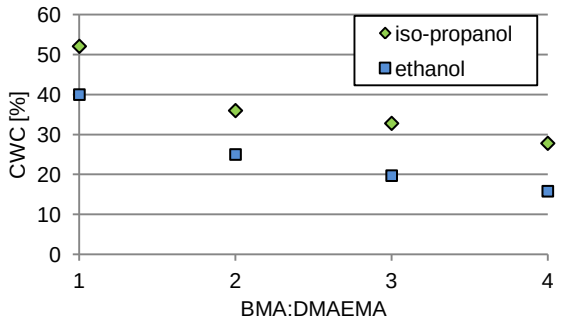

Figure 5-6 Critical water content for solutions of 1 g/L of macromolecules with different BMA:DMAEMA ratios in *iso*-propanol and ethanol (determined by optical transmittance).

With increasing amount of BMA in the macromolecules, the CWC was reduced. The tolerated amount of water before agglomerates were formed was 10 % higher for solutions in *iso*-propanol over the whole range of BMA:DMAEMA ratios. The strongest decrease in CWC was observed upon increase in the BMA:DMAEMA ratio from 1:1 to 1:2. When adding a small amount (5 – 10 mmol/L) of HCl to the alcohol first, any amount of water could be added without causing turbidity.

Critical micelle concentration

The CMC of redox co-initiators with different BMA:DMAEMA ratios is shown in Figure 5-7.

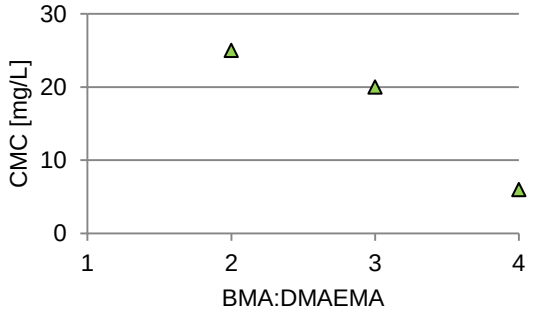

Figure 5-7 Critical micelle concentration for solutions of polymers with different BMA:DMAEMA ratios in 20 % 2-propanol containing 10 mmol/L HCl (determined by pyrene method).

No CMC could be determined for a BMA:DMAEMA ratio of 1:1 since no shift in the fluorescence intensities was detected. For the other ratios, a decreasing CMC (25 mg/L to 6 mg/L) was observed; when increasing the BMA content.

5.2.2.2 Azo based thermal initiator

Azo modified pSMA was soluble in water up to concentrations of 26 g/L and no CWC could be determined.

The determined CMC for hydrolysed and azo modified pSMA is given in Figure 5-8.

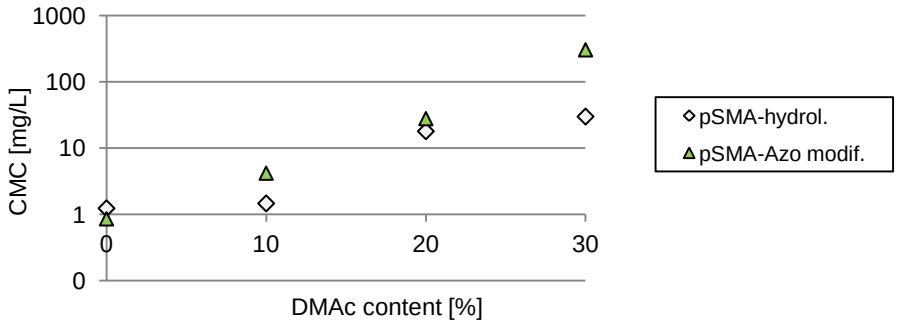

Figure 5-8 Critical micelle concentration of hydrolysed and azo modified pSMA depending on the content of DMAc.

The CMC showed an increase for both polymers, when increasing the DMAc content of the solution. The CMC of the hydrolysed polymer ranged from 1.2 mg/L in pure water to 30 mg/L with 30 % DMAc. The CMC of the azo modified polymer increased nearly exponentially ($R^2 = 0.99$) in the observed range, starting at 0.9 mg/L in water to 300 mg/L with 30 % DMAc content.

5.2.2.3 Peroxide based thermal macro initiator

Peroxide modified pSMA polymers were less soluble than azo modified. However, by first dissolving in DMAc and diluting with 100 mM NaOH solution, the polymers could be well dissolved. The CMC in these solutions is given in Table 5-13.

Table 5-13 CMC of hydroperoxide macro initiators in 100 mM NaOH containing 2 % DMAc

Macro initiator	CMC [mg/L]
^{t}Bu-OO-pSMA	5.6
Cumyl-OO-pSMA	34

The CMCs for both modified polymers were significantly different, with the cumyl peroxide modified pSMA showing a CMC more than 5 times higher than the ^{t}Bu peroxide modified pSMA.

5.2.3 Adsorption behaviour

The adsorption to PES model surfaces was surveyed to find best suited conditions for membrane modification. The standard test SPR was performed for all initiators. Since ellipsometry turned out to be difficult with the surveyed layer systems, it was only applied to analyse the redox and azo based initiators. QCM was only used later in the project to deliver supporting data for the redox co-initiator, since this was the initiator used for actual membrane modification.

5.2.3.1 Redox co-initiator

Surface plasmon resonance

Two exemplary time plots of the resonance angle during SPR experiments are shown in Figure 5-9.

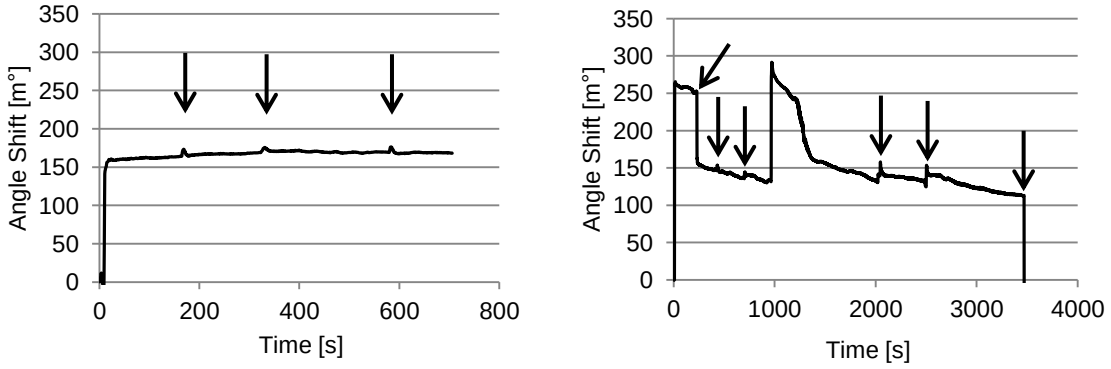

Figure 5-9 Angle shift during SPR experiment with 5 g/L MB13 (left) and 5 g/L MB11 (right) in IPA/water pH 3 starting with sample injection followed by washing steps with pure solvent indicated by arrows.

The typical behaviour is shown in Figure 5-9 (left). The data are displayed, starting with initiator injection at t=0 and multiple washing steps with background solution indicated by peaks. The angle shift achieved a stable value after some time and did not return to its initial value upon washing. MB11 (Figure 5-9 right) did not show the same behaviour. Here no stabilization was achieved and the angle did change abruptly upon washing with a tendency to decrease. Finally the angle dropped to its original baseline value. The average angle shifts of 3 measurements per initiator were calculated after three washing steps. The results are given in Figure 5-10.

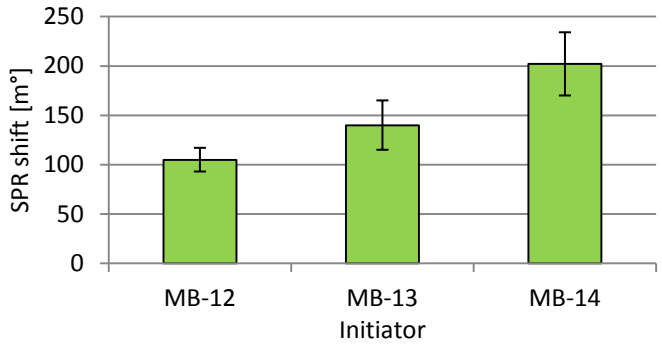

Figure 5-10 Average angle shift by adsorption of macromolecules with different BMA content 5 g/L in IPA/water pH 3.

The average angle shift as was increasing with increasing amount of BMA, ranging from 100 m° to 200 m°.

Quartz crystal microbalance

The frequency development during the QCM experiments and the derived adsorbed masses of redox co-initiator are summarized in Figure 5-11.

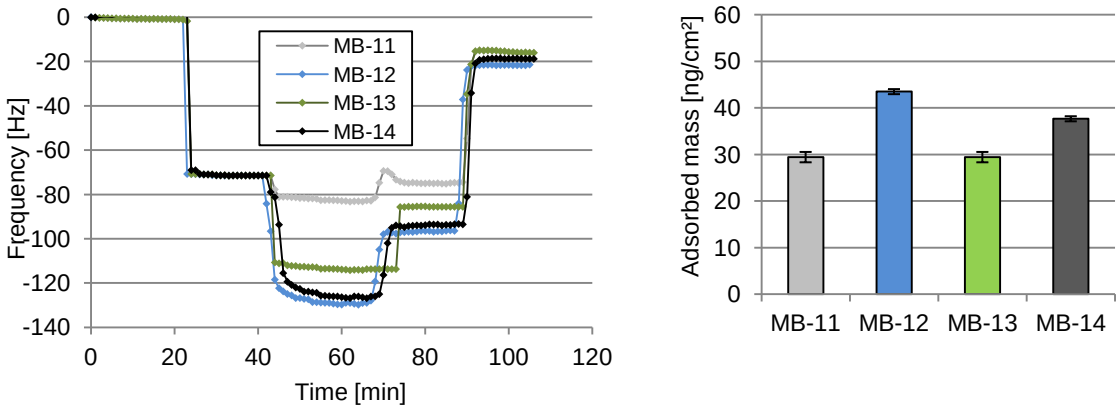

Figure 5-11 QCM frequency change due to adsorption of macro co-initiators; water, solvent mixture, sample solution (1 g/L), solvent, water.

In the strongest frequency shift (Figure 5-11 left) occurred, when water was exchanged for the background solution containing 20 % *iso*-propanol and 10 mmol/L HCL. The adsorption of MB-12 and MB-14 led to the most pronounced shifts in frequency during adsorption. For both the

onset was fast, indicated by a steep slope of the curve. After that the adsorption was slower. Adsorption and saturation occurred within the next 7 min. After changing back to pure background solution, both curves showed some extend of desorption within approx. 5 min. About half of the frequency change was irreversible. The response for MB-13 was less pronounced and occurred with steeper slopes. The general trend however was similar. The lowest response was observed for MB-11 and in this case the frequency almost returned to its initial value in background solution.

From the frequency changes between the two measurements in water at the beginning and at the end, the adsorbed mass was determined and is given in Figure 5-11 (right). The adsorbed mass was relatively equal (30 – 42 mg/cm²) for all macromolecules with no recognizable correlation.

Layer thickness by ellipsometry

The apparent layer thicknesses determined by ellipsometry are given in Table 5-14. Each measurement was performed on two separate chips. First, refractive index and layer thickness of the adsorbed initiator layer were both fitted freely, starting from different assumed layer thicknesses (0 nm, 100 nm and 1000 nm). Only physically reasonable solutions where accepted (i.e. no negative refractive index and layer thicknesses $0 \leq d \leq 10000$ nm). When using the model to determine both refractive index and layer thickness from the collected data, these criteria could not be met in any attempt. Therefore the refractive index curve was fixed to values taken from the software database (assuming n should be comparable to poly methyl methacrylate[141]). The fitting quality was rated based on the correlation of calculated and determined Δ and Ψ trajectories. A good fitting was achieved when the calculated Δ and Ψ correlate with the measured values. An average rating was achieved, when Δ or Ψ were deviating. A poor rating was achieved when Δ and Ψ were deviating. Typical comparisons of measured and calculated trajectories are shown in Figure 5-12.

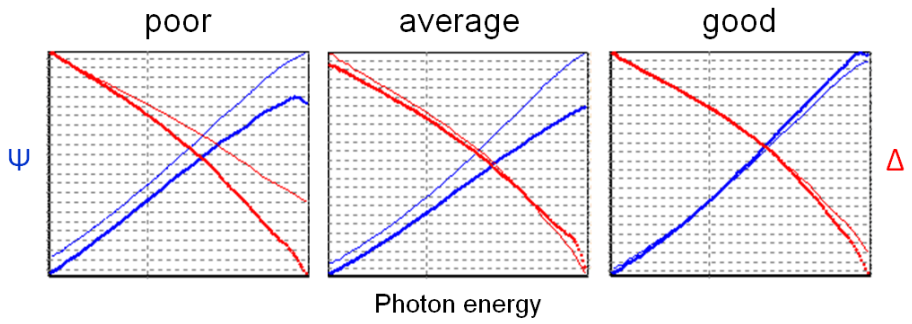

Figure 5-12 Fitting curves for Ψ and Δ, bold lines represent measured and thin lines represent calculated values, photon energy 1.5 to 2.9 eV, typical Ψ values 20 to 47 °, Δ values 40 to 96 °.

Table 5-14 Layer thickness of redox co initiator on PES spin coated Si wafers

Initiator	Thickness [nm]	Fitting
MB-11	15.4	poor
MB-11	2.5	average
MB-12	5.5	good
MB-12	n.d.	not possible
MB-13	3.1	average
MB-13	0	average
MB-14	1.9	good
MB-14	12.8	average

The determined thicknesses varied from 1.9 nm to 15.4 nm. The two best fittings indicated layer thicknesses of 1.9 and 5.5 nm. The mean layer thickness derived from all average and good fittings, weighing the good fittings twice, was 4.2 (± 2.8) nm.

5.2.3.2 Azo based thermal initiator

Surface plasmon resonance

Two SPR runs were performed with pSMA-azo. The results are given in Figure 5-13.

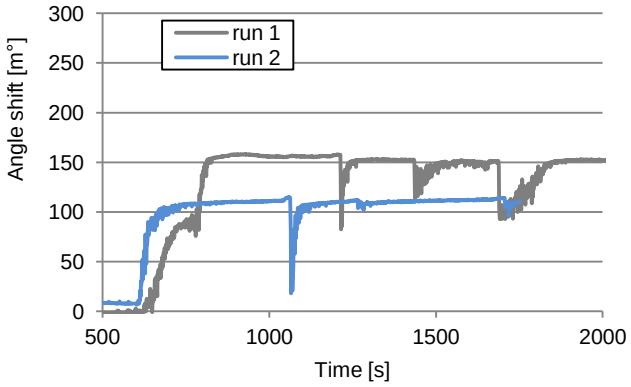

Figure 5-13 Angle shift during surface plasmon resonance experiment with 1 g/L pSMA-azo in 20 % DMAc/water. First positive slope indicates the samples injection, drops indicate the washing steps.

In both runs, a steady angle shift occurred within 220 s. The polymer was not removed from the surface during the subsequent washing steps (washing steps are indicated by dents in the curve). The average angle shift was 131 (± 21) m°.

Layer thickness by ellipsometry

For the ellipsometry evaluation of pSMA-azo modified PES films, similar specifications like for the redox co-initiator measurements were stated (cf. Chapter 5.2.3.1). The results are given in Table 5-15.

Table 5-15 Layer thickness determined by ellipsometry on PES spin coated Si wafers

Polymer	Concentration [g/L]	Solvent	Thickness [nm]	Fitting
pSMA hydrolysed	0.1	H_2O	n.d.	impossible
pSMA hydrolysed	0.1	H_2O	4.1	poor
pSMA hydrolysed	0.1	20 % DMAc	8.3	poor
pSMA hydrolysed	0.1	20 % DMAc	n.d.	impossible
pSMA hydrolysed	1	20 % DMAc	10.5	poor
pSMA hydrolysed	1	20 % DMAc	12.9	poor
pSMA-azo	1	H_2O	9.5	average
pSMA-azo	1	H_2O	n.d.	impossible
pSMA-azo	0.1	20 % DMAc	10.4	very poor
pSMA-azo	0.1	20 % DMAc	11.5	poor
pSMA-azo	1	20 % DMAc	9	poor
pSMA-azo	1	20 % DMAc	11.4	average

No good fitting could be achieved for the azo modified pSMA and hydrolysed pSMA. Due to the poor fitting quality, no tendencies could be derived. The average layer thicknesses (regardless of solvent or polymer content) were 9 (± 2.8) nm for hydrolysed pSMA and 10.4 (± 0.9) nm for pSMA-azo.

5.2.3.3 Peroxide based thermal initiator

Surface plasmon resonance

The resonance curves of SPR experiments with tBu-OO-pSMA and cumyl-OO-pSMA can be found in the appendix (11.2). The summarized angle shifts are given in Figure 5-14.

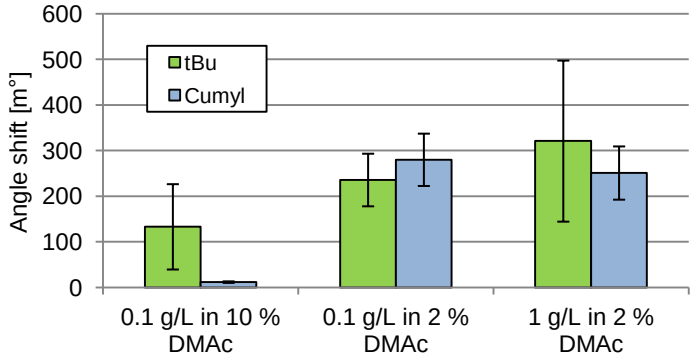

Figure 5-14 SPR angle shift as measure for adsorption of modified pSMA to PES model surfaces (30 nm dense film).

Only tBu-OO-pSMA showed significant angle changes in 10 % DMAc. Reducing the DMAc content to 2 %, the angle shift increased for both polymers. A further increase in polymer concentration did not lead to a significant increase in angle shift. The strongest deviation (± 50 %) was observed for a concentration of 1 g/L tBu-OO-pSMA in 2 % DMAc.

5.2.4 Initiator activity

5.2.4.1 Redox co-initiator

In situ rheology

In situ rheology was used for the determination of gel point. The gel point was determined as the intercept between storage and loss modulus. Exemplary raw data are given in Figure 5-15.

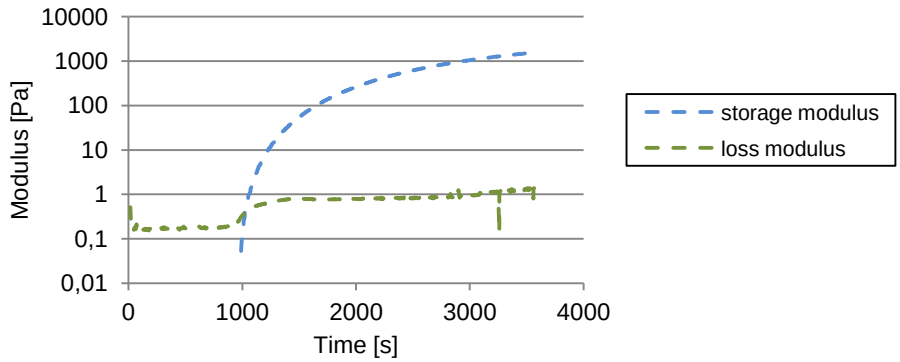

Figure 5-15 Typical storage and loss modulus curve for in situ rheology during gelation of SPP - here 0.56 M SPP DC 6.7 with 7.5 mM APS and 15 mM TMED (30 mM amine) as redox couple.

The combined data for different redox co-initiators at different pH are given in Figure 5-16. In case of the reference samples not containing tertiary amine co-initiator, no gelation occurred within twelve hours.

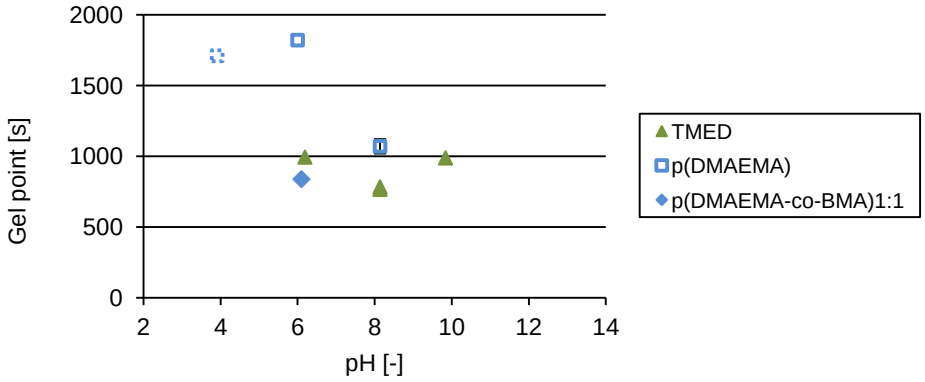

Figure 5-16 Gelation times for SPP solutions (0.56 M SPP DC 6.7) containing different polymeric and monomolecular tertiary amines (30 mM amine) as redox co-initiators and 7.5 mM APS.

The gelation time for the TMED – persulfate redox couple as initiator was low for a broad pH range (6 – 10). The polymerized DMAEMA showed comparable activity at pH 8, but gelation was slower at lower pH (4 – 6). At higher pH precipitates were forming. The gelation time at pH 4 was doubtful, since the detected storage modulus was very low (~4 Pa. cf. Figure 5-17). For TMED no gelation was detected at pH 5. The macromolecule with a BMA:DMAEMA ratio of

1:1 (MB-11) could only be dissolved to a pH up to 6. However at this pH it showed slightly faster gelation than TMED. The steady state storage moduli (i.e. the storage moduli of the formed gel at the end of the measurements) are plotted in dependence of pH in Figure 5-17.

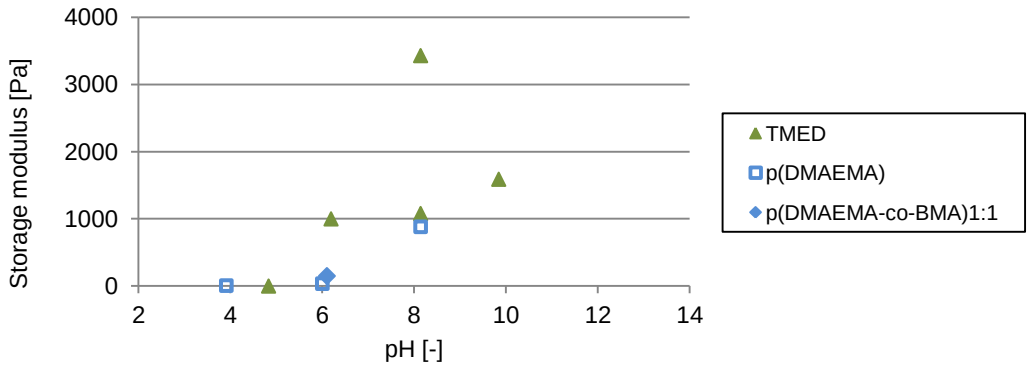

Figure 5-17 Storage modulus of the formed hydrogels at the end of the measurement.

The storage moduli increased with increasing pH. Very low storage moduli (< 6 Pa) were observed at pH < 6.

Additional tests were performed varying the temperature and the persulfate concentration. The results are given in Figure 5-18.

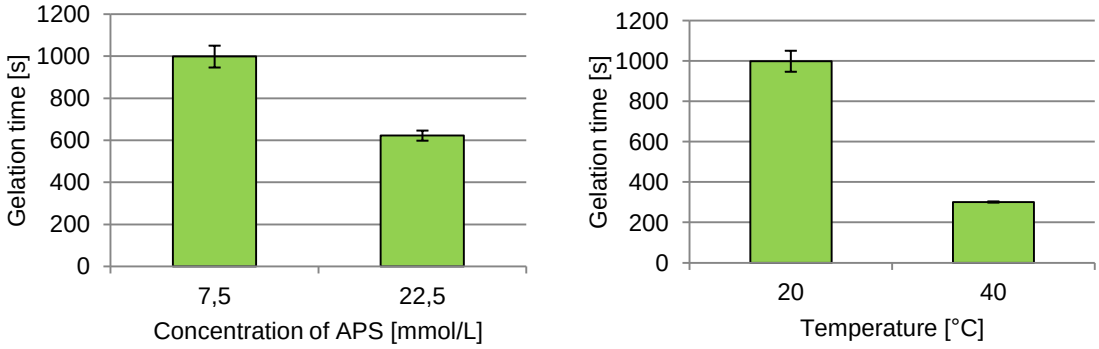

Figure 5-18 Dependency of the gelation time on the APS concentration (left, T = 20 °C) and the temperature (right, c(APS) = 7.5 mM), using MB-11 (30 mM amine) as co-initiator.

A three times increase in the persulfate concentration led to a 40 % lower gelation time (Figure 5-18 left). Increasing the temperature by 20 °C led to a 70 % decrease in gelation time (Figure 5-18 right).

5.2.4.2 Azo based thermal initiator

In situ rheology

No initiator activity could be found for the azo modified pSMA. A 0.56 M SPP DC 6.7 test solution containing 1 g/L of the polymer did not gelate within 75 min at 80 °C.

UV-Vis after thermal and UV exposure

Since no initiator activity could be detected during in situ rheology, UV-Vis spectra were recorded before and after heating. Since the synthesized azo group is known to be cleaved much faster by UV irradiation than by thermal energy[93], UV treatment was also applied for comparison. The results are shown in Figure 5-19.

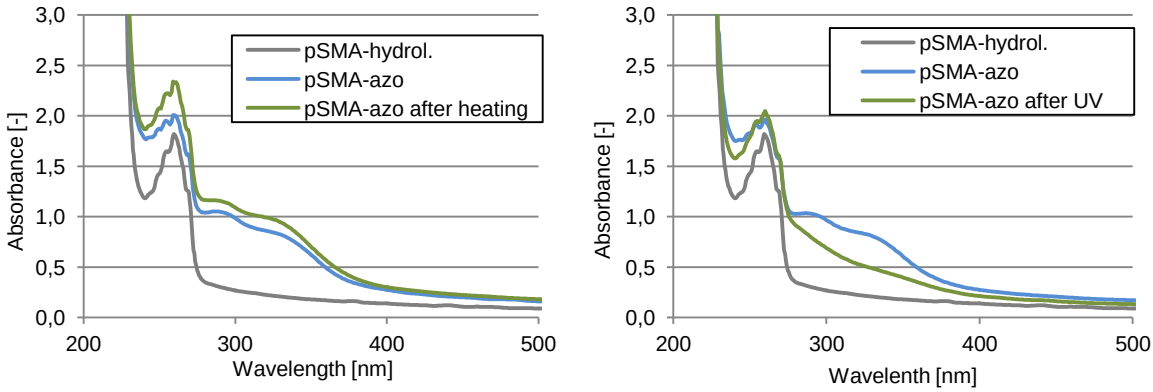

Figure 5-19 Change in UV-Vis spectra due to boiling (left, 285 min reflux in water) and UV irradiation (right, 40 mW/cm², 5 min).

Even after 285 min in boiling water (Figure 5-19 left), no change in the UV-Vis spectrum was detected. After 5 min UV treatment, the bands at λ = 290 nm and λ = 330 nm vanished.

5.2.4.3 Peroxide modified polymer as thermal initiator

In situ rheology

The gelation times determined by rheology at different temperatures with and without added macromolecular thermal initiators are summarized in Figure 5-20.

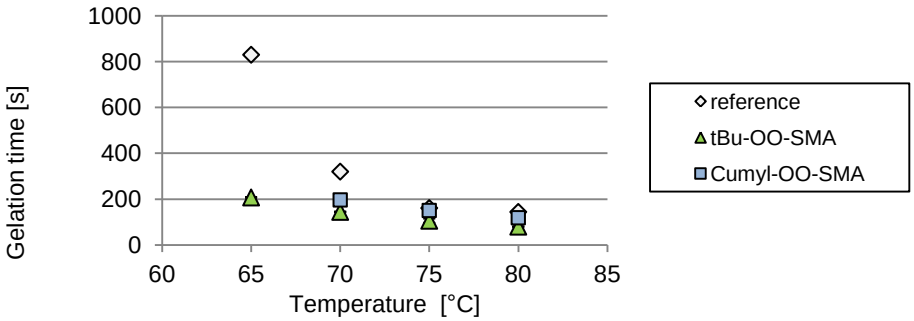

Figure 5-20 Gelation time vs. temperature for 0.56 M SPP DC 6.7 with and without peroxide modified polymer.

All solutions showed fast gelation (< 200 s) at 80 °C and 75 °C. The first significant difference in gelation time was observed at 70 °C. At this temperature gelation without thermal initiator took twice as long as with the ^{t}Bu-OO-pSMA thermal initiator. Gelation with the cumyl-OO-pSMA

initiator was 36 % slower than with ^{t}Bu-OO-pSMA. At 65 °C the gelation without initiator took four times as long as with the tBu-OO-pSMA initiator.

5.3 Modification of dense films with redox co-initiator

Zeta potential

Some preliminary tests were carried out on dense PES films in order to determine suitable conditions for surface grafting. ZP measurements were carried out to determine influences of the macromolecular redox-co initiator on the surface charge. The results are shown in Figure 5-21.

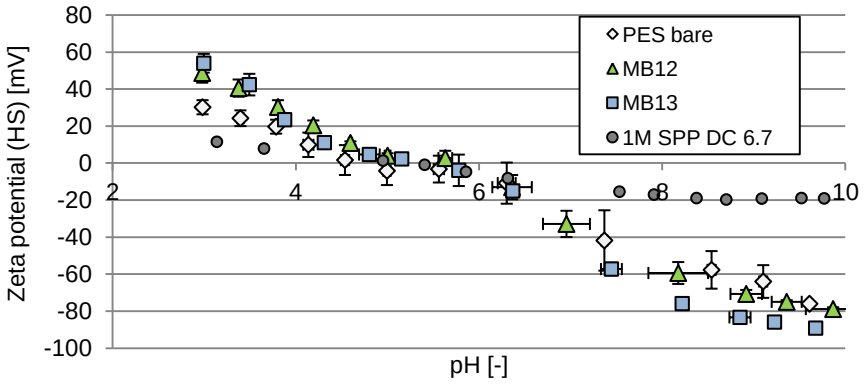

Figure 5-21 Zeta potential determined from streaming current on dense thin films. Modified, premodified and bare PES.

At high pH (>7), the ZP for bare PES as well as for the premodified samples was deviating more than at low pH. The IEP was between 4.5 and 6 for all three sample types. At low pH (<4) the ZP of premodified samples was slightly more positive (~20 mV) than for pristine PES. The increased slope of the ZP curve could be compensated, when grafting the film with a high concentration of SPP (1 M SPP DC 6.7). The IEP for the grafted film was almost unchanged, while the slope of the ZP curve was much smaller than for the premodified or unmodified films. Interestingly the thickly grafted film still showed a slightly positive ZP (12 mV) at low pH and a slightly negative ZP (- 15 mV) above pH 7.5.

Degree of grafting

The gravimetrical DG under varied conditions are summarized in Table 5-16.

Table 5-16 Gravimetric DG experiments with dense PES films premodified with MB-12 (*saturated solution, *[2] sample was removed, when bulk polymerization was starting to occur).

Concentration of SPP [mol/L]	DC [%]	Concentration of APS [mmol/L]	$MgCl_2$ conc. [mmol/L]	pH	Result
1	6.7*	50	50	2.2	no DG
1	6.7*	50	100	2.2	no DG
1	6.7*	50	500	2.2	no DG
1	6.7*	15	0	2.2	no DG
1	6.7*	50	0	2.2	no DG
1	6.7*	100	0	2.2	no DG
1	3.35	50	100	7.4	bulk polymerization
1	3.35	50	500	7.4	bulk polymerization
1	3.35	100	100	7.4	bulk polymerization
1	3.35	100	500	7.4	bulk polymerization
0.5	3.35	50	100	7.4	-2.2 [µg/cm²]
0.5	3.35	50	500	7.4	5.5 [µg/cm²]
0.5	3.35	100	100	7.4	14.3 [µg/cm²]
0.5	3.35	100	500	7.4	49.6 [µg/cm²]
1	6.7*	50	0	7.4	747*2 [µg/cm²]
1	6.7*	50	50	7.4	bulk polymerization
1	6.7*	50	100	7.4	bulk polymerization

At low pH (2.2) and high DC (6.7 %) no grafting was detected. Increasing the pH led to fast bulk polymerization. When reducing the monomer concentration to 0.5 M, a detectable DG was observed.

Stability test

Another batch of dense films was modified later in the project using the grafting conditions established for membrane modification. These films were used for stability tests. The CA after different times in the test solutions is shown in Figure 5-22.

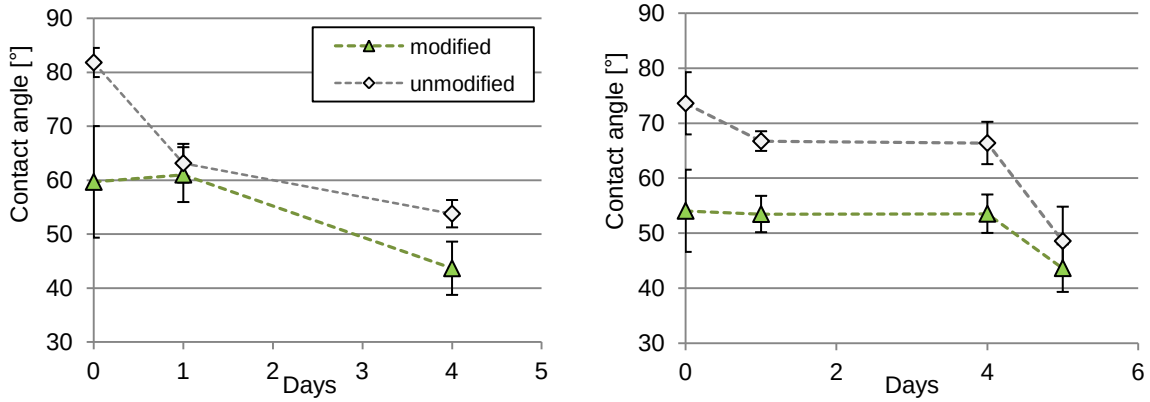

Figure 5-22 Contact angle of modified (MB12, 0.25 M SPP DC 3.35, 5 mM APS) and unmodified films vs. time in 1 M HCl (left) and 0.1 M NaOH (right).

The CA the modified films were significantly lower than for unmodified films. In HCl (Figure 5-22 left) the CA of the unmodified films decreased about 20 ° after the first day, while the CA of the modified film remained constant. During the next 3 days the CA of both unmodified and modified films decreased further. In NaOH (Figure 5-22 right) the CA of modified films remained

constant the first four days and then decreased by 10 ° between day 4 and 5. The unmodified films CA decreased within the first day by 5 ° and another 18 ° between day 4 and 5.

5.4 Structural differences in used membrane types

SEM was used to evaluate whether the cross-section and surface morphology of the used flat-sheet and multibore membranes differed significantly. SEM images of the surface (a) and cross section (b,c) of used multibore and flat sheet membranes are compiled in Figure 5-23.

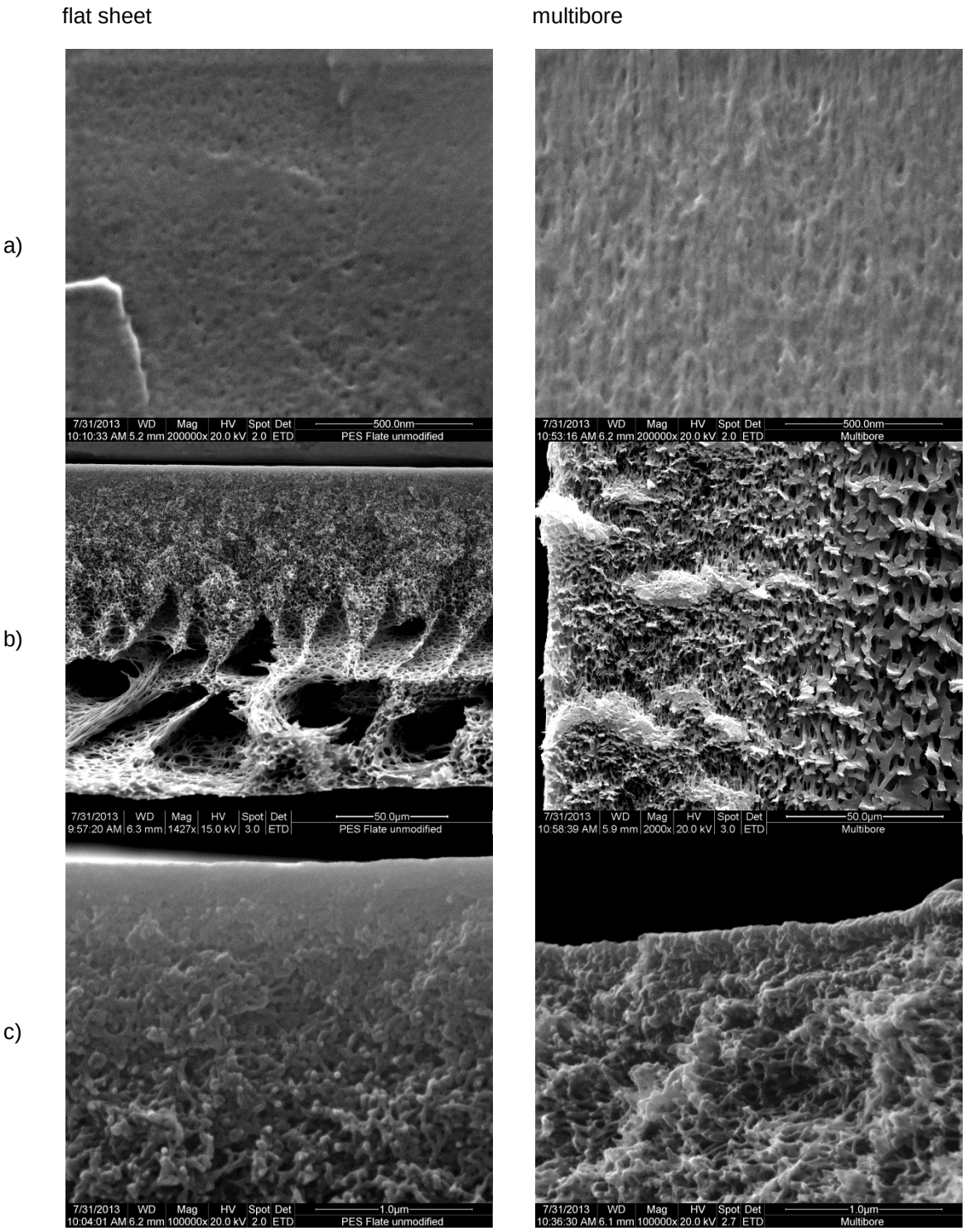

Figure 5-23 SEM images of flat sheet (left) and multibore (right) membranes; a) surface. b) cross section overview. c) cross section selective layer.

Similarities between both membranes can be observed in the pictures of the surface (a) as well as the total cross section (b) and selective layer (c). Dark pore-like holes of 20 to 50 nm can be observed in both surfaces (a). The flat sheet featured an asymmetric structure with macro voids in the lower half and a sponge-like support in the upper half. The multibore substructure was anisotropic as well, but did not contain macro voids (Figure 5-23 a) left vs. right). The cross

section of the selective layer showed ~100 nm of a very dense layer at the surface on top of the porous support (Figure 5-23 c). The top layer of the multibore membrane appeared to be broken in a more grainy structure.

The full cross sections of both membranes are shown in Figure 5-24 with different scale.

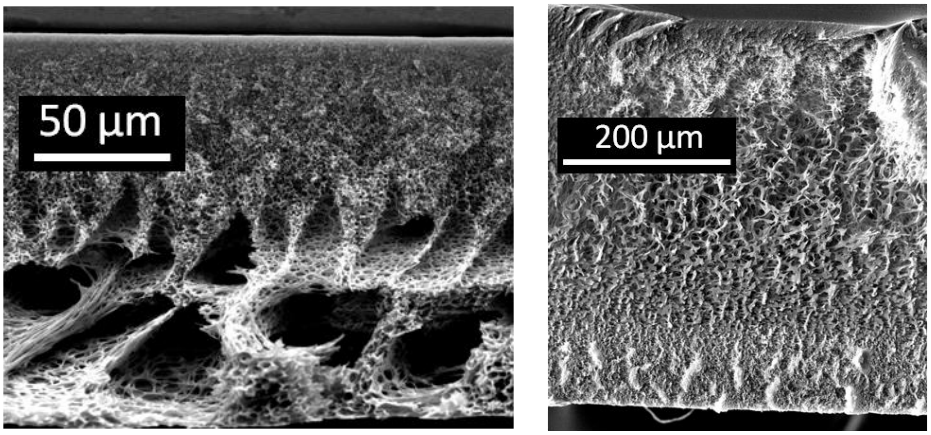

Figure 5-24 SEM cross section of flat sheet (left) and multibore (right) membranes.

The support layer of the multibore was much thicker than the support of the flat sheet membrane. While the flat sheet became more porous towards the permeate side, the multibore comprised the most porous part in the middle section of the support. The permeate side of the multibore was again more dense.

5.5 Flat sheet membranes

Unless stated otherwise, all membranes were modified using self synthesized SPP. However some measurements were performed using SPP provided by ChemicalPoint. In the latter case this will be stated in the figures caption.

5.5.1 Thermal macro initiator mediated modification

The influence of the thermal macro initiator on grafting was surveyed in a similar way like for the redox-co-initiator. Static adsorption of the initiator did not influence the permeability detectably. The filtration of initiator reduced the permeability by ~25 (± 1) %. This reduction was completely reversible, when heating the modified membranes in water at similar conditions like in the subsequent grafting procedure. Therefore the results data are given relative to the initial water permeability. The changes in permeability due to thermal grafting with and without the initiator are given in Figure 5-25.

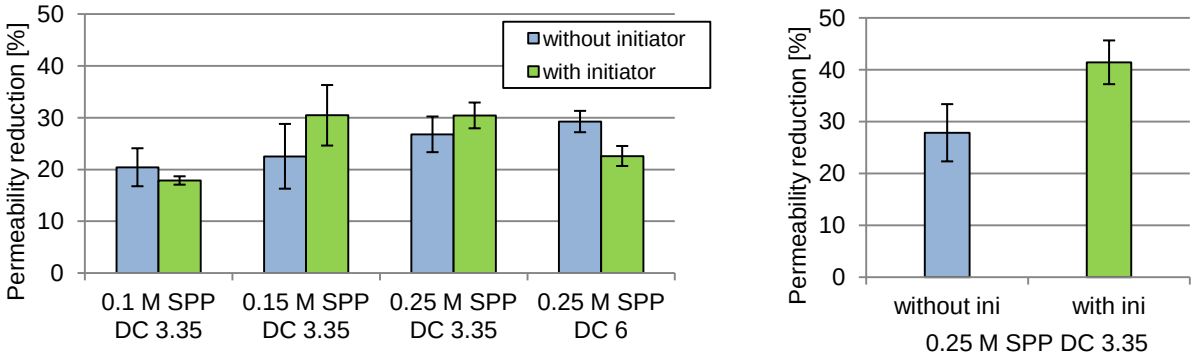

Figure 5-25 Permeability decrease by thermal (65 °C) modification for varied compositions of grafting solution with and without initiator;10 min initiator adsorption 0.1 g/L (left) and filtration of 2/15 mL 0.2 g/L (right).

When just adsorbing the initiator to the surface (Figure 5-25 left), the effect of the initiator was small. At low monomer concentration and DC (0.1 M SPP DC 3.35) the grafting appeared even less effective than without initiator. At medium and high monomer concentration (0.15 M and 0.25 M SPP) and DC 3.35 the initiator effect was most pronounced but still small, taking into account the error bars. At higher DC (6.7) the grafting effect with initiator was again less pronounced than without. The permeability reduction was in no case higher than 30 %.

When filtering the initiator onto the membrane (Figure 5-25 right), a stronger permeability decrease was achieved with initiator (40 ± 4 %) than without (28 ± 5 %). The bars in Figure 5-25 (right) represent data from 9 membranes in 3 batches without, and 5 membranes in 2 batches with initiator.

To further investigate the reasons for the reversible permeability decrease, CA was determined before and after initiator filtration and after heating the premodified membrane in pure water. The results are shown in Figure 5-26.

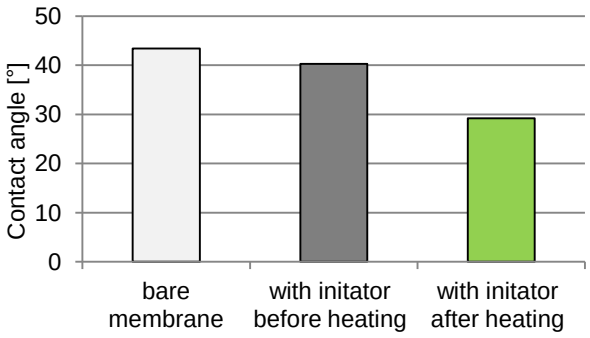

Figure 5-26 Changes of CA due to initiator immobilization and subsequent heating in water.

The CA slightly decreased, when adsorbing the thermal macro-initiator. When heating in pure water without monomers, the CA decreased further to a value of 30 °.

For different reasons, discussed in Chapter 6.2.3, the modification using the redox system was deemed to be more feasible.

5.5.2 Redox co-initiator mediated grafting

The gravimetrical DG, determined by drying is shown in Figure 5-27.

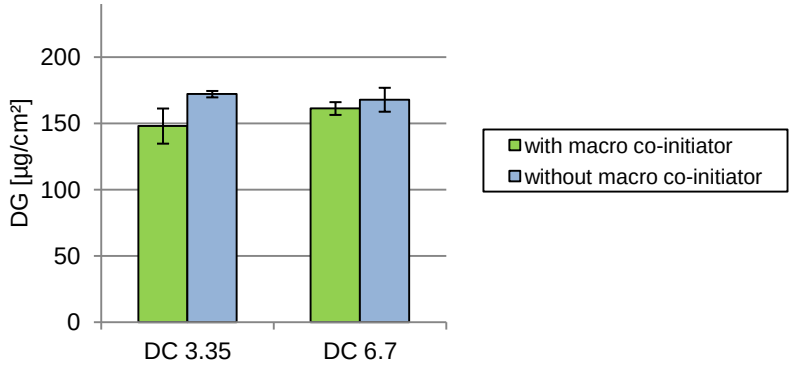

Figure 5-27 Gravimetrical DG for different cross-linker contents (0.25 M SPP).

The DG was very similar (150 – 170 µg/cm²) for all samples regardless of whether the membrane was premodified or not. DC did not have an influence on the gravimetrical DG.

5.5.2.1 Permeability

With another set of membranes, permeability measurements were performed before and after grafting to estimate the changes in permeability due to grafting. The initial permeability of pristine flat sheet samples was 670 ± 120 L/hm²bar. Due to the broad variety of initial permeabilities, the data are represented as average values of at least three independent membrane samples modified in separate vessels. The pre modification with redox co-initiator reduced the permeability by ~8 (± 5) %. The data are given relative to the permeability of the premodified membrane. In some cases modifications were repeated with new monomer solution. Since the initial permeabilities of the used membranes varied (660 ± 120 L/hm²bar) permeability data is expressed as relative changes. Figure 5-28 summarizes permeability changes after modification with commercial SPP.

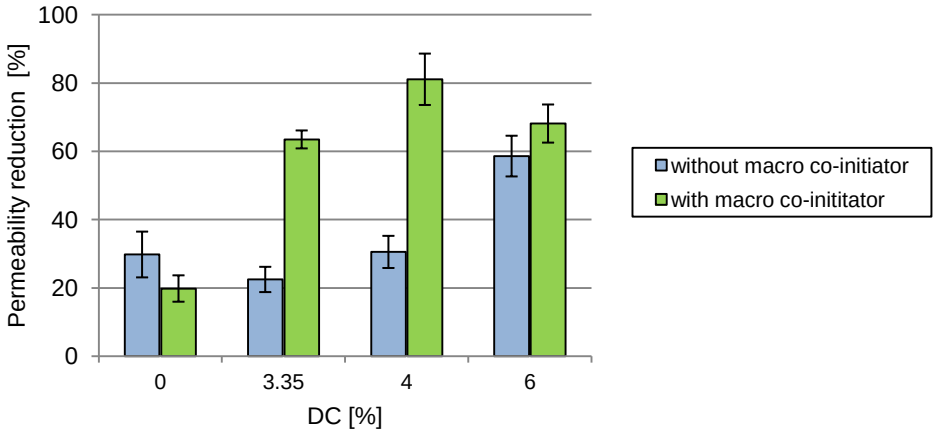

Figure 5-28 Permeability reduction by grafting procedure in dependence of different cross-linker contents (0.25 M SPP from ChemicalPoint).

Each column represents permeability data from three independent flat sheet samples from one batch. Without cross-linker (DC 0), the permeability was reduced by 25 (± 5) % with and without macromolecular co-initiator. With a low and medium DC (DC 3.35 and 4), the macromolecular co-initiator showed the strongest effect. The permeability of modified membranes without co-initiator decreased only by 25 (± 5) % in both cases. The permeability of samples modified with co-initiators was reduced by63 (± 4) % at a DC 3.35 and by 80 (± 8) % at DC 4. With DC 6.7, the permeability reduction was almost similar for modified samples with and without co-initiator. With co-initiator however the average reduction was still 10 (± 4) % higher than without.

Figure 5-29 represents the permeability changes due to modification with self synthesized SPP.

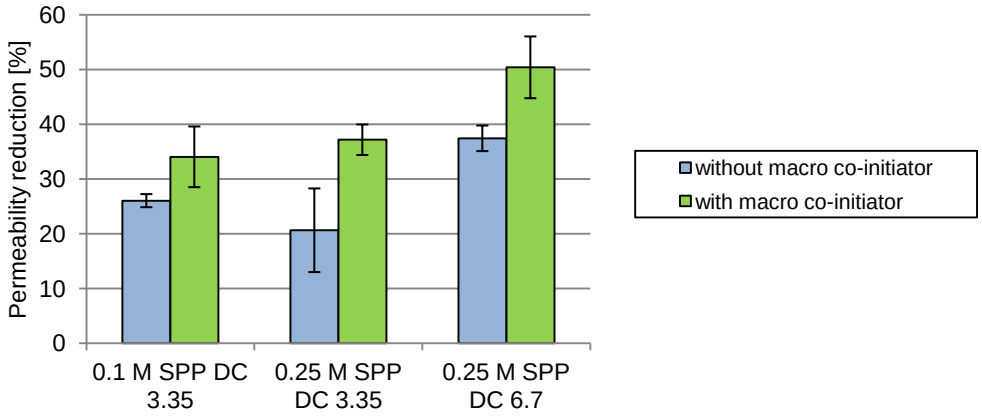

Figure 5-29 Permeability reduction for different grafting conditions with self synthesized SPP.

The grafting showed significantly less influence on permeability with the self synthesized monomer than with commercial SPP, when using the macromolecular co-initiator. The modification with 0.25 M SPP DC 3.35 caused a similarly low reduction (21 %) without co-initiator. With co-initiator, the reduction was higher than without co-initiator, but lower than with

the commercial SPP (37 % vs. 63 %). When grafting with higher cross-linker content, a similar trend like in Figure 5-28 was observed. However now the total influence on permeability was lower (50 % vs. 68 %). The low monomer concentration tested in this series also caused clearly more permeability reduction (34 %) with co-initiator than without (26 %).

5.5.2.2 Morphological changes

Close views of the surfaces of a pristine, a premodified and two modified membranes are shown in Figure 5-30.

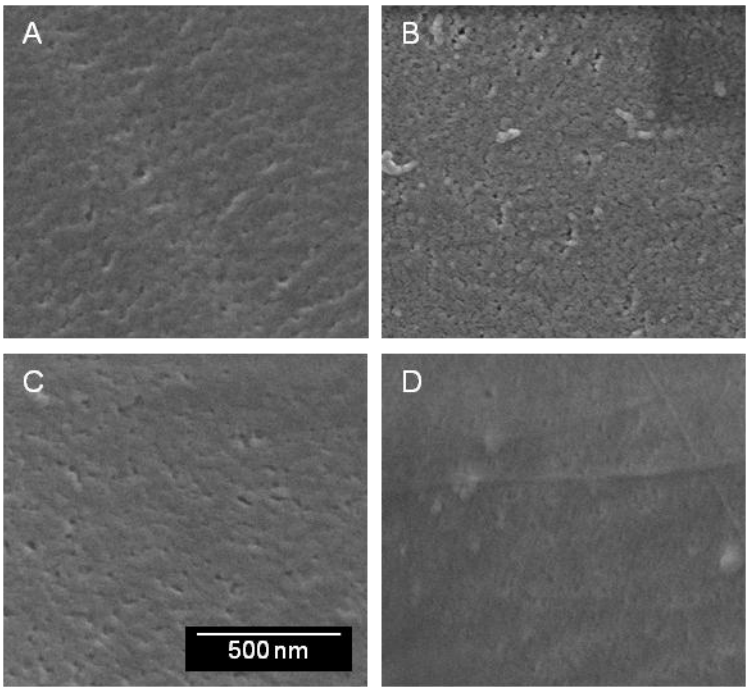

Figure 5-30 Surface SEM image; A pristine. B premodified. C 0.1 M SPP. D 0.5 M SPP DC 3.35.

The porous structure of the premodified membrane appeared slightly more porous than the pristine sample (Figure 5-30 B vs. A). The modification with 0.1 M SPP did not cause observable changes in the surface structure (Figure 5-30 C vs. A). The surface of the membrane modified with higher monomer content appeared much smoother with less observable pore-like structures than pristine and premodified membranes (Figure 5-30 D vs. A, B).

The changes in the cross section of the selective were also surveyed by SEM. The pictures are shown in Figure 5-31.

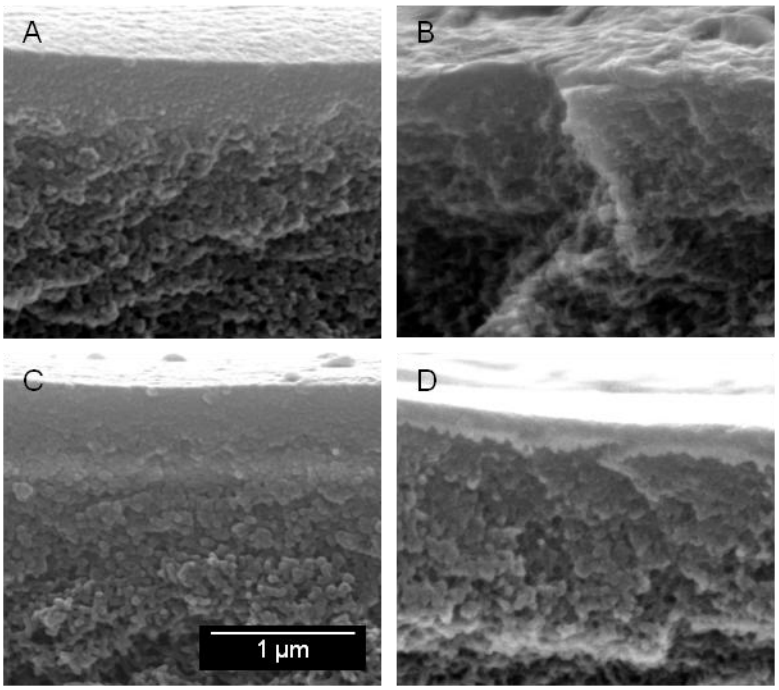

Figure 5-31 SEM images of cross section of the selective layer of (A) pristine, (B) premodified and modified membranes with (C) 0.1 M SPP and (D) 0.5 M SPP (DC 3.35).

The cross section break of the premodified membrane appeared to be rougher than of the pristine membrane. Also the part of the surface visible in cross section was less smooth than of the pristine membrane (Figure 5-31 B vs. A). No significant changes were detected after modification at low monomer concentration either (Figure 5-31 C, vs. A, B). Only at the high monomer concentration (0.5 SPP) the structure appeared different. A dense layer was observed on top of the membrane, which was in this case thinner (~200 nm) than for the unmodified and premodified membranes (~500 nm) (Figure 5-31 D vs. A, B).

5.5.2.3 Energy dispersive x-ray spectroscopy

The upper 100 nm of the cross sections shown in Figure 5-31 were surveyed by XPS during the scan. For comparison similar scans were performed in the lower part of the membrane cross section. The results are summarized in Figure 5-32.

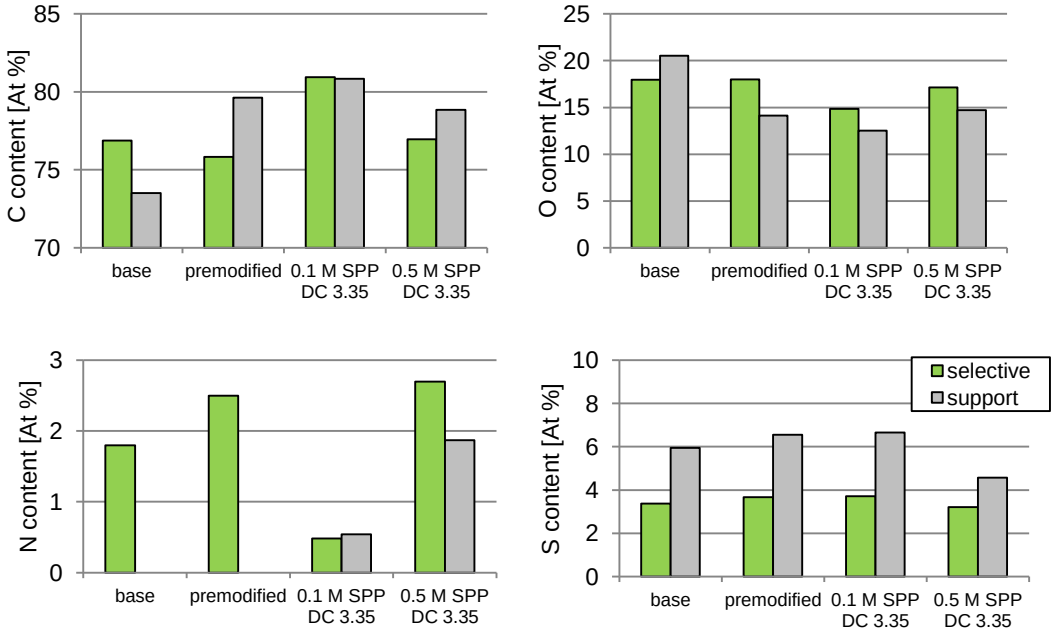

Figure 5-32 Elemental composition C (upper left), O (upper right), N (lower left) and S (lower right) determined by EDX of membrane cross section.

Upon premodification with initiator, only the N content of the upper cross section increased. The carbon content decreased slightly while S and O stood similar. No N was detected in the support before or after pre modification. The O content in the support was decreased about 6 % while the C content was increased during premodification.

Upon modification with the low monomer concentration (0.1 M SPP), the C content increased by 5 % in the support and selective side. During modification the N content in the support was increased from 0 % to 0.5 %, while the N content at the surface was reduced from 2.5 % to 0.5 %. The increase in N content in the support was even more pronounced in the membrane modified with 0.5 M SPP. In the selective layer, however, the elemental composition was very similar to the composition of the premodified sample.

5.5.2.4 SIMS-mapping

In the following, the SIMS-mapping images of grafted and ungrafted membrane surfaces are presented. The order is always from left to right: pristine membrane, grafted without initiator and grafted with initiator with a concentration of 0.25 M SPP DC 6.7.

Negative ions

Figure 5-33 shows the distribution of CN^- sources on the membranes.

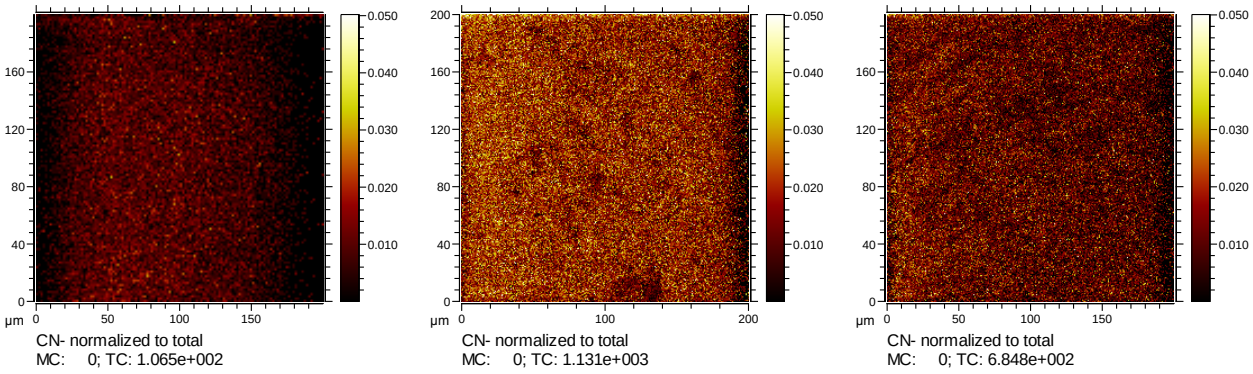

Figure 5-33 Local distribution of CN^- sources determined by SIMS-TOF; from left to right: pristine membrane, grafted without initiator and grafted with initiator with a concentration of 0.25 M SPP DC 6.7.

The pristine sample showed the lowest amount of CN- sources along the surface, while the membrane modified without initiator showed the highest density. However the differences between the two grafted membranes were small compared to the difference to the pristine sample. The normalized distributions of S- sources are shown in Figure 5-34:

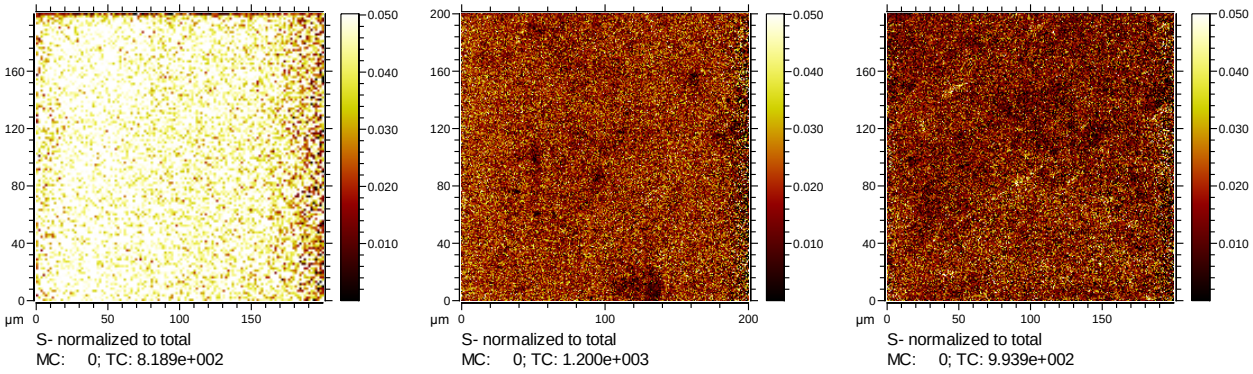

Figure 5-34 Local distribution of S^- sources determined by SIMS-TOF; from left to right: pristine membrane, grafted without initiator and grafted with initiator with a concentration of 0.25 M SPP DC 6.7.

A very high amount of S^- was observed on the pristine membrane. Both grafted membranes showed significantly lower amounts of S^-. The amount of S^- was very similar for both grafted membranes.

Second layer scan negative ions

The measurements were repeated at the same spot after a sputter cleaning with an 200 eV Cs^+ beam. The beam was used to remove adsorbed fragments from the first scan. These data thus represent a scan app. 10 nm below the initial surface which was removed by the first scan. The results are given in the following starting with the CN^- source distribution in Figure 5-35.

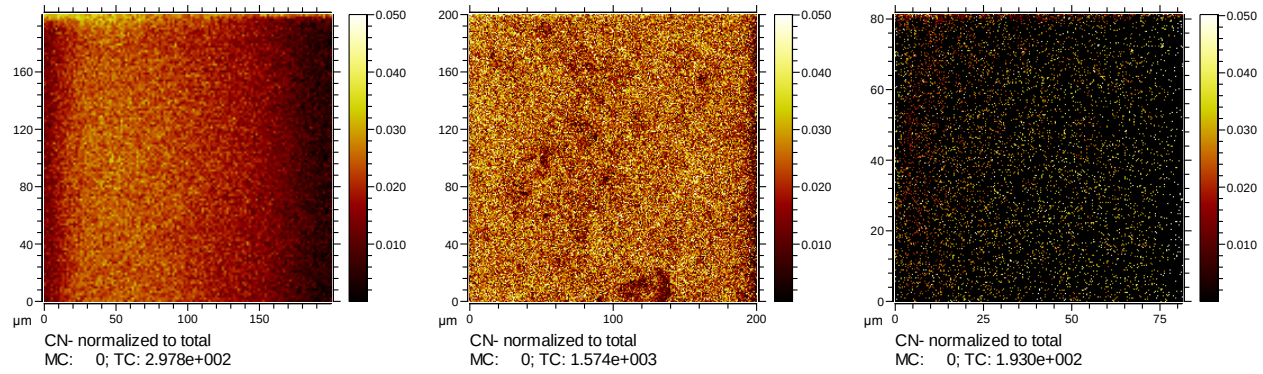

Figure 5-35 Local distribution of CN^- sources determined by SIMS-TOF after sputter cleaning with 200 eV Cs^+; from left to right: pristine membrane, grafted without initiator and grafted with initiator with a concentration of 0.25 M SPP DC 6.7.

Comparing (Figure 5-35 to Figure 5-33), much more CN- was observed for the pristine sample, while the amount on the sample grafted without initiator was quite similar. The amount of CN- of the sample modified with initiator decreased.

The distribution of S- on the surface after sputter cleaning is shown in Figure 5-36.

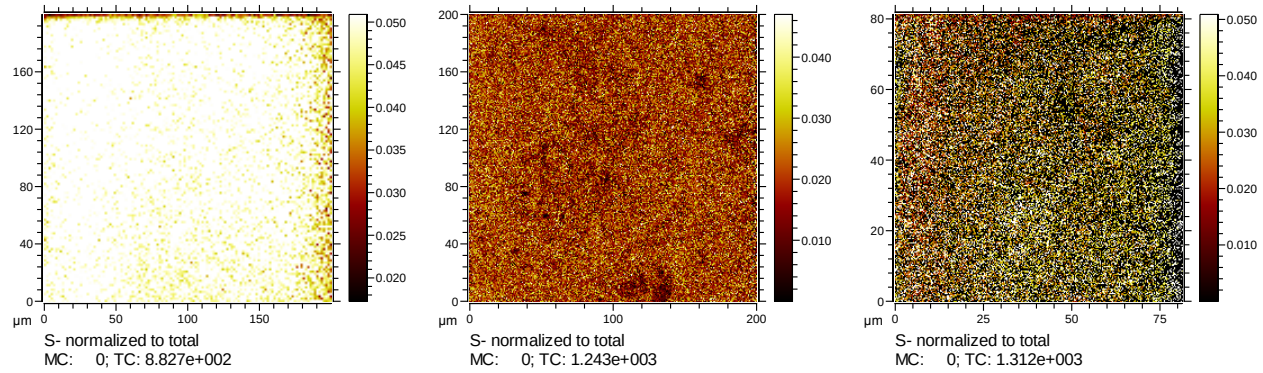

Figure 5-36 Local distribution of S^- sources determined by SIMS-TOF after sputter cleaning with 200 eV Cs^+; from left to right: pristine membrane, grafted without initiator and grafted with initiator with a concentration of 0.25 M SPP DC 6.7.

For the pristine membrane the S^- concentration slightly increased after cleaning. The sample modified without initiator showed similar concentrations like before the sputter cleaning. For the sample modified with initiator the concentration was also increased slightly (Figure 5-36 vs. Figure 5-34).

Positive ions

The distribution of sources for the larger positive fragments CH_4N^+ and $C_3H_8N^+$ are presented in the following, starting with the total distribution of positive ion sources in Figure 5-37.

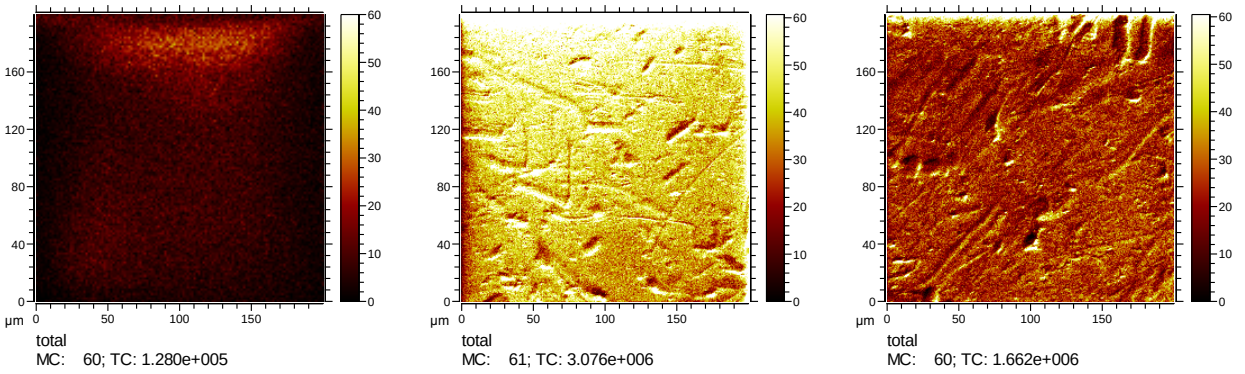

Figure 5-37 Sources of total positive Ions by SIMS-TOF; from left to right: pristine membrane, grafted without initiator and grafted with initiator with a concentration of 0.25 M SPP DC 6.7.

The pristine sample showed the lowest amount of positive ions. Both grafted membranes released more positive ions, while the amount was higher on the membrane grafted without initiator. Furthermore, both membrane surfaces appear more structured than the pristine sample. The distribution of CH_4N^+ is given in Figure 5-38.

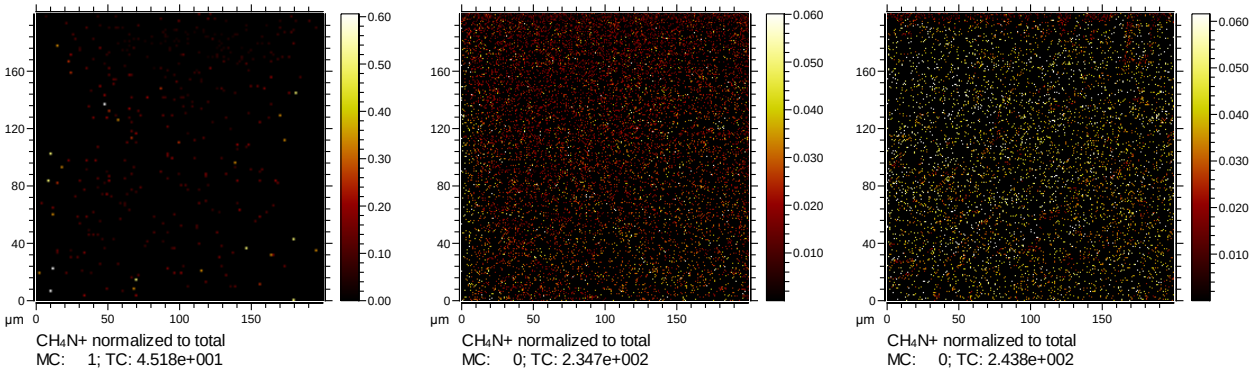

Figure 5-38 Local distribution of CH_4N^+ sources determined by SIMS-TOF; from left to right: pristine membrane, grafted without initiator and grafted with initiator with a concentration of 0.25 M SPP DC 6.7.

Almost no CH_4N^+ was observed on the pristine membrane. The highest amount was observed on the membrane grafted with initiator. The amount of CH_4N^+ detected on the membrane grafted without initiator was average. The distribution of the larger fragment $C_3H_8N^+$ is shown in Figure 5-39.

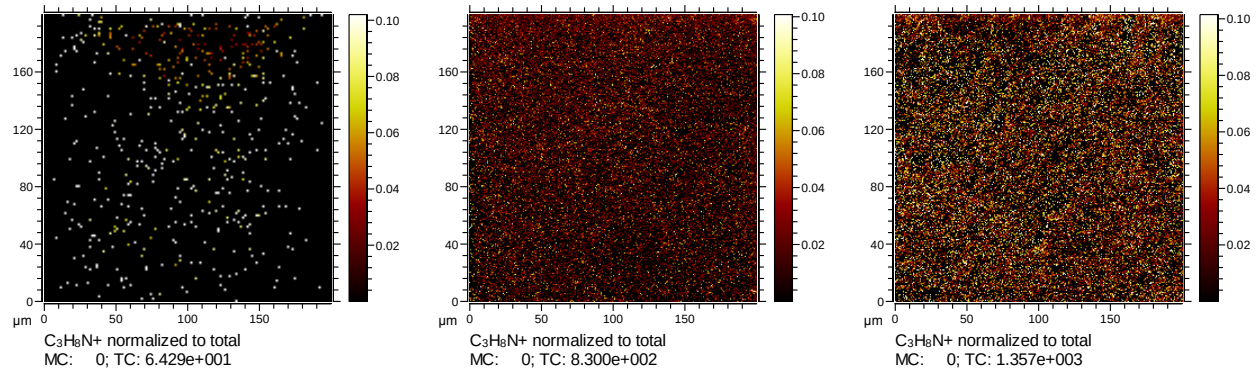

Figure 5-39 Local distribution of $C_3H_8N^+$ sources determined by SIMS-TOF; from left to right: pristine membrane, grafted without initiator and grafted with initiator with a concentration of 0.25 M SPP DC 6.7.

The pristine sample released no $C_3H_8N^+$ in wide areas but showed some spots of high concentration. Overall the amount of $C_3H_8N^+$ released from the pristine membrane was lowest. Again the amount was highest for the membrane grafted with macromolecular co-initiator and average for the membrane grafted without co-initiator.

Second layer scan positive ions

Like for the negative ions, the measurements were repeated after a sputter cleaning with an 200 eV Cs^+ beam. The results are given in the following, starting with the distribution of CH_4N^+ in Figure 5-40.

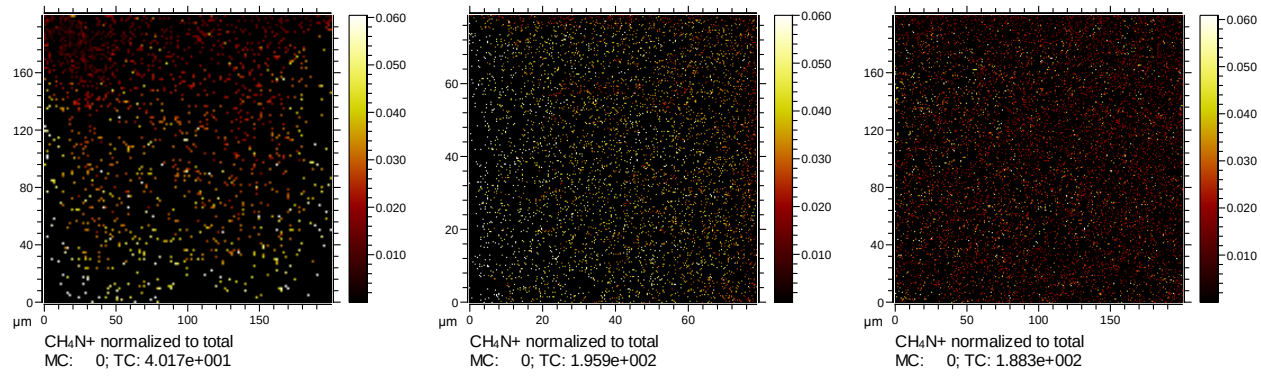

Figure 5-40 Local distribution of CH_4N^+ sources determined by SIMS-TOF after sputter cleaning with 200 eV Cs^+; from left to right: pristine membrane, grafted without initiator and grafted with initiator with a concentration of 0.25 M SPP DC 6.7.

After sputter cleaning, CH^4N^+ was released from more spots than before from the pristine membrane sample. Also from the membrane modified without co-initiator, more intense spots were observed. On the membrane grafted with co-initiator, the intensity was lower but more homogenous after sputtering (Figure 5-40 vs. Figure 5-38). The distribution of C^3H8N^+ after sputtering is shown in Figure 5-41.

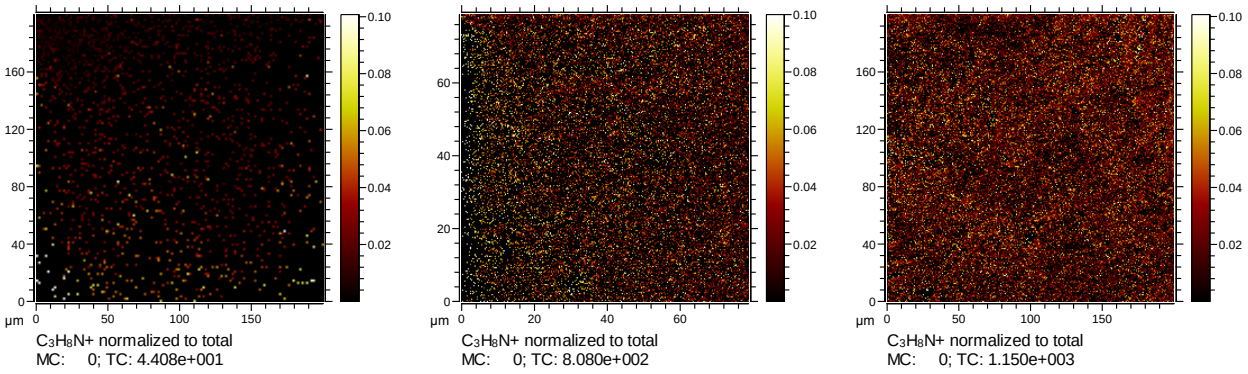

Figure 5-41 Local distribution of $C_3H_8N^+$ sources determined by SIMS-TOF after sputter cleaning with 200 eV Cs^+; from left to right: pristine membrane, grafted without initiator and grafted with initiator with a concentration of 0.25 M SPP DC 6.7.

The intensities for the pristine sample were the lowest, but higher than before sputtering. The two grafted membranes showed significantly higher intensities than the pristine membrane, while the intensity for the membrane grafted with initiator was highest. In both cases the intensities were slightly lower than before sputtering (Figure 5-41 vs. Figure 5-39).

5.5.2.5 ATR-IR spectroscopy

The changes in IR upon premodification with MB12 were surveyed by ATR-IR. The spectra are given in Figure 5-42.

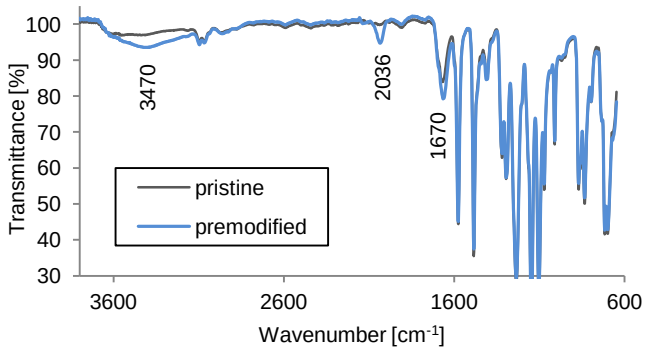

Figure 5-42 ATR-IR spectra of pristine and premodified (MB12) membrane selective layer.

After premodification a broad band occurred at 3470 cm^{-1}. This is typically the area for O-H vibration[139]. Another new band occurred at 2036 cm^{-1} which could not be attributed to any of the expected groups of either initiator or PES/PVP or used solvents.

The IR spectra of the selective side and the support side of modified and unmodified membranes are shown in Figure 5-43.

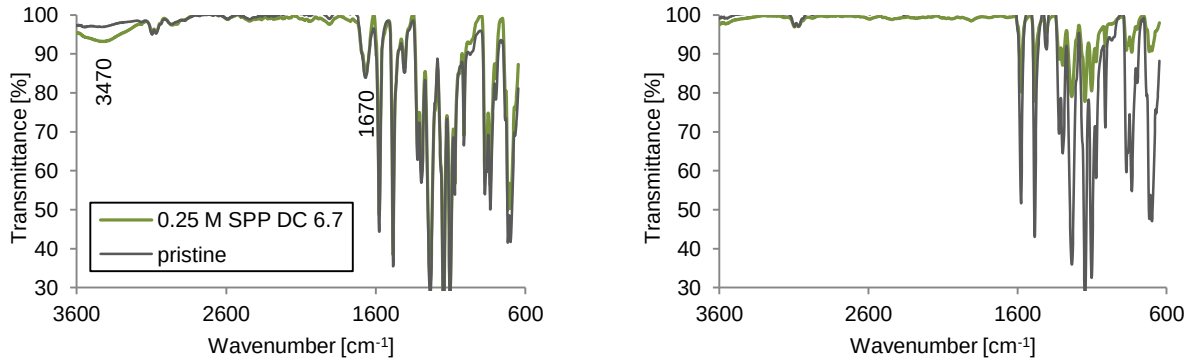

Figure 5-43 ATR-IR spectra of selective side (left) and support side (right) of modified and unmodified membranes.

Considering the spectra of the modified and unmodified surfaces, no remarkable/significant changes occurred. The most pronounced change on the selective layer was the occurrence of a broad O-H band at 3470 cm^{-1}. In this range, also N-H vibrations could be expected to cause a band pair. However due to the broadness of the band it was more likely caused by O-H valence[139].

The most pronounced difference between the spectra of the selective and the support side of all membranes was the band at 1670 cm^{-1} attributed to C=O in PVP[139]. The band was strong on the selective side of the modified and unmodified samples and absent in spectra of the support side (the full spectra are presented in the Appendix Figure 11-9). The same band was also unchanged in upon premodification (Figure 5-42).

5.5.2.6 X-Ray photo electron spectroscopy

The elemental compositions on the selective layers, determined by XPS are given in the following Figure 5-44 and compared to theoretical values.

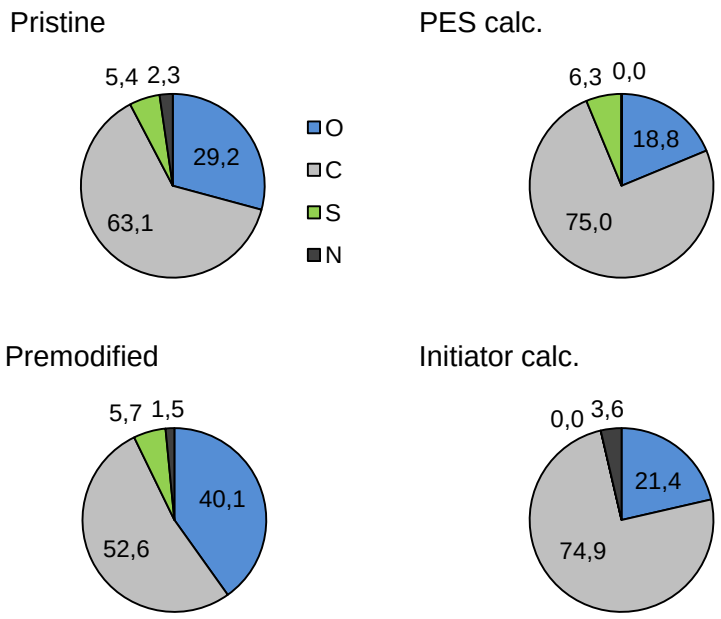

Figure 5-44 Elemental composition (At %) of pristine and premodified membrane surface (left) compared to calculated values for pure PES and a pure initiator layer (right).

Figure 5-44 shows changes due to initiator adsorption. The theoretical composition of the pristine membrane was assuming a pure PES surface. Comparing the measured and calculated compositions, the actual sample contained much more oxygen and less carbon. Also a significant amount of nitrogen was present, where no nitrogen would be expected for a pure PES surface. The determined N/S ratio was 0.43.

Upon premodification, the O content was still increasing, while N was slightly reduced. The determined N/S ratio was 0.27, with an increased S content compared to the base membrane. A detailed survey of the binding energies of carbon in the pristine and premodified membrane was conducted. The results are summarized in Table 5-17.

Table 5-17 Allocation of C in different binding states in the pristine and premodified membrane.

Binding state	**Energy [eV]**	**Pristine**		**Premodified**	
		Area [CPS eV]	Content [At %]	Area [CPS eV]	Content [At %]
C1s	285	342.65	74.51	170.41	74.67
C-O / C-S	286	92.64	20.14	43.65	19.13
C=O	288	4.6	1.00	0	0.00
O=C-O	289	0	0.00	4.85	2.13
Pi-Pi	291,5	20.01	4.35	9.32	4.08

The most remarkable changes are the disappearance of the C=O bonds and the appearance of ester groups upon premodification.

The elemental composition after grafting is given in Figure 5-45.

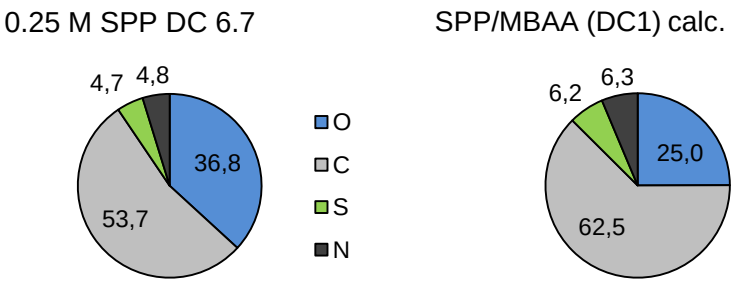

Figure 5-45 Elemental composition (At %) of modified membrane surface (left) compared to calculated values for SPP-co-MBAA hydrogel containing 6.7 % MBAA (right).

After grafting, the O content was slightly decreased from 40 % to 37 % (cf. Figure 5-44). The S content also decreased slightly from 5.7 % to 4.7 %. The N content significantly increased from 1.5 % to 4.7 % leading to an N/S ratio of 1.01.

A detailed survey of the carbon binding energies after modification was conducted and the results are summarized in Table 5-18.

Table 5-18 Allocation of C to different binding states in the modified sample.

Binding state	Energy [eV]	Area [CPS eV]	Content [At %]
C 1s	285	257.02	74.95
C-O / C-S	286	66.65	19.44
C=O	288	18.4	5.37
O=C-O	289	0.85	0.25
PiPi	291	0	0.00

The main change compared to the premodified membrane (cf. Table 5-17) is the increase in the energy area 288-289 eV suggested as C=O or O=C-O.

5.5.2.7 Contact angle

Contact angle on flat sheets

The determined CA during the grafting process on flat sheet membranes are summarized in Figure 5-46.

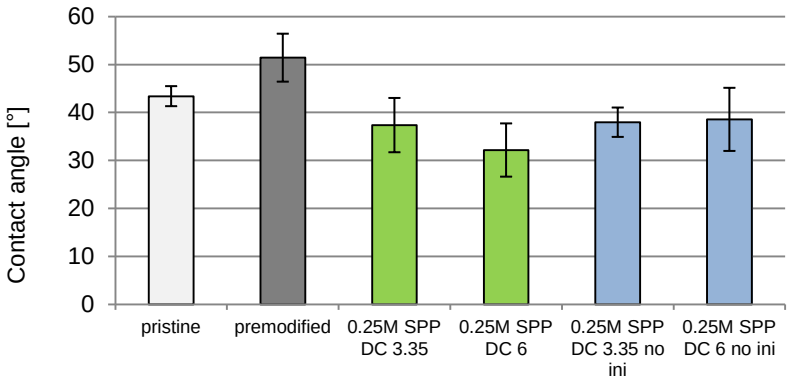

Figure 5-46 Water contact angle determined by captive bubble method for treated samples at different conditions.

The CA increased significantly (by ~8 °) upon premodification. The effect was overcompensated by the hydrogel modification. The decrease in CA was more pronounced for the higher DC, but both modifications led to surfaces with slightly (by ~6 ° for low and ~9 ° for high DC) lower CA than the base membrane. A similar modification without premodification caused less pronounced changes. The decreases in CA observed here were small taking into account the error bars.

Contact angle on hollow fibre membranes

A method for comparative CA determination on multibore samples could not be developed. However measuring on the single bore was possible. Pictures of a measurement during sessile drop and captive bubble are shown in Figure 5-47.

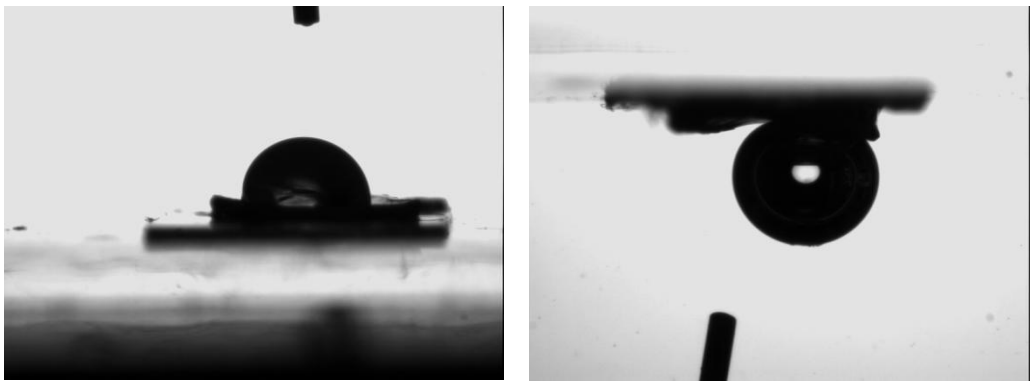

Figure 5-47 Water contact angle measurement. sessile drop (left) and captive bubble (right) with single bore membrane.

The contact angle in sessile drop mode (Figure 5-47 left) was ca. 91° (± 2° average of 4 samples). Figure 5-47 (right) shows the typical result of a captive bubble measurement. In 90 % of all attempts, the bubble did not stay at the membrane surface. Since the bubble sticked preferably at curved parts of the surface, no CA could be determined in captive bubble mode.

5.5.2.8 Zeta potential

The results of the ZP measurements on flat sheet membranes are summarized in Figure 5-48.

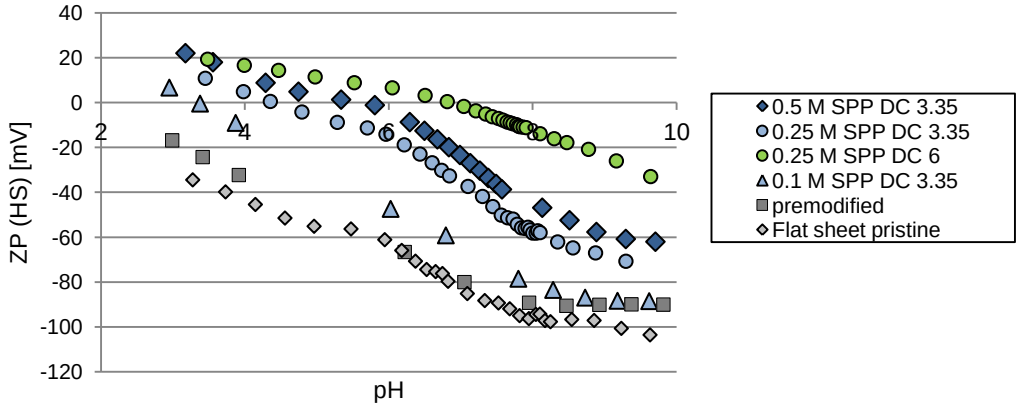

Figure 5-48 Zeta potential (HS) vs. pH of membranes in different steps of the grafting process.

The pristine flat sheet membranes showed a negative zeta potential over the whole surveyed pH range. The zeta potential started at -40 mV and dropped to a steady value of – 100 mV at pH 8. After premodification the ZP at lower pH (< 4) was slightly (~ 15 mV) higher than the ZP of the pristine membrane. Modification with a low monomer concentration (0.1 M) and low DC (3.35) led to an increase in ZP, still maintaining the slope of the curve. IEP was about 3.2 for this membrane. By increasing the monomer concentration, the IEP shifted towards ~ pH 4.2 with an unchanged slope. Doubling the DC at a similar monomer concentration led to a flatter curve with an IEP of 7 and a low maximum charge (~20 mV). Doubling the monomer concentration (0.5 M) and keeping DC low (3.35) had no influence on the curves slope and only shifted it towards an IEP of ~ pH 6.

5.5.2.9 Sieving curve analysis and molecular weight cut-off

The effect of the grafting procedure on rejection behaviour was evaluated in dead-end filtration of dextran. Exemplary sieving curves are shown in Figure 5-49.

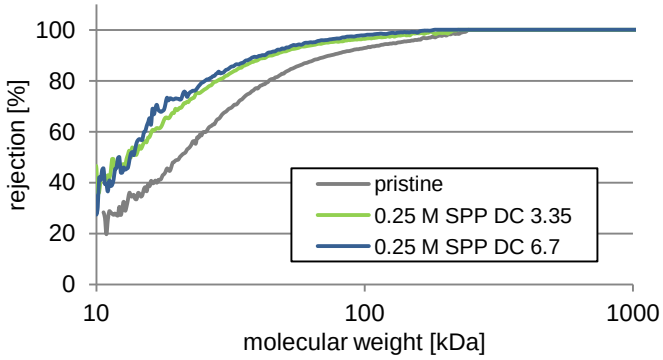

Figure 5-49 Dextran sieving curves of modified and unmodified flat sheet membranes in dead-end mode.

Both modifications shifted the sieving curve towards lower MW. The shift was only slightly more expressed for the higher DC (6.7). The MWCO was determined from the presented sieving curves and one repetition of the experiment with another set of membranes. The average MWCO and the average deviation are summarized in Figure 5-50.

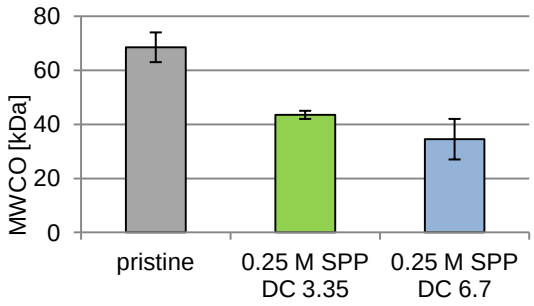

Figure 5-50 MWCO for dextran of modified and unmodified flat sheet membranes in dead-end mode.

The grafting with a DC of 3.35 reduced the MWCO from ca. 69 kDa to ca. 44 kDa. Grafting with a higher DC of 6.7 reduced the MWCO further to ca. 35 kDa.

The estimated pore sizes of the membranes according to Eq. 11 are given in Table 5-19.

Table 5-19 Membrane pore diameter derived from the dextran MWCO.

	MWCO [kDa]	Pore size [nm]
Pristine	69	14
0.25 M SPP DC 3.35	44	11
0.25 M SPP DC 6.7	35	9

5.5.2.10 Fouling resistance

Bovine serum albumin

Static adsorption

Protein fouling was surveyed using BSA as a model protein. First tests were performed in static mode. The results are summarized in Figure 5-51 with each bar representing a measurement on two independent samples.

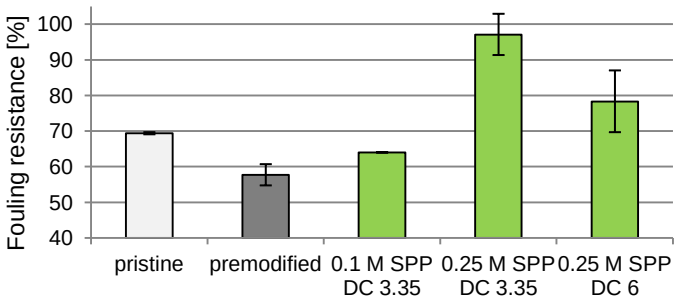

Figure 5-51 Static fouling resistance towards 1 g/L BSA solutions (1 h pH 7.4) (SPP from ChemicalPoint).

The deviation in fouling resistance was only low for the membrane modified with 0.1 M SPP and DC 3.35. The pristine membrane already showed a quite high resistance towards protein fouling at static conditions. Upon premodification with the macromolecular redox co-initiator, the fouling resistance was decreased by 10 %. Grafting with 0.1 M SPP DC 3.35 slightly compensated the effect, but did not restore the initial fouling resistance. Both modifications with higher monomer concentrations (0.25 M SPP) led to higher resistance than the base membrane. While the high cross-linker content (DC 6) yielded a fouling resistance of ~ 79 %, the membranes modified with a DC of 3.35 showed almost 100 % fouling resistance.

Dead-end filtration

The fouling resistance during filtration was determined. All filtrations were run at the same constant starting pressure and the same volume was filtrated. The bars in Figure 5-52 represent the average of three independent membranes. Only the measurements on pristine, premodified and modified membranes with 0.1 M SPP DC 3.35 represent the average of seven independent samples instead. For some samples, TOC of retentate and permeate was measured to estimate rejection (cf. Appendix Table 11-1). The pristine samples already showed BSA rejection > 99 % and modification with or without co-initiator did not change this detectably.

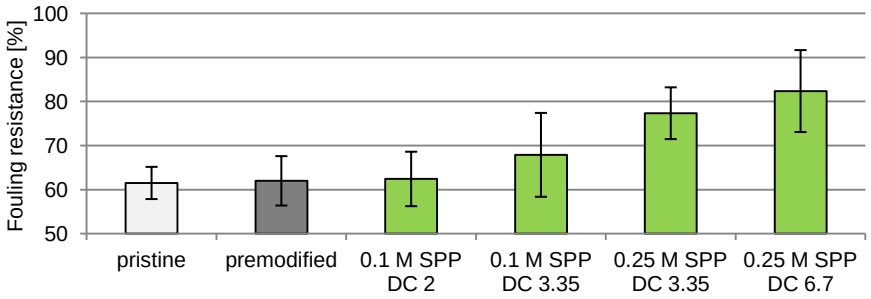

Figure 5-52 Fouling resistance towards BSA (10 mL permeate of 15 mL feed, 1 g/L BSA, pH 7.4, 0.4 bar, 300 rpm) (SPP from ChemicalPoint).

The premodification and the modification at low monomer concentration and DC (0.1 M SPP DC 2) did not have a detectable influence on the fouling resistance under filtration conditions. When increasing the DC to 3.35, a slight increase in fouling resistance was observed but this was small relative to the deviation. Increasing the monomer concentration to 0.25 M SPP significantly increased the fouling resistance to 77 (± 6) % for DC 3.35 and 82 (± 9) % for DC 6.7.

Extracts from membrane bioreactor

The first filtrations with EPS and SMP were performed at similar flux conditions like the BSA fouling tests. Due to the broader mixture of molecular sizes in EPS and SMP, a deviating rejection can be expected for membranes with different permeability. For better comparison a Nadir UP020 membrane with similar starting permeability like the modified membranes was used in these tests. All bars with error bars represent the average of two individual samples. Due to the low absolute concentrations, no TOC could be measured in the collected permeate and feed samples. Figure 5-53 shows the results of the fouling tests.

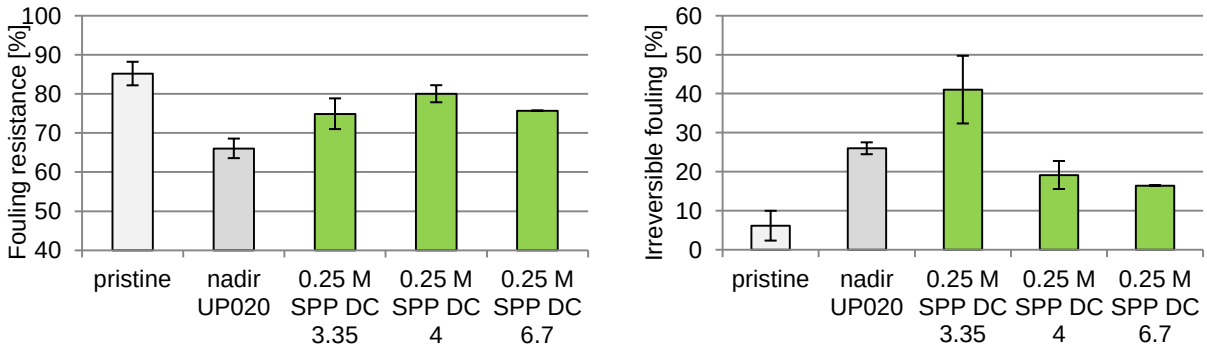

Figure 5-53 Fouling resistance during filtration of 10/15 mL 25 mg/L EPS in PBS at 0.4 bar, 300 rpm (left) and irreversible flux reduction after 24 h in PBS solution (right)(SPP from ChemicalPoint).

At similar constant pressure, all surveyed membranes showed quite high fouling resistance towards EPS. The pristine membrane showed the highest fouling resistance (85 ± 3 %) while

the UP020 membrane showed the lowest (66 ± 2 %). All modified membranes showed a higher fouling resistance than UP020 but lower fouling resistance than the pristine membrane.

The data in Figure 5-53 (right) represent irreversible fouling after rinsing the samples 24 h in PBS solution. The irreversible fouling of the pristine membrane (Inge), was ca. 6 %, whereas the irreversible fouling of the nadir membrane was 26 %. The modified membranes with a higher DC (DC 4 and DC 6.7) showed a permanent flux reduction between the Inge and Nadir membranes. The permanent reduction for the membrane with DC 6.7 was slightly lower than for the membrane with a DC of 4 (16 % vs. 19 %). Interestingly the fouling of the modified membrane with the lowest DC even increased during rinsing in PBS and was 41 % after the rinsing step.

Another series of fouling experiments was run with EPS, where all experiments were started at similar flux. The fouling resistance at similar initial flux conditions is shown in Figure 5-54.

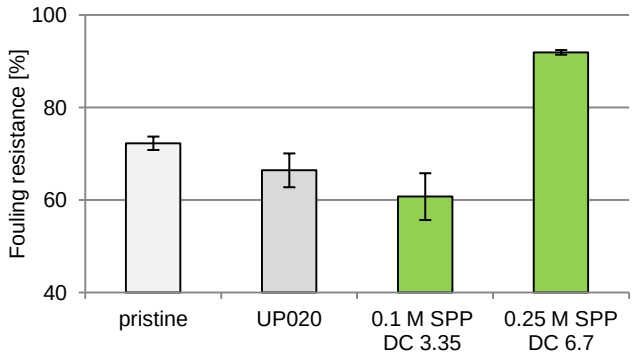

Figure 5-54 Fouling resistance during dead-end filtration of a 10 mg/L EPS solution (0.15 mL/min. pH 7.4 in PBS).

The fouling resistance of the pristine Inge membrane was 72 %. The fouling resistance of the Nadir membrane was slightly lower (66 %). The membrane modified with low monomer concentration (0.1 M SPP) and DC 3.35 showed even less fouling resistance (61 %). The best performing membrane under these conditions was the membrane modified with 0.25 M SPP and a DC of 6.7. In this case the fouling resistance was 91 %.

UV absorption at 284 nm was used to determine the feed and permeate concentrations. The calculated rejections are shown in Figure 5-55.

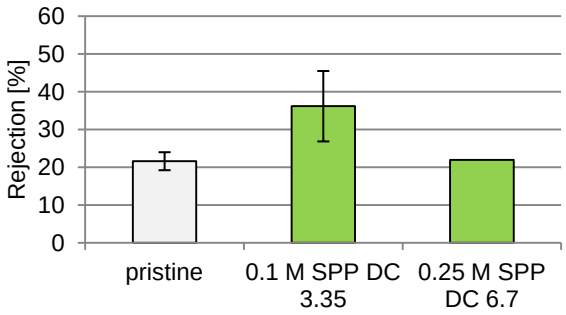

Figure 5-55 EPS rejection during dead-end filtration with pristine and modified membranes, determined by UV absorption at 284 nm.

The determined rejection was higher for the membrane modified with low DC and monomer concentration than of the pristine membrane(36 % vs. 22 %). Interestingly the rejection of the membrane modified with high monomer concentration and DC was very similar to the rejection of the base membrane.

Similar filtration experiments were performed with SMP, however here no calibration of UV could be achieved and TOC concentrations were not detectable due to the low concentrations and sample volumes. The fouling resistances are given in Figure 5-56.

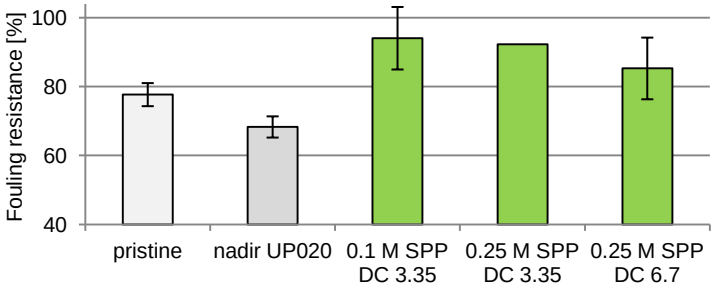

Figure 5-56 Fouling resistance during dead-end filtration of a 40 mg/L SMP solution (0.15 mL/min. pH 7.4 in PBS).

The pristine membrane already showed a quite high fouling resistance of 78 %. The Nadir membrane performed with a resistance of 68 (± 3) %. All modified membranes were significantly better than both unmodified membranes, with the highest fouling resistance for the membrane modified with low monomer content (0.1 M SPP) and DC of 3.35.

Flower soil extract

Dead-end filtration of flower soil extract was performed in a different way to compare the results from flat sheet filtration with the results of filtration experiments with hollow fibres performed at Inge's production site. Figure 5-57 shows three circles of filtration at constant pressure (adjusted for each membrane) with similar initial flux for all membranes. After every 20 min the membrane was removed from the cell and rinsed with water.

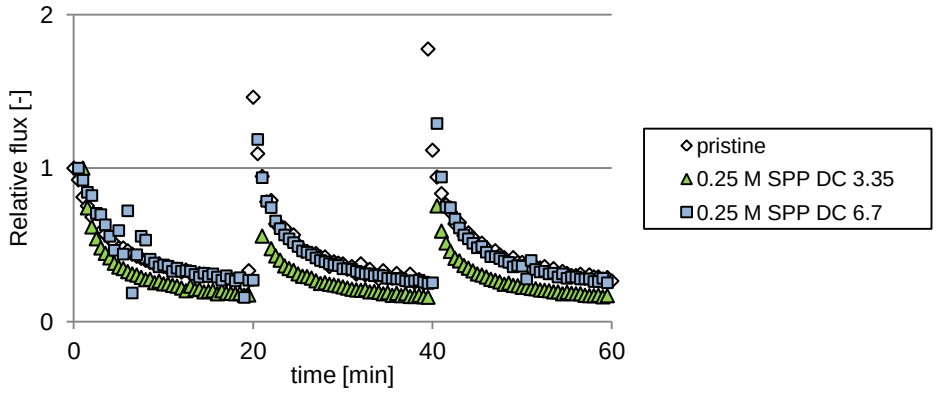

Figure 5-57 Relative flux vs. time for flower soil dead-end filtration; initial flux 0.6 mL/min, 0.42 - 0.55 bar, no stirring.

Without stirring, membranes with high DC performed similar like pristine membrane. In both cases a slight increase in permeability (expressed as higher relative flux at similar TMP) was observed after each rinsing step. This effect is more pronounced for the pristine sample. The sample modified with lower DC showed stronger flux decrease. After rinsing with water the initial flux of the pristine and the modified membrane with DC 6.7 during each further cycle was higher than during the previous cycle. This was not the case for the modified membrane with DC 3.35.

To determine the influence of stirring, the same samples were used for filtration at a stirring rate of 300 rpm at constant pressure (Figure 5-58).

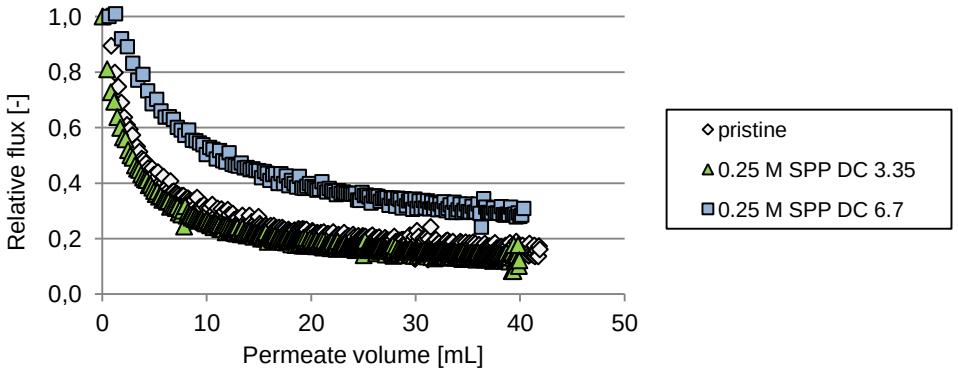

Figure 5-58 Relative flux vs. permeate volume during dead-end filtration at 300 rpm stirring, 0.6 mL/min initial flux.

Under stirring conditions the membrane with a higher DC (6.7) performed better than the pristine membrane and the membrane modified with low DC (3.35). The membrane with high DC lost only 50 % of its initial flux during permeation of the first 10 mL, while the pristine membrane and the membrane modified with low DC lost 73 % and 74 % respectively. During permeation of the next 30 mL the flux decrease was slower. The membrane modified with a high DC levelled off to 28 % of the initial flux, while the flux of the unmodified membrane decreased to 14 %. The flux of the membrane with low DC decreased to 13 %.

Permeate and feed samples were taken during filtration and the rejection was determined by TOC measurement. The results are summarized in Figure 5-59 together with a photograph of feed and permeate of one membrane.

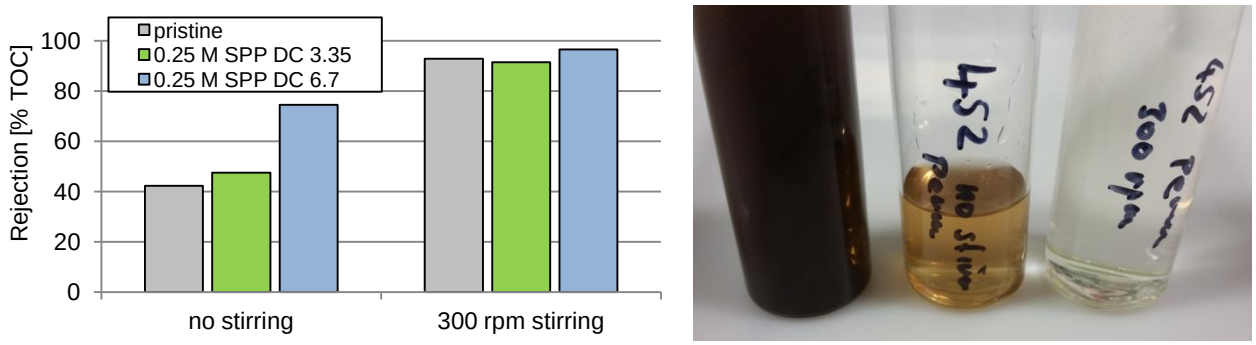

Figure 5-59 Rejection determined by TOC during dead-end filtration with and without stirring (left), right: photograph of feed solution (left vial), filtration without stirring (middle vial) and with stirring (right vial) 0.25 M SPP DC 3.35.

It was observed, that the modified sample had a significant rejection for the flower soil extract treated here, even without stirring. With stirring the rejection for modified and pristine membranes was similarly high. The higher rejection in the stirred mode could even be observed as a decolouring of permeate (Figure 5-59 right).

Before and after the whole fouling cycle, the contact angles of two samples were determined. Also the CEB treatment (cf. Chapter 4.6.4) was simulated by immersing the samples in 0.03 M H_2SO_4 and 0.03 M NaOH for 15 min respectively and measuring the CA in between.

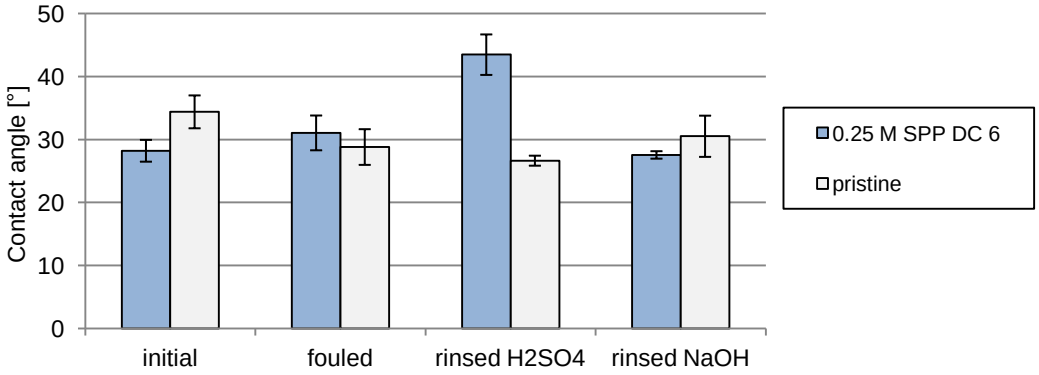

Figure 5-60 Contact angle of tested membranes after different treatment steps.

A slight decrease in CA after fouling was observed for the pristine sample, leaving it with similar hydrophilicity like the best modified samples. No change in CA was detected after immersion in H_2SO_4 or NaOH. For the modified sample a strong increase in CA was observed after H_2SO_4 treatment. After the whole cleaning cycle, the modified membrane maintained a similar CA like before the test, whereas the pristine sample was slightly more hydrophilic than initially.

5.5.2.11 Stability

The results of the performed stability tests, performed by backflushing with NaOH and soaking in H_2O_2 are shown in Figure 5-61.

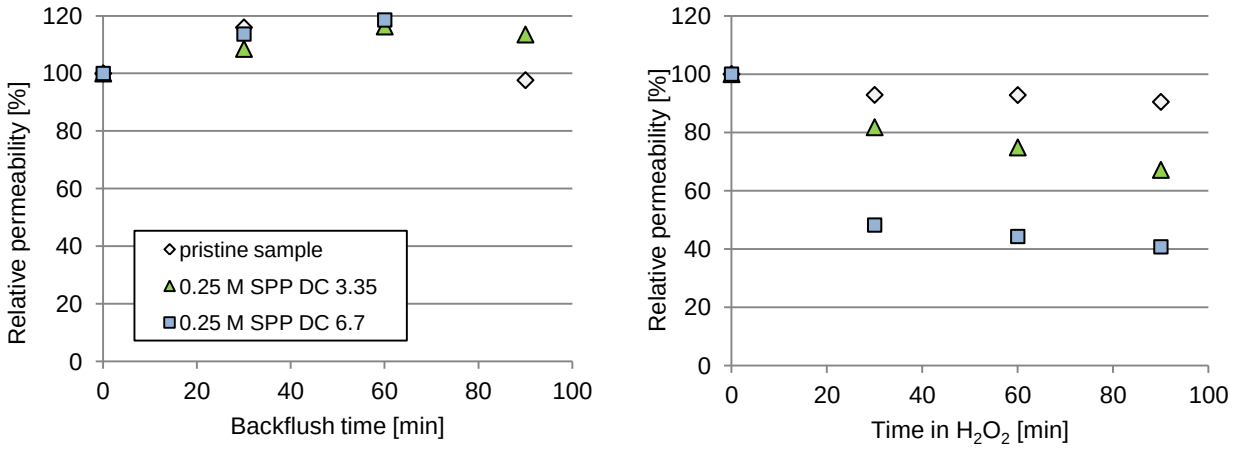

Figure 5-61 Stability of modification, indicated by permeability change during backflushing with 0.1 M NaOH solution at 0.4 bar (left) and soaking in 1 % H_2O_2 solution (right).

During NaOH backwash (Figure 5-61 left) the permeability of all used membranes increased slightly (8 – 13 %) in the first 30 min. The strongest increase was observed for the pristine membrane (19 %).

Upon immersion in H_2O_2 (Figure 5-61 right) all samples permeabilities were reduced. The permeability of the unmodified membrane decreased least with a final permeability of 90 % of the initial permeability. The permeability of the membrane modified with 0.25 M SPP DC 3.35 decreased to 67 % of the initial permeability. The permeability of the membrane with a DC of 6.7 was decreased at strongest. The decrease was fast in the initial 30 min and levelled off to 41 % after 90 min.

In order to further evaluate the origin of the permeability change observed in Figure 5-61 right, a new set of membranes was modified. Half of the samples were treated in HCl and the stability experiment was repeated. The results are given in Figure 5-62.

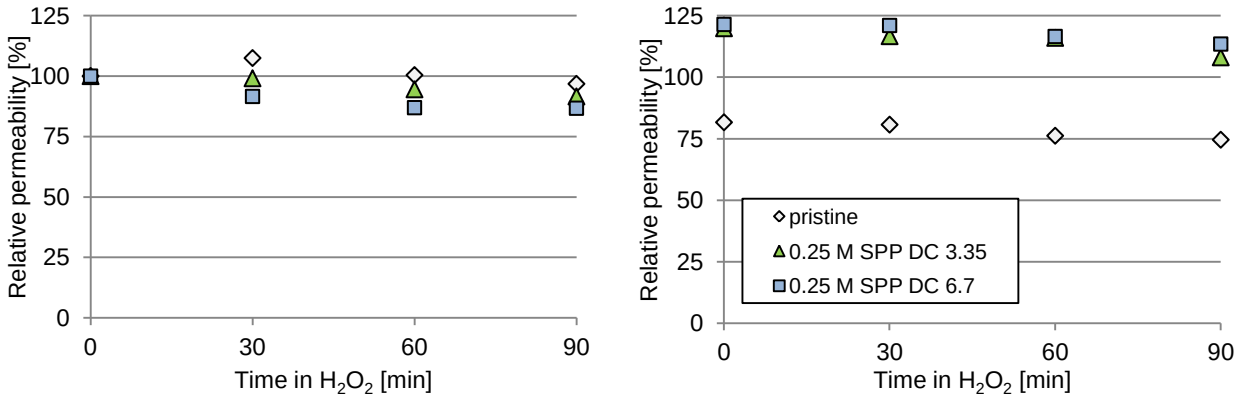

Figure 5-62 Permeability change by soaking of modified and unmodified membranes in 1 % H_2O_2 without (left) and with HCl pretreatment (right).

This time the observed decrease was lower than in the previous experiment under similar conditions (Figure 5-62 left vs. Figure 5-61 right). Still the decrease was strongest for the membrane with the highest DC. When soaked in 3 M HCl solution over night, both modified samples increased their permeability, while the permeability of the pristine membrane decreased. During the subsequent H_2O_2 treatment, none of the membranes changed its permeability significantly.

An interesting observation can be made evaluating the metadata from the performed fouling tests. Comparing the water permeabilities of modified membranes with their PBS permeabilities, differences occurred between samples modified with and without initiator. The available data is compiled in Figure 5-63.

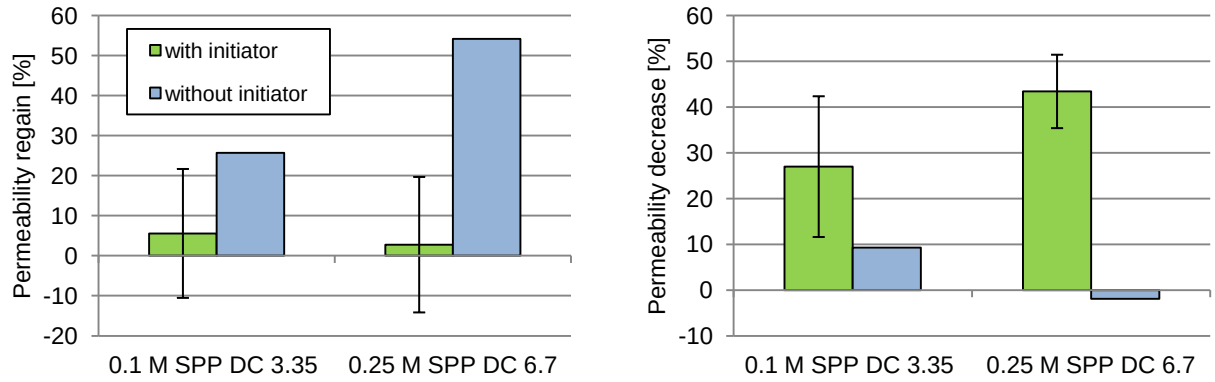

Figure 5-63 Effect of PBS solution on permeability, expressed as permeability regain (left) and remaining decrease (right).

Figure 5-63 (left) expresses the observed change as increase in PBS permeability relative to the water permeability of the newly modified membranes. The changes were relatively low (~ 3 - 5 % increase ± 16 %) for the membranes modified with initiator. At low monomer concentration and DC (0.1 M SPP DC 3.35) the membrane modified without initiator slightly increased its permeability. The membrane modified without initiator and a high monomer concentration and

DC (0.25 M SPP DC 6.7) significantly increased its permeability upon equilibration in PBS. For premodified and pristine membranes, no significant (± 3 %) changes were observed.

Figure 5-63 (right) expresses the same set of data as remaining permeability decrease in PBS solution. The grafting effect on permeability almost vanished for the samples modified without initiator, when filtrating PBS solution.

5.6 Modification of lab scale modules

The initial water permeabilities of the tested lab scale modules were mostly ranging from 600 to 1000 L/hm²bar. The redox co-initiator was used in all cases, where an initiator was used.

5.6.1 Modification effect on the permeability

The gravimetrical determination showed 99 % initiator rejection by the modules in cross-flow mode. The permeability reduction by modification is shown in Figure 5-64.

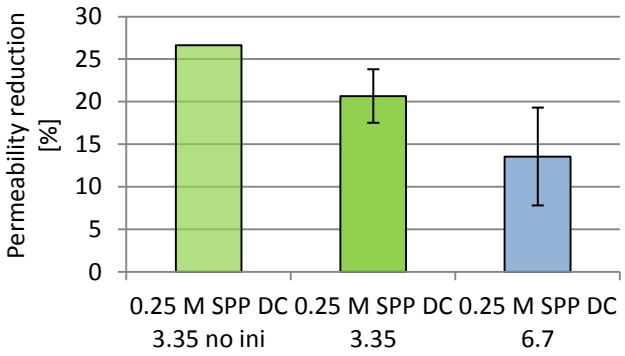

Figure 5-64 Permeability reduction by modification in lab scale modules.

The reduction was slightly lower for modules modified with initiator than without, for the modification with a DC of 3.35. Modification with a DC of 6.7 caused even lower permeability reduction (ca. 15 %).

For some samples a time dependency of permeability was observed (Figure 5-65).

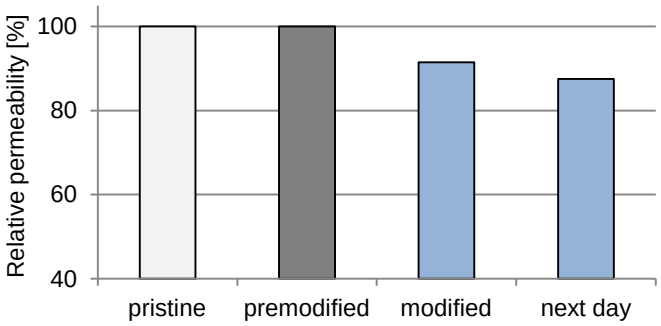

Figure 5-65 Relative permeability of small lab scale module after different steps of modification and filtration experiments.

In the sequence in Figure 5-65, pure water permeability was measured and then the module was premodified. After pre modification, the module was stored in water for one night and permeability was measured again. In this step the permeability did not change. Then the module was modified (0.25 M SPP DC 6.7) and the permeability was measured again, showing a decrease of 9 %. This decrease was even larger after storage in water over night (12 %).

5.6.2 Molecular weight cut off

The sieving curves of the unmodified and modified modules are presented in Figure 5-66.

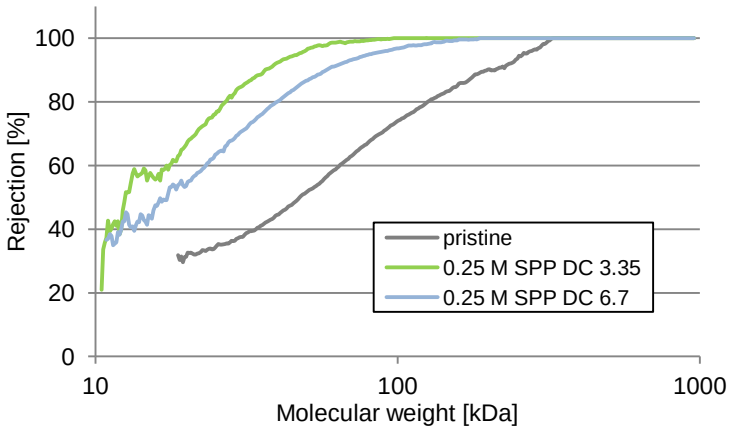

Figure 5-66 Sieving curves of modified and unmodified modules in cross-flow operation.

Both modifications shifted the sieving curves left towards lower MW. The shift was more pronounced for the membrane modified with lower cross-linker content. The MWCO was determined from the sieving curves and is given in Figure 5-67.

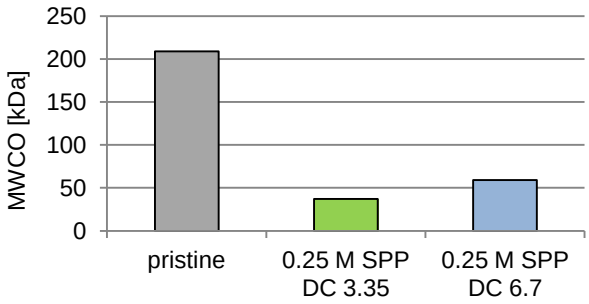

Figure 5-67 MWCO of grafted and pristine membrane modules in cross-flow operation.

The MWCO is significantly reduced by the grafting process in both cases. The decrease is slightly stronger for the membrane grafted with a lower DC.

5.6.3 Zeta potential of modified modules

Zeta potential measurements were carried out in modules to proof the hydrogel modification. The results achieved with commercial SPP are shown in Figure 5-68.

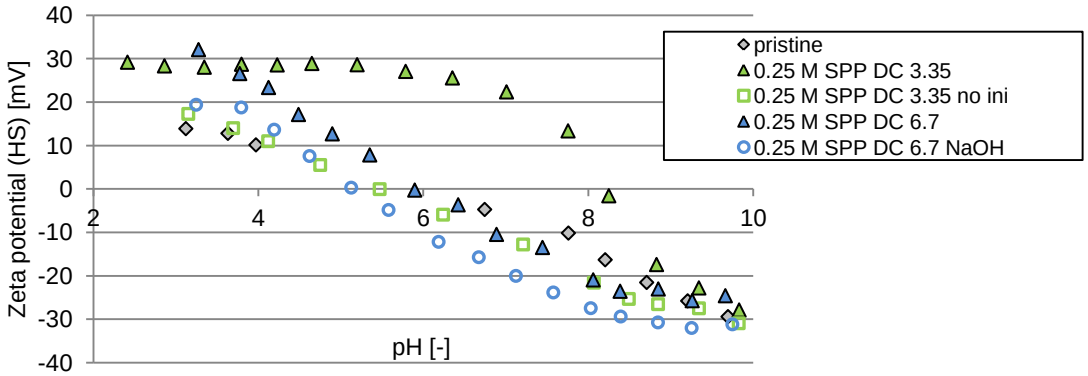

Figure 5-68 Tangential zeta potential from streaming current (SPP from ChemicalPoint).

The pristine module showed a ZP ranging from 14 mV at low pH (pH 3) to -30 mV at high pH (.8) with an IEP at pH 6.5. The modification without redox co-initiator (0.25 M SPP DC 3.35) did not lead to significant changes of the curve. Modification at similar conditions, but utilizing the redox co-initiator, led to a strong positive charge (24 mV) at a broad pH range (pH 3 – 6). The IEP of this membrane was ~ 8.2. The modification with initiator and a high DC (6.7) led to an increase in the slope compared to the pristine membrane. The IEP of this membrane was 6 and the absolute charge ranged from 32 mV (at pH 3) to – 22 (pH 9). Washing the so modified module with 0.1 M NaOH shifted the curve and IEP to lower pH (IEP at pH 5), without changing the slope.

Figure 5-69 shows a set of ZP curves, recorded with one single module during the different steps of modification (using self synthesized SPP).

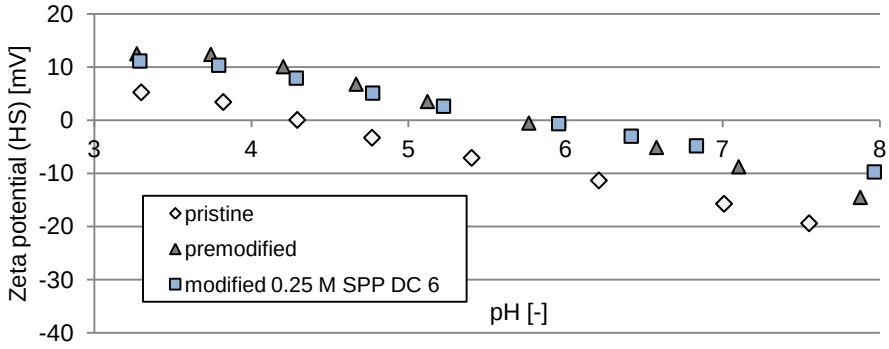

Figure 5-69 Tangential zeta potential of pristine and modified hollow fibre modules.

Interestingly the IEP (pH 4.3) of the unmodified module was different than of the one tested before (cf. Figure 5-68). However the slope of the curve was quite comparable. Upon premodification with redox co-initiator, the curve shifted towards higher ZP and an IEP at pH 5.8. Upon grafting the slope of the curve was slightly lower, with a similar IEP. However this effect was almost negligible compared to the effect of premodification.

For comparison another test was carried out by modifying a pristine module with a polycation. Unlike all other ZP data in this work, the data shown here was gathered measuring from high to low pH.

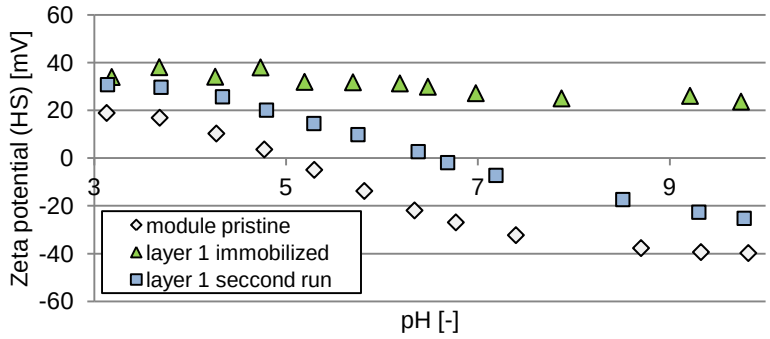

Figure 5-70 Tangential zeta potential from streaming current for pristine module and module with adsorbed cationic layer (two subsequent runs).

The absolute values determined in this test were generally higher than for the other tests with modules (cf. Figure 5-68 and Figure 5-69). The pristine module had a ZP of ~ 20 mV at pH 3 with an IEP at pH 5. The ZP at high pH (> 8.7) was – 40 mV. When immobilizing the polycation, the ZP became positive (~ 20 – 40 mV) over the whole pH range. During the second run, the module showed a negative ZP at high pH (- 25 mV at pH 9.8) and an IEP at pH 6.5. The overall behaviour in this second run was roughly between the first run and the pristine module.

5.6.4 Fouling experiments with modules

5.6.4.1 BSA fouling

BSA fouling tests were performed in cross-flow mode. The results are given in Figure 5-71.

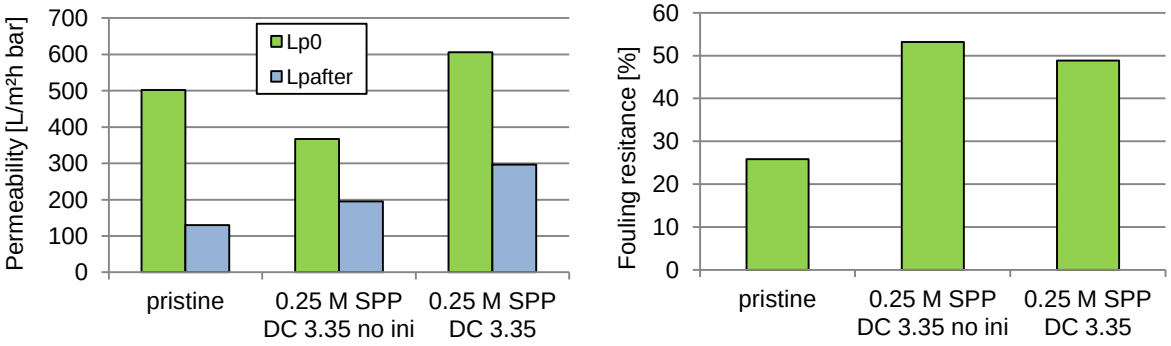

Figure 5-71 Results for fouling during BSA ultrafiltration (20 min recirculation. 1 g/L BSA. pH 7.4 in PBS. 0.4 bar). expressed as absolute permeability (left) and fouling resistance (right).

In Figure 5-71 (right) the relative fouling resistance is given. The fouling resistance of the pristine module was smallest (25 %) at the given conditions. The fouling resistance of the two modules modified with and without redox co-initiator (0.25 M SPP DC 3.35) was about twice as high. The relative fouling resistance of the module modified without redox co-initiator was slightly higher than of the module modified with redox co-initiator (4 %).

The absolute permeabilities before and after fouling (Figure 5-71 left) showed differences between the two modified modules and the unmodified module. The absolute permeability of the unmodified module was lowest after the fouling test. Since the module modified without redox co-initiator showed the lowest initial permeability in PBS, it performed worse than the module modified with redox co-initiator, despite the higher relative fouling resistance. The final permeability of the module modified with co-initiator was 300 l/hm²bar after the fouling test. This was almost three times higher than the final permeability of the unmodified module (130 L/hm²bar).

5.6.4.2 EPS fouling

The results of the EPS fouling test with single fibre modules are summarized in Figure 5-72. Error bars represent the average deviation from two subsequent flux measurements with the same module.

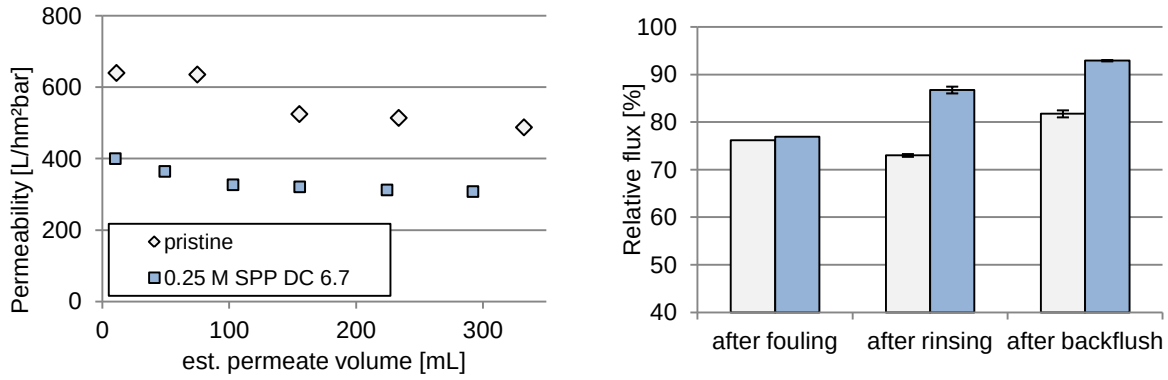

Figure 5-72 Fouling data cross-flow filtration 10 mg/L EPS in PBS buffer, permeability change during filtration (left) and flux reduction (right).

The development of the absolute permeabilities is shown in Figure 5-72 (left). The permeability of the unmodified module decreased by ~ 18 % during permeation of the first 155 mL. The permeability of the modified module decreased by ~ 19 % during the permeation of the first 100 mL. After this, both modules permeabilities only decreased slowly. The relative flux (Figure 5-72 right) derived from PBS flux before and after the test was 24 % and 23 % for the unmodified and modified module respectively. After rinsing the modules at high cross-flow velocity the flux of the unmodified module decreased another 3 % (to 63 % relative flux).The flux of the modified module was restored by 10 % (to 87 % relative flux). The back flush with water increased both permeabilities. The relative flux was then 82 % for the unmodified and 93 % for the modified module.

5.6.4.3 SMP fouling

Due to the low number of modules available, the modules used for SMP fouling were the same modules used for the EPS fouling tests. The modules were cleaned by a CEB sequence comparable to Chapter 4.6.4 before the test. The SMP fouling data is summarized in Figure 5-73.

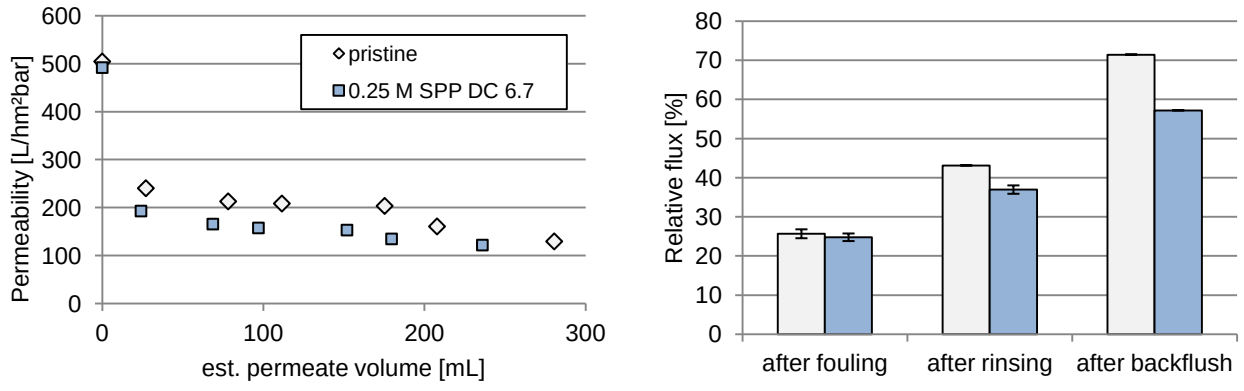

Figure 5-73 Fouling data from cross-flow filtration of 40 mg/L SMP in PBS pH 7.4, permeability change during filtration (left) and flux reduction after different steps (right).

The absolute permeability of the modified module was slightly higher (490 instead of 400 L/hm²bar) and the permeability of the unmodified module was slightly lower (500 instead of 640 L/hm²bar) than in the EPS test (cf. Figure 5-72 left). Both modules permeabilities dropped quickly (~ 60 %) during the permeation of the first 25 mL. After the initial drop the permeability decline was slower. The rinsing at high cross-flow velocity restored part of the flux of both modules. The effect was slightly stronger for the unmodified module (18 % regain instead of 12 %). Back flush with water restored more of the initial flux and again the effect was slightly stronger for the unmodified module (28 % instead of 20 % flux regain).

5.6.5 Flower soil fouling

The results of the fouling experiments with flower soil extract are given in the following. The development of TMP over time during 2 h dead-end filtration of flower soil is shown in Figure 5-74.

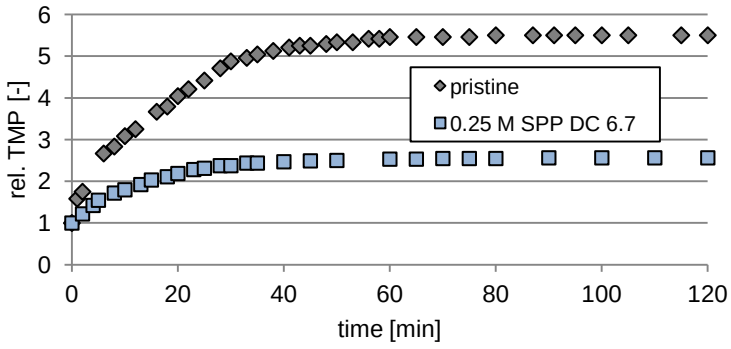

Figure 5-74 Relative TMP (TMP/initial TMP) vs. time during dead-end filtration of flower soil with small lab scale module at a constant flux rate.

The modified module started at a higher TMP (0.32 bar) compared to the pristine module (0.12 bar). The TMP in both modules increased within the first 40 min and then reached a constant value of 0.8 bar for the modified and 0.65 bar for the pristine module. The relative increase in TMP was much more expressed for the pristine module than for the modified module.

Pure water flux was measured before and after the fouling test. Figure 5-75 compares the so determined fouling resistance in cross-flow and dead-end mode.

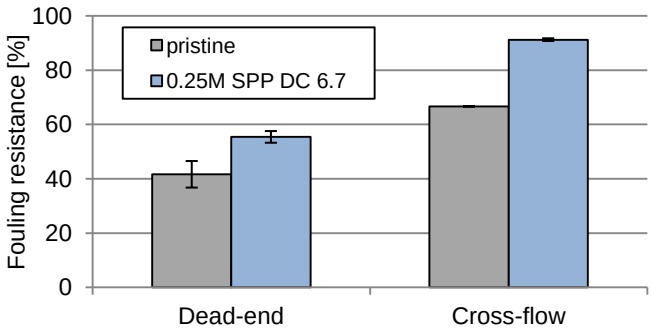

Figure 5-75 Fouling resistance towards flower soil extract for unmodified and modified modules in dead-end and cross-flow mode.

The fouling resistance was lowest (ca. 41 %) for the pristine module in dead-end mode. The fouling resistance of the modified module was significantly higher (ca. 55 %). In cross-flow operation the fouling resistance was further increased for both module types. The pristine module showed a fouling resistance of 67 % (single experiment) and the modified module showed a fouling resistance of ca 91 %. The TOC rejection determined during the experiments is summarized in Figure 5-76.

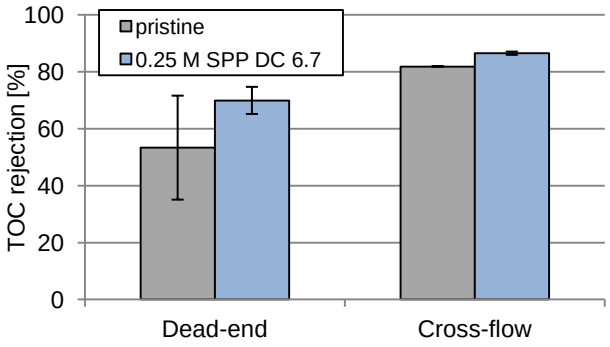

Figure 5-76 TOC rejection of modified and unmodified modules in cross-flow and dead-end filtration of flower soil extract.

The rejection was slightly higher for the modified modules in both operation modes. Also for both modules it was higher in cross-flow than in dead-end mode.

5.7 Five fibre test modules

5.7.1 Flower soil fouling

The development of TMP during cross-flow filtration is shown in Figure 5-77.

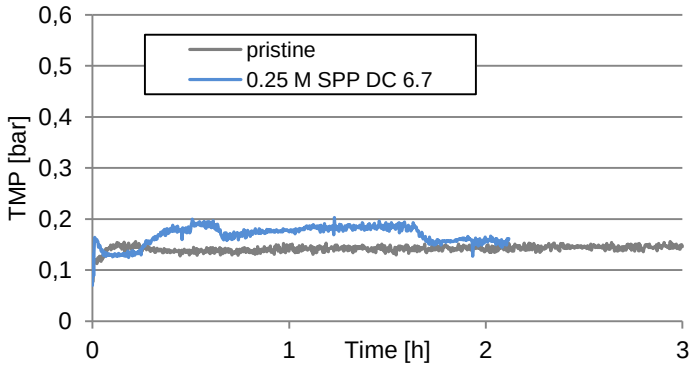

Figure 5-77 TMP vs. time during cross-flow filtration of flower soil in five fibre module.

The modified module performed similar to the pristine module. No fouling was observed for either module. The main difference was a varying TMP in case of the modified module.

The TMP development over time during dead-end filtration is shown in Figure 5-78.

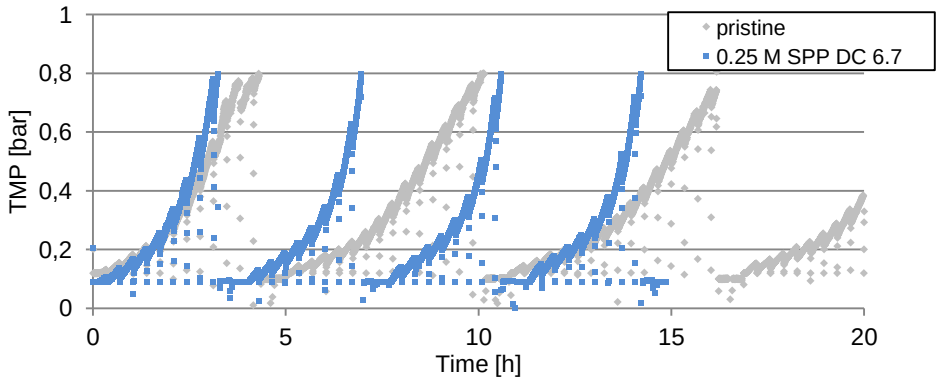

Figure 5-78 TMP vs. time during dead-end filtration of flower soil in five fibre module.

In dead-end mode a significant TMP increase was observed. The modified module showed a constant performance during four filtration cycles. The cycle duration was 3.5 h for each cycle. The pristine module increased in performance after the first cycle with cycle durations of 4, 5.4 and 5.7 h for the subsequent three cycles.

The TOC content and calculated rejection under the examined filtration conditions are summarized in Figure 5-79.

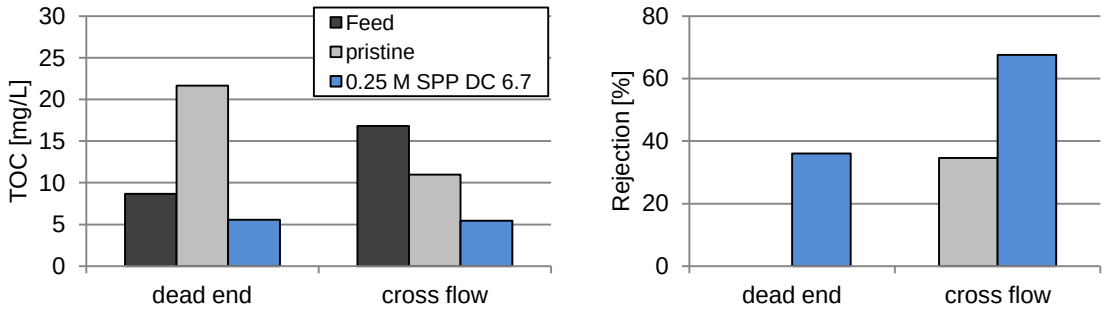

Figure 5-79 TOC rejection of modified and pristine five fibre modules in flower soil filtration.

The feed concentration was higher during cross-flow operation. The highest TOC concentration was measured in the permeate of the pristine sample. It was more than two times higher than the TOC concentration in the feed solution. Therefore no rejection could be determined for the pristine module. The TOC in the permeate of the modified module was significantly decreased and the calculated rejection was 36 %. A similar rejection was determined for the pristine module in cross-flow operation, while the rejection of the modified module was even higher (68 %). The inorganic carbon (IC) content was significantly higher than the TOC in all cases. The average determined IC was 60 (± 1) mg/L and thus three times higher than the highest determined TOC.

5.7.2 Stability during chemical enhanced back-wash

The stability data for two modified modules and a pristine module is presented in Figure 5-80.

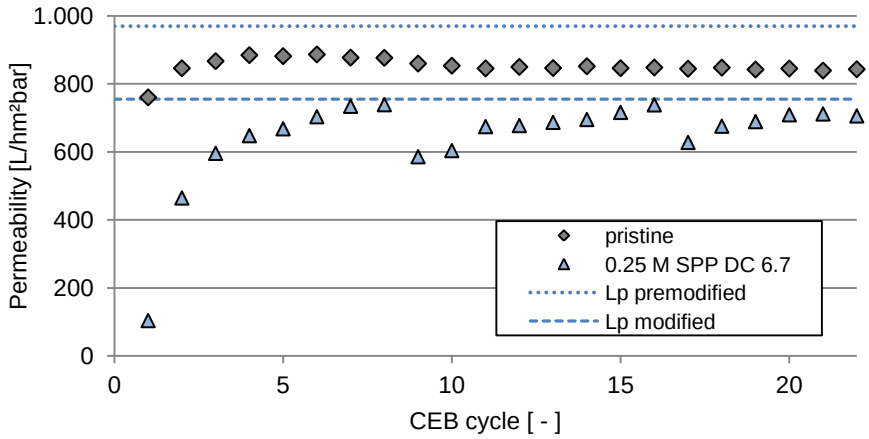

Figure 5-80 Permeability development during multiple CEB cycles.

The initial permeability was smaller than the permeability of the newly modified module and pristine module because the modules were used for flower soil fouling experiments before the stability test (due to the limited number of available modules). During the first CEB, the permeability increased significantly in case of the modified module. In the second CEB the observed increase was much lower. For the pristine module the increase was less expressed

but also took place within the first two cycles. After the third and all subsequent CEBs, the permeability was only varying around values of 600-740 L/hm²bar for the modified module. The pristine module also increased its permeability during the first four cycles, but the increase was less pronounced. The final value was varying between 840 and 880 L/hm²bar. The permeability of the modified module was never higher than the permeability directly after hydrogel modification or premodification with initiator (as indicated by the blue lines).

5.8 Pilot scale modules

The permeability decrease by modification for the two pilot scale modules was 18 (± 4) %. Besides the named adaptations for the initiator adsorption (cf. Chapter 4.6.5), no technical difficulties occurred.

6 Discussion

6.1 Bulk hydrogels

The bulk hydrogels were prepared in order to determine optimal grafting conditions for surface modification. The hydrogel based on the zwitterionic SPP has the advantage that the local charge distribution is always balanced and no sections with net positive or negative net charge are formed. The gelation times (Table 5-1 and Table 5-2) show that a minimum amine concentration is needed to catalyze the gelation. This concentration seems to be significantly higher for the mixture of cationic and anionic AATAC/AAMPSA. A possible explanation could be the coordination of the sulfonic acid groups in AAMPSA to the tertiary amine in TMED. This observation is a major drawback, when applying the hydrogel modification on a membrane using the macromolecular redox co-initiator. The amount of available amine groups on the surface is limited and cannot be increased beyond a certain level. SPP has a clear advantage due to the close vicinity of its positive and negative charge. This difference is depicted in Figure 6-1.

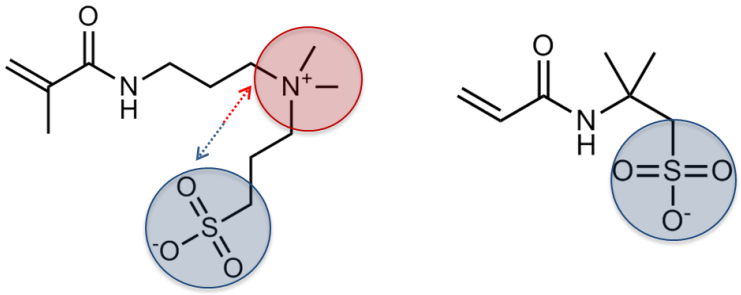

Figure 6-1 Comparison of SPP (left) and AAMPSA (right) regarding their local charge.

Due to the local charge balance, it can be expected that the tendency for coordination is lower, when using SPP.

Since only 80 % of the monomer mixture of AATAC/AAMPSA is incorporated in the bulk hydrogels, certain conclusions about the monomer reactivity can be made: The calculated N/S ratios from elemental analysis (Table 5-3) indicate similar reactivity for both monomers. Furthermore the swelling experiments (Figure 5-1) show an antipolyelectrolyte effect, indicating a homogenous charge distribution[142]. Also the homogeneity seems to be independent on the ionic strength in the monomer solution during preparation, as can be concluded from the composition of the synthesized hydrogels with different salt concentrations in the monomer mixture (Table 5-3).

It was expected that the hydrogel containing zwitterionic SPP would show increased swelling with increased salt concentration. This antipolyelectrolyte effect[143] arises due to the decreased attractive forces between the homogenously distributed charges in the polymer. When increasing the ionic strength, the electrostatic attractions are reduced and the polymer chains expand[144]. In case of a polyelectrolyte, the opposite would be observed, since the increased ionic strength should reduce the repulsive interactions of similar charges along the polymer chain and thus enable a deswelling. A homogenously charge balanced hydrogel comprising similar amounts of AATAC and AAMPSA should also show the antipolyelectrolyte effect. In case of an inhomogeneous incorporation of AATAC or AAMPSA into the hydrogel, the swelling behaviour should change to a more polyelectrolyte like behaviour[142].

The significantly higher degree of swelling (~ two times at 0 mmol NaCl) for the AATAC/AAMPSA based hydrogel compared to the SPP based hydrogel (DC 6.7) (cf. Figure 5-1) may be explained by the lower conversion (80 % vs. 87 %). However since the difference in conversion is low, the lower conversion is not likely the only explanation for the different swelling degree. Especially the lower slope of the swelling curve with increasing NaCl concentration indicates a less homogenous charge distribution compared to the SPP hydrogel. Possibly the stronger swelling in the beginning is caused by repulsion of local charges, which are countered at increasing ionic strength. This would lead to a reduction in the antipolyelectrolyte behaviour like reported by Gao[142] for zwitterionic hydrogels with a local charge imbalance.

In the SPP hydrogel the DC was also increased two times compared to the standard DC of 6.7. Interestingly, at low salt concentrations this had a negligible influence on the swelling degree. Apparently in this case the attractive ionic interactions in the hydrogel are more significant than the cross-linker content. Figure 6-2 depicts the situation in a cross-linked pSPP hydrogel.

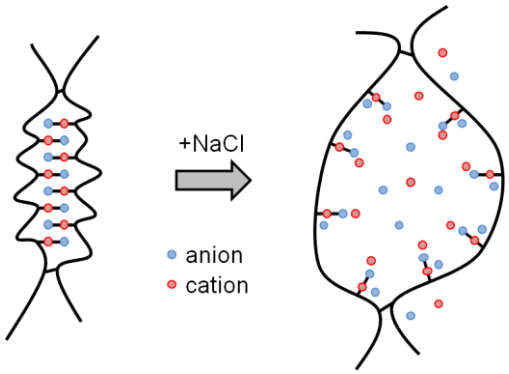

Figure 6-2 Swelling of a pSPP loop between two MBAA cross-links upon increase of ionic strength in solution.

In the absence of ions in the surrounding solution, the polymer chains are closely packed due to ionic interactions of the sulfobetaine groups. Upon addition of salt the attractive interactions are

minimized and the limiting factor for the mesh size is the amount of chemical cross-links. It is thus easy to understand why the influence of the cross-linker content on swelling degree diminishes at the absence of salt. This observation is one reason to conduct all fouling experiments (except for flower soil experiments) in PBS buffer as standard solution. Under these conditions (high ionic strength) it is expected that the actual mesh size is mainly determined by the cross-linker content. On the other hand, the permeability of membranes before and after grafting is determined in pure water in order to minimize the effect of different mesh-size on the permeability change due to the modification. By reducing the effect of DC on swelling and hence on permeability, the permeability data collected in such experiments is more apt to allow conclusions about grafting efficiency.

Due to the better compatibility with the redox co-initiator and especially since the observed difference in swelling degree becomes almost negligible for higher ionic strength, SPP seems the more promising monomer for membrane modification. Therefore SPP was chosen as the monomer system for hydrogel grafting on membranes.

6.2 Macromolecular initiator systems

6.2.1 Synthesis

6.2.1.1 Redox co-initiator

A copolymer of BMA and DMAEMA can be synthesized easily by free radical copolymerization. The used analytical methods give an indication on the possibilities to control the composition and the MW of the polymer.

The main source for losses during the preparation process is expected to be adhesion to the used glass vessels in the precipitation process. Still even when trying to minimize these effects by collecting most of the attached material in *iso*-propanol, the highest achieved yield was 70 %. Besides incomplete conversion, incomplete precipitation may be a good explanation for the observed moderate yields. Probably the smaller molecular mass fraction of the initiator is easier to be dissolved in water than the higher molecular masses. In this case the smaller polymer fraction would not precipitate and would be removed during the washing steps. This assumption is well in accordance with the observed moderate (compared to other polymers [145, 146]) PDIs during SEC (Table 5-5). Also the increased PDI at increased overall molecular mass supports this theory. When the molecular weight is increased and a similar weight distribution is maintained, less polymer will be dissolved during the precipitation step. Thus the effect of molecular weight discrimination in the precipitation step diminishes.

Assuming that the tertiary amine group in DMAEMA is mainly responsible for water solubility, a discrimination of DMAEMA rich polymer chains may be expected during the precipitation process. Indeed, in the ^{1}H-NMR evaluation (Table 5-4) a slightly higher amount of BMA is found in the copolymer than expected for the two lowest BMA:DMAEMA ratios. When comparing the EA data (Table 5-6), the N content is often higher than expected. This effect is in contrast to the observations from NMR. A possible explanation for the slightly higher N content determined by EA may be an insufficient removal of DMF. This would be detected in EA but would not interfere in the ^{1}H-NMR determination. The incorporation of isobutyronitrile as head groups resulting from the starter radicals should only have a minor influence on the elemental composition, taking into account the molecular weight of the copolymer.

Overall, the discussed effects are small and the main conclusion from the EA and NMR evaluation is that the amount of adhesive and initiator groups in the polymer can be controlled easily by adjusting the educt composition. This is also in accordance with the very similar free radical reactivity ratios of the monomers[147].

The broad variety in molecular mass distribution observed in SEC (Table 5-5) can have different reasons. The monomer mixture is already heated during the bubbling with Ar, but the temperature is only controlled in the oil bath and not in the reaction mixture. Thus, possibly the temperature, at which AIBN was added, differed between different batches. Also differences in the temperature and pH of the precipitation bath can have an influence on the molecular mass discrimination effect discussed above. The most important result of the SEC is that the molecular mass of the first series of polymers is just below the MWCO of the membranes (~70 kDa dextran). The MW can be well increased by simply reducing the initiator amount. The so produced polymer with a MW of 344 kDa should be well rejected by the used membranes. Also the low PDI is beneficial, since no lower weight fraction of polymer will penetrate into the membrane support.

The IR spectrum of MB12 (Figure 5-2) shows two characteristic bands, which may be used for identification of the initiator on the premodified membrane. However, for a quantitative interpretation the C-H band in R_2NCH_3 is not specific enough. Furthermore, this band may only be compared to the C=O band in the backbone for quantification. Since both bands are overlapped by other bands, the quantification would be less accurate than the evaluation of NMR and EA above.

Summarizing it can be concluded, that the ratio of BMA:DMAEMA, as well as the MW, can be adjusted easily by changing the composition of the educts. The synthesized polymers are expected to be random copolymers, since the reactivity rates for both monomers are very similar[147]. Furthermore, macromolecules with sufficiently high MW to feature surfactant

properties and to be rejected by the UF membrane can be synthesized by reducing the AIBN content relative to the monomer concentration.

6.2.1.2 Azo based thermal initiator

The modification of pSMA to introduce a new azo functionality is a more complex approach. Different problems occurred during the synthesis and characterization. These are discussed in the following section.

The observed changes in MW (Table 5-8) cannot be explained by the expected modification. Hydrolysis alone should not increase the MW significantly, since only one additional O and two H atoms are introduced per MA group. Furthermore, only 26 % of the polymer is composed of MA. The decrease in PDI is similarly unexpected. A possible explanation may be the hydrogen bond donor capacity introduced by the hydrolysis of the MA groups. The polymer can thus interact with the polyester material in the SEC column via hydrogen bonds. Probably the smallest molecules adsorb in the column and are thus not detected. Especially the fact that the universal calibration delivers a similar result supports this theory. The PMMA calibration is determining the MW only by retention time in the column, while the universal calibration uses intrinsic viscosity to determine MW after the separation based on retention. Therefore in case of a sole increase of interaction with the column both methods should deliver different results. On the other hand, the maleic acid groups in the hydrolysed polymer can also serve as hydrogen bond acceptors. Intermolecular hydrogen bonding could thus lead to formation of polymer aggregates with higher molecular weight.

Considering the deviation between the two measurements of pure pSMA (Table 5-8 and Table 5-11), the azo modification does not lead to significant changes in MW. The sole hydrolysis increases the determined MW. Since the modification includes the same hydrolysation step, a similar increase would be expected after azo-modification. A possible explanation for the almost unchanged apparent MW is successful introduction of the azo side group. Due to the bulkyness and hydrophobic nature of the introduced azo side group, the effect of the hydrolysis (hydrogen bonding) on apparent MW is compensated and the MW is only slightly increased.

The elemental composition of pSMA determined by EA (Table 5-9) is very close to the expected values. However the sum of detected elements is only 98 %. This deviation is likely due to an experimental error, since in a later measurement (cf. Table 5-12) the matching composition is found. After simply hydrolyzing the polymer, the sum of detected elements is only 94 % (Table 5-9). This is possibly due to the presence of remaining NaCl from the hydrolysis procedure. Also presence of Na^+ as counter ion of the maleic acid groups is possible. This effect is even more pronounced after combined modification and hydrolysis. The determined O contents are too

high in both cases. A possible explanation may be an interference of the inorganic components on the O determination. Since O is determined in an independent analysis, the ratios of the other elements should still be precise. Most interesting is the N:C ratio in the azo modified pSMA. The determined ratio is 0.014, while 0.018 would be expected for 10 % modification of MA. The determined N:C ratio is corresponding to a modification of 8.3 % of the MA groups.

A successful modification with the azo group is also indicated by UV-VIS spectroscopy (Figure 5-3). The strong absorption of azo-benzyl alcohol (expected at 289 nm) can also be found in the modified pSMA, but not in the solely hydrolysed polymer.

The ATR-IR spectra (Figure 5-4) clearly show the successful hydrolysis of all MA groups, since the characteristic bands for anhydrides (1774 and 1849 cm^{-1}) are disappearing. Azo groups are known to feature very low and often not existing IR activity[139]. The observed similarity in IR spectra of azo-modified and hydrolysed pSMA besides the fingerprint region does therefore not contradict a successful modification.

Summarizing, it can be concluded that ~ 8 % of the MA groups are modified with a new side group and the subsequent hydrolysis is successful. However the arguments for successful introduction of the azo-functionality are mainly indicative.

6.2.1.3 Peroxide based thermal initiator

The synthesis and characterization of the peroxide based thermal initiator was successful and is discussed in the following section:

Due to the higher degree of modification and generally better solubility in NMR solvents (compared to the azo modification), the modification degree of MA with organic peroxides can be determined by ^{1}H-NMR (Table 5-10). For the ^{t}Bu-OO-pSMA this determination is relatively precise, since the peaks used for determination are well separated. The determination is much less reliable in case of cumyl-OO-pSMA, since the bands of aromatic CH in the cumyl- and styrene groups are overlapping and multiple correction steps are needed. The ^{1}H-NMR can therefore proof successful modification in both cases but only indicates a slightly higher degree of modification for cumyl-OO-pSMA than for ^{t}Bu-OO-pSMA.

The MW determined by SEC significantly differs depending on the detection and evaluation method. This behaviour is completely different than for the azo modification, where both evaluation methods lead to similar results (cf. Table 5-8). The universal calibration uses intrinsic viscosity for MW determination. Since the modification procedure introduces new side groups to the pSMA, the probability for entanglements becomes larger. Due to more entanglements the

detected viscosity can be increased further than by sole increase of the chain length. However, the effect of this “branching” is likely to be low due to the short length of the side groups[148]. Hydrogen bonds could be another explanation. The increase in intrinsic viscosity always occurs after hydrolysis of the MA, which creates two carboxylic acid groups capable to act as H-bond donors and acceptors. Thus, the combination of increased branching and increased intermolecular hydrogen bonding can lead to an increase in intrinsic viscosity and hence apparent molecular weight.

The lower apparent molecular weights in case of the evaluation based on RI and PMMA calibration can only be explained by longer rejection times in the column. This can be due to hydrogen bonding to the polyester material in the column. While this bonding was strong in case of the azo modification and pure hydrolysis (cf. Chapter 6.2.1.2), it is likely less expressed here. The main reason can be the introduction of bulky cumyl and ^{t}Bu perester groups to the polymer. The cumyl hydroperoxide modification is apparently more efficient (like derived from ^{1}H-NMR), and the cumyl group is more bulky than the ^{t}Bu group. Therefore the introduction of the cumyl side group may shield the hydrophilic maleic acid groups located at the polymer backbone. This would lead to lower rejection times in the column due to less hydrogen bonding and hence explain the observed higher apparent MW.

The elemental analysis of modified and unmodified pSMA (Table 5-12) is to some extend inconclusive. The composition of pSMA is similar to the theoretical composition. This indicates that the MA is not hydrolysed during storage. The high O content of cumyl-OO-pSMA could be explained by incomplete drying, especially since the H content is also higher than expected. The presence of N indicates also incomplete removal of Et_3N from the synthesis (cf. Chapter 4.4.1.2). However in the ^{1}H-NMR spectrum (cf. Appendix Figure 11-5), the characteristic peaks for Et_3N in DMSO at 0.93 ppm and 2.43 ppm[149] are missing. Also the water peak at 3.33 ppm is very small. The missing 5 % in the elemental composition may be Na^+ counterions and/or NaCl from the hydrolysis and neutralization step as discussed for the azo-pSMA. This may lead to similar problems in the O determination.

Since the C, H and O content of ^{t}Bu-OO-pSMA covers 100 % of the composition, a presence of Na and Cl is unlikely in this case. The low O content can thus be explained best by incomplete hydrolysis of the MA groups. This explanation is unlikely, taking into account the disappearing MA band in IR (Figure 5-5) clearly indicating hydrolysis of most of the MA groups during both modifications (with cumyl- and ^{t}Bu- hydroperoxide). However the oxygen content is still increased compared to the base polymer. The EA therefore indicated successful modification, but does not allow a quantification of the incorporated perester bonds.

Besides the hydrolysis, IR is also indicating successful introduction of a new peroxide group into the polymer causing an absorbance band at 830 cm^{-1} for both modifications (Figure 5-5). However the new band is in the fingerprint region and thus only indicative[139].

Summarizing it can be concluded that the modification was successful. NMR indicates different modification degrees with cumyl and ^{t}Bu- hydroperoxide and IR indicates complete hydrolysis and introduction of the new peroxide group.

6.2.2 General applicability

Since the membranes and especially the membrane modules are expected to only tolerate a small content of organics in aqueous solution, compositions must be determined, where the initiators can be dissolved but will still adsorb to the membrane surface. For this reason the main goal is to create solution systems close to the solubility limit, where the macromolecular initiators/co-initiators act as surfactants. On the other hand, the synthesized polymers need to maintain a maximum initiator activity. The best initiator should be large enough to be completely rejected by the used UF membranes. Also the initiator has to adsorb well to the PES membrane surface, while featuring a high activity.

6.2.2.1 Redox co-initiator

The composition of the DMAEMA-co-BMA copolymer is strongly influencing its water tolerance. The CWC decrease with increased BMA content (Figure 5-6) can be attributed to the decreased hydrophilicity. The increased solubility at low pH can be explained by protonation of the DMAEMA groups. With its pKa of 7.4[150], the DMAEMA will be easily protonated thus making the polymer water soluble. Since the polymers are not soluble in diluted HCl alone within reasonable time (< 1 day), the polymer is first dissolved in alcohol and then mixed with diluted HCl solution. Since the CWCs are higher for solutions in *iso*-propanol, this solvent is the better choice for surface modification. Due to the higher CWC, a lower solvent content is needed. The used solvent composition for all initiator adsorption steps (Chapter 4.4.2.3) was developed from the observations during the CWC experiments. The composition was not further optimized here, but the solvent content may likely be further reduced for less solvent tolerating systems in future applications.

The CMC decreases with increasing fraction of hydrophobic BMA in the polymer (Figure 5-7). As discussed in Chapter 2.5, the structure of hydrophobic groups is crucial for the micelle formation and the adsorption efficiency. Due to the expected random copolymerization, the formation of larger hydrophobic sections becomes less likely when reducing the BMA amount in the educt mixture. Since the initiator with a 1:1 ratio of hydrophobic BMA and hydrophilic

DMAEMA shows no shift in pyrene fluorescence, absence of micelle formation can be concluded. Likely this is due to the close vicinity of the hydrophilic groups in this polymer. The different behaviour of the polymer with a ratio of 1:1 (MB11) is also observed in the SPR and QCM adsorption experiments (Figure 5-9 right and Figure 5-11 left). It can therefore be concluded, that the amount of hydrophobic BMA is not sufficient in MB11.

Except for MB11 with the lowest amount of BMA groups, all redox co-initiators show irreversible adsorption to PES model surfaces in SPR (Figure 5-10). The amount of initiator adsorbed to the surface seems to increase with increasing BMA content. However in the QCM studies (Figure 5-11) this trend is not confirmed. The main difference between the two measurements is that QCM was measured under flow through conditions, while SPR was measured with a constant volume, which was only mixed. In order to avoid drying of the PES surface in SPR, the surface could only be rinsed by dilution and partial removal of the analyte (i.e. 40 µL of 50 µL sample solution are replaced by 40 µL background solution in each rinsing step cf. 4.4.2.3), while in QCM the sensors could be rinsed several minutes with fresh background solution. Also in QCM the difference between the frequencies in water was determined (with the sequence water, background solution, sample, background solution, water), while the angle shift in SPR represents the shift in background solution with the sequence background solution, sample, rinsing, background solution). The differences in absolute values can therefore be explained by the different experimental procedures. The SPR experiments represent the situation during initiator immobilization, while the QCM experiments give additional information on the stability during the subsequent treatment process (i.e. rinsing with water and permeability determination). Both methods indicate a very stable adsorption of the polymer to the PES surface. Furthermore the adsorption happens very fast and seems to reach saturation. Assuming a density of 1 g/cm³ for the polymers, a layer thickness of 0.3 to 0.43 nm can be calculated for the masses determined by QCM. This is significantly lower than the layer thickness determined by ellipsometry (cf. Table 5-14) which indicates layer thicknesses of about 4 nm. The reason for this is probably that the layers are not dense polymer films with a density of 1 g/cm³ but are better described as layers with cavities and defects. In this case the actual refractive index would be different than assumed for an optically homogeneous polymer film. Unfortunately a combined determination of layer thickness and refractive index was not possible here because of the high complexity of the model system. The main problem is the usually bad fitting in the multilayer measurements. For the PES coated sensors, the thickness of the single PES layer could be well determined. The evaluation of the multilayer system (Si, SiO_2, PES and initiator) makes assumptions regarding the thickness of SiO_2 and uses Δ and Ψ values from one single spot of the PES coated surface as a basis for the evaluation of subsequent measurements. A slight deviation in the actual PES thickness on one chip can therefore lead to problems in the determination of subsequent layers, when not measuring at the exactly same

spot. The determined layer thicknesses are therefore not to be taken as absolute values, but more as indicators for the presence of a very thin layer of initiator on the surface.

Summarizing, the adsorption onto PES model surfaces is proved by SPR and QCM. QCM and ellipsometry indicate the formation of a very thin layer in the range of a monolayer. This will be beneficial for membrane modification, since such a thin layer should not cause a significant permeability decrease. The initiator with the largest fraction of DMAEMA groups (that will act as co-initiator) and still featuring good adsorptive behaviour is MB12 with a BMA:DMAEMA ratio of 1:2. This polymer appears therefore most promising as a co-initiator for membrane modification.

The co-initiator activity of the synthesized poly BMA-co-DMAEMA copolymers is proven by in situ rheology (Chapter 5.2.4.1). The longer reaction times at low pH may be attributed to protonation of the tertiary amine groups. In the protonated state, the tertiary amine group has no free electron pair and can thus not act as an electron donor in the initiation mechanism (cf. Figure 3-3). Interestingly the TMED/APS initiated reaction seems less sensitive to pH. This can be explained by the close vicinity of the two amine groups in TMED. Since they are only separated by two carbon atoms, the charge of the first amine groups impedes protonation of the second[151]. Therefore one amine group will stay unprotonated and active at lower pH values. Also the 1:1 copolymer of BMA and DMAEMA shows faster gelation than the pure pDMAEMA. This observation can be explained, taking into account the amounts of polymer used in the experiment. The experiment was performed with similar concentrations regarding the concentration of amine groups. Therefore the polymer concentration in the solution is twice as high in case of the MB-11 (8.98 g/L) as for the pDMAEMA (4.72 g/L). From the intrinsic viscosity determined for MB-11 in the SEC detector, the overlap concentration can be estimated. The overlap concentration characterizes the point, where polymer coils start to interact and are thus capable to form cross-links. Its value can be estimated as the reciprocal of the intrinsic viscosity[152]. For MB-11 the so estimated overlap concentration is 98 g/L, which is in a comparable range like reported overlap concentrations of methacrylate polymers of similar molecular weight[152]. The concentrations of solutions prepared here are approximately 10 times lower than the overlap concentration. During the polymerization reaction the macromolecular initiators are grafted with the SPP-co-MBAA polymer. This increases their molecular weight and will hence decrease the overlap concentration until the gel point is reached, at which the independently growing polymer structures start to interact and cross-link. Since the concentration of growing polymer molecules is twice as high in the case of MB-11, the gel point is reached earlier in this case. The observed effect is significantly lower than the actual co-initiating effect of the amino groups as can be derived from the much faster gelation in all cases where initiator was used (10 – 30 min with and > 12 h without co-initiator). Therefore, it can be

concluded that the incorporation of amine groups to polymers does not significantly reduce their co-initiator activity in the case studied here.

In the rheology experiments, a general trend of increasing storage moduli with increasing pH (in the range from pH 4 – 10) is observed (Figure 5-17). The observation may be due to less chemical cross-links at lower initiator concentrations; at low concentrations of active starter radicals longer separated chains will form. With a lower amount of growing polymer chains, the propensity for the growing chain to meet a double bond in a cross-linker molecule of another growing chain is lower. Interestingly the use of polymeric co-initiators also leads to lower storage moduli than TMED at higher pH (pH 6 and 8) and similar concentrations. This may be explained by the co-promoting effect of the second amine group in close vicinity in the TMED molecule making TMED a better co-initiator, when no protonation occurs[94].

Summing up the data shows that the polymerized tertiary amines can be used as co-initiators with APS in a similar way like TMED. Even though the activity seems slightly lower than for TMED, the system seems well applicable to initiate polymerization of a cross-linked polySPP hydrogel network. In combination with the good adsorption performance, the system appears very promising for membrane modification.

6.2.2.2 Azo based thermal initiator

The azo modified pSMA is well soluble in water which is likely due to the low modification degree of only 8 % (cf. Chapter 6.2.1.2) and hence the high amount of hydrophilic maleic acid groups. The strong increase in CMC (Figure 5-8) at higher DMAc contents is another indication for successful modification. The chemical properties of the side groups can have a strong influence on the micelle formation[153]. Due to the large number of carbon-nitrogen bonds in the azo side group, interaction with DMAc is more likely than in case of the unpolar styrene or the charged maleic acid groups in the unmodified polymer[154]. The data shows furthermore that the micelle formation can be well controlled by adjusting the DMAc content of the prepared solutions.

The SPR experiments (Figure 5-13) show similarly fast and strong adsorption to PES like the redox co-initiators (cf. Figure 5-9 (left)). The absolute changes are also in a similar range like for the co-initiator. The angle shift of 130 m° can be considered moderate in comparison to other studies with the same device (60 m° - 600 m° for different proteins on different polymer surfaces)[155].

Especially after adsorption in 20 % DMAc solutions, the evaluation of ellipsometry measurements is almost impossible (Table 5-15). One reason may be the swelling of PES in

DMAc containing solutions[107] probably leading to rearrangements or partial detachments of the PES layer. In this case the assumptions regarding PES layer thickness and the existence of two well separated layers could be invalid leading to the observed strong deviations.

Overall, it is concluded that the modified polymer can be adsorbed onto PES surfaces in a similar way like the macromolecular redox-co initiators. Furthermore the MW should be sufficient, so that the molecule is well rejected by the used UF membranes.

No thermal initiator activity is found for the azo modified pSMA at 80°C. This is unexpected because a pure monomer solution with similar monomer concentrations shows a gel point after only 140 s (cf. Figure 5-20). A possible explanation may be that the quite high concentration of 1 g/L polymer inhibits the self initiated thermal polymerization by increasing viscosity and reducing the general monomer mobility in the solution. Due to the low content of azo groups (0.2 mmol/L assuming 8 % of the MA groups are modified) this negative effect cannot be countered by the thermal radical formation. Hindered diffusion is known to increase the reaction speed in some cases like described by Trommsdorff et al. [156]. The Trommsdorff effect occurs, when the growing polymer chains are more hindered from diffusion than the monomers and chain termination is thus inhibited. The hindered mobility of growing chains can be expected to lead to less cross-linking, since the propensity of two chains to meet is reduced. Furthermore the polyanionic hydrolyzed pSMA chains may act as a kind of spacer due to electrostatic repulsion. During membrane modification, the modified pSMA will be adsorbed on the membrane surface so the described problems should not occur. However, besides the inhibiting effect on bulk hydrogel formation, the azo compound is not cleaved by thermal energy but only by UV irradiation as can be derived from the UV measurements (Figure 5-19). The observed UV degradation is in accordance with the half life time of 135 s at 50 mW/cm² reported in literature[93]. Nevertheless, the thermal decomposition should also be detectable due to the reported half life time of 180 min at 80 °C[93].

Summarizing, it can be said that the modified and hydrolysed pSMA shows strong and fast adsorption to PES model surfaces. The polymer seems therefore suitable for synthesis of a macromolecular thermal initiator. On the other hand, the thermal initiator activity could not be proven. A possible explanation for the low activity may be decomposition of the azo compound during hydrolysis of the MA, since similar azo compounds are instable in aqueous solution[100]. In this case the detected nitrogen could be explained by decomposition byproducts, which are UV degradable but not thermally degradable. A possible pathway for the hydrolysis may be a hydrolysis analogous to the Japp-Klingemann synthesis[157]. The suggested mechanism is shown in Figure 6-3.

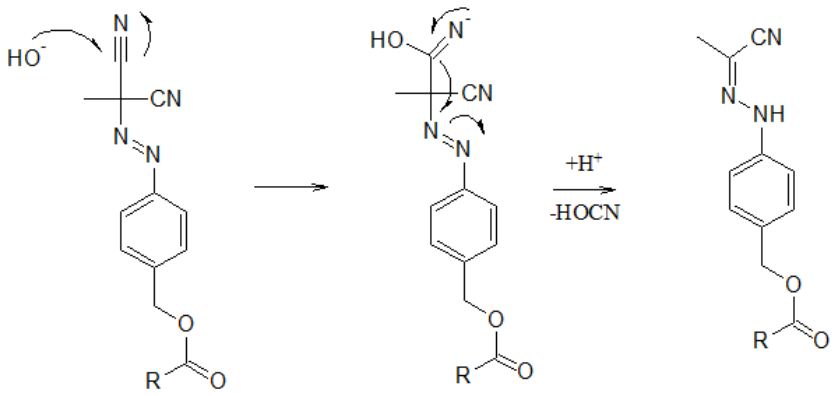

Figure 6-3 Suggested mechanism for hydrolysis of azo group.

In this case a large fraction of the nitrogen would still be detected in the modified polymer. Indeed it has been reported that similar water soluble azo compounds form hydrazones under alkaline conditions (pH ≥ 8)[158]. Milder conditions during the hydrolysis (i.e. lower pH) could avoid this side reaction. On the other hand, longer hydrolysis times would lead to more thermal decomposition of the azo compound.

The presented approach to a thermal macro initiator has two inherent weak points, which are caused by the ester bond of the azo functional group to the base polymer and the azo bond itself. Furthermore, the multistep synthesis of the azo functional group is a significant disadvantage and source for arising difficulties. It is therefore considered reasonable to stop the development of the azo based initiator and instead use the proven good adsorption properties of the easy to modify base polymer, but change the initiator group to an easier to achieve peroxide based modification.

6.2.2.3 Peroxide based thermal initiator

The peroxide based thermal initiator seems much more feasible than the azo based thermal initiator. The pSMA base polymer as well as the used hydroperoxides are available in large scale[96, 159].

The modified polymers can be well dissolved in an aqueous alkaline solution containing only 2 % DMAc. This may enable an application of the initiator in situations, where the redox initiator solution (acidic aqueous solution containing 20 % *iso*-propanol cf. 5.2.2.1) cannot be applied.

The CMC of cumyl-OO-pSMA is slightly higher than for ^{t}Bu-OO-pSMA (Table 5-13). Two obvious differences between the polymers could explain the disparity: The *tert*-butyl and cumyl substituents have a different size and flexibility and can therefore be expected to shield the modified MA group in the base polymer to a different extend. Also the degree of modification is different for both polymers (cf. Table 5-10). Due to the higher degree of modification, the maleic

acid groups in the cumyl modified polymer are less accessible for hydration. Therefore a lower CMC would be expected for this polymer. Since this is not the case, the CMC is likely more influenced by the bulkiness and conformation of the cumyl group than by the number of hydrophilic units. This observation is also in accordance with the fact that benzene rings reduce the CMC less than six single CH_2 groups[80]. Due to the lower CMC the ^{t}Bu-OO-pSMA initiator is expected to show better adsorption performance. But considering the error bars, the differences observed in the SPR adsorption experiments (Figure 5-14) are low. Both initiators show a fast and irreversible adsorption to the PES surfaces. Only at higher concentrations of DMAc the response decreases. This is well in accordance with an increase in CMC like it was observed for the azo modified and hydrolyzed pSMA (cf. Figure 5-8). From the data it can be concluded that the membrane premodification should be performed at concentrations of 0.1 g/L initiator in a solution containing 2 % DMAc.

The initiator activity for both modifications is well proven by in situ rheology (Figure 5-20). Gelation with both of the two thermal initiators is generally faster than the spontaneous thermal polymerization of the monomers. The polymerization initiated by ^{t}Bu-OO-pSMA is always faster than with cumyl-OO-pSMA. This is unexpected when taking into account the half-life times of the hydroperoxides used for modification (Figure 6-4).

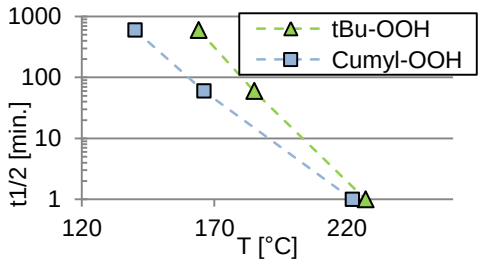

Figure 6-4 Half-life times for hydroperoxides at different temperatures[160].

Assuming a similar reactivity trend for the peresters, a faster gelation with cumyl-OO-pSMA would be expected due to the shorter half life time (i.e. faster radical formation). Due to the low precision of the determined modification degree in case of cumyl-OO-pSMA, the perester concentrations were probably not the same during the in situ rheology experiments causing the apparent lower reactivity.

Both initiators seem suitable for membrane modification according to the adsorption and activity tests. Since the determination of perester groups in ^{t}Bu-OO-pSMA is more precise and the CMC is lower for this macromolecule, thermal membrane modification is conducted with this initiator.

6.2.3 Suitability for membrane modification

Suitable conditions for membrane grafting were found for the developed thermal- and redox co-initiator systems. The determination of the degree of grafting was complicated for the used membranes. Generally, a very simple way to determine grafting efficiency is the gravimetric method, which was tested with the redox system (Figure 5-27). Since the samples have to be dried before and after each step, changes in the membrane structure are possible. Since the dried membranes cannot be directly immersed in aqueous solution, they were rewetted in *iso*-propanol with a subsequent solvent exchange before the grafting step. Since *iso*-propanol is a good solvent for the used initiators and also causes swelling of the membranes, initiator desorption can be a problem in this step. This may be the main reason, why no significant differences are observed between samples modified with or without initiator.

A more promising way to rate the grafting efficiency by a simple method uses the grafting effect on permeability. The grafting on the surface influences the permeability by adding an additional layer, that causes further hydraulic resistance. The same applies for grafting in the membrane support. Generally, more grafting should therefore lead to a lower permeability. However, the permeability change cannot directly be correlated to DG, since the DC and the location of grafting will also have an influence on the permeability. Figure 6-5 depicts the main hydraulic resistance layer for a base membrane and two grafted membranes.

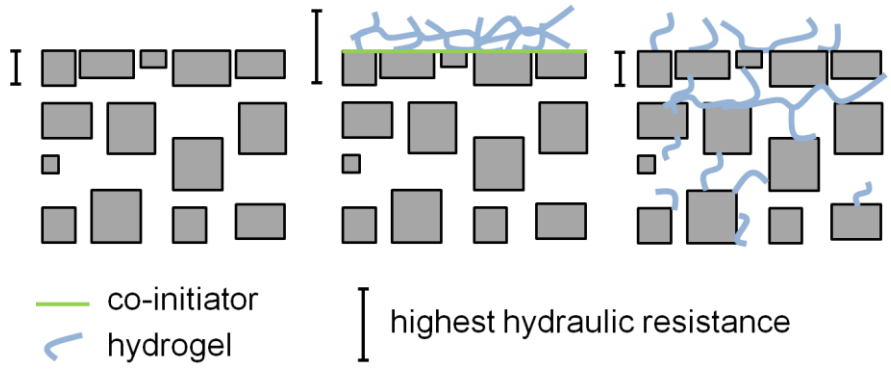

Figure 6-5 Main hydraulic resistance (left to right) of a pristine membrane, a membrane grafted using co-initiator and a membrane grafted homogeneously over the entire cross section (the polymer amount is identical).

In case of the base membrane, the selective layer is forming the main hydraulic resistance. In case of the membrane grafted using the redox co-initiator, the grafting is concentrated on the membrane surface forming an additional dense layer. Thus, the area of high hydraulic resistance becomes larger. In case of the membrane grafted homogeneously with a lower DG (i.e. similar amount of hydrogel on more surface area), the main hydraulic resistance is still caused by the selective layer. Since the main part of the hydrogel is covering the pore walls of the porous support, its influence on permeability is minimal.

When the grafting is only located at the surface, the DC is also expected to influence the permeability. In case of a more cross-linked hydrogel network, the permeability should be lower due to the higher hydraulic resistance of the hydrogel. Pure water was used for permeability determination to keep the effect of DC on swelling low (cf. Chapter 6.1), therefore the correlation of the observed flux decreases to grafting efficiency appears valid.

The reason for the strongly differing influence of commercial (Figure 5-28) and self synthesized (Figure 5-29) SPP on membrane permeability remains unclear. A possible explanation may be pre-polymerization of the monomer due to improper transport and storage conditions. This could be evaluated by SEC, but due to possible damage of the column in case of a different problem with the monomer, this test was not carried out. With the commercial SPP a very strong effect of the initiator on grafting is achieved for medium DC. At higher DC the grafting efficiency is also high in the absence of initiator. Also when using the self synthesized SPP, a significant increase in unspecific grafting is observed upon raising the DC (Figure 5-29). This can be partly explained by the lower swelling degrees due to higher cross-linker content, which leads to lower permeability through the network. Also polymers formed in the bulk solution in the porous support are more like to get trapped there, when the network is more cross-linked and thus less flexible.

A similar but less pronounced effect is observed for the thermal grafting (Figure 5-25). When just adsorbing the thermal initiator to the membrane, its activity is obviously not high enough to cause a significant effect on grafting. The reversible decrease in permeability by initiator filtration can be explained by a combination of possible influences. The membrane polymer is likely swelling in the initiator solution containing 2 % DMAc. This may lead to stronger compaction during the initiator filtration step. The compaction would then be reversed partially in the subsequent heating step without pressure. Also the observed increase in hydrophilicity upon heating of the premodified membrane in pure water (Figure 5-26) may cause an increase in permeability. Furthermore the change in CA indicates a successful cleaving of the peroxide bond at the surface, as presented in Figure 6-6.

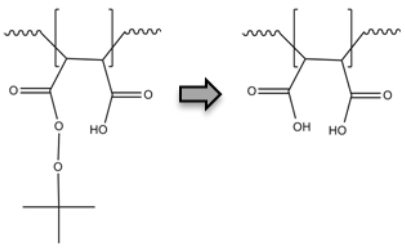

Figure 6-6 Cleaving of the perester bond in the polymer side group.

When the perester bond is cleaved by heating in water, the bulky hydrophobic *tert*-butyl group is removed, exposing the hydrophilic maleic acid group. This may cause the observed decrease in contact angle.

Summarizing, the initiator applicability could be proven for both systems. The redox co-initiator features a better control over unspecific polymerization in the bulk. This is indicated by the lower changes in permeability, when modifying without macromolecular co-initiator. Since an unspecific polymerization will lead to undesired grafting in the membrane support, this is a clear advantage of the redox-co initiator system. Another draw-back for the application of the thermal initiator is the need for heating and heat control. The heat is well controllable, when grafting flat sheet samples. However, when grafting in membrane modules, heat control is likely more difficult. Also, heating a membrane module composed of different materials can possibly cause problems due to different material expansion or softening. In terms of applicability it is therefore concluded to use the redox co-initiator for further modification experiments and subsequent fouling experiments.

6.3 Modification and performance of flat sheet membranes

6.3.1 Membrane morphology

A comparison of the used multibore and flat-sheet membranes (Figure 5-23) shows that both membranes are very similar. The similar structure of the surface layer allows comparable initiator adsorption and grafting.

When pre-modifying the flat sheet membrane, its surface becomes rougher (Figure 5-30). This is possibly due to a removal of PVP from the membrane, when swelling in the *iso*-propanol solution used for initiator adsorption. The smoother membrane surfaces after grafting with a 0.1 M and 0.5 M monomer solution can be attributed to successful grafting.

The thin dense layer in the cross-section near the top surface of the membrane modified at high monomer concentration (Figure 5-31 D) may be dried hydrogel. The layer has a thickness of ~ 200 nm. This is slightly higher than the thickness one can derive from the gravimetrical DG (cf. Figure 5-27). Assuming a density of 1 g/cm³ the layer thicknesses of all membranes modified with 0.25 M SPP and different cross-linker contents are ~150 nm. However, the SEM images can only allow a rough estimation, since the observed layer thicknesses or pore sizes are strongly depending on the conditions during drying and breaking of the sample. Also due to the sputtering process small structures can be covered. Therefore EDX was used as an additional tool to gain information on the chemical composition of the membrane top layer and support. The results are discussed and compared to XPS in the following Chapter.

6.3.2 Effects on surface chemistry

6.3.2.1 Chemical composition

EDX

EDX scans of the upper and lower part of membranes in different stages of modification were performed (Figure 5-32). The given elemental compositions can only give a rough estimation of, whether modification was successful and how surface selective the modification was. Even though only an area of 100 nm x 100 nm was scanned, the actual measuring area can be expected to be much larger. The main reason is the lateral expansion of the electron beam in the material caused by electro scattering. In a self supporting polymer film this lateral expansion can be up to several microns[161]. The expected distribution of electrons in the membrane sample is illustrated schematically in Figure 6-7.

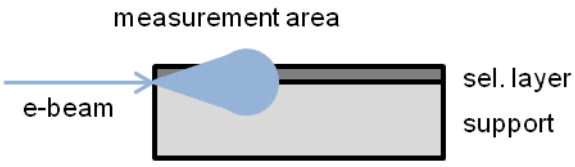

Figure 6-7 Expansion of electrons in the membrane sample during EDX scan of a membrane cross-section.

Due to the expansion of the electron coil, the actual measurement senses large parts of the membrane support, when only the selective layer is scanned. Still several conclusions appear valid. No N content is found in the support before or after initiator immobilization. The presence of N at the surface can be explained by the orientation of PVP towards the surface, which is also observed in ATR-IR (cf. Chapter 5.5.2.5). Furthermore the increase in N content upon premodification in the upper part of the membrane is likely caused by the adsorption of macromolecular co-initiator on the UF membrane surface. This observation is only qualitative, but the complete absence of N in the deeper membrane support indicates successful rejection of the initiator on the surface. Also the increase of N content upon modification is interesting. The stronger increase of N in the support at higher monomer concentration (as compared to the increase of N content in the support at low monomer concentration) indicates more undesired grafting in the support at this concentration. The other changes in elemental composition are difficult to interpret. The main reason is the discussed scattering of electrons in the sample, likely leading to an overlapping of zones with different compositions. Especially for the measurements of the selective layer it can be expected, that the collected data also arises from the support close to the surface.

SIMS-mapping

The SIMS-mapping gives another strong indication for successful grafting. A quantitative evaluation of the presented data is difficult. This is because the matrix of grafted and pristine membranes is expected to be completely different. Since the matrix effect on ion quantities can be very strong in SIMS[119]; the discussion will be more qualitative.

CN^- ions (Figure 5-33) can arise either from PVP in case of the pristine membrane or from MBAA and SPP in case of grafted membranes. The higher intensities on the grafted membranes can either be related to more N content at the surface, if matrix effects are low, or to a different influence of the surrounding matrix on CN^- release. In both cases, the higher CN-release from the grafted samples indicates a changed surface composition and thus successful grafting. S^- ions (Figure 5-34) can be generated either from the PES membrane polymer or from grafted SPP. Again the significantly changed intensity is a good indication for a change of the surface composition by the grafting process.

The CN^- intensity changes observed after sputtering with a low energy ion beam (Figure 5-35) are similar for the membrane modified without initiator and the unmodified membrane, while the membrane modified with initiator behaves different. The different behaviour can indicate a removal of a thin grafting layer in case of the membrane modified with initiator, while the membrane modified without initiator is modified also in the deeper membrane layers. Regarding the S^- ions after sputter cleaning (Figure 5-36), the sample modified with initiator behaves different from the two other samples. Since the reason for the observed changes remains unclear, the main conclusion drawn is that the distribution of sources for both surveyed negative ions is homogenous in all cases.

The distribution of sources for positive ions is more relevant than for the negative ions. The observation that more positive ions are created from both grafted membranes (Figure 5-37) indicates once more a significant difference between grafted and pristine samples. Possible sources for CH_4N^+ are either PVP in the base membrane or SPP in the hydrogel. Possible fractionation patterns, which lead to formation of CH_4N^+ from the two materials, are shown in Figure 6-8.

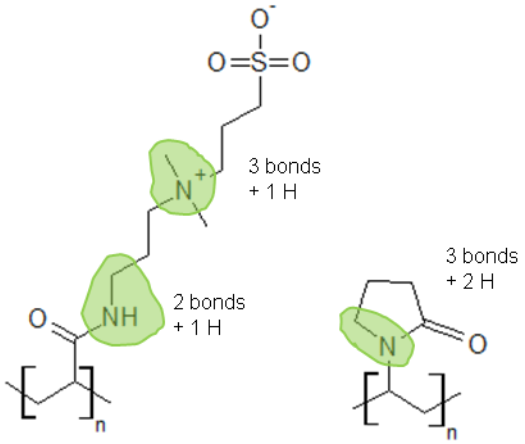

Figure 6-8 Possible origin of secondary CH_4N^+ ions from PVP and pSPP (number of broken bonds and transferred H is given beside each possible fragment).

The formation of the CH_4N^+ fragment appears more likely from pSPP, since two possibilities exist. Also one of the possible formation pathways only contains two bond breaks and a single H transfer. A formation from PVP seems unlikely, since three bonds need to be broken and two H atoms transferred. This is likely the reason, why almost no CH_4N^+ ions are generated from the pristine membrane (Figure 5-38). The generated ions from both modified membranes on the other hand indicate presence of SPP at the surface.

The formation of the $C_3H_8N^+$ fragment is expected to be even more specific. It can easily be created from pSPP, as indicated in Figure 6-9.

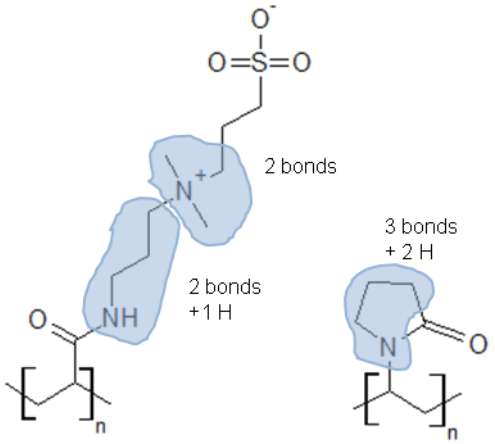

Figure 6-9 Possible origin of secondary $C_3H_8N^+$ ions from PVP and pSPP (number of broken bonds and transferred H is given beside each possible fragment).

Two possible fragmentations can create the $C_3H_8N^+$ fragment from pSPP with only two bond breaks, while three bond breaks and two H transfers are needed to generate the fragment from PVP. The significantly higher abundance of the fragment on the membrane grafted using the initiator indicates more successful grafting in this case. The lower amount of $C_3H_8N^+$ released from the membrane modified without initiator may be explained by a thinner grafting layer,

inhomogeneous grafting or grafting mainly in the support. A “dilution” of the hydrogel specific signal would arise from the present membrane material. Another possible source for the fragment is the DMAEMA side group in the macromolecular co-initiator, which would also explain the higher abundance on the surface modified with initiator. It is expected that the assumed monolayer of initiator should have only a small influence with regard to the typical diameter (i.e. penetration depth) of the fragmentation cascade of 10-50 nm[119]. Since the same trends are observed after the first scan with subsequent sputter cleaning for both positive fragments (Figure 5-40 and Figure 5-41), it can be concluded that the observed differences are not caused by loosely adsorbed material or a thin (<10-50 nm) layer. Summarizing, it can be said that the SIMS mapping gives strong indication for successful modification. The modification is very homogenous and without defects. Furthermore, the results indicate more successful grafting, when employing the pre-adsorbed co-initiator.

ATR-IR

The observed changes in the IR spectra upon premodification (Figure 5-42) are very small. The new OH vibration is likely caused by insufficient drying or uptake of humidity from the air. The band at 2036 cm^{-1} can be attributed to CO_2 from the surrounding air. The adsorbed layer of initiator is likely too thin to be detected by ATR-IR. This is also in accordance with the observations made during the ellipsometry and QCM measurements in Chapter 5.2.3.1. The main conclusion is therefore that no material seems to be leached out of the membrane during initiator adsorption. Also the measurement gives another indication for the good rejection of the initiator, since a permeating initiator could be expected to adsorb also in the membrane pores and support and should thus cause a stronger response in the ATR-IR spectrum.

The grafted hydrogel layer is expected to be thicker and could thus cause a signal in the IR spectrum (Figure 5-43). However a determination of DG by ATR-IR as a ratio of band intensities[162, 163] is not possible here, since the strong C=O bands of the methacrylamide backbone[139] of the grafted polymer are concealed by the presence of PVP in the selective layer. On the other hand, the absence of the band in the spectrum of the bottom side of the membrane is another indication for the surface selectivity of the grafting procedure.

XPS

The elemental surface composition determined by XPS (Figure 5-44 and Figure 5-45) reveals significant changes. However the interpretation remains difficult. The pristine PES membrane (Figure 5-44 top) comprises a significant amount of N. This can be explained by the presence of PVP at the surface as observed in EDX and IR. However the amount of O is significantly higher than expected for PES. In other XPS studies of PES UF membranes, a composition of 71.8 %

C, 22 % O and 5.3 % S has been found[164]. This means a C/S ratio of 13.5, while the expected ratio for pure PES is 12 and the observed ratio in this study is 11.8. The C/S ratio in Figure 5-44 is close to the expected ratio, so the high O content is likely due to some sort of contamination. The presence of water is an unlikely reason, since the samples were equilibrated in ultra high vacuum for several hours before the actual measurement. The observed N/S ratio of 0.43 corresponds to a PVP content of 30 % at the surface. Assuming this PVP content, the O content should only be 17.6 %. A possible explanation for the observed high oxygen content may be photo oxidation of the base polymer by sunlight or oxidation of additives like PVP during the post treatment process, e.g. with hypochlorite, which can be used to remove PVP from PES membranes and increase the porosity[165]. Since the exact post treatment conditions of the membranes used here are not provided, the latter explanation remains unproven but likely.

The determined N/S ratio in the premodified membrane of 0.27 corresponds to a coverage with initiator of 45 %, assuming the initiator composition determined by ^{1}H-NMR (Table 5-4). However, in this case the determined O content (40 % at) is still two times higher than expected (20 % at). Also the increase in S content is unexpected, since the initiator does not contain S. A possible explanation for the increased S and decreased N content may be the removal of PVP from the membrane during the initiator immobilization. Due to the *iso*-propanol content a slight swelling of the polymer could lead to a release of PVP. However, the strong increase in O content is not explained by PVP removal alone. The survey of C binding states (Table 5-17) gives a strong indication for a successful initiator immobilization. The appearing ester groups are likely attributed to the methacrylate backbone of the redox co-initiator. The disappearance of C=O groups is another indication for PVP removal during the initiator immobilization.

After grafting (Figure 5-45), the O content is still higher than expected. From the N/S ratio after grafting, an MBAA content of only 1 % can be derived (assuming 100 % coverage of the PES surface). Regarding the elemental composition, the main indicator for successful grafting is the increased N content. Another indication for successful grafting can be found in the binding energies (Table 5-18). A binding energy of 288.3 eV has been reported for C=O in poly methacrylamides[166]. Therefore the observed increase in C atoms with binding energies in that area can likely be attributed to –NH-C=O in the methacrylamide backbone of the grafted hydrogel. Even though a quantitative evaluation of the grafting process based on XPS remains difficult, the analysis gives strong indication for successful initiator immobilization and subsequent grafting.

Summarizing, the changes in surface chemistry prove successful rejection and adsorption of the macromolecular co-initiator on the membrane selective layer. Furthermore, the application of the macromolecular co-initiator is beneficial for the subsequent grafting step, since more

hydrogel is formed on the membrane surface. On the other hand, a quantification based on chemical methods remains difficult due to the complex nature of the samples. The main problem is the multi component system with several overlapping layers, while the layers of interest are thin compared to the matrix.

6.3.2.2 Surface hydrophilicity

The grafting procedure can be well surveyed by CA measurements before and after each grafting step (Figure 5-46). Upon adsorption of the initiator, the membrane becomes more hydrophobic. This can be attributed to the hydrophobic nature of the macromolecular co-initiator. Another explanation for an increase in CA would be a leaching of PVP from the membrane during the initiator immobilization step. The IR determination shows no changes in the PVP peak upon premodification (cf. Figure 5-42 and Chapter 6.3.2.1), while XPS analysis reveals changes that could be attributed to a PVP removal from the membrane surface (cf. Figure 5-44 and Chapter 6.3.2.1). Even though the reason for the increased CA after initiator adsorption remains speculative, the subsequent modification is proven by the corresponding increase in hydrophilicity during the grafting step. The main difficulty regarding the determined CAs is the quite high hydrophilicity of the base membrane on one side and the limitation of the method on the other side. Due to the slight curvature or roughness on the sample surface, the captive bubble does not always stick to highly hydrophilic samples. On the other hand, the bubble is more apt to get trapped at less hydrophilic spots or defects. Zhao et al.[167] reported CAs of 20 ° (captive bubble in water) for an MF membrane grafted with poly sulfobetaine methacrylate (SPE) via ATRP after long reaction times. The CAs in this work are in a similar range. A main reason for the slightly higher CAs could be the use of the less hydrophilic cross-linker MBAA leading to a less hydrophilic polymer hydrogel.

The application of the captive bubble method to capillary membranes was not possible. The sessile drop method can be applied to single bore capillaries, but this method is less applicable for the surveyed membrane system. The sample has to be dried before measuring, possibly damaging the surface structure and changing the hydrogel to a collapsed polymer layer, which is less or not porous and not containing water. Upon addition of the droplet, it will also be absorbed by the membrane surface, constantly changing the CA. Furthermore, the method is only applicable with single bore fibres, so for detailed analysis multiple single fibre modules would have to be prepared and destroyed. Taking into account the minor significance of the information gained from sessile drop measurements on flat sheets, it was therefore decided to not further develop the CA determination on modified capillary membranes.

6.3.2.3 Surface charge

The grafting process can be monitored in the performed ZP measurements (Figure 5-48). The increase in ZP upon initiator immobilization can be explained by the presence of tert. amine groups, which can be protonated easily (pKa=7.4[150]). The observation thus indicates successful initiator immobilization. Interestingly, the effect of grafting on the ZP is higher, when increasing the DC at constant monomer concentration than when increasing monomer concentration at constant DC. A similar trend is observed regarding the effect of cross-linker content on permeability (cf. Figure 5-29). From the combined results it can be concluded that a higher cross-linker content is beneficial for the grafting efficiency. This is also supported by the slightly lower CA of membranes grafted with higher DC (cf. Figure 5-22), since a higher content of hydrophobic MBAA should actually increase the CA.

Former studies[168] have reported ZPs of 0 mV over broad pH ranges for polySPE grafted membranes. SPE is a methacrylate, carrying the same zwitterionic sulfobetaine group like the SPP used in this work. Therefore, it may be expected that polySPP graft hydrogels show a similar behaviour. The main differences are the different membrane type, the use of cross-linker and the measuring mode for ZP. The amount of cross-linker may have an influence on the ZP curve by “diluting” the zwitterionic polymer on the surface. A stronger influence can be expected from the different operation mode and membrane geometry. In the cited study, a polyethylene terephthalate (PET) track etched membrane was surveyed by streaming potential. Compared to the PES anisotropic membranes used here, the pore sizes are larger and the pores in the support can be expected to be much less interconnected, hence flux through the membrane support is less likely occurring during the ZP measurement. Figure 6-10 depicts the different streaming situation for the two membrane types.

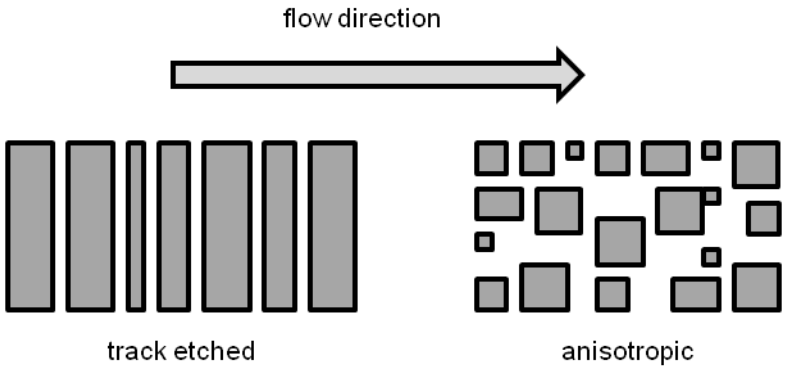

Figure 6-10 Flow conditions during ZP measurement with track etched and anisotropic membranes.

In the idealized presentation in Figure 6-10 it is obvious that the actual membrane surface, which interacts with the liquid flux, is likely larger in case of the anisotropic PES membranes. In order to minimize the effect of surface conductivity and conductivity in the membrane support[169]

on the result, streaming current was measured instead of streaming potential[124]. However it can still be expected that the actual interacting surface area is larger than the actual separation layer. In the Helmholtz Smoluchowski equation (used to determine the ZP (Eq. 7)), the geometric L/A term is only valid for a streaming channel, which is formed by two flat rectangular surfaces. In case of a very porous support the geometry becomes more complex and the interacting surface is likely larger. This may lead to higher absolute values of the ZP. This also explains the significant differences compared to the measurements on dense films (cf. Figure 5-21), where much more effect is observed at lower monomer concentrations. The IEP should be more reliable, since it is independant from the described effects. Therefore the IEP shift towards a neutral pH of 7 with increased monomer concentration and cross-linker content indicates a clear benefit of the grafting procedure.

On the other hand, the observations are only indicative. Due to the manual membrane production, the thickness of the membrane support layer often varied. For a new batch of membranes, ZP values were often unreasonably low (< -200 mV). This could well be related to a larger interacting surface area.

The redox co-initiator was also used to modify dense PES films of 30 µm thickness. The ZP measurement of such dense films (Figure 5-21) features the possibility to measure with precisely defined cell geometry. This helps to avoid the above discussed problems, which arise from contributions of the membrane support. The observed increase in ZP of the films treated with MB12 and MB13 at low pH can be attributed to the protonation of the tert. amine groups in the copolymers (pKa=7.4[150]). The slightly lower ZP of the film treated with MB13 at high pH is probably due to more adsorbed anions. MB13 contains more hydrophobic BMA groups than MB12, thus it may be arranged differently at the surface – with more of the ester groups between backbone and side groups being exposed to the solution. The most important observation is the strong influence of the grafting on the ZP. This indicates successful grafting even at low monomer concentrations.

6.3.3 Permeability and rejection

The observed permeability decrease by the grafting procedure (Figure 5-29) correlates with the decrease in MWCO (Figure 5-50). Interestingly, the effect of the DC on the decrease in MWCO is not very pronounced. Probably this is due to the observed effect of salt concentration on the swelling of SPP hydrogels with low DC (cf. Figure 5-1), as discussed in Chapter 6.1. Since the salt concentration in the feed solution is very low during the dextran filtration, both hydrogels are likely similarly swollen. This may explain the similarity under these filtration conditions. Another possible source for a misleading interpretation of the results is the operation at constant and

similar pressure for grafted and pristine membranes. Since the permeability differs for the surveyed membranes, the operation at similar pressure will lead to different initial fluxes. Also, due to the different rejections different degrees of CP may occur. The selection of a constant very low pressure of 0.03 bar was the attempt to minimize such effects.

Especially, since the filtration experiments with modules under much more controlled flux conditions showed similar results for the modified membranes (cf. Figure 5-67), the gathered data for the flat sheet membranes is considered reliable.

Interestingly, when filtering flower soil extract (Figure 5-59) the influence of DC on the TOC rejection is much more pronounced. This observation is in good accordance with the hypothesis that the gel with low DC is strongly influenced by the ion concentration in the feed. The flower soil is extracted with a 250 mM NaOH solution and neutralized by adding HCl (cf. Chapter 4.5.3.3). Also some additional amount of different salts can be expected to be present in the soil. Also the extract is diluted with tap water (~2 mmol/L Na^+ and ~1 mmol/L Ca^{2+})[170] instead of ultrapure water. The strong effect of stirring on the TOC rejection during the flower soil filtration can be explained by CP. The application of a stirrer reduces the expansion of the CP layer by turbulent mixing. Thereby the driving force for the solute permeation is reduced. The rejection data indicates that cross-flow operation may be an option to increase the TOC rejection in water filtration for the base membrane. The modification with a DC of 6.7 can significantly improve the rejection in dead-end operation.

6.3.4 Fouling resistance and cleanability

Bovine serum albumin

The results of the static fouling experiments with BSA (Figure 5-51) correlate to some extend with the determined CAs (Figure 5-46). The more hydrophobic premodified membrane performs worst in the static fouling test. This can only slightly be compensated by grafting with a low monomer concentration and DC. Interestingly, for the higher monomer concentrations the benefit is larger with a low DC. This is unexpected, because the modification with high DC is more hydrophilic, as can be derived from the CA measurements. It is known that the hydrophobic cross-linker MBAA can significantly reduce the protein fouling resistance of sulfobetaine hydrogels[171]. Therefore a careful adjustment of the DC is important to find the right balance of grafting efficiency and fouling resistance. Another factor, which may influence the static adsorption of BSA, is the swelling in the feed solution with a high ionic strength. This is in good agreement with the results from the swelling experiments with bulk hydrogels, where the swelling in salt solution strongly depended on the DC of the hydrogel (cf. Chapter 6.1).

During the filtration of BSA the samples modified with the highest DC perform best. All samples show BSA rejections > 99 %, therefore different fouling mechanisms (pore blocking vs. cake layer formation) appear unlikely. The hydrodynamic radius of the BSA molecule can be expected to be between 4.5 and 6 nm at the pH during the filtration experiments[172]. This is slightly smaller than the apparent pore radii derived from the dextran filtration (Table 5-19). The observed increase in fouling resistance with increased monomer concentration and DC may be due to an increasing exclusion of the BSA by the hydrogel. The filtration experiments are performed at high ionic strength, so the swelling is expected to be controlled by the DC (cf. Chapter 6.1). In case of the hydrogel with low DC, the BSA is probably partly entrapped in the highly swollen hydrogel. The smaller mesh size in case of the high DC is sufficient to reject BSA completely.

Interestingly, the negative effect of the premodification on the static fouling is not observed during the filtration operation. The initiator is only adsorbed in a thin layer on the membrane surface. It thus forms the main interacting layer in case of the static fouling experiments. During filtration operation the flow conditions become more important, since BSA molecules can penetrate into the membrane pores and cause pore narrowing[173]. The absence of initiator on the membrane pore walls explains the similar behaviour of premodified and pristine membrane during BSA filtration.

Summarizing, it can be concluded that the modification with a high DC leads to a significant increase in protein fouling resistance under filtration conditions, while a lower DC can be beneficial under static conditions.

Membrane bioreactor extracts

EPS

When filtering 25 mg/L EPS at similar pressure like during filtration of BSA (Figure 5-53), the modification appears to have a negative effect on the membrane performance. The increased fouling tendency compared to the pristine membrane may be attributed to an increase in rejection. Even though the EPS rejection cannot be determined with sufficient reliability, a higher rejection is expected due to the lower MWCO (cf. Chapter 5.5.2.9). The MW distribution of the EPS used here is not known, but other studies have found the largest amount of EPS in an MBR treating municipal wastewater with a MW of 10 kDa to 100 kDa[174]. This is in the same range, in which the dextran MWCO of the membranes varies. Therefore, increased rejection appears a possible reason for the increased fouling. Interestingly, the Nadir membrane with similar permeability shows significantly less fouling resistance. Therefore it can be concluded that the inherent anti fouling properties compared to a similar membrane are increased. When

rinsing the membrane in PBS buffer, fouling is almost reversible in most cases (Figure 5-53, right). The amount of irreversible fouling is highest for the membrane with low DC (3.35). This is probably because part of the fouling substances is trapped in the swollen hydrogel. Due to the high salt concentration in the buffer solution a lower swelling is expected for the higher DCs. The amount of irreversible fouling seems to correlate with this trend. The stronger permeability decrease after regeneration of the membranes modified with low DC (3.35) is difficult to explain from the available data. Possibly the additional flux decrease is due to a rearrangement of the EPS during the 24 h immersion in PBS.

During filtration at lower EPS feed concentration and at similar initial flux for all membranes (Figure 5-54), the pristine samples show less fouling resistance than in the longer filtration at higher flux and higher concentration (Figure 5-53). This is unexpected, because the increased flux and concentration can be expected to cause stronger CP and hence more fouling. A possible explanation is an inconsistent composition of the feed solution. The used EPS have a grainy structure with each grain having a different colour shade. Possibly due to the low amounts needed to prepare a solution, the selection of EPS grains has an influence on the composition of the feed solution. Also a different temperature during the filtration process could have an influence on fouling. The effect of temperature on the performance can be considered low, since the temperature did not vary more than ± 2 °C. Since the filtrations for one set of data were always conducted on the same day using the same feed solution, a comparison within one set of data appears still valid.

Under the defined comparable flux conditions, the modified membrane with a high DC is superior to both unmodified membranes. The membrane grafted with a low DC and a low monomer concentration performs worse than all other membranes. This is in accordance with the observations from the BSA filtration, where the low DG is not sufficient to compensate the negative effect of premodification on the fouling resistance.

The analysis of the feed and permeate samples via UV absorption indicates an increased rejection for the EPS, as can be expected from the reduced MWCO. However, since the observed rejection is small and the used concentrations are very low, a high experimental error is expected for the data. Mainly adsorption in the membrane support, as well as dilution by buffer in the filtration cell, can cause apparently higher rejections. On the other hand, leaching of material from the used membranes can lead to higher apparent EPS concentrations, since the absorption at 284 nm is quite unspecific.

SMP

The SMP filtration (Figure 5-56) also indicates a lower fouling resistance of the Nadir membrane than of the pristine standard membrane. All modified membranes perform significantly better than both unmodified membranes. This is interesting because the MW of the SMP should be much lower than of the EPS and a main part of the SMP should have MW lower than the MWCO of all membranes. Typically most of the SMP is smaller than 10 kDa[175]. Unfortunately, the used feed solutions do not sufficiently absorb UV to get a useful calibration in the used concentration range, but it is expected that the rejection for SMP is very low. In this case the fouling mechanism is mainly pore narrowing and plugging. The positive effect of the grafting on the SMP fouling is likely due to additional undesired grafting in the porous support. The unspecific grafting is indicated by the experiments in the absence of macromolecular co-initiator (Figure 5-29) – it is possibly making the pore walls more hydrophilic and hence less prone to protein adsorption.

The slightly decreased fouling resistance at higher DC is likely due to an adverse effect of the MBAA cross-linker on the antifouling properties of SPP as described by Carr et al.[176].

Based on the fouling experiments performed with MBR extracts, modification with a high DC (6.7 %) appears most promising to increase the fouling resistance. The large benefit of the high DC on the EPS fouling may likely compensate the slight adverse effect on the SMP fouling resistance. Further studies with membranes, which are more suitable for MBR applications, may be a promising future direction. For example, the application to comparable PES outside-in capillary membranes could be well feasible.

Flower soil extract

The modified membrane with high DC and the pristine membrane perform similar in dead-end mode (Figure 5-57). Interestingly the modified membrane with a low DC performs significantly worse. As discussed before (cf. Chapter 6.3.3), the swelling of this membrane is expected to be higher at high ionic concentrations like in the feed solution. Due to the similar rejection of the low DC and the pristine membrane under dead-end conditions, it can be expected that a similar amount of foulant is rejected at the membrane surface. Even though the hydrogel does not affect the membrane rejection in the swollen state, it could still hinder the removal of the foulants between two filtration cycles. This hypothesis is schematically represented in Figure 6-11.

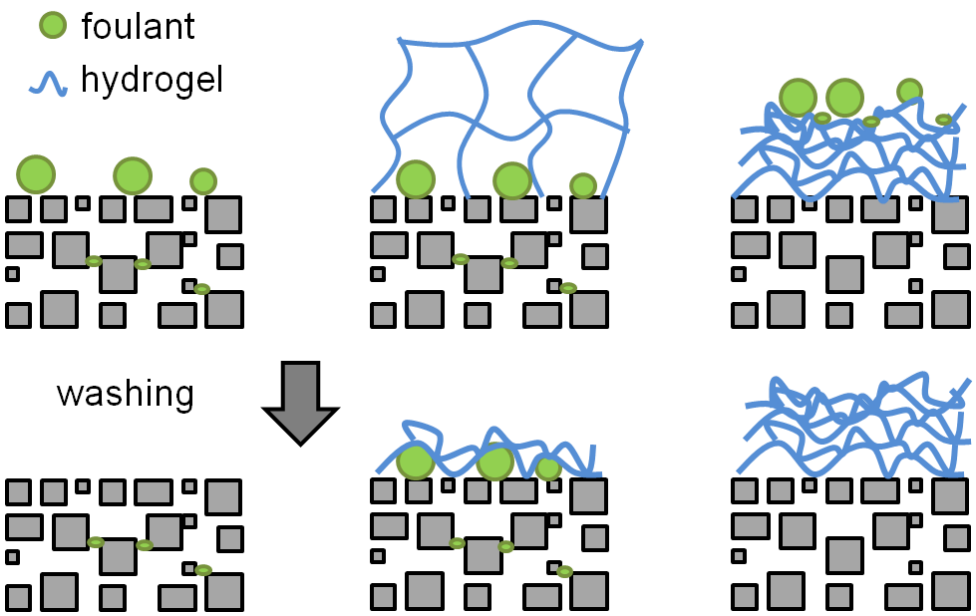

Figure 6-11 Foulant adsorption and removal or capture during the fouling process with high and rinsing with low salt concentration: pristine membrane (left) modified membrane with DC 3.35 (middle) and DC 6.7 (right).

In case of the pristine sample only part of the foulant penetrates into the pores and causes irreversible pore blocking. The situation is the same in case of the membrane modified with a DC of 3.35 (in the middle). However upon rinsing with pure water the hydrogel traps the adsorbed solutes possibly by a fast deswelling. The right side represents the situation on the membrane with a high DC. Here most of the foulant is rejected by the strongly cross-linked hydrogel. Therefore the fouling is decreased. The observed increase in permeability after each rinsing step is probably due to a decompaction of the membrane.

In the stirred dead-end operation (Figure 5-58), the modified membrane with a high DC performs significantly better than both other membranes. This can be explained by the high rejection of the compact hydrogel, keeping the solutes close to the shear plane. Due to its hydrophilic nature the solutes do not adsorb to the hydrogel surface. In case of the highly swollen hydrogel with a lower DC, the solutes can penetrate into the network, where the shear stress is reduced. They can thus get trapped in the hydrogel layer. In case of the unmodified membrane, the surface is more hydrophobic (cf. Figure 5-46). This likely causes a stronger adsorption to the membrane surface.

The changes in CA after fouling (Figure 5-60) are very small, taking into account the error bars. The observed increase of CA upon H_2SO_4 treatment of the modified membrane is unlikely due to a removal of the grafting layer, since the CA is even higher than of the pristine membrane. A possible explanation is a measuring error, which can occur due to the curved surfaces, hiding part of the captive bubble and thus concealing the actual baseline. Taking into account that the

membranes exhibit their initial CA after treatment with NaOH, this explanation seems reasonable.

6.3.5 Stability

The performed stability tests (Figure 5-61) show a high stability under alkaline conditions. All membrane samples show a slight increase in permeability after back flushing with NaOH. Since this is also valid for the unmodified membrane, a removal of grafting seems not to occur. No significant compaction effects were observed in this study, whereas membrane compaction is known as a factor influencing membrane permeability for several UF membranes[177]. The observed increase in permeability after back flush may therefore be caused by a decompaction of the membrane. When treating the membranes in H_2O_2 solution, the permeability decreases for all samples. A possible reason for this may be an additional cross-linking of the hydrogel via reactivation of unreacted double bonds. This would lead to a narrower mesh and increased hydraulic resistance (Figure 6-12).

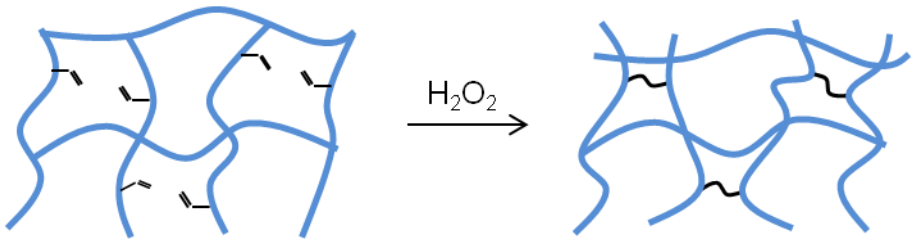

Figure 6-12 Cross-linking via unreacted double bonds.

The explanation is plausible because the effect is almost unnoticeable for the unmodified membrane and increases with increasing amount of cross-linker in the modified membranes. The results from the control experiment (Figure 5-62) support the hypothesis to some extent. After the treatment of the membranes with HCl the decrease in permeability is similar for both modified membranes and much less than before the treatment. On the other hand, the HCl treatment increases the overall permeability of the modified membranes. This can be due to removal of the grafting layer during treatment with high HCl concentrations. Another possible explanation for the increased permeability is the removal of unspecifically polymerized hydrogel from the membrane support during the HCl treatment.

A removal of unspecific grafting due to bulk polymerization is also indicated by the effect of PBS solution on the membranes grafted with and without initiator (Figure 5-63). The data indicates that most of the grafting is removed, when equilibrating the samples modified without initiator in saline buffer solution. This can be caused by an increase in pSPP solubility due to the higher salt concentrations. The higher solubility can be derived from the swelling data of bulk hydrogels (Figure 5-1). The membranes grafted using the co-initiator, are not influenced by the PBS,

which indicates a stronger adhesion to the membrane surface. A stability increase due to the use of the macromolecular co-initiator is probably not explained by the strong adsorption of the initiator alone. A combination of chemical grafting onto the partly entrapped co-initiator and physical adherence in the selective layer is a more plausible explanation. The idea is illustrated in Figure 6-13.

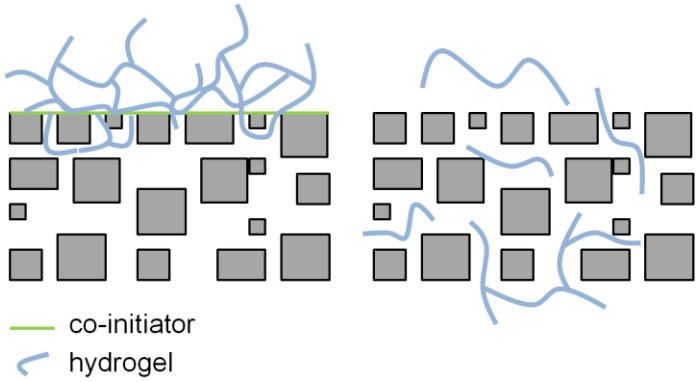

Figure 6-13 Illustration of grafting, facilitated on the surface by redox co-initiator (left) and by unspecific bulk polymerization (right).

Due to entanglements inside the membrane selective layer and chemical grafting to the adsorbed co-initiator, the hydrogel is anchored to the membrane (left). On the right side in the absence of co-initiator, part of the hydrogel is only loosely trapped in the porous support.

The presented data shows that a stable grafting can be achieved using the redox co-initiator. Possibly an optimization of the MBAA content combined with an additional cross-linking step after grafting would lead to a further increase in stability in the future.

6.4 Transfer to modules

The transfer to hollow fibre modules is not a straight forward upscaling procedure. The main differences are the cross-flow operation and the different modification procedure. The cross-flow operation influences the adsorption of the macromolecular co-initiator, which can be considered a special kind of membrane fouling (cf. Chapter 2.3.1). The grafting step differs, because the module has a high volume on the permeate side. This needs to be filled to avoid permeation of the monomer solution during grafting. The main difference is thus that the capillaries contain monomer solution in the membrane lumen, with the permeate side and support filled with degassed water. The flat sheet samples on the other hand are completely immersed in monomer solution. Also the membrane characterization is more difficult due to the low accessibility. The different aspects of the procedure are discussed in the following Chapters.

6.4.1 Permeability and rejection

The significantly different effect of the grafting on the permeability of the hollow fibre modules (Figure 5-64) compared to the flat sheets (cf. Figure 5-29) can be explained by the differences in the hydrogel grafting step. Figure 6-14 depicts the starting situation, where the lumen side of the module is filled with the grafting solution and the permeate side is filled with water.

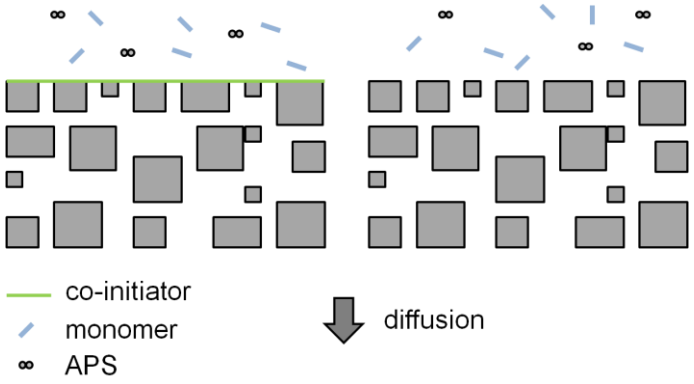

Figure 6-14 Diffusion of monomers and APS into the membrane support of membrane modules with premodified (left) and pristine (right) membranes.

Since only the membrane lumen is filled with monomer solution, unspecific grafting in the membrane support can be largely suppressed. This is especially the case, when using the redox co-initiator, since the monomers and APS must pass the premodified selective layer to enter the membrane pores. Here the vicinity to the co-initiator groups triggers the initiation reaction. Furthermore, the growing hydrogel layer will also decrease the diffusion of monomers into the support.

Interestingly, the permeability decrease is slightly more expressed, when the membrane is modified with lower DC. The effect is small compared to the error bars. A possible explanation may be the undesired grafting in the support. This could be due to the larger mesh size and hence less hindrance in monomer diffusion to the membrane support during the grafting step.

The broad deviation of the apparent membrane permeabilities between the different modules is probably due to the small dimensions of the lab scale modules. The fibres are potted using resins of sufficiently low viscosity to fill the membrane pores. Part of the membrane fibre (1-2 cm on each side) is therefore sealed by the potting resin. Variations in the potting length may cause an error of the actual surface area of up to 20 % in addition to variations of the membranes permeability. Therefore, the tests on small scale modules should be regarded in a semi quantitative way, keeping in mind that the used modules are never completely identical.

The time dependency in the permeability of the modified membranes (Figure 5-65) is possibly due to additional cross-links of unreacted double bonds, as indicated by the stability tests (cf. Chapter 6.3.5).

The MWCO of the pristine modules (Figure 5-67) is unexpectedly high (200 kDa), while the MWCO of both grafted membranes (37 and 59 kDa) is in a similar range like the MWCO of grafted flat sheet samples (44 and 35 kDa, cf. Figure 5-50). Also the higher MWCO of the grafted membrane with higher DC compared to the grafted membrane with low DC is unexpected. A possible reason for the discrepancies is the already mentioned inhomogeneous potting of the small modules. If a differently large part of the tube is sealed by potting resin either in the beginning or in the end of the module, a different TMP at the actual active membrane surface can occur. The arising pressure difference for a 20 cm tube with 0.9 mm inner diameter at the volumetric retentate fluxes can be calculated to be roughly 10 mbar according to Hagen-Poiseuille´s law. This indicates that a large part of the applied TMP (30 mbar) is contributed by the resistance of the tube walls. However, for the 20 cm module this should only contribute a deviation of about 2 mbar, assuming potting inhomogeneities of 4 cm. The different MWCO can also be attributed to the different membrane permeabilities. The typical permeability of the used pristine flat sheet samples is much lower (670 L/hm²bar) than the permeability of the used hollow fibres (1000 L/hm²bar, cf. Table 4-1). This can explain the strongly differing MWCO of the pristine samples. The SEM pictures of the surfaces of both membrane types (Figure 5-23 a) also show a slightly smoother surface in case of the flat sheet. Also in the cross section (Figure 5-23 c) the selective layer of the flat sheet appears denser than the selective layer of the multibore. Taking into account the different MWCO and permeability, both observations may be attributed to less or smaller pores in the flat sheet membrane.

The changes in MWCO and permeability indicate a successful transfer of the modification procedure to capillary modules. Due to the favourable conditions during grafting (cf. Figure 6-14), the modification is even more successful than the modification on flat sheet samples – a similar MWCO reduction is achieved with less influence on permeability.

From the observed changes in permeability and MWCO due to the modification procedure a successful modification of the modules can be concluded.

6.4.2 Zeta potential in modules

The ZP determination in modules (Chapter 5.6.3) is difficult to interpret, since the conditions are significantly different from the measurements on flat sheet samples. The most important difference is the additional contribution of the electrolyte filled permeate side of the module and the membrane support. By measuring the streaming current instead of streaming potential this

problem is avoided. However, due to the porous nature of the membrane support part of the streaming current may still flow in the membrane support and contribute to the ZP, as discussed for the flat sheet membranes[137]. The above discussed (cf. Chapter 6.4.1) variations in potting can also influence the contribution of the membrane support to the streaming current. When more support is filled with potting resin, the contribution of the support to the measurement will decrease. Furthermore, also the conductivity and electrolyte exchange between feed and permeate side will be decreased in the potted membrane area. The combination of these effects can explain the largely differing ZP curves of different modules.

The strong positive surface charge over a broad pH range after grafting with commercial SPP and a DC of 3.35 (Figure 5-68) is unexpected. The curve indicates a cationic polymer at the surface. A possible explanation would be a degradation of the SPP monomer via Hofmann elimination before the grafting step. In this case decomposition at the quaternary amine would lead to a poly DMAEMA like polymer after grafting. However none of the other samples shows a similar behaviour. Also Hofmann elimination at similar sulfobetaine functional groups has been reported to occur only at high temperatures (~ 500 – 700 K)[178]. Therefore the observation is likely due to a measuring error. The other samples do not show very pronounced changes.

Also the measurements with self synthesized SPP grafted modules do not indicate any changes by the grafting process. The main change occurs upon initiator immobilization. This may be explained by two different reasons. The slope of the ZP curve of the pristine modules is already lower than the slope of the hydrogel grafted dense PES films (cf. Figure 5-21). Therefore changes might not be detectable since they do not occur. The other explanation would be an error in the measuring method. This is possible, since the method was developed using a measuring device that was constructed for other geometries. Contributions of the self designed fittings and the module itself could influence the measurement. The performed test with a poly cation adsorbed to a module surface indicates that the method is in fact suitable to detect changes of the surface charge. The observed changes clearly show a successful adsorption of the poly cation to the surface. At low pH, the PES surface bears a positive charge and the poly cation is partly removed at the end of the first run (the measurement was performed from high to low pH). In the second run the charge behaviour is thus closer to the pristine module. The method therefore seems suitable to detect pronounced changes in modules. However for the SPP grafting surveyed here, the changes are too small to be observed with the method.

6.4.3 Fouling experiments

BSA fouling

The fouling resistance towards BSA (Figure 5-71) cannot be compared directly to the fouling experiments with flat sheet membranes (cf. Figure 5-52) due to the different operation conditions. The main reason for the significantly lower fouling resistance is the longer filtration time. Still, the modified membranes perform significantly better than the unmodified sample. Interestingly, the effect of PBS on the permeability of membranes modified with and without redox co-initiator is the opposite of what is observed with modified flat sheets (cf. Figure 5-63). The permeability decrease in case of the module modified without redox co-initiator is probably linked to a loosening of unspecifically polymerized hydrogel in the membrane support. This led to increased permeabilities in case of the flat sheet membranes (cf. Chapter 6.3.5). However, the support structure is very different between the two membrane types (Figure 5-24). The narrow support structure of the multibore at the outer side of the fibre (i.e. the permeate side) may act as a second layer with low permeability, trapping removed hydrogel parts from the membrane support, thus reducing the overall permeability. This may also explain the often observed decrease of membrane permeability over time (Figure 5-65). Pieces of polymer loosely stuck in the membrane support could become free and slowly accumulate at the outer membrane surface.

Membrane bioreactor extracts

The strong effect of the grafting on the EPS fouling resistance observed during dead-end filtration with flat sheet samples (cf. Figure 5-54) diminishes, when filtering a similar feed in cross-flow operation (Figure 5-72). Similar to the case of BSA filtration, the higher filtrate volume is the main difference between the two experiments. The permeate volume per membrane area is 81 L/m² in the cross-flow filtration and only 32 L/m² in dead-end operation of flat sheets. Even though the fouling resistance of the grafted and pristine membrane modules appears to be similar, the absolute permeability (Figure 5-72, left) seems to be more stable for the grafted membrane. Also, the membrane cleaning is much easier with the grafted membrane. This may be explained by the expected different fouling principles – fouling in case of the grafted membrane takes place mainly on the outer surface of the grafting layer, while fouling on the pristine membrane is also caused by pore blocking, where the foulant is much harder to remove by physical cleaning.

In case of SMP fouling (Figure 5-73), the results are completely different from the results gathered during dead-end operation of flat sheets (cf. Figure 5-56). Again, a possible explanation is the larger permeated volume. The main flux decrease occurs very early, after

6 L/m² passed the membrane in cross-flow operation. The dead-end filtration with flat sheets was only carried out until 4.7 L/m² passed the membrane, so probably no steady state was achieved yet. In both cases, the rejection of the SMP is expected to be low, taking into account the MWCO and the typical MW of SMP. As discussed in Chapter 6.3.4, a large part of the SMP has MW below 10 kDa and thus significantly below the MWCO of the modified and unmodified membranes. The predominating fouling mechanism is therefore likely pore blocking and internal fouling and is not affected by the grafting layer on top of the membrane. The slightly lower efficiency of the physical membrane cleaning (Figure 5-73 right) in case of the modified membrane is probably due to the additional hydraulic resistance of the grafting layer. It is expect that the solutes would adsorb mainly in the more hydrophobic and less fouling resistant membrane pores and support. Therefore solutes, which desorb from the pristine membrane during physical cleaning, are directly released to the surrounding bulk solution and carried off. In case of the grafted membrane, the hydrogel probably hinders the transport and thus decreases the driving force for desorption.

Flower soil extract

The relative TMP increase in dead-end mode (Figure 5-74) is significantly lower for modified modules than for unmodified modules. Due to the lower permeability of the modified module a higher initial TMP is needed to achieve a similar flux. Relative to this higher initial pressure, the TMP stays more constant. The higher initial fouling rate of the pristine membrane is well observable, when the slopes from Figure 5-74 vs. time are plotted (Figure 6-15).

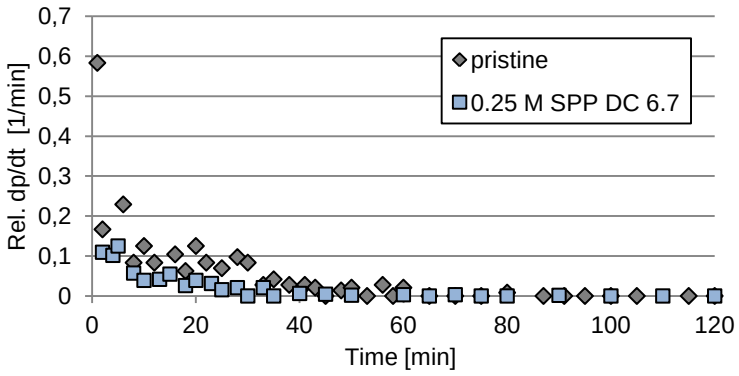

Figure 6-15 Relative TMP increase rate vs. time during dead-end filtration of flower soil extract with lab scale modules.

The initial TMP increase rate of the pristine module is much higher than the increase rate of the modified module. The observed TMP increase is caused by the combined effects of CP and membrane fouling. The effect of CP on TMP increase should be higher in case of the modified module, due to the higher TOC rejection (Figure 5-76) and similar flux. Since the rate of TMP increase is much higher for the pristine module, it can be concluded that the influence of fouling

is higher in this case. The lower rate of TMP increase, combined with the higher TOC rejection is thus a good indication for an increased inherent fouling resistance. The benefit of the modification becomes more obvious, when taking into account the resistance towards irreversible fouling. The fouling resistance of modified modules towards flower soil extract is significantly higher than for the pristine modules in both operation modes (Figure 5-75). This indicates that the hydrogel is shielding the membrane surface from the foulant effectively. The advantage is more pronounced in cross-flow than in dead-end mode. The observation is in accordance with the observed fouling resistance during dead-end filtration with flat sheet samples (cf. Figure 5-57 and Figure 5-58). Since the rejection and flux conditions are comparable for modified and unmodified membranes, the CP is expected to be comparable as well. The effect can be explained by different adsorptive interactions between membrane and foulant. Due to the lower adhesion of foulants to the hydrogel, removal by the applied turbulence (Re = 7400) is easier in case of the hydrogel modified membranes. In case of the pristine samples, the attraction between membrane surface and foulant is stronger and therefore the turbulence is not sufficient to remove the foulants effectively.

An additional benefit of the modification in dead-end operation is the significantly increased TOC rejection compared to the pristine membrane (Figure 5-76). Again the data is very similar to the data collected during flower soil extract filtration experiments with flat-sheets (cf. Figure 5-59). The increased rejection in dead-end mode can be attributed to a smaller effective pore size due to the hydrogel grafting, which is also effectively reducing the MWCO (cf. Figure 5-50 and Figure 5-67). According to the differences in MWCO between the grafted and pristine membrane modules (Figure 5-67), a more pronounced difference in the TOC rejection between the modified and unmodified modules can be expected. Also the pristine module shows a broad variation in TOC rejection. Both observations may be explained by the above discussed (Chapter 6.4.1) possible inhomogeneities of the lab scale modules.

Considering the fouling experiments with EPS (cf. Figure 5-72), the modified membranes are much easier to clean by a short cross-flow flushing of the modules at low TMP and high linear velocity. A continuous cross-flow operation is likely too cost intensive for surface water treatment. Nevertheless, this result can be used in the future to replace the back-flush steps in dead-end operation by low pressure “cross-flush” steps. Furthermore, the increased TOC rejection may be useful to minimize the need of a feed pretreatment. A further increase in TOC rejection can probably be achieved by further adjusting the DC of the grafting layer.

6.4.4 Five fibre test modules

With modified and unmodified modules, no detectable fouling occurs during the cross-flow filtration at constant permeate flux (Figure 5-77). A possible reason is the lower permeate flux (59 L/hm²) compared to the single fibre modules (300 L/hm²). The set permeate flux was the maximum achievable flux, when maintaining a comparable linear velocity. The main problem is that the setup is mainly designed for dead-end operation and thus had to be operated under quite undefined conditions in cross-flow. Therefore the cross-flow data from the five fibre modules remains to some extend inconclusive.

The lower TOC rejection (Figure 5-79) compared to the small lab scale modules (cf. Figure 5-76) and flat sheet membranes (cf. Figure 5-59) is unexpected. The TOC rejections in dead end filtration of flower soil extract are summarized in Table 6-1.

Table 6-1 TOC rejection during dead-end filtration of flower soil extract with different membrane types.

System	TOC rejection pristine [%]	TOC rejection 0.25 M SPP DC 6.7 [%]
Flat sheet	42	74
Lab scale	53	70
Five fibre	-	36

The flux per membrane area is lower during the filtrations with the larger modules (75 L/hm² vs. 170 L/hm² to 100 L/hm²). Therefore a higher rejection would be expected. Possible explanations for the difference are dilution and saturation effects in the smaller setups. Since the large setup was filtering feed solution for at least two hours before taking samples, all adsorption processes of not rejected components may be in equilibrium. The increase in the permeate TOC of the pristine module may be due to a leaching of PVP from the production process or glycerine (used for membrane storage). However, such leaching is usually not observed by the project partner Inge. It is unlikely, because all fibres are post treated to remove loosely incorporated PVP. Bacterial growth in the sample or solvent evaporation cannot be excluded, since the TOC samples were stored (7 °C, no stabilizer) for up to one week before the TOC measurement. Besides, the amount of inorganic carbon (IC) is significantly higher than in the small scale experiments, since tap water was used for the feed solution. Due to the combined measuring errors of total carbon (TC) and IC determination, a large error can occur, when the IC is higher than the TOC[179]. Summarizing, it can be concluded, that the filtration experiments show a similar trend like the experiments with flat sheets and single fibre modules. Since only single experiments could be conducted the uncertainty of the results is slightly higher than for the previous experiments.

The increasing cycle duration during the operation of the pristine module in dead-end mode (Figure 5-78) is unexpected. Taking into account the increased TOC of the permeate (Figure

5-79 left), a leaching of components from the module seems a possible explanation. No CEB is applied before or during the cross-flow test and in this case also no increase of TOC in the permeate occurs (Figure 5-79). This indicates that a release of material is probably caused by the CEB in case of the pristine module. The modified module features a stable filtration performance during dead-end operation (Figure 5-78). Interestingly, in both cases the back flush (every 20 min) has much less effect than the rinsing step conducted with the flat sheet samples (cf. Figure 5-57). This is likely due to the different flux conditions. Flat sheets had to be operated at constant pressure, while the five fibre modules were operated at constant flux. The flux per membrane area is 75 L/hm² in case of the modules, while it starts at 210 L/hm² and decreases rapidly to 22 L/hm² in case of the flat sheets, so that the flat sheets were operated at lower fluxes most of the time. Figure 6-16 compares the fluxes during dead-end operation of flat sheet membranes (cf. Figure 5-57) and five fibre modules (cf. Figure 5-78).

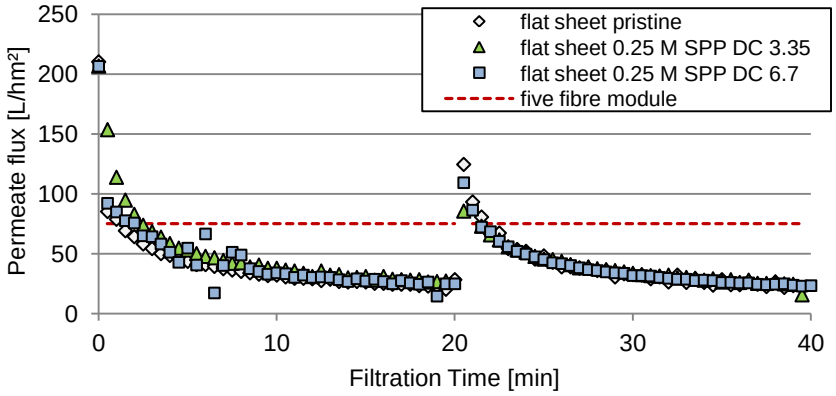

Figure 6-16 Permeate flux vs. time during dead-end operation of flat sheet membranes and five fibre membrane modules (flower soil extract as model foulant).

From Figure 6-16, it can be derived that the flat sheet membranes operated at higher fluxes only about 10 to 20 % of the time and at significantly lower fluxes during the rest of the filtration. As a result, the fouling rate in case of the modules could be higher due to higher permeate flux and hence more CP.

The chemical stability test (Figure 5-80) is important to rate the applicability of the modification under real operation conditions. The initial permeability increase during the stability test can be attributed to the removal of a fouling layer. This is because the modules had to be reused due to the low number of available modules. In fact, the pristine module seems to be irreversibly fouled since the initial permeability of 1000 L/hm²bar is only regained to 85 % during the 22 CEB cycles. This is another good indication for the improved cleanability of the grafted membrane modules.

The permeability data of the modified module indicates a high stability under the applied cleaning conditions. Since the permeability never exceeds the permeability of the newly

modified module, removal of the grafting layer seems not to occur. The strong variation in permeability of the modified module could be due to swelling and deswelling of the hydrogel. Since the module is exposed to high changes in pH and ion concentration during the test, swelling and deswelling likely occur. Also the streaming conditions rapidly change from forward flux to back flushing, with soaking steps in between (cf. Chapter 4.6.4). Probably the measuring time of only 10 min after each CEB is too short to reach equilibrium flux conditions.

Still the conclusion of a high stability appears valid, since a removal of the grafting layer should reduce the effect of the discussed swelling and deswelling processes on the measurement and the behaviour should be more similar to the pristine module in case of a removal of the grafting layer.

Summarizing, the tests with five fibre test modules show that the modification can be transferred to larger modules. Furthermore, the modification remains stable under typical cleaning conditions. Therefore the transfer to a pilot plant seems promising.

6.4.5 Pilot phase tests

The grafting procedure was successfully applied in pilot scale modules as can be seen from the comparison of permeability reduction caused by the procedure in lab scale and pilot scale (Figure 6-17).

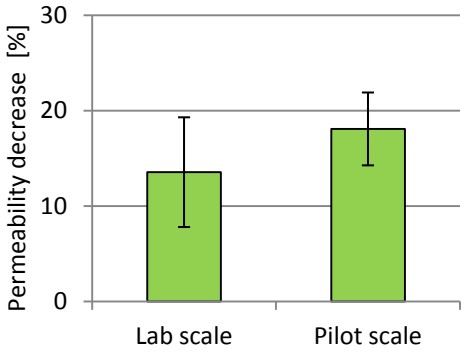

Figure 6-17 Comparison of permeability reduction by modification procedure in lab scale and pilot modules.

A very important factor besides the technical applicability is the economical feasibility of the process. Based on the quantities of different substances needed for the modification of pilot scale modules and the current prices for these substances[180], the costs for the modification can be estimated. The main cost factors (excluding labour and energy cost and minor expenses) are summarized in Table 6-2.

Table 6-2 Material cost for modification of pilot scale modules per module and per membrane area.

Substance	Amount [g]	Cost per module [€]	Cost per membrane area [€/m²]
m SPP	6.87	7.42	53.00
MBAA	0.49	0.11	0.79
MB-12	1.00	0.05	0.36
IPA	157	2.96	21.14
total		7.58	75.28

The main bottleneck of the presented grafting technique is the availability of SPP. The monomer is currently only available in small scale for scientific studies. The resulting high price of currently 53 €/m² can be a drawback for the application. Also the solvent amount needed for initiator immobilization contributes significantly to the total modification cost. On the other hand, the technical applicability of the modification method was demonstrated. In future work, the presented initiator system could be used to graft other polymeric hydrogels onto PES UF membranes. Also regain of not reacted monomer from the modification solution could be investigated in future studies. Reducing the amount of *iso*-propanol can be beneficial for both the material cost and cost for precaution measures in the process. Furthermore a reuse of the initiator solution for premodification could be possible, since most of the macromolecular co-initiator is likely contained in the retentate stream.

7 Conclusions and outlook

7.1 Initiator systems

The presented study shows that the macromolecular initiators and co-initiator systems can be well adjusted to adsorb on PES membranes and dense films. The Initiators can be used for surface modification on membranes and membrane modules by surface initiated cross-linking polymerization. Thus polymer hydrogel layers can be created on the treated surfaces and the key concept of this work could be proven.

A thermal initiator could be synthesized and applied to PES membranes. However, problems occurred regarding the control of undesired grafting in the membrane support. Also the application of a constant high temperature to membrane modules, when using the thermal initiator is expected to be more difficult than the redox co-initiator approach. Even though the thermal approach was not further pursued, it may be useful for other applications of the macromolecular initiator concept in the future. Further optimization of the premodification procedure (regarding filtration time, temperature, initiator concentration and solvent composition) and the grafting conditions (temperature, monomer concentration and grafting duration) can possibly improve the procedure.

The redox co-initiator approach was very successful. Good indications for high surface selectivity as well as high grafting stability were found. The macromolecular co-initiator does not influence the membrane characteristics detectably, but helps to increase the surface selectivity and stability of the grafting layer. Since the role of the redox co-initiator is only a radical formation, the system can likely be applied to graft other hydrogel systems on PES membranes. Generally every monomer, which can be polymerized via free radical polymerization, should be suitable for grafting. The main limitation is that the grafting solution should not be too acidic (optimal pH ≥ 7), in order to avoid protonation of the amine groups and loss of initiator activity. Since the driving force for adsorption is believed to be mainly hydrophobic interactions, the synthesized material is expected to be suitable for many other hydrophobic membranes. By changing the adhesive group in the co-initiator, the system may be optimized for other membrane materials. For example, methacrylate monomers with fluorinated side groups could increase the affinity to PVDF membranes. Also optimization of the ratio of initiator groups to adhesive groups may further improve the benefits of the co-initiator.

7.2 Membrane performance

The applied polyzwitterionic modification increases the membrane hydrophilicity and turns the zeta potential from a strong negative value to a more neutral behaviour. This improvement in chemical properties is accompanied by an increased resistance towards protein fouling in static adsorption as well as filtration experiments. An improvement of fouling resistance was also found for more complex mixtures of substances typically encountered in MBR effluents or surface water treatment. The presented data indicates that the hydrogel grafting technique is useful to improve anti fouling performance in real membrane processes and not only with simple model foulants. Future works should focus on the optimization of parameters like DC and DG to achieve optimal anti fouling properties for such applications. For MBR applications, other PES membrane types, like outside-in capillaries, should be modified.

The modification reduces the membrane permeability, but this is compensated by the decrease in MWCO and corresponding increase in TOC rejection. By adapting the DC, the grafted membranes may be adjusted to achieve an even higher TOC rejection in order to minimize the need for flocculation pre-treatment during surface water filtration. Also the modification of base membranes with higher permeability and MWCO can be tested. In this case membranes with similar filtration performance compared to the standard UF membrane and increased antifouling properties can probably be achieved. In this case the co-initiator rejection needs to be tested and the co-initiator MW probably has to be increased.

The presented study is mainly focused on proving the concept of a macromolecular co-initiator and its application for hydrogel grafting. Future studies may focus on further optimization of the monomer concentration and DC of the grafted hydrogel. The used cross-linker MBAA is hydrophobic and indications were found that a higher cross-linker content can have a negative influence on the antifouling properties. Zwitterionic cross-linkers, like carboxybetaine dimethacrylate may be used as a cross-linker to further increase the antifouling properties. In other studies it has been demonstrated that this can be a versatile approach in order to reduce fouling propensity[176].

The bulk hydrogel experiments indicate responsivity to ion concentration for the pSPP hydrogel. During the membrane filtration experiments many indications were found that this stimuli responsive behaviour is transferable to the modified membrane. Stimuli responsive membranes are a field of growing interest since they offer many interesting possibilities[64]. For example, the swelling and deswelling can be used for improved cleaning during back-flush at high salt concentrations. Thus, the need for chemical cleaning may be reduced. The self cleaning efficiency of a pSPE UV-grafted membrane is currently surveyed in the workgroup[181]. The

grafting technique presented here may help to transfer the findings from the other study to applications, where UV grafting cannot be used, i.e., in hollow fibre membranes.

Different chemical cleaning experiments show a high chemical and mechanical stability of the grafted hydrogel layer. Future work should focus on the optimization and adaption of the filtration process to the new membranes. The performed tests in this study assume the standard cleaning procedures for conventional membranes. Due to the increased antifouling properties, milder conditions may probably be used in the future to increase the membrane lifetime and reduce the operational costs. Also, the increased TOC rejection may be used to reduce the need for feed pretreatment. By replacing the back flush steps with low pressure “cross-flush” (i.e. rinsing the module in cross-flow at high retentate flux) steps, the energy efficiency of the filtration process could be improved.

7.3 Technical feasibility

The main benefit of the presented redox co-initiator over established techniques like UV-grafting or plasma treatment is the easy applicability. The method can be applied without any additional equipment. Potentially the grafting could even be applied on-site in a filtration plant. This can especially be useful, if the long term stability of the grafting layer should prove to be shorter than the membrane lifetime. In this case the grafting may be reapplied after an intensified cleaning. Since no suitable conditions for the complete removal of the grafting layer from the membrane surface were found, future research may focus on this point. For example, chemical weak points could be implemented into the initiator or hydrogel, so that the modification may be degraded chemically. By chemically triggering an accelerated decomposition, the hydrogel layer and all possibly incorporated fouling substances could be removed from the membrane surface. After such an intensified cleaning, the grafting may be reapplied within one day.

In this study, the applicability in membrane modules of different scale, ranging from single fibre small scale to 1.5 m pilot scale modules could be proven. The new grafting technique can therefore help to decouple the membrane grafting from the membrane production. This can be beneficial for special applications, which need only small amounts of membranes with a special performance feature like biocompatibility for example. If the membrane cannot be feasibly produced in large amounts, a commercial membrane module can be modified to achieve the desired properties. The high cost of the SPP monomer can be a drawback for the presented hydrogel modification. On the other hand, it was proven that the method can be technically realized. Especially, due to the possibility to adjust the hydrogel system and utilize other monomers or use the technique with other membranes, the method appears to be a versatile and promising approach for future development in the field of surface functionalized membranes.

8 Literature

[1.] Baker, R.W., *Membrane Technology and Application*. 2 ed. John Wiley & Sons, Chichester, **2004**.

[2.] He, X. and M.-B. Hägg, *Membranes for Environmentally Friendly Energy Processes.* Membranes, **2012**. *2*(4): p. 706-726.

[3.] Zhang, W., et al., *A Review on Flux Decline Control Strategies in Pressure-Driven Membrane Processes.* Industrial & Engineering Chemistry Research, **2015**. *54*(11): p. 2843-2861.

[4.] Samhaber, W.M., *Die industrielle Anwendung der Nanofiltration – Potenziale, Erfahrungen und Grenzen.* Chemie Ingenieur Technik, **2005**. *77*(5): p. 566-572.

[5.] Shannon, M.A., et al., *Science and technology for water purification in the coming decades.* Nature, **2008**. *452*(7185): p. 301-310.

[6.] Baldasso, C., T.C. Barros, and I.C. Tessaro, *Concentration and purification of whey proteins by ultrafiltration.* Desalination, **2011**. *278*(1-3): p. 381-386.

[7.] Tutunjian, R.S., *Ultrafiltration Processes in Biotechnology.* Annals of the New York Academy of Sciences, **1983**. *413*(1): p. 238-253.

[8.] Schäfer, A.I., A.G. Fane, and T.D. Waite, *Cost factors and chemical pretreatment effects in the membrane filtration of waters containing natural organic matter.* Water Research, **2001**. *35*(6): p. 1509-1517.

[9.] Kabasch-Korbutowicz, M., *Ultrafiltration as a method of separation of natural organic matter from water* Materials Science-Poland, **2008**. *26*(2): p. 460-467.

[10.] Mutamim, N.S.A., et al., *Application of membrane bioreactor technology in treating high strength industrial wastewater: a performance review.* Desalination, **2012**. *305*(0): p. 1-11.

[11.] Le-Clech, P., V. Chen, and T.A.G. Fane, *Fouling in membrane bioreactors used in wastewater treatment.* Journal of Membrane Science, **2006**. *284*(17).

[12.] Meng, F., et al., *Recent advances in membrane bioreactors (MBRs): Membrane fouling and membrane material.* Water Research, **2009**. *43*(6): p. 1489-1512.

[13.] Yune, P.S., J.E. Kilduff, and G. Belfort, *Fouling-resistant properties of a surface-modified poly(ether sulfone) ultrafiltration membrane grafted with poly(ethylene glycol)-amide binary monomers.* Journal of Membrane Science, **2011**. *377*(1–2): p. 159-166.

[14.] Jönsson, C. and A.-S. Jönsson, *Influence of the membrane material on the adsorptive fouling of ultrafiltration membranes.* Journal of Membrane Science, **1995**. *108*(1–2): p. 79-87.

[15.] Song, L., *Flux decline in crossflow microfiltration and ultrafiltration: mechanisms and modeling of membrane fouling.* Journal of Membrane Science, **1998**. *139*(2): p. 183-200.

[16.] Van den Berg, G.B. and C.A. Smolders, *Flux decline in ultrafiltration processes.* Desalination, **1990**. *77*(0): p. 101-133.

[17.] Kimura, K., et al., *Irreversible membrane fouling during ultrafiltration of surface water.* Water Research, **2004**. *38*(14–15): p. 3431-3441.

[18.] Kuzmenko, D., et al., *Chemical cleaning of UF membranes fouled by BSA.* Desalination, **2005**. *179*(1–3): p. 323-333.

[19.] Asatekin, A., et al., *Anti-fouling ultrafiltration membranes containing polyacrylonitrile-graft-poly(ethylene oxide) comb copolymer additives.* Journal of Membrane Science, **2007**. *298*(1–2): p. 136-146.

[20.] Chen, F., et al., *Pilot-scale investigation of drinking water ultrafiltration membrane fouling rates using advanced data analysis techniques.* Water Research, **2014**. *48*(0): p. 508-518.

[21.] Porter, M.C., *Concentration Polarization with Membrane Ultrafiltration.* Product R&D, **1972**. *11*(3): p. 234-248.

[22.] Wijmans, J.G., et al., *Hydrodynamic resistance of concentration polarization boundary layers in ultrafiltration.* Journal of Membrane Science, **1985**. *22*(1): p. 117-135.

[23.] Chan, R. and V. Chen, *Characterization of protein fouling on membranes: opportunities and challenges.* Journal of Membrane Science, **2004**. *242*(1–2): p. 169-188.

[24.] Blatt, W., et al., *Solute Polarization and Cake Formation in Membrane Ultrafiltration: Causes, Consequences, and Control Techniques*, in *Membrane Science and Technology*, J. Flinn, Editor. **1970**. Springer US. p. 47-97.

[25.] Sioutopoulos, D.C. and A.J. Karabelas, *The effect of permeation flux on the specific resistance of polysaccharide fouling layers developing during dead-end ultrafiltration.* Journal of Membrane Science, **2015**. *473*(0): p. 292-301.

[26.] Xiao, F., et al., *Identification of key factors affecting the organic fouling on low-pressure ultrafiltration membranes.* Journal of Membrane Science, **2013**. *447*(0): p. 144-152.

[27.] Zularisam, A.W., A.F. Ismail, and R. Salim, *Behaviours of natural organic matter in membrane filtration for surface water treatment — a review.* Desalination, **2006**. *194*(1–3): p. 211-231.

[28.] Hao, Y., et al., *Effect of metal ions on humic acid fouling of hollow fiber ultrafiltration membrane.* Journal of Membrane Science, **2011**. *376*(1–2): p. 247-253.

[29.] Yuan, W. and A.L. Zydney, *Humic Acid Fouling during Ultrafiltration.* Environmental Science & Technology, **2000**. *34*(23): p. 5043-5050.

[30.] Kunacheva, C. and D.C. Stuckey, *Analytical methods for soluble microbial products (SMP) and extracellular polymers (ECP) in wastewater treatment systems: A review.* Water Research, **2014**. *61*(0): p. 1-18.

[31.] Flemming, H.-C., T.R. Neu, and D.J. Wozniak, *The EPS Matrix: The "House of Biofilm Cells".* Journal of Bacteriology, **2007**. *189*(22): p. 7945-7947.

[32.] Laspidou, C.S. and B.E. Rittmann, *A unified theory for extracellular polymeric substances, soluble microbial products, and active and inert biomass.* Water Research, **2002**. *36*(11): p. 2711-2720.

[33.] Bae, T.-H. and T.-M. Tak, *Interpretation of fouling characteristics of ultrafiltration membranes during the filtration of membrane bioreactor mixed liquor.* Journal of Membrane Science, **2005**. *264*(1–2): p. 151-160.

[34.] Bacchin, P., P. Aimar, and V. Sanchez, *Model for colloidal fouling of membranes.* AIChE Journal, **1995**. *41*(2): p. 368-376.

[35.] Xiong, Y. and Y. Liu, *Biological control of microbial attachment: a promising alternative for mitigating membrane biofouling.* Applied Microbiology and Biotechnology, **2010**. *86*(3): p. 825-837.

[36.] Flemming, H.-C., *Microbial biofouling: unsolved problems, insufficient approaches and possible solutions*, in *Biofilm Highlights*. **2011**. Springer: Heidelberg, New York. p. 81-109.

[37.] Shi, X., et al., *Fouling and cleaning of ultrafiltration membranes: A review.* Journal of Water Process Engineering, **2014**. *1*(0): p. 121-138.

[38.] Shirazi, S., C.-J. Lin, and D. Chen, *Inorganic fouling of pressure-driven membrane processes — A critical review.* Desalination, **2010**. *250*(1): p. 236-248.

[39.] Peeva, P.D., et al., *Cross-flow ultrafiltration of protein solutions through unmodified and surface functionalized polyethersulfone membranes – Effect of process conditions on separation performance.* Separation and Purification Technology, **2012**. *92*(0): p. 83-92.

[40.] Bacchin, P., P. Aimar, and R.W. Field, *Critical and sustainable fluxes: Theory, experiments and applications.* Journal of Membrane Science, **2006**. *281*(1–2): p. 42-69.

[41.] Field, R.W., et al., *Critical flux concept for microfiltration fouling.* Journal of Membrane Science, **1995**. *100*(3): p. 259-272.

[42.] Wu, D., J.A. Howell, and R.W. Field, *Critical flux measurement for model colloids.* Journal of Membrane Science, **1999**. *152*(1): p. 89-98.

[43.] Peter-Varbanets, M., et al., *Stabilization of flux during dead-end ultra-low pressure ultrafiltration.* Water Research, **2010**. *44*(12): p. 3607-3616.

[44.] Liang, S., et al., *Organic fouling behavior of superhydrophilic polyvinylidene fluoride (PVDF) ultrafiltration membranes functionalized with surface-tailored nanoparticles: Implications for organic fouling in membrane bioreactors.* Journal of Membrane Science, **2014**. *463*(0): p. 94-101.

[45.] Rajasekhar, T., et al., *Oil–water emulsion separation using ultrafiltration membranes based on novel blends of poly(vinylidene fluoride) and amphiphilic tri-block copolymer containing carboxylic acid functional group.* Journal of Membrane Science, **2015**. *481*(0): p. 82-93.

[46.] Pellegrin, B., et al., *Multi-scale analysis of hypochlorite induced PES/PVP ultrafiltration membranes degradation.* Journal of Membrane Science, **2013**. *447*: p. 287-296.

[47.] Shon, H.K., et al., *Influence of Flocculation and Adsorption as Pretreatment on the Fouling of Ultrafiltration and Nanofiltration Membranes: Application with Biologically Treated Sewage Effluent.* Environmental Science & Technology, **2005**. *39*(10): p. 3864-3871.

[48.] Mao, R., et al., *Impact of various coagulation technologies on membrane fouling in coagulation/ultrafiltration process.* Chemical Engineering Journal, **2013**. *225*(0): p. 387-393.

[49.] Huang, H., K. Schwab, and J.G. Jacangelo, *Pretreatment for Low Pressure Membranes in Water Treatment: A Review.* Environmental Science & Technology, **2009**. *43*(9): p. 3011-3019.

[50.] Kurita, T., K. Kimura, and Y. Watanabe, *The influence of granular materials on the operation and membrane fouling characteristics of submerged MBRs.* Journal of Membrane Science, **2014**. *469*(0): p. 292-299.

[51.] Schwinge, J., et al., *Characterization of a zigzag spacer for ultrafiltration.* Journal of Membrane Science, **2000**. *172*(1–2): p. 19-31.

[52.] Fritzmann, C., et al., *Helically microstructured spacers improve mass transfer and fractionation selectivity in ultrafiltration.* Journal of Membrane Science, **2014**. *463*(0): p. 41-48.

[53.] Yan, L., et al., *Effect of nano-sized Al2O3-particle addition on PVDF ultrafiltration membrane performance.* Journal of Membrane Science, **2006**. *276*(1–2): p. 162-167.

[54.] Susanto, H. and M. Ulbricht, *Characteristics, performance and stability of polyethersulfone ultrafiltration membranes prepared by phase separation method using different macromolecular additives.* Journal of Membrane Science, **2009**. *327*(1–2): p. 125-135.

[55.] Nunes, S.P., M.L. Sforça, and K.-V. Peinemann, *Dense hydrophilic composite membranes for ultrafiltration.* Journal of Membrane Science, **1995**. *106*(1–2): p. 49-56.

[56.] Freeman, B.D. and I. Pinnau, *Gas and Liquid Separations Using Membranes: An Overview*, in *Advanced Materials for Membrane Separations*. **2004**. American Chemical Society. p. 1-23.

[57.] Yang, Q., et al., *Composites of functional polymeric hydrogels and porous membranes.* Journal of Materials Chemistry, **2011**. *21*(9): p. 2783-2811.

[58.] Chapman, R.G., et al., *Surveying for Surfaces that Resist the Adsorption of Proteins.* Journal of the American Chemical Society, **2000**. *122*(34): p. 8303-8304.

[59.] Prime, K. and G. Whitesides, *Self-assembled organic monolayers: model systems for studying adsorption of proteins at surfaces.* Science, **1991**. *252*(5009): p. 1164-1167.

[60.] Chen, S. and S. Jiang, *An New Avenue to Nonfouling Materials.* Advanced Materials, **2008**. *20*(2): p. 335-338.

[61.] Chiang, Y.-C., et al., *Sulfobetaine-grafted poly(vinylidene fluoride) ultrafiltration membranes exhibit excellent antifouling property.* Journal of Membrane Science, **2009**. *339*(1–2): p. 151-159.

[62.] Zhang, Z., et al., *Superlow Fouling Sulfobetaine and Carboxybetaine Polymers on Glass Slides.* Langmuir, **2006**. *22*(24): p. 10072-10077.

[63.] Eshet, I., et al., *Chemical and Physical Factors in Design of Antibiofouling Polymer Coatings.* Biomacromolecules, **2011**. *12*(7): p. 2681-2685.

[64.] Wandera, D., S.R. Wickramasinghe, and S.M. Husson, *Stimuli-responsive membranes.* Journal of Membrane Science, **2010**. *357*(1–2): p. 6-35.

[65.] Yang, Q., et al., *Designing magnetic field responsive nanofiltration membranes.* Journal of Membrane Science, **2013**. *430*(0): p. 70-78.

[66.] Peeva, P.D., T. Pieper, and M. Ulbricht, *Tuning the ultrafiltration properties of anti-fouling thin-layer hydrogel polyethersulfone composite membranes by suited crosslinker monomers and photo-grafting conditions.* Journal of Membrane Science, **2010**. *362*(1–2): p. 560-568.

[67.] Susanto, H., M. Balakrishnan, and M. Ulbricht, *Via surface functionalization by photograft copolymerization to low-fouling polyethersulfone-based ultrafiltration membranes.* Journal of Membrane Science, **2007**. *288*(1–2): p. 157-167.

[68.] Yasuda, H., A.K. Sharma, and T. Yasuda, *Effect of orientation and mobility of polymer molecules at surfaces on contact angle and its hysteresis.* Journal of Polymer Science: Polymer Physics Edition, **1981**. *19*(9): p. 1285-1291.

[69.] Wavhal, D.S. and E.R. Fisher, *Membrane Surface Modification by Plasma-Induced Polymerization of Acrylamide for Improved Surface Properties and Reduced Protein Fouling.* Langmuir, **2003**. *19*(1): p. 79-85.

[70.] Yu, H.-Y., et al., *Surface modification of polypropylene microporous membrane to improve its antifouling property in MBR: CO2 plasma treatment.* Journal of Membrane Science, **2005**. *254*(1–2): p. 219-227.

[71.] Gu, M., J.E. Kilduff, and G. Belfort, *High throughput atmospheric pressure plasma-induced graft polymerization for identifying protein-resistant surfaces.* Biomaterials, **2012**. *33*(5): p. 1261-1270.

[72.] Shenton, M.J., M.C. Lovell-Hoare, and G.C. Stevens, *Adhesion enhancement of polymer surfaces by atmospheric plasma treatment.* Journal of Physics D: Applied Physics, **2001**. *34*(18): p. 2754.

[73.] Schulze, A., et al., *Permanent surface modification by electron-beam-induced grafting of hydrophilic polymers to PVDF membranes.* RSC Advances, **2013**. *3*(44): p. 22518-22526.

[74.] Frost, S. and M. Ulbricht, *Thermoresponsive ultrafiltration membranes for the switchable permeation and fractionation of nanoparticles.* Journal of Membrane Science, **2013**. *448*(0): p. 1-11.

[75.] Singh, N., et al., *Modification of regenerated cellulose ultrafiltration membranes by surface-initiated atom transfer radical polymerization.* Journal of Membrane Science, **2008**. *311*(1–2): p. 225-234.

[76.] Yue, W.-W., et al., *Grafting of zwitterion from polysulfone membrane via surface-initiated ATRP with enhanced antifouling property and biocompatibility.* Journal of Membrane Science, **2013**. *446*(0): p. 79-91.

[77.] Jain, P., et al., *Completely Aqueous Procedure for the Growth of Polymer Brushes on Polymeric Substrates.* Langmuir, **2007**. *23*(23): p. 11360-11365.

[78.] Lei, J. and M. Ulbricht, *Macroinitiator-mediated photoreactive coating of membrane surfaces with antifouling hydrogel layers.* Journal of Membrane Science, **2014**. *455*: p. 207-218.

[79.] Adrus, N., *Stimuli - Responsive Hydrogels and Hydrogel Pore - Filled Composite Membranes*. Lehrstuhl für Technische Chemie II, Duisburg-Essen, Essen, **2012**.

[80.] Cosgrove, T., *Colloid science*. 2. ed. ed. principles, methods and applications. John Wiley & Sons**,** Chichester, **2010**.

[81.] Raffa, P., et al., *Polymeric Surfactants: Synthesis, Properties, and Links to Applications.* Chemical Reviews, **2015**. *115*(16): p. 8504-8563.

[82.] Théodoly, O., et al., *Adsorption Kinetics of Amphiphilic Diblock Copolymers: From Kinetically Frozen Colloids to Macrosurfactants.* Langmuir, **2009**. *25*(2): p. 781-793.

[83.] Johner, A. and J.F. Joanny, *Block copolymer adsorption in a selective solvent: a kinetic study.* Macromolecules, **1990**. *23*(26): p. 5299-5311.

[84.] Park, J.-W., H. Kim, and M. Han, *Polymeric self-assembled monolayers derived from surface-active copolymers: a modular approach to functionalized surfaces.* Chemical Society Reviews, **2010**. *39*(8): p. 2935-2947.

[85.] Lee, J.H., J. Kopecek, and J.D. Andrade, *Protein-resistant surfaces prepared by PEO-containing block copolymer surfactants.* Journal of Biomedical Materials Research, **1989**. *23*(3): p. 351-368.

[86.] Wang, Y., et al., *Improved permeation performance of Pluronic F127–polyethersulfone blend ultrafiltration membranes.* Journal of Membrane Science, **2006**. *282*(1–2): p. 44-51.

[87.] Zhao, W., et al., *Fabrication of antifouling polyethersulfone ultrafiltration membranes using Pluronic F127 as both surface modifier and pore-forming agent.* Journal of Membrane Science, **2008**. *318*(1–2): p. 405-412.

[88.] Edmondson, S., et al., *Surface Polymerization from Planar Surfaces by Atom Transfer Radical Polymerization Using Polyelectrolytic Macroinitiators.* Macromolecules, **2007**. *40*(15): p. 5271-5278.

[89.] Lei, J. and M. Ulbricht, *Macroinitiator-mediated photoreactive coating of membrane surfaces with antifouling hydrogel layers.* Journal of Membrane Science, **2014**. *455*(0): p. 207-218.

[90.] Nuyken, O. and B. Voit, *Polymeric Azo Initiators*, in *Macromolecular Design - Concept and Practice*, M.K. Mishra, Editor. **1994**. Polymer Frontiers International: Hopewell. p. 313-354.

[91.] Nuyken, O., R. Rengel, and R. Kerber, *Copolymerisation von 4-(1,1-dicyanoethylazo)benzylmethacrylat mit styrol, methacrylonitril und methylmethacrylat mit anschließender Pfropfung der Azocopolymere.* Die Makromolekulare Chemie, **1980**. *181*(8): p. 1565-1577.

[92.] Voronov, S., et al., *Polyperoxide surfactants for interface modification and compatibilization of polymer colloidal systems. I. Synthesis and properties of polyperoxide surfactants.* Journal of Applied Polymer Science, **2000**. *76*(8): p. 1217-1227.

[93.] Anders, C., et al., *Surface Modification with Hydrogels via Macroinitiators for enhanced Friction Properties of Biomaterials.* Journal of Macromolecular Science, Part A, **1999**. *36*(7-8): p. 1017-1029.

[94.] Feng, X.-D., *The role of amine in vinyl radical polymerization.* Makromolekulare Chemie. Macromolecular Symposia, **1992**. *63*(1): p. 1-18.

[95.] Guo, T.-Y., et al., *Copolymerizations of butyl methacrylate and fluorinated methacrylates via RAFT miniemulsion polymerization.* Journal of Polymer Science Part A: Polymer Chemistry, **2007**. *45*(22): p. 5067-5075.

[96.] Polyscope Polymers, *Company Website.* **2015.** Available from: http://www.polyscope.eu/products/xiran-resins.aspx.

[97.] Dobbins, S.C., D.E. McGrath, and M.T. Bernards, *Nonfouling Hydrogels Formed from Charged Monomer Subunits.* The Journal of Physical Chemistry B, **2012**. *116*(49): p. 14346-14352.

[98.] Cao, B., et al., *The impact of structure on elasticity, switchability, stability and functionality of an all-in-one carboxybetaine elastomer.* Biomaterials, **2013**. *34*(31): p. 7592-7600.

[99.] Gao, J., et al., *Multidimensionally stimuli-responsive phase transition of aqueous solutions of poly((N,N-dimethylamino)ethyl methacrylate) and poly(N,N-dimethyl-N-(methacryloyl)ethyl ammonium butane sulfonate).* Journal of Applied Polymer Science, **2008**. *107*(6): p. 3548-3556.

[100.] Kerber, R., J. Gerum, and O. Nuyken, *Azoinitiatoren, 9.Synthese und pfropfung azogruppenhaltiger polycarbonate.* Die Makromolekulare Chemie, **1979**. *180*(3): p. 609-614.

[101.] Ghorai, M.K., R. Talukdar, and D.P. Tiwari, *A Route to Highly Functionalized β-Enaminoesters via a Domino Ring-Opening Cyclization/Decarboxylative Tautomerization Sequence of Donor–Acceptor Cyclopropanes with Substituted Malononitriles.* Organic Letters, **2014**. *16*(8): p. 2204-2207.

[102.] Steinert, V., M. Raetzsch, and S. Reinhardt, *Preparation of maleic acid copolymers with lateral per-ester Groups. - by forming addition product of triethylamine with maleic anhydride copolymer, reacting with hydroperoxide, and hydrolysing*, DE19904034902, **1992**. Patentamt Germany.

[103.] Shen, H. and A. Eisenberg, *Morphological Phase Diagram for a Ternary System of Block Copolymer PS310-b-PAA52/Dioxane/H2O.* The Journal of Physical Chemistry B, **1999**. *103*(44): p. 9473-9487.

[104.] De Vendittis, E., et al., *A fluorimetric method for the estimation of the critical micelle concentration of surfactants.* Analytical Biochemistry, **1981**. *115*(2): p. 278-286.

[105.] Kalyanasundaram, K. and J.K. Thomas, *Environmental effects on vibronic band intensities in pyrene monomer fluorescence and their application in studies of micellar systems.* Journal of the American Chemical Society, **1977**. *99*(7): p. 2039-2044.

[106.] Dominguez, A., et al., *Determination of Critical Micelle Concentration of Some Surfactants by Three Techniques.* Journal of Chemical Education, **1997**. *74*(10): p. 1227.

[107.] Berndt, E.M., *Schaltbare und biozide Antibiofouling-Beschichtungen durch funktionale Block- und Pfropfcopolymere mit definierter Architektur* Lehrstuhl für Technische Chemie II, Univ. Duisburg-Essen, Essen, **2010**.

[108.] Hall, D.B., P. Underhill, and J.M. Torkelson, *Spin coating of thin and ultrathin polymer films.* Polymer Engineering & Science, **1998**. *38*(12): p. 2039-2045.

[109.] Pieracci, J., J.V. Crivello, and G. Belfort, *UV-Assisted Graft Polymerization of N-Vinyl-2-pyrrolidinone onto Poly(ether sulfone) Ultrafiltration Membranes Using Selective UV Wavelengths.* Chemistry of Materials, **2002**. *14*(1): p. 256-265.

[110.] Tompkins, H.G., *A User´s Guide to Ellipsometry*. Academic Press, Inc.**,** San Diego, **1993**.

[111.] Kretschmann, E., *Die Bestimmung optischer Konstanten von Metallen durch Anregung von Oberflächenplasmaschwingungen.* Zeitschrift für Physik, **1971**. *241*(4): p. 313-324.

[112.] Green, R.J., et al., *Surface plasmon resonance analysis of dynamic biological interactions with biomaterials.* Biomaterials, **2000**. *21*(18): p. 1823-1835.

[113.] Yang, H., D. Lazos, and M. Ulbricht, *Thin, highly crosslinked polymer layer synthesized via photoinitiated graft copolymerization on a self-assembled-monolayer-coated gold surface.* Journal of Applied Polymer Science, **2005**. *97*(1): p. 158-164.

[114.] Sauerbrey, G., *Verwendung von Schwingquarzen zur Wägung dünner Schichten und zur Mikrowägung.* Zeitschrift für Physik, **1959**. *155*(2): p. 206-222.

[115.] Chiou, B.-S. and S.A. Khan, *Real-Time FTIR and in Situ Rheological Studies on the UV Curing Kinetics of Thiol-ene Polymers.* Macromolecules, **1997**. *30*(23): p. 7322-7328.

[116.] Muller, R., et al., *Rheological characterization of the gel point: a new interpretation.* Macromolecules, **1991**. *24*(6): p. 1321-1326.

[117.] Mezger, T.G., *Das Rheologie Handbuch*. Vincentz**,** Hannover, **2010**.

[118.] Ocampo, A.M., *Persulfate activation by organic compounds*. Department of civil and Environmental Engineering, Washington State University, **2009**.

[119.] Van der Heide, P., *Secondary Ion Mass Spectrometry*. John Wiley & Sons**,** Hoboken, New Jersey, **2014**.

[120.] Otto, M., *Analytische Chemie*. WILEY-VCH**,** Weinheim, **2006**.

[121.] Cammann, K., *Instrumentelle Analytische Chemie*. Spektrum Akademischer Verlag**,** Berlin, **2001**.

[122.] Verma, H.R., *Atomic and Nuclear nalytical Methods*. Springer**,** Heidelberg, **2007**.

[123.] Palacio, L., et al., *Contact angles and external protein adsorption onto UF membranes.* Journal of Membrane Science, **1999**. *152*(2): p. 189-201.

[124.] Werner, C., et al., *Extended Electrokinetic Characterization of Flat Solid Surfaces.* Journal of Colloid and Interface Science, **1998**. *208*(1): p. 329-346.

[125.] Buksek, H., T. Luxbacker, and I. Petrinic, *Zeta Potential Determination of Polymeric Materials Using Two Differently Designed Measuring Cells of an Electrokinetic Analyzer.* Acta Chimica Slovenica, **2010**. *57*(3): p. 700-706.

[126.] Koros, W.J., Y.H. Ma, and T. Shimidzu, *Terminology for membranes and membrane processes (IUPAC Recommendations 1996)* Pure and Applied Chemistry, **1996**. *68*(7): p. 1479-1489.

[127.] Peeva, P.D., *Thin-Layer Hydrogel Composite Membranes with Tailored Antifouling and Ultrafiltration Properties: Preparation, Characterisation and Performance in Bioseparation*. Lehrstuhl für Technische Chemie II, Univ. Duisburg-Essen, Essen, **2011**.

[128.] Schock, G., A. Miquel, and R. Birkenberger, *Characterization of ultrafiltration membranes: cut-off determination by gel permeation chromatography.* Journal of Membrane Science, **1989**. *41*(0): p. 55-67.

[129.] Sarbolouki, M.N., *A General Diagram for Estimating Pore Size of Ultrafiltration and Reverse Osmosis Membranes.* Separation Science and Technology, **1982**. *17*(2): p. 381-386.

[130.] Becht, N.O., D.J. Malik, and E.S. Tarleton, *Evaluation and comparison of protein ultrafiltration test results: Dead-end stirred cell compared with a cross-flow system.* Separation and Purification Technology, **2008**. *62*(1): p. 228-239.

[131.] Peeva, P.D., et al., *Performance of Thin-Layer Hydrogel Polyethersulfone Composite Membranes during Dead-End Ultrafiltration of Various Protein Solutions.* Industrial & Engineering Chemistry Research, **2012**. *51*(21): p. 7231-7241.

[132.] Yune, P.S., J.E. Kilduff, and G. Belfort, *Searching for novel membrane chemistries: Producing a large library from a single graft monomer at high throughput.* Journal of Membrane Science, **2012**. *390–391*(0): p. 1-11.

[133.] Herzberg, M. and E. Asa, *unpublished data GelMem cooperation project*. **2015**. Ben Gurion Univ. of the Negev: Israel.

[134.] Heijnen, M. and M. Krug, *Composition of flower soil extract*. **2014**. Inge GmbH: Greifenberg.

[135.] Volk, C.J., C.B. Volk, and L.A. Kaplan, *Chemical composition of biodegradable dissolved organic matter in streamwater.* Limnology and Oceanography, **1997**. *42*(1): p. 39-44.

[136.] Merker, G.P. and C. Baumgarten, *Fluid- und Wärmetransport Strömungslehre*. B. G. Teubner**,** Wiesbaden, **2000**.

[137.] Lanteri, Y., et al., *Electrokinetic characterization of hollow fibers by streaming current, streaming potential and electric conductance.* Journal of Membrane Science, **2012**. *411–412*(0): p. 193-200.

[138.] Vaterrodt, A. and M. Ulbricht. *Novel antifouling surface functionalizations using polymeric zwitterions via adsorption/entrapment and layer-by-layer deposition*. at *8th Int. Conference on Polymer and Fiber Biotechnology*. **2014**. Braga, Potrugal.

[139.] Hesse, M., H. Meier, and B. Zeeh, *Spektroskopische Methoden in der organischen Chemie*. Thieme**,** Stuttgart, **2005**.

[140.] Oxley, J., et al., *Raman and Infrared Fingerprint Spectroscopy of Peroxide-Based Explosives.* Applied Spectroscopy, **2008**. *62*(8): p. 906-915.

[141.] Franke, H., *Optical recording of refractive-index patterns in doped poly-(methyl methacrylate) films.* Applied Optics, **1984**. *23*(16): p. 2729-2733.

[142.] Gao, M., K. Gawel, and B.T. Stokke, *Polyelectrolyte and antipolyelectrolyte effects in swelling of polyampholyte and polyzwitterionic charge balanced and charge offset hydrogels.* European Polymer Journal, **2014**. *53*(0): p. 65-74.

[143.] Kudaibergenov, S.E. and V.B. Sigitov, *Swelling, Shrinking, Deformation, and Oscillation of Polyampholyte Gels Based on Vinyl 2-Aminoethyl Ether and Sodium Acrylate.* Langmuir, **1999**. *15*(12): p. 4230-4235.

[144.] Wang, F., J. Yang, and J. Zhao, *Understanding anti-polyelectrolyte behavior of a well-defined polyzwitterion at the single-chain level.* Polymer International, **2015**. *64*(8): p. 999-1005.

[145.] Wang, J.-S. and K. Matyjaszewski, *Controlled/"living" radical polymerization. atom transfer radical polymerization in the presence of transition-metal complexes.* Journal of the American Chemical Society, **1995**. *117*(20): p. 5614-5615.

[146.] Paik, H.-j., et al., *Block Copolymerizations of Vinyl Acetate by Combination of Conventional and Atom Transfer Radical Polymerization.* Macromolecules, **1999**. *32*(21): p. 7023-7031.

[147.] Lee, S.B., A.J. Russell, and K. Matyjaszewski, *ATRP Synthesis of Amphiphilic Random, Gradient, and Block Copolymers of 2-(Dimethylamino)ethyl Methacrylate and n-Butyl Methacrylate in Aqueous Media.* Biomacromolecules, **2003**. *4*(5): p. 1386-1393.

[148.] Striegel, A.M. and M.R. Krejsa, *Complementarity of universal calibration SEC and 13C NMR in determining the branching state of polyethylene.* Journal of Polymer Science Part B: Polymer Physics, **2000**. *38*(23): p. 3120-3135.

[149.] Gottlieb, H.E., V. Kotlyar, and A. Nudelman, *NMR Chemical Shifts of Common Laboratory Solvents as Trace Impurities.* The Journal of Organic Chemistry, **1997**. *62*(21): p. 7512-7515.

[150.] Van de Wetering, P., et al., *Structure−Activity Relationships of Water-Soluble Cationic Methacrylate/Methacrylamide Polymers for Nonviral Gene Delivery.* Bioconjugate Chemistry, **1999**. *10*(4): p. 589-597.

[151.] Paoletti, P., et al., *Thermodynamics of protonation of amines. Values of log K, ΔH, and ΔS for the protonation of NN´- and NN-dimethylethylenediamine and NNN´N´-tetramethylethylenediamine.* Journal of the Chemical Society A: Inorganic, Physical, Theoretical, **1971**(0): p. 310-313.

[152.] Gupta, P., et al., *Electrospinning of linear homopolymers of poly(methyl methacrylate): exploring relationships between fiber formation, viscosity, molecular weight and concentration in a good solvent.* Polymer, **2005**. *46*(13): p. 4799-4810.

[153.] Dörfler, H.-D., *Grenzflächen- und Kolloidchemie*. WILEY-VCH**,** Weinheim, **1994**.

[154.] Hansen, C.M., *The Three Dimensional Solubility Parameter And Diffusion Coefficient*. Danish Technical Press**,** Copenhagen, **1967**.

[155.] Lazos, D., S. Franzka, and M. Ulbricht, *Size-Selective Protein Adsorption to Polystyrene Surfaces by Self-Assembled Grafted Poly(ethylene Glycols) with Varied Chain Lengths.* Langmuir, **2005**. *21*(19): p. 8774-8784.

[156.] Trommsdorff, V.E., H. Köhle, and P. Lagally, *Zur polymerisation des methacrylsäuremethylesters.* Die Makromolekulare Chemie, **1948**. *1*(3): p. 169-198.

[157.] Uhl, W. and A. Kyriatsoulis, *Namen- und Schlagwortreaktionen in der Organischen Chemie*. Springer**,** Wiesbaden, **1984**.

[158.] Nuyken, O. and R. Kerber, *Über die Eigenschaften einiger wasserlöslicher Azo-Initiatoren.* Die Makromolekulare Chemie, **1978**. *179*(12): p. 2845-2857.

[159.] Pergan GmbH, *Company Website.* **2015.** Available from: http://www.pergan.com/.

[160.] Pergan GmbH, *Product Catalog: Organische Peroxide für die Polymerisation*. **2012**.

[161.] Hawryluk, R.J., A.M. Hawryluk, and H.I. Smith, *Energy dissipation in a thin polymer film by electron beam scattering.* Journal of Applied Physics, **1974**. *45*(6): p. 2551-2566.

[162.] Bernstein, R., S. Belfer, and V. Freger, *Surface Modification of Dense Membranes Using Radical Graft Polymerization Enhanced by Monomer Filtration.* Langmuir, **2010**. *26*(14): p. 12358-12365.

[163.] Freger, V., J. Gilron, and S. Belfer, *TFC polyamide membranes modified by grafting of hydrophilic polymers: an FT-IR/AFM/TEM study.* Journal of Membrane Science, **2002**. *209*(1): p. 283-292.

[164.] Liu, S.X. and J.-T. Kim, *Characterization of Surface Modification of Polyethersulfone Membrane.* Journal of Adhesion Science and Technology, **2011**. *25*(1-3): p. 193-212.

[165.] Qin, J.-J., M.H. Oo, and Y. Li, *Development of high flux polyethersulfone hollow fiber ultrafiltration membranes from a low critical solution temperature dope via hypochlorite treatment.* Journal of Membrane Science, **2005**. *247*(1–2): p. 137-142.

[166.] Naukin, A.V., et al., *NIST X-ray Photoelectron Spectroscopy Database*. **2000**. US Measurement Services Division of the National Institute of Standards and Technology.

[167.] Zhao, Y.-H., K.-H. Wee, and R. Bai, *Highly hydrophilic and low-protein-fouling polypropylene membrane prepared by surface modification with sulfobetaine-based zwitterionic polymer through a combined surface polymerization method.* Journal of Membrane Science, **2010**. *362*(1–2): p. 326-333.

[168.] Yang, Q. and M. Ulbricht, *Novel Membrane Adsorbers with Grafted Zwitterionic Polymers Synthesized by Surface-Initiated ATRP and Their Salt-Modulated Permeability and Protein Binding Properties.* Chem. Mater., **2012**. *24*(15): p. 2943-2951.

[169.] Fievet, P., et al., *Determining the ζ-potential of plane membranes from tangential streaming potential measurements: effect of the membrane body conductance.* Journal of Membrane Science, **2003**. *226*(1–2): p. 227-236.

[170.] *Analyse 2014 für das Trinkwasser aus dem Wasserwerk Essen-Überruhr*. **2014**. Westfälische Wasser- und Umweltanalytik GmbH (WWU) und Hygiene-Institut des Ruhrgebiets: Essen.

[171.] Bai, T., et al., *Restraint of the differentiation of mesenchymal stem cells by a nonfouling zwitterionic hydrogel.* Angew Chem Int Ed Engl, **2014**. *53*(47): p. 12729-34.

[172.] Böhme, U. and U. Scheler, *Effective charge of bovine serum albumin determined by electrophoresis NMR.* Chemical Physics Letters, **2007**. *435*(4–6): p. 342-345.

[173.] Nabe, A., E. Staude, and G. Belfort, *Surface modification of polysulfone ultrafiltration membranes and fouling by BSA solutions.* Journal of Membrane Science, **1997**. *133*(1): p. 57-72.

[174.] Wang, Z., Z. Wu, and S. Tang, *Extracellular polymeric substances (EPS) properties and their effects on membrane fouling in a submerged membrane bioreactor.* Water Research, **2009**. *43*(9): p. 2504-2512.

[175.] Kuo, W.-C. and G.F. Parkin, *Characterization of soluble microbial products from anaerobic treatment by molecular weight distribution and nickel-chelating properties.* Water Research, **1996**. *30*(4): p. 915-922.

[176.] Carr, L.R., H. Xue, and S. Jiang, *Functionalizable and nonfouling zwitterionic carboxybetaine hydrogels with a carboxybetaine dimethacrylate crosslinker.* Biomaterials, **2011**. *32*(4): p. 961-8.

[177.] Persson, K.M., V. Gekas, and G. Trägårdh, *Study of membrane compaction and its influence on ultrafiltration water permeability.* Journal of Membrane Science, **1995**. *100*(2): p. 155-162.

[178.] Cardoso, J., L. Rubio, and M. Albores-Velasco, *Thermal degradation of poly(sulfobetaines).* Journal of Applied Polymer Science, **1999**. *73*(8): p. 1409-1414.

[179.] Shimadzu, *TOC-VCPH/CPN User Manual*. Kyoto, **2003**.

[180.] Sigma Aldrich, *Company Website.* **2015.** Available from.

[181.] Birkner, M. and M. Ulbricht. *Stimuli-responsive ultrafiltration membranes based on grafted zwitterionic polymers*. at *CHISA*. **2014**. Prague.

9 Curriculum Vitae

The Curriculum Vitae is not contained in the online version

The Curriculum Vitae is not contained in the online version

10 Publications

Oral Presentations

01.2015, Essen	M. Quilitzsch, M. Ulbricht "Reaktive Beschichtung von Membranoberflächen mit Antifouling Hydrogelen" GDCh Neujahrskolloquium 2015
10.2014, Aachen	M. Quilitzsch, M. Ulbricht "A novel and easy to apply process for in-module surface selective modification of membranes and its application to increase fouling resistance of UF membranes" 15. Aachener Membran Kolloquium
07.2014, Suzhou	M. Quilitzsch, M. Ulbricht "A novel macromolecular co-initiator system for surface selective modification of membranes in modules with fouling resistant hydrogel layers" 10^{th} International Congress on Membranes and Membrane Processes (ICOM2014)

Poster Presentations

04.2014, Frankfurt a.M.	M. Quilitzsch, M. Ulbricht "A new macromolecular initiator system for surface selective modification of UF membranes applicable in ready to use modules" ProcessNet Infotag Membrantechnik "Neuentwicklungen Cross Flow Filtration - Membranen, Module und Prozesse"
07.2013, Essen	M. Quilitzsch, M. Ulbricht "A new macromolecular surfactant as a co-initiator for grafting an anti-fouling coating onto polymeric ultrafiltration membranes" 30th EMS Summer School on Membranes
09.2013, Pisa	M. Quilitzsch, M. Ulbricht "Macromolecular surfactants as co-initiators for surface selective synthesis of hydrogel layers on ultrafiltration membranes" Congress of the European Polymer Federation
09.2012, London	M Quilitzsch, M. Ulbricht "Low-fouling UF membranes for water treatment by surface modification with hydrogel layers via a new macro-initiator" Euromembrane 2012
10.2012, Aachen	M. Quilitzsch, M. Ulbricht "Low-fouling hydrogel-coated UF membranes for treatment of waste effluents in an membrane Bioreactor" 14. Aachener Membran Kolloquium

11 Appendix

11.1 NMR spectra of synthesized initiators

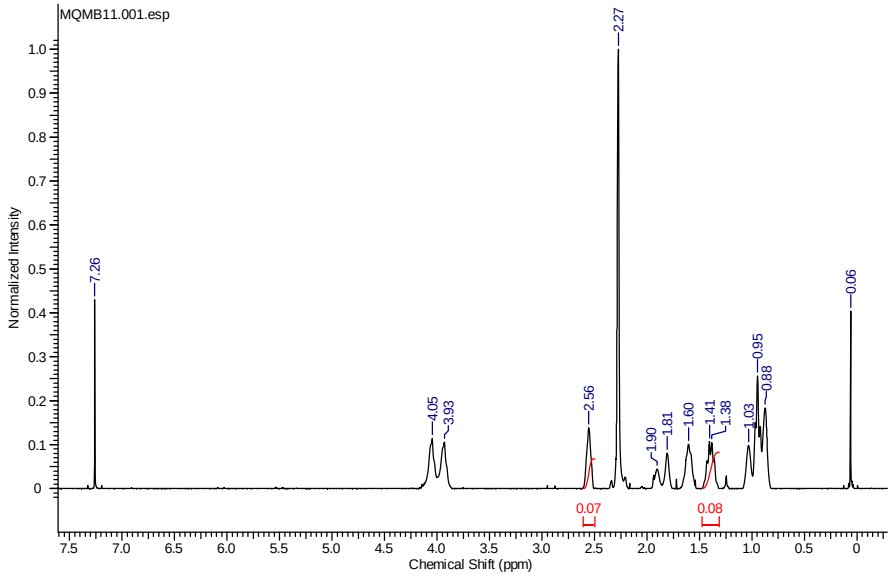

Figure 11-1 300 MHz ^{1}H-NMR spectrum of MB11 in $CDCl_3$.

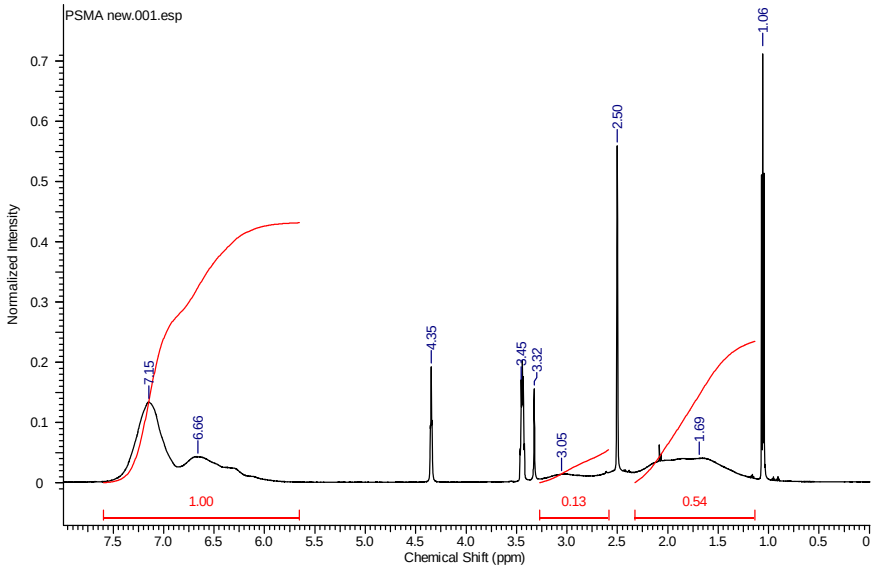

Figure 11-2 600 MHz ^{1}H-NMR Spectrum of pSMA in DMSO.

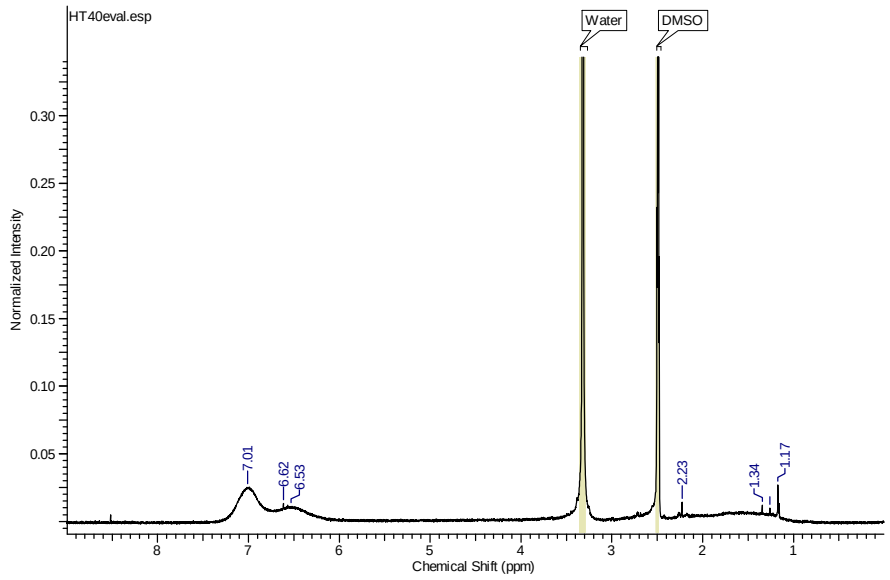

Figure 11-3 500 MHz 1H-NMR spectrum of azo modified pSMA in DMSO.

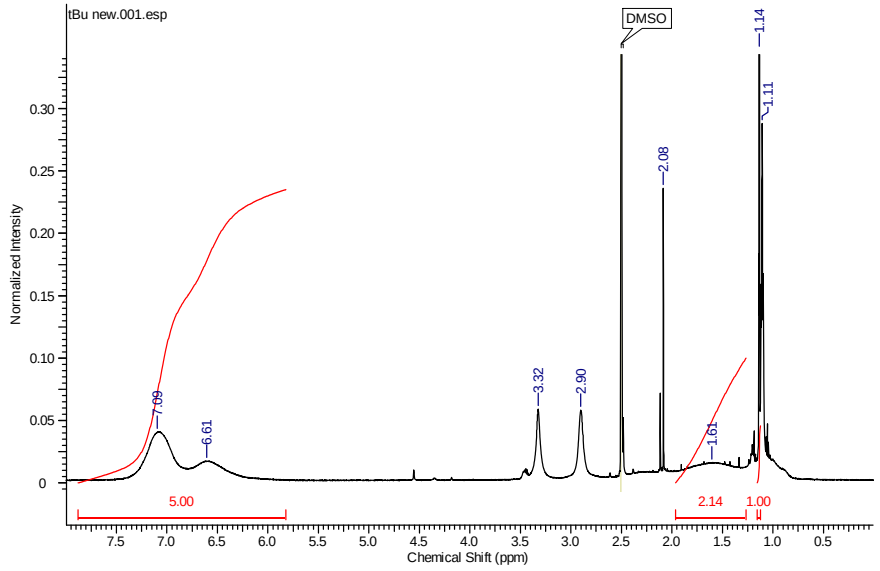

Figure 11-4 600 MHz ^{1}H-NMR spectrum of *tert.* butyl peroxide modified pSMA in DMSO.

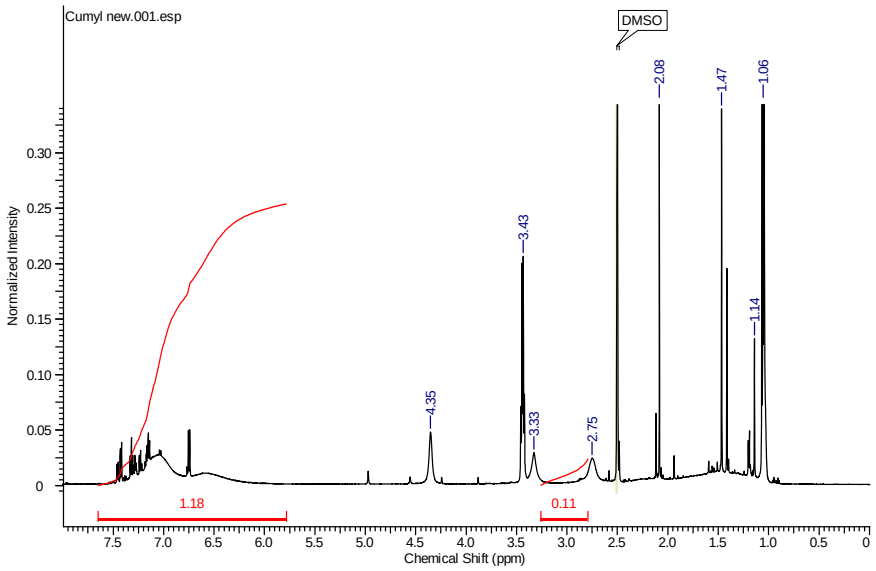

Figure 11-5 600 MHz ^{1}H-NMR spectrum of cumyl peroxide modified pSMA in DMSO.

11.2 SPR resonance curves

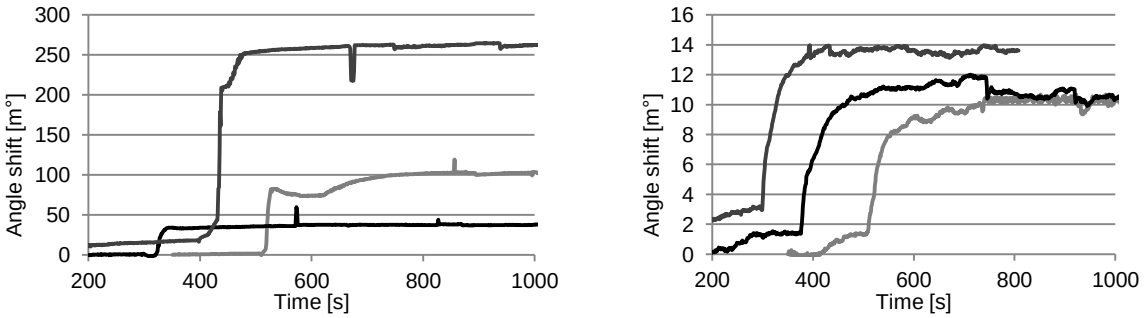

Figure 11-6 SPR resonance curve 0.1 g/L in 10 % DMAc tBu-pSMA (left) and cumyl-OO-pSMA (right).

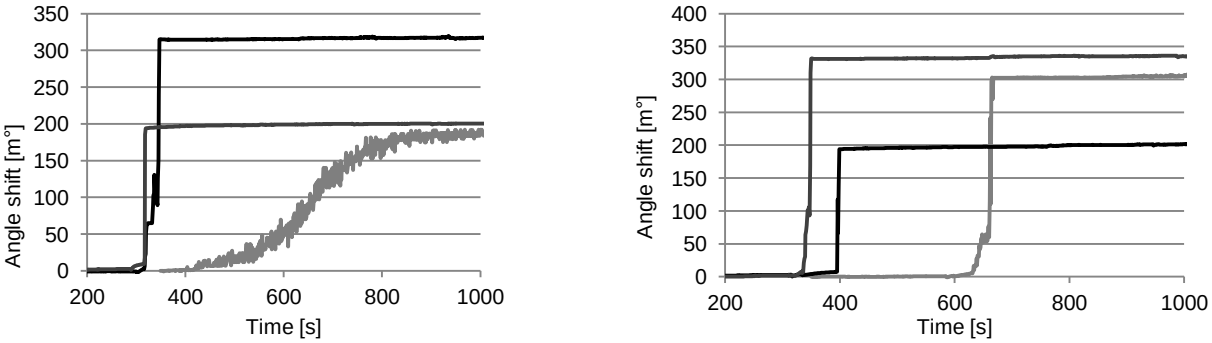

Figure 11-7 SPR resonance curves 0.1 g/L in 2 % DMAc, tBu-pSMA (left) and cumyl-OO-pSMA (right).

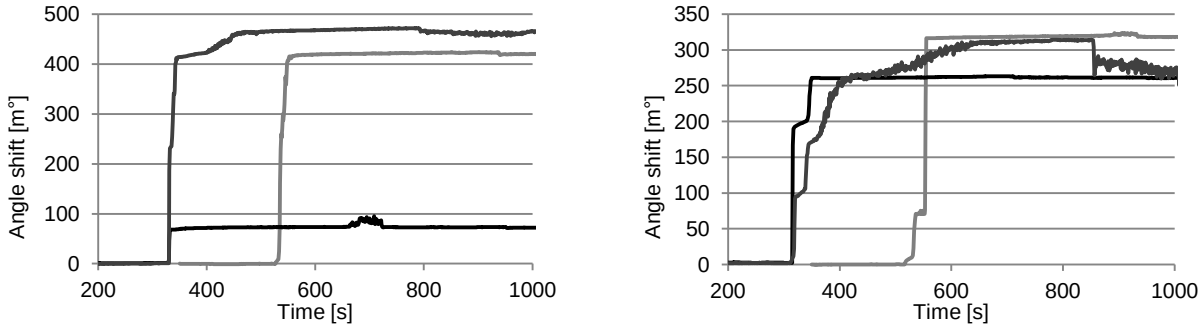

Figure 11-8 SPR resonance curves 1 g/L in 2 % DMAc, tBu-pSMA (left) and cumyl-OO-pSMA (right).

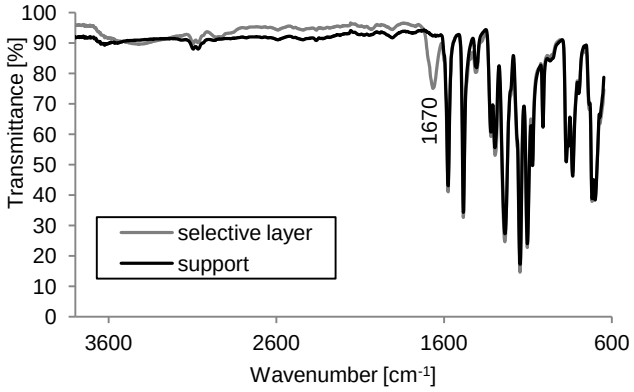

Figure 11-9 ATR-IR spectra of selective layer and membrane support of pristine PES flat sheet membrane.

Table 11-1 BSA rejection for selected samples determined by TOC

Modification	BSA rejection [% TOC]
0.1 M SPP DC 3.35 sample 1	99.6
pristine	99.7
0.1 M SPP DC 3.35 sample 2	99.8
0.1 M SPP DC 3.35 sample 3	93.7
0.1 M SPP DC 3.35 no co-ini	97.2